SCUOLA DI DOTTORATO
UNIVERSITÀ DEGLI STUDI DI MILANO-BICOCCA

Department of Physics

PhD program in Physics and Astronomy

Non-perturbative thermal QCD at all temperatures: the case of hadronic screening masses

Davide Laudicina

25th January 2024

Supervisor: Prof. Leonardo Giusti

Academic Year 2023/2024

Abstract

In the literature, thermal QCD has been explored non-perturbatively on the lattice up to $T \sim 1$ GeV and in perturbation theory, with analytical calculations, in the corresponding dimensional reduced effective theory. Nevertheless, there is much evidence, both on the theoretical and on the numerical side, that a perturbative approach is not guaranteed to be reliable even at very high temperature. For instance, for the Equation of State, perturbation theory can predict the coefficients of the expansion up to a finite order in the strong coupling, due to non-perturbative effects. In the $SU(3)$ Yang-Mills theory, these effects have been found to be significant even at the electroweak scale. For this reason, a non-perturbative approach up to very high temperature is crucial for the understanding of the high temperature regime of QCD.

The long-term objective of this thesis is to explore non-perturbatively the properties of thermal QCD in a wide range of temperatures, from 1 GeV up to the electroweak scale, beyond which other SM degrees of freedom have to be taken into account. In order to do so, the original contribution to this thesis contains two different aspects.

The first part is related to the specific strategy we implemented to simulate very large temperatures on the lattice. This strategy exploits a non-perturbative definition of the strong coupling constant in a finite volume to renormalize the theory and allows us to simulate an extremely large range of temperature with a moderate numerical effort.

In the second part of this thesis we provide a first, concrete application of this strategy, by computing the hadronic screening spectrum, i.e. the mesonic and the baryonic screening masses, from about 1 GeV up to approximately 160 GeV.

In the mesonic sector the bulk of the masses is given by the tree-level value $2\pi T$ with a few percent positive deviation. Furthermore, the spin splitting between the vector and the pseudoscalar masses turns out to be $O(g^4)$ in the entire range of temperature and remains clearly visible up the electroweak scale. At low temperatures the competition between quadratic and quartic terms in the coupling constant leads, in the pseudoscalar mass, to an effective slope with opposite sign with respect to the analytical result. At $T \sim 1$ GeV, the various terms due to inter-

actions accidentally cancel each other and the pseudoscalar mass turns out to be very close to the free theory value $2\pi T$. Given this cancellation, the $O(g^4)$ spin-dependent term is responsible for the deviation of the vector mass from $2\pi T$ at the lower end of the range of temperatures that we simulated. These considerations show that the 1-loop order correction to the free theory value is not sufficient to explain our results, in the entire range of temperature.

The exploration of the baryonic sector has been feasible thanks to the fact that at sufficiently high temperature no depletion of the signal-to-noise ratio occurs. The corresponding masses have been obtained with a few permille accuracy and show at most a 8% positive deviation with respect to the free theory value $3\pi T$. As for the mesonic case, other contributions are still relevant both at high and low temperatures. At the electroweak scale, the competition between cubic and quartic terms in the coupling constant provides about 20% of the total contribution due to interactions and, at $T \sim 1$ GeV, those terms are responsible for the flattening of the baryonic masses. This behaviour, however, cannot be explained by the $O(g^2)$ perturbative correction.

Both in the mesonic and in the baryonic sector we observed chiral symmetry restoration in the entire range of temperatures. Its manifestation results in the degeneracy of various masses, a fact which is in agreement with Ward-Takahashi identities obtained in presence of chiral symmetry.

These non-perturbative results are compatible with the effective field theory prediction, while it is clear that the reliability of 1-loop order perturbation theory is limited to temperatures well above the electroweak scale. These considerations call for a non-perturbative study of thermal QCD up to very high temperatures and the strategy proposed here provides a general framework to do that.

Acknowledgements

I would like to thank my supervisor Leonardo for all the support and the valuable advise during these three years. Together with him I would like to express my gratitude to Michele for his constant help, to Tim for being my first guide in this journey from the very beginning and to Prof. Mikko Laine for all the precious discussions during my stay in Bern. I warmly thank all the members of the lattice group of Milano-Bicocca: Matteo, Pietro, Matteo, Gabriele, Luca, Mitsuaki, Mattia and Marco. Thank you all for being an endless source of discussion and inspiration. A special mention goes to all the guys who passed by room 5016 over the past three years: it's been a wonderful journey.

To conclude, I would like to thank my parents, my sister and all the people who supported me in the last three years. Thank you for the endless support and patience: all of this would not have been possible without you all.

List of publications

For an updated list see https://inspirehep.net/authors/d.laudicina.1

Articles

[1] M. Dalla Brida, L. Giusti, T. Harris, D. Laudicina and M. Pepe, *Non-perturbative thermal QCD at all temperatures: the case of mesonic screening masses* *JHEP* 04 (2022) 034 [2112.05427]

[2] L. Giusti, T. Harris, D. Laudicina, M. Pepe and P. Rescigno, *Baryonic screening masses in QCD at high temperature, in preparation.*

[3] D. Laudicina et al., *Analytic calculation of baryonic screening masses at 1-loop order in perturbation theory, in preparation.*

Proceedings

[4] D. Laudicina, M. Dalla Brida, L. Giusti, T. Harris and M. Pepe, *Computation of QCD meson screening masses at high temperature*, *PoS* LATTICE2021 (2022) 190 [2112.06662]

[5] M. Dalla Brida, L. Giusti, T. Harris, D. Laudicina and M. Pepe, *QCD mesonic screening masses up to high temperatures*, *PoS* ICHEP2022 (2022) 829 [2211.11549]

[6] D. Laudicina, M. Dalla Brida, L. Giusti, T. Harris and M. Pepe, *QCD mesonic screening masses and restoration of chiral symmetry at high T*, *PoS* LATTICE2022 (2023) 182 [2212.02167]

[7] P. Rescigno, L. Giusti, T. Harris, D. Laudicina and M. Pepe, *Baryonic Screening Masses in High Temperature QCD*, in *40th International Symposium on Lattice Field Theory*, 11, 2023 [2311.17761]

Contents

Introduction and motivation

The Standard Model of Particle Physics (SM) is the Quantum Field Theory (QFT) which describes three of the four fundamental interactions of nature, namely electromagnetic, weak and strong interactions. At the most fundamental level, it provides a quantum description of elementary particles in a relativistic framework. In this sense, elementary particles in the SM are treated as excitations of the underlying fundamental fields.

Since the second half of the XX century, when it was introduced, it passed several experimental tests and, to date, it provides the best theoretical description of fundamental interactions at the sub-nuclear level. Nonetheless, many physical phenomena, ranging from gravitational interaction to dark matter and many others, still remain outside any theoretical description provided by the SM.

In this context, Quantum Chromodynamics (QCD) is the Quantum Field Theory which describes the strongly interacting sector of the SM [8]. The work presented in this thesis especially deals with the description of strongly interacting matter under extreme conditions.

QCD at high temperatures plays a fundamental rôle in particle and nuclear physics, and in cosmology. Apart from its intrinsic theoretical interest, the collective behaviour of strongly-interacting particles is a crucial input for determining the evolution of the early Universe. Today the quark-gluon plasma is also produced and investigated at heavy-ion colliders, where some of its basic properties are essential to analyze the experimental data. Due to asymptotic freedom, one could hope that the dynamics of the quark-gluon plasma could be efficiently described by a perturbative approach in the high temperature regime. Nevertheless, it is well known, both on the experimental [9, 10] and on the theoretical side [11], that the behaviour of the theory is strongly interacting.

In this sense, a perturbative approach is not guaranteed to be reliable even at very large temperatures [12]. Therefore, the lattice regularization provides the only theoretical framework, in which a first principle, non-perturbative study of the non-trivial dynamics of this plasma is possible. By construction thermal lattice QCD is defined in euclidean space-time. Therefore it provides a useful tool for studying euclidean observables, such as screening masses and other QCD thermodynamics quantities. On the contrary, the calculation of real-time observables, like particle production rates and other quantities, is more involved since it requires an analytical continuation from imaginary to real times [13].

The work in this thesis is part of a much wider project which aims to a non-perturbative study of thermal QCD up to very high temperatures.

The original contribution to this thesis contains two different aspects. The first part is related to the specific strategy we implemented to simulate very large temperatures on the lattice. Here we generalize to QCD the strategy which has been successfully implemented for the $SU(3)$ Yang-Mills theory in Ref. [14]. This strategy exploits a non-perturbative definition of the strong coupling constant in a finite volume to renormalize the theory and allows us to simulate an extremely large range of temperature with a moderate numerical effort.

In the second part of this thesis we provide a first, concrete application of this strategy, by computing the hadronic screening spectrum, i.e. the mesonic and the baryonic screening masses, from about 1 GeV up to approximately 160 GeV. These masses characterize the exponential decay of two-point correlation functions of interpolating operators carrying mesonic and baryonic quantum numbers. They are the inverse of the spatial correlation lengths which encode how the plasma react when a state with that given set of quantum numbers is injected into the system. Screening masses can be easily investigated numerically, they are related to spectral functions and they signal the restoration of chiral symmetry at high temperature.

In the literature, the calculations of these observables are limited to temperatures below 1 GeV and in some cases, e.g. for the baryonic screening masses, no result in the continuum limit is available yet.

The study contained in this thesis provides the first non-perturbative study of the mesonic and baryonic screening masses from about 1 GeV up to the electroweak

scale, with a very high accuracy. The high precision of our results allowed us to analyze in details the temperature dependence induced by interactions.

In the mesonic sector, $O(g^4)$ terms are relevant in the entire range of temperatures. On one hand these terms are responsible for the accidental approach of the pseudoscalar mass to the free theory value $2\pi T$ at $T \sim 1$ GeV. On the other hand, spin dependent terms, which turn out to be $O(g^4)$ over the entire range of temperatures explored, are clearly visible at the highest temperatures where the vector and the pseudoscalar masses are still different and at low temperature where those are responsible for the 4% positive deviation of the vector mass with respect to the free theory value $2\pi T$. This behaviour cannot be explained by the 1-loop order perturbative correction obtained in the framework of the effective field theory and the pattern of different contributions that we have found explains why it has been difficult in the past to match lattice results at lower temperature with the analytical behaviour at asymptotically high temperatures.

Similarly, in the baryonic sector, at the electroweak scale, the competition between cubic and quartic terms in the coupling constant amounts to $\sim 20\%$ of the total contribution due to interactions and those terms are crucial to explain the behaviour of the baryonic screening masses at the lower end of the range of temperatures that we simulated. As for the mesonic case, the 1-loop order perturbative correction is not sufficient to explain the non-perturbative lattice data over the entire range of temperature.

These findings confirm previous lattice results obtained in the $SU(3)$ Yang-Mills theory and motivate a complete and systematic non-perturbative study of thermal QCD up to the electroweak scale.

This thesis is organized as follows. In Chapter 1 we give a general outline on the theory of strong interactions at zero temperature. QCD is defined in terms of the continuum path intergral formulation, with a particular focus on its main features, such as field content and renormalizability. A dedicated section is devoted to discuss the QCD spectrum and its relations to the action symmetries and their breaking. Chapter 2 is dedicated to introduce thermal QCD. The dimensionally reduced effective theory is discussed as well as the consequences of thermal effects on the hadronic screening spectrum. Chapter 3 is dedicated to give a general introduction to the lattice regularization, which is the only theoretical framework

which allows a non-perturbative study of QCD. To conclude this Chapter we spend some time to discuss how the hadronic spectrum can be extracted from lattice observables. In Chapter 4 we outline the lattice setup and the strategy used for our lattice simulations. Finally Chapter 5 and 6 are dedicated to the numerical results of this work. In the former we focus on the non-perturbative calculation of the mesonic screening masses, while the latter is devoted to the baryonic ones. In both cases, at the beginning of these Chapters some time is spent to discuss the 1-loop order perturbative result for these masses which is obtained in the framework of the dimensionally reduced effective theory [15].

Chapter 1

Quantum Chromodynamics

Quantum Chromodynamics is the fundamental theory of strong interactions [8] (for a reference textbook see ref. [16] and ref. [17, 18] for a perturbative and a lattice approach respectively). It is defined as a renormalizable Quantum Field Theory built on the $SU(N_c)$ gauge symmetry group, where $N_c = 3$ is the number of colours and describes the quantum interactions between colour-charged particles like quarks and gluons. By construction QCD is a non-abelian theory, a fact which makes its dynamics highly non-trivial. In contrast with Quantum Electrodynamics (QED), which is the only abelian theory within the Standard Model, QCD exhibits many non-perturbative features, like colour confinement and is able, by itself, to explain the hadronic spectrum of QCD.

In the following sections we will review the main building-blocks to construct QCD, i.e. its field content and the concept of renormalization, in euclidean space-time[1]. Along with these definitions, we will devote some time to discuss some of the main theoretical successes of QCD.

1.1 SU(3) Yang-Mills theory

In terms of field content, the $SU(3)$ Yang-Mills theory contains the gauge field $A_\mu(x)$ where $\mu = 0, \ldots, 3$ is a Lorentz index. From a representation theory point

[1] The usual (3+1)-dimensional minkoskian theory is mapped to the corresponding 4-dimensional euclidean theory by a *Wick's rotation* ($t_{\mathrm{M}} = -it_{\mathrm{E}}$)

of view this field transforms under the adjoint representation of $SU(3)$, which translates into having $a = 1, \ldots, N_c^2 - 1$ independent real gauge fields $A_\mu^a(x)$ so that $A_\mu(x) = A_\mu^a(x) T_a$, where T_a is a basis of the $SU(3)$ algebra (see App. A.1 for some useful definitions). By taking into account a generic element of the $SU(3)$ group which can be written as

$$\Omega(x) = \exp\left[i\epsilon^a(x) T_a\right] , \tag{1.1}$$

we can define the $SU(3)$ gauge transformations as local transformations acting on the gauge field as

$$A_\mu(x) \longrightarrow A'_\mu(x) = i\Omega(x) D_\mu \Omega(x)^\dagger , \tag{1.2}$$

where we defined the covariant derivative as

$$D_\mu = \partial_\mu - i A_\mu . \tag{1.3}$$

From these definitions, the QCD field strength tensor reads

$$F_{\mu\nu} = i\left[D_\mu, D_\nu\right] = \partial_\mu A_\nu^a - \partial_\nu A_\mu^a - i\left[A_\mu, A_\nu\right] , \tag{1.4}$$

and by writing $F_{\mu\nu} = F_{\mu\nu}^a T_a$ and using the properties of the generators of the $SU(3)$ algebra (see eq. A.6), it can be written in the familiar form

$$F_{\mu\nu}^a = \partial_\mu A_\nu^a - \partial_\nu A_\mu^a + f^{abc} A_\mu^b A_\nu^c , \tag{1.5}$$

where f^{abc} are the anti-symmetric structure constants of the $SU(3)$ gauge group defined in App. A.1. Notice that under gauge transformations the field strength tensor transforms as

$$F_{\mu\nu}(x) \longrightarrow F'_{\mu\nu}(x) = \Omega(x) F_{\mu\nu}(x) \Omega^\dagger(x) . \tag{1.6}$$

In order to build the Yang-Mills action for the gluon field we require this to be gauge invariant and the corresponding theory to be renormalizable, which translates into taking into account only operators with mass dimension $d \leq 4$, see Sec.

Figure 1.1: On the left, the three point gluonic interaction and on the right the four point gluonic interaction. The appearance of this type of interactions is due to the non-abelian nature of QCD.

1.4 for a further discussion on this topic. There are only two different composite operators which satisfy these requirements and, as a consequence, the action reads[2]

$$S_g[A] = \int \mathrm{d}^4x \left\{ \frac{1}{2g_0^2} \mathrm{Tr}\left[F_{\mu\nu}F_{\mu\nu}\right] - \frac{i\theta}{32\pi^2}\epsilon_{\mu\nu\rho\sigma} \mathrm{Tr}\left[F_{\mu\nu}F_{\rho\sigma}\right] \right\}, \tag{1.7}$$

where the trace is over colour indices. While the abelian Yang-Mills action is a theory of non-interacting massless gauge bosons, non-abelian theories, like the $SU(3)$ Yang-Mills theory, contain cubic and quartic terms in A_μ, which give rise to gluonic self-interaction terms, whose Feynaman diagrams are depicted in Fig. 1.1.

Let us notice that gauge invariance allows the presence of the second term on the r.h.s in the action, the so called *θ-term*, which would be responsible for the breaking of the CP symmetry.

1.2 Fermions

Once the Yang-Mills sector of the action has been properly defined, QCD requires the presence of quarks. Furthermore in order to preserve gauge invariance, quarks must interact with gluons. In the most general case, the gauge field is coupled to N_f different flavours of Dirac fermions transforming under the fundamental representation of the colour group $SU(3)$, namely each Dirac fermion is a three-component vector in colour space, which transforms under gauge transformations

[2]Notice that the standard perturbative convention is easily recovered by simply making the substitution $A_\mu(x) \to g_0 A_\mu(x)$, where g_0 is the bare coupling constant.

as

$$\begin{aligned}\psi(x) &\longrightarrow \psi'(x) = \Omega(x)\psi(x) \\ \bar{\psi}(x) &\longrightarrow \bar{\psi}'(x) = \bar{\psi}(x)\Omega^{\dagger}(x)\,,\end{aligned} \tag{1.8}$$

In terms of the Lorentz group a Dirac fermion transforms as a reducible representation of dimension 4, composed by a left-handed and a right-handed Weyl spinor, which on the other hand transform as a $(1/2, 0)$ and $(0, 1/2)$ representation of the Lorentz group respectively[3]. As for the pure gauge case, once the field content is defined, the action is simply constructed by requiring it to be gauge invariant and the corresponding theory to be renormalizable. There are only two operators with mass dimension $d \leq 4$, namely the kinetic and the mass term. This leads to the usual expression for the Dirac action

$$S_f[\bar{\psi}, \psi, A] = \int \mathrm{d}^4x\, \bar{\psi}(x)\left[\gamma_\mu D_\mu + M_0\right]\psi(x)\,, \tag{1.9}$$

where the covariant derivative naturally introduces interactions with the gauge fields. γ_μ are the Dirac gamma matrices, satisfying the Clifford algebra (see eq. A.8) and M_0 is the mass matrix, which can always be diagonalized with an appropriate field redefinition. The action in eq. 1.9 holds for each of the quark flavours. The full QCD action is finally given by

$$S_{QCD}[\bar{\psi}, \psi, A] = S_g[A] + S_f[\bar{\psi}, \psi, A]\,, \tag{1.10}$$

where the fermionic sector is meant to include all the possible fermion flavours, i.e. in eq. 1.9 a sum over all the flavours is understood. Notice that the θ-term appearing in eq. 1.7 is constrained by several experimental measurements of the neutron electric dipole moment [19, 20, 21], which provides the upper limit $\theta \lesssim 10^{-10}$ [22]. For this reason, it is often assumed $\theta = 0$.

[3]Here we exploit the isomorphism between the proper Lorentz group $SO(1,3)$ and $SU(2) \times SU(2)$

1.3 Path integral formulation

The action defined in eq. 1.10 is enough to define the theory at the classical level. The corresponding quantum field theory is obtained by exploiting the path integral formulation [23], where the formal partition function in euclidean space-time is defined as

$$\mathcal{Z} = \int DA\, D\bar{\psi}\, D\psi\, D\bar{c}\, Dc\, e^{-S_{QCD}}\,, \tag{1.11}$$

where $D[\cdot]$ denotes the path integral measure over all the possible fields configurations. Let us stress that the definition in eq. 1.11 is purely formal and a rigorous definition can be formulated on the lattice, see Chapter 3. In the expression above, in order to keep Fermi-Dirac statistics for fermions, quark fields ψ and $\bar{\psi}$ are not simply c-number, but are Grassmann variables, i.e. they are anti-commuting objects, satisfying the *Grassmann algebra*. Furthermore the integral over the gluonic fields is not well defined, since the integration is over an infinite number of equivalent gauge configurations. The introduction of a gauge fixing term is needed and in the Faddeev-Popov formalism it is achieved by introducing two additional terms in the action, which now reads

$$S_{QCD}[\bar{\psi}, \psi, A, \bar{c}, c] = S_g[A] + S_f[\bar{\psi}, \psi, A] + S_{FP}[\bar{c}, c] + S_{GF}[A]\,, \tag{1.12}$$

where the Faddeev-Popov [24] and the gauge fixing contributions are respectively

$$S_{FP} = -\int \mathrm{d}^4x \frac{2}{g_0^2} \mathrm{Tr}\left[\bar{c}\partial_\mu D_\mu c\right]\,, \tag{1.13}$$

$$S_{GF} = \int \mathrm{d}^4x \frac{\lambda_0}{g_0^2} \mathrm{Tr}\left[\partial_\mu A_\mu \partial_\nu A_\nu\right]\,, \tag{1.14}$$

where λ_0 is the gauge fixing parameter and again the trace is over colour indices. In the expression above the two fields c and $\bar{c}$, which are called *ghost* and *anti-ghost* fields respectively, have been introduced to make the integral over the gauge fields finite. Those are Grassmann variables, but in order to preserve Lorentz invariance, they transform as scalar fields under Lorentz transformations.

Let us stress that the Faddeev-Popov procedure holds to all orders in perturba-

tion theory, but it does not apply at the non-perturbative level. Indeed, as pointed out by Gribov, in a non abelian gauge theory the gauge fixing condition could have multiple solutions leading to the so called Gribov copies, which limit this procedure only to the perturbative analysis [25]. As a final remark, let us stress again that the above expressions are just formal definitions. When the correct definition of the path integral is introduced with a lattice regularization, the gauge fixing and the Faddeev-Popov terms will be no longer required, as we will see in Chapter 3.

1.4 Renormalization

As mentioned in Sec. 1.1 after defining the field content of the theory and imposing gauge invariance, the last step in order to define the QFT is the *renormalization* step. This procedure is by itself composed of two different parts. The first one is the so called *regularization* step and the second one is the one which defines the renormalization *scheme*.

The regularization step is needed in order to define physical observables. In this step one typically introduces a cut-off (or a regulator) to tame the ultraviolet (UV) divergences in momentum integrals. Obviously the divergent part of the integrals is recovered by taking the limit of vanishing regulator.

The regularization technique we use in this work is the so called *lattice* regularization, which provides the only theoretical framework which allows a non-perturbative definition of QCD, see Chapter 3 for a further discussion. This kind of procedure consists in discretizing the theory on a lattice with a spacing a, which provides a cut-off at extremely small distances or, equivalently, in the high momentum region, i.e. we take into account momenta $p < \pi/a$ only.

The path integral in eq. 1.11 is defined in terms of bare parameters, e.g. bare quark masses and bare coupling constant. The choice of a set of renormalization conditions defines the renormalization scheme and naturally introduces a dependence on the cut-off in the bare parameters. On the lattice this is achieved by using a so called *hadronic scheme*. In this kind of schemes bare parameters are kept fixed for a give lattice spacing and their dependence on the cut-off is constrained by fixing the value of some computable observables, like hadron masses

(e.g. M_π, M_N, M_K), to some value which is kept constant in the lattice spacing [26, 27]. Given its importance in the present thesis, in Chapter 3 a section will be dedicated to non-perturbative renormalization with further details and discussions.

At the perturbative level, dimensional regularization [28] is the most common regularization procedure. It consists in computing all the amplitudes in $D = 4 - 2\varepsilon$ dimensions. Other procedures deal with the introduction of a hard cut-off Λ which implies to consider only momenta $p < \Lambda$ [29].

The most common perturbative renormalization scheme is the so called *minimal subtraction* (MS) scheme, in which any divergent term in the cut-off is subracted order by order [30, 31].

The general criterion to establish the renormalizability of a theory depends on the mass dimension of the operators appearing in the action. Any operator O can be classified in terms of the dimensionality of its coupling $d_g = d_O - 4$ as

- $d_g > 0$: *relevant* operator.
- $d_g = 0$: *marginal* operator.
- $d_g < 0$: *irrelevant* operator.

A theory is renormalizable if contains all possible relevant and marginal operators with the appropriate symmetries and in such case, it is sufficient to set a finite number of renormalization conditions only. This is the case of QCD as for any other theory within the Standard Model.

In the context of renormalization one can introduce the cut-off independent renormalized parameters, which are defined as

$$g^2(\mu) = Z_g(g_0, a\mu) g_0^2 \,, \qquad M(\mu) = Z_M(g_0, a\mu) M_0 \,, \tag{1.15}$$

where the dimensionless constants Z_i are renormalization scheme dependent and depend both on the cut-off and on the so called *renormalization scale* μ. In the same way, if one is interested in correlation functions involving fundamental fields, we can define the renormalized fields as

$$A_\mu^R = Z_3^{1/2}(g_0, a\mu) A_\mu \,, \qquad \psi_R = Z_2^{1/2}(g_0, a\mu) \psi \,, \tag{1.16}$$

Once the cut-off is removed, this procedure introduces a dependence on the scale μ in the renormalized coupling and in the quark masses. This scale dependence has deep implications for what concerns the nature of a QFT. As a final remark, notice that, even though the renormalized parameters gain a scale dependence, any physical observable, e.g. hadron masses, has to be scale and scheme independent (see Sec. 1.4.2).

1.4.1 Renormalization group equations

Due to the renormalization procedure, some renormalized quantities, e.g. renormalized parameters and renormalized correlation functions of fundamental operators, might gain an explicit dependence on the renormalization scale μ. This dependence is embedded in the so called *renormalization group equations* [32]. Let us consider the most general case with n_{G} gauge fields, n_{F} fermionic fields and a generic scale dependent correlation function $\Gamma^{n_{\mathrm{G}},n_{\mathrm{F}}}$. One can show that bare and renormalized quantities are related by

$$(Z_3^{-1/2})^{n_{\mathrm{G}}}(Z_2^{-1/2})^{2n_{\mathrm{F}}}\Gamma_R^{n_{\mathrm{G}},n_{\mathrm{F}}}(\{x_j\};\mu,g,M) = \Gamma_0^{n_{\mathrm{G}},n_{\mathrm{F}}}(\{x_j\};g_0,M_0)\,, \tag{1.17}$$

where $\Gamma_0^{n_{\mathrm{G}},n_{\mathrm{F}}}$ is the bare correlation function, which depends on the bare quantities and implicitly on the cut-off, while $\Gamma_R^{n_{\mathrm{G}},n_{\mathrm{F}}}$ is the renormalized correlation function which depends on the renormalized quantities and on the scale μ only. Since the bare correlation function does not depend on the scale, its derivative with respect to μ vanishes. This leads to the well known non-perturbative Callan-Symanzik equation [33, 34]

$$\left[\mu\frac{\partial}{\partial\mu} + \beta\frac{\partial}{\partial g} + \tau M\frac{\partial}{\partial M} - n_{\mathrm{G}}\gamma_3 - 2n_{\mathrm{F}}\gamma_2\right]\Gamma_R^{n_{\mathrm{G}},n_{\mathrm{F}}} = 0\,, \tag{1.18}$$

where for the renormalized coupling and the renormalized quark masses it holds

$$\beta(g) = \mu\frac{\partial g}{\partial\mu}, \qquad \tau(g) = \frac{\mu}{M}\frac{\partial M}{\partial\mu}, \tag{1.19}$$

and in the same way for the renormalized gluonic and fermionic fields

$$\gamma_3(g) = \frac{1}{2}\mu\frac{\partial}{\partial\mu}\ln Z_3, \qquad \gamma_2(g) = \frac{1}{2}\mu\frac{\partial}{\partial\mu}\ln Z_2. \tag{1.20}$$

These equations encode how the renormalized parameters of the theory depend on the scale, i.e. how a change in the renormalization scale affects the renormalized parameters. In perturbation theory the β-function and the τ-function can be expressed as an expansion in the renormalized coupling. For example, for the β-function we obtain

$$\beta(g) = -g^3 \sum_{k=0}^{\infty} b_k g^{2k}\,, \tag{1.21}$$

where coefficients b_k are computed at $(k+1)$-th order in perturbation theory and depend on the number of flavours N_f and on the number of colours N_c, thus on the physical theory we are considering.

An interesting property of the above expansion is that the b_0 and b_1 coefficients do not depend on the renormalization scheme, i.e they are universal and their values are [35, 36]

$$b_0 = \frac{1}{(4\pi)^2}\left[\frac{11}{3}N_c - \frac{2}{3}N_f\right], \qquad b_1 = \frac{1}{(4\pi)^4}\left[\frac{34}{3}N_c^2 - \left(\frac{13}{3}N_c - \frac{1}{N_c}\right)N_f\right], \tag{1.22}$$

while b_2 and b_3, namely the 3-loop and 4-loop coefficients, are scheme dependent and their value in the $\overline{\text{MS}}$ scheme can be found in Ref. [37, 38]. Analogously, for the τ-function for the quark masses it holds

$$\tau(g) = -g^2 \sum_{k=0}^{\infty} d_k g^{2k}\,. \tag{1.23}$$

In this case the only universal coefficient is the one at 1-loop order in perturbation theory, which reads

$$d_0 = \frac{1}{(4\pi)^2}\frac{3\,(N_c^2-1)}{N_c}\,. \tag{1.24}$$

As a final remark, notice that the expressions in eq. 1.19 define a *flow* in parameters space, which describes how the theory behaves at different energy scales. In this

sense, the value of the coefficients in the perturbative expansion (see eq. 1.21 and 1.23) have a crucial rôle in the description of this flow.

A different, but equivalent, approach to renormalization was provided by Wilson in Ref. [39]. In this approach every QFT comes with an intrinsic cut-off and represents a low energy description of a more fundamental theory, i.e. it is an effective theory which describes the infrared (IR) behaviour of the fundamental theory below a certain UV energy scale. In this sense, the renormalization group provides a map that link the fundamental theory to the QFT by integrating out high energy scales. In this sense, the effects of relevant operators become increasingly important at lower energies, while irrelevant operators give relevant contributions only at high energy.

1.4.2 Λ-parameter

Phyical observables $G_R(\mu, g, M)$ are independent of fundamental fields renormalization and must be scale invariant, then, from eq. 1.18, they must satisfy the renormalization group equation

$$\left\{\mu\frac{\partial}{\partial\mu} + \beta\frac{\partial}{\partial g} + \tau M\frac{\partial}{\partial M}\right\} G_R(\mu, g, M) = 0\,. \tag{1.25}$$

These quantities are usually called *renormalization group invariant* (RGI). Maybe the simplest RGI quantity with mass dimension 1, one can obtain is the so called Λ-parameter. We assume it to be independent of the quark mass, a fact which can be achieved by employing a mass-independent renormalization scheme. In such case we can choose a Λ-parameter of the form $G_R(\mu, g) = \Lambda_{\rm QCD}(\mu, g) = \mu f(g)$, i.e. the scale dependence appearing in $f(g)$ is cancelled by the factor μ. As a consequence it has to satisfy

$$\left\{1 + \beta\frac{\partial}{\partial g}\right\} f(g) = 0\,. \tag{1.26}$$

This equation has a simple solution in terms of the β-function which reads

$$\Lambda_{\rm QCD}(\mu, g) = \mu \exp\left\{-\int_{\bar{g}}^{g} \frac{dx}{\beta(x)}\right\}. \tag{1.27}$$

Notice that for $\bar{g} \to 0$ the integral is divergent due to the vanishing β-function in the weak coupling limit. In order to deal with this divergence we employ the 2-loop perturbative expansion for the β-function defined in eq. 1.21. This leads to

$$\Lambda_{\rm QCD}(\mu, g) = \mu \left(b_0 g^2\right)^{-b_1/2b_0^2} e^{-1/2b_0 g^2} \exp\left\{ - \int_0^{g(\mu)} \mathrm{d}x \left[\frac{1}{\beta(x)} + \frac{1}{b_0 x^3} - \frac{b_1}{b_0^2 x} \right] \right\} . \tag{1.28}$$

A couple of comments are in order. First of all it is worth noticing that the definition of $\Lambda_{\rm QCD}$ in eq. 1.28 is totally non-perturbative and, even if b_0 and b_1 are scheme independent, $\Lambda_{\rm QCD}$ is not, i.e. the Λ-parameter is a *scheme dependent* RGI quantity. On the other hand, notice that the appearance of the Λ-parameter, which is - by definition - a dimensionful quantity, is due to the renormalization procedure which takes place when defining a QFT. Even if we considered QCD in the massless limit, which is, at classical level, a scale invariant theory, the quantization of the theory breaks this symmetry leading to the appearance of $\Lambda_{\rm QCD}$, which then defines the typical scale of QCD.

This phenomenon, which generates a dimensionful quantity from a theory which is scale invariant at the classical level is called *dimensional transmutation*. In a very similar fashion, by solving the τ-function defined in eq. 1.23 we can define the *invariant quark mass* M_q, which, in contrast with $\Lambda_{\rm QCD}$, is not only a RGI quantity, but is also *scheme independent*.

So far the renormalization scale was unphysical, however if we take it to be of the order of the momentum transfer for a particular process $\mu \simeq Q$, then the renormalized coupling provides the strength of the strong interaction at that energy scale. In this way, by applying the same analysis that led us to eq. 1.28, a generic renormalization group invariant quantity with mass dimension d is a function of the renormalized parameters and of scale Q and can be written as

$$G_R \equiv \mu^d G\left(\frac{Q^2}{\mu^2}, g(\mu), M(\mu)\right) = Q^d G\left(1, g(Q), M(Q)\right) . \tag{1.29}$$

If we restrict ourselves to the massless limit of QCD, then the Λ-parameter, being the only energy scale of the theory, is sufficient to define the typical energy scale of the observable. By taking advantage of dimensional transmutation, the above

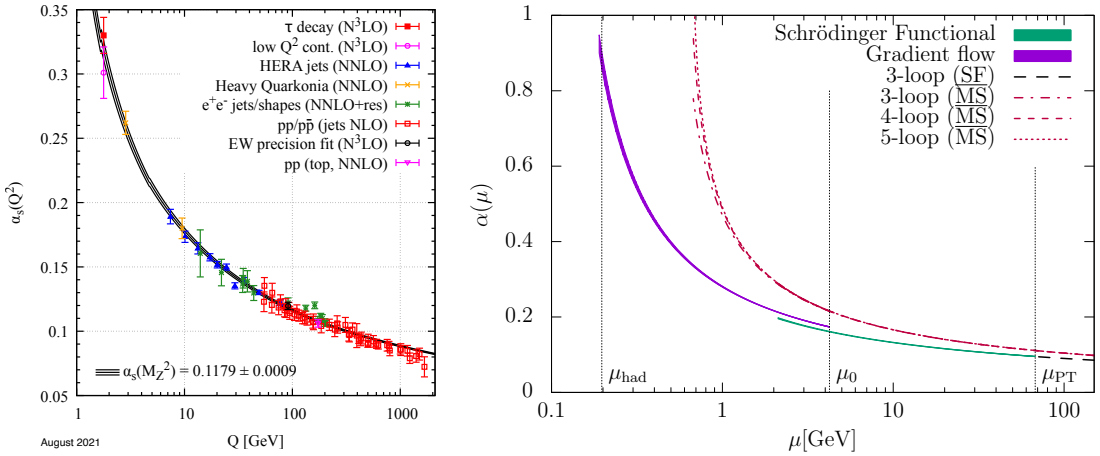

Figure 1.2: Left: the measurements of α_s, as a function of the energy scale Q at different orders in perturbation theory. Data from Particle Data Group, See Ref. [22]. Right: Non-perturbative determination of the strong coupling constant on the lattice using Schrödinger functional and gradient flow schemes. Data from the ALPHA collaboration, see Ref. [40]

observable can be written as

$$G_R \;=\; \Lambda_{\rm QCD}^{d}\, G\left(1, g\left(Q\right)\right)\,, \tag{1.30}$$

For instance, for hadron masses $G_R = M_H$ $(d = 1)$, it holds

$$M_H \;=\; \Lambda_{\rm QCD} \times \mathcal{K}\,, \tag{1.31}$$

where $\mathcal{K}$ is a dimensionless, non-perturbative, scheme-dependent coefficient. As we will see in Sec. 1.5, this has deep implications in hadron spectroscopy.

1.4.3 Running coupling and asymptotic freedom

The definition of the Λ-parameter in Sec. 1.4.2 fixes the value of the renormalized coupling in a physical process which occurs at the energy scale Q.

An explicit solution to eq. 1.28 is easily obtained in the weak coupling limit, by simply using the 2-loop perturbative expansion for the β-function which involves

the b_0 and b_1 coefficients defined in eq. 1.22 and leads to

$$\alpha_s(Q) = \frac{g^2(Q)}{4\pi} = \frac{1}{4\pi b_0 \ln\left(\frac{Q^2}{\Lambda^2}\right)}\left[1 - \frac{b_1}{b_0^2}\frac{\ln\left(\ln\left(\frac{Q^2}{\Lambda^2}\right)\right)}{\ln\left(\frac{Q^2}{\Lambda^2}\right)}\right]. \tag{1.32}$$

Notice that the behaviour of the *running coupling* depends on the sign of the b_0 parameter in eq. 1.22 which is a function of the number of flavours N_f and of the number of colours N_c. In particular, a negative-valued b_0 would lead to a *Landau pole* which makes the coupling divergent at a specific value of Q. On the other hand for positive values of the 1-loop coefficient, the coupling vanishes for $Q \to \infty$ and this somehow justifies *a posteriori* the weak coupling expansion we performed in eq. 1.32 leading to what is called *asymptotic freedom* of the theory. Physical QCD, with $N_c = 3$ and $N_f = 6$ falls in the latter case. The vanishing coupling for $Q \to \infty$ implies the validity of perturbation theory to be restricted to the high energy regime and the value of Λ_{QCD} provides the energy scale at which the perturbative expansion breaks down and non-perturbative effects start to become relevant.

The Q-dependence of the running coupling can be extracted precisely by using a variety of experimental inputs using perturbation theory. This kind of determinations involves at least NLO pre-

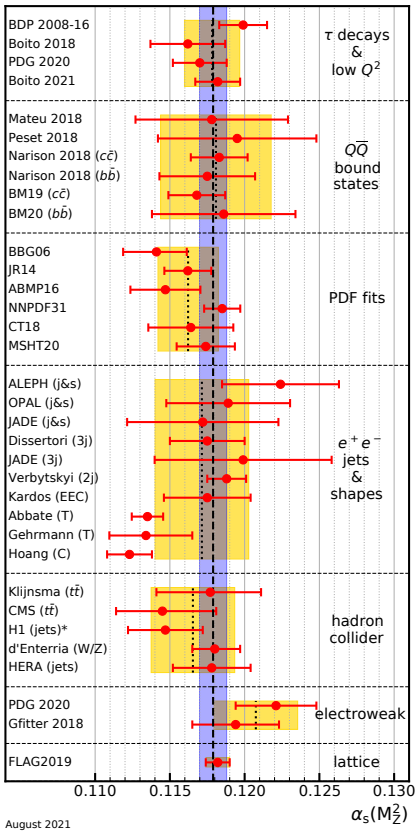

Figure 1.3: Summary of the determinations of the running coupling both perturbatively and non-perturbatively. Yellow bands show the average of each field, while the blue band corresponds to the overall world average. From Ref. [22]. Notice that the lattice average does not include the latest results reported in Ref. [41] but is limited to the FLAG 19 report (see Ref. [42]).

	Meson	Mass (MeV)
8	π^+	139.57039(18)
	π^0	134.9768(5)
	π^-	139.57039(18)
	K^+	493.677(16)
	K^0	497.611(13)
	$\bar{K}^0$	497.611(13)
	K^-	493.677(16)
	η	547.862(17)
1	η'	957.78(6)

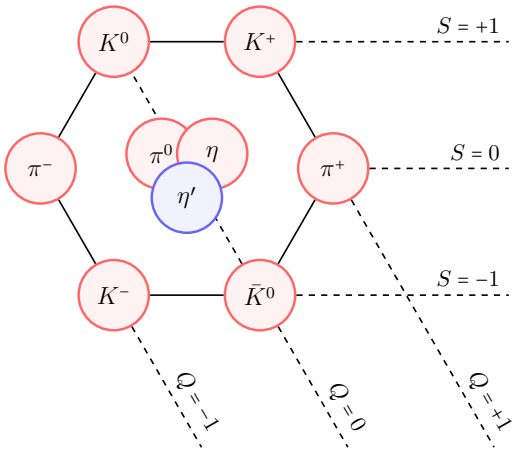

Table 1.1: On the right the mesonic octet in blue and the singlet (η') in red. Q is the electric charge and S the strangeness quantum number. Isospin projection along the third axis can be obtained by using the Gell-Mann-Nishijima formula [50, 51]. On the left the corresponding masses. Data from Ref. [22].

dictions for τ decays [43], heavy quarkonia decays [44], PDF fits [45], hadronic final states from e^+e^- annihilations [46], jets and $t\bar{t}$ production in hadron colliders [47, 48] and electroweak precision fits [49]. In order to compare different determinations of α_s those are typically rescaled to a standard energy scale, given by the Z mass. In fig. 1.2 on the left the calculation of α_s from different experimental input at different orders in perturbation theory is shown, leading to the perturbative average $\alpha_s(M_Z) = 0.1176(10)$ [22].

In addition to the perturbative determination of the running coupling, progresses in lattice calculations have made possible a non-perturbative determination of the QCD running coupling from a few hundred MeV up to the electroweak scale. In fig. 1.2 on the right the non-perturbative running of the coupling obtained in Ref. [40] is shown. The world average lattice determination of the running coupling is provided by the FLAG collaboration [41] and includes several determinations based on step-scaling methods, potential at short distances, Wilson loops and heavy quark two-point functions, leading to the final estimate $\alpha_s(M_Z) = 0.1184(8)$, which provides a remarkable check that the experimental running of the coupling is perfectly reproduced by the theory. By combining perturbative and non-perturbative

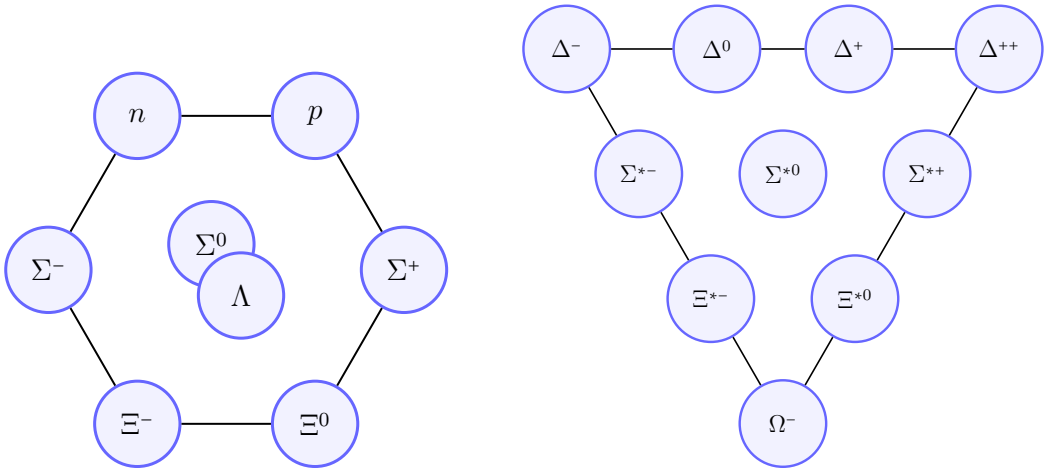

(a) (b)

Figure 1.4: (a) Baryon octet, masses span from 938 MeV (p) to 1321 MeV (Ξ^-). (b) baryon decuplet, masses span from 1232 MeV (Δ^{++}) to 1672 MeV (Ω^-).

determinations of the running coupling at the M_Z scale, the final world average quoted in Ref. [22] is $\alpha_s(M_Z) = 0.1179(9)$ (see fig. 1.3).

1.5 QCD hadronic spectrum

As we have seen in Sec. 1.4.3 at low energy the strong coupling constant diverges making quarks and gluons strongly interacting. This behaviour suggest the phenomenon of *colour confinement* and implies that neither free quarks nor free gluons can be directly observed, but, on the contrary, only colour-singlet states are physical observables. The multiple experimental evidences of new particles made the classification of hadronic states a long-standing problem well before QCD was introduced. The first attempt to systematically classify the hadronic spectrum was done by Gell-Mann in his seminal paper on the so-called Eightfold Way [52]. This classification was based on global quantum numbers of hadrons, such as *strangeness*, *isospin* and *electric charge* and led, for $N_f = 3$, to the standard organization for mesons into a singlet and an octet depicted in fig. 1.1, while for the baryons it led to the octet and decuplet representations (see fig. 1.4a and 1.4b). Such organization encodes the underlying $SU(3)$ flavour symmetry of the theory.

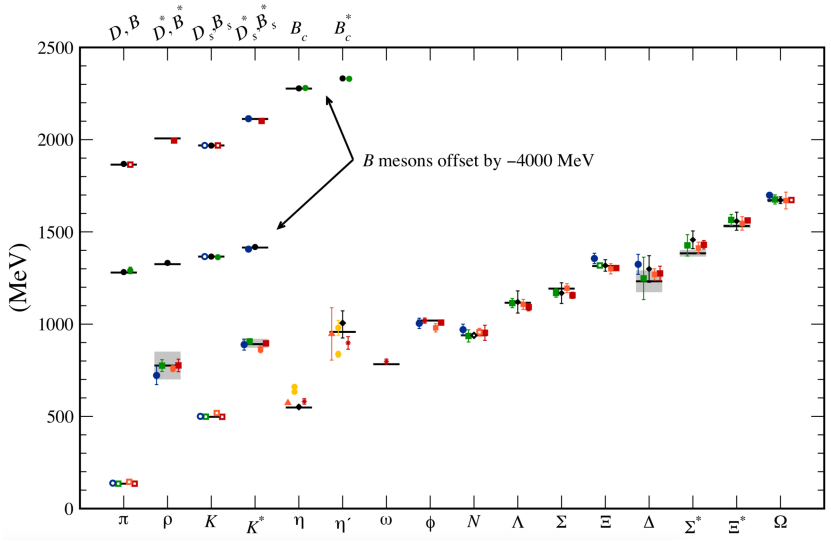

Figure 1.5: Lattice determinations of the hadronic spectrum. Black horizontal lines and grey boxes represent the experimental value of the masses and the corresponding widths, while the remaining symbols denote the lattice estimate provided by different collaborations. Different symbols correspond to different lattice discretizations for the Dirac operator. The plot includes results obtained with Wilson, Staggered, Twisted-mass Wilson and domain wall fermions. Open symbols for π, K, N, Ξ, Ω denotes the masses used to fix the lines of constant physics, see Sec. 3.4.

In this way, if a (anti-)quark transforms as a (anti-)fundamental representation of the flavour group $SU(3)$, any mesonic state $q\bar{q}$ can be expressed in terms of irreducible representation of the flavour group $SU(3)$ as

$$\mathbf{3} \otimes \bar{\mathbf{3}} = \mathbf{1} \oplus \mathbf{8}\,, \tag{1.33}$$

and in the same way a baryonic state qqq is represented as

$$\mathbf{3} \otimes \mathbf{3} \otimes \mathbf{3} = \mathbf{10}_S \oplus \mathbf{8}_M \oplus \mathbf{8}_M \oplus \mathbf{1}_A\,, \tag{1.34}$$

where the subscripts are related to the symmetric properties of the state under the exchange of two quarks (symmetric, mixed-symmetry and antisymmetric).

The prediction of the hadronic spectrum is one of the great success of QCD at the non-perturbative level. In fig. 1.5 we report a summary of the most recent

lattice determinations from different collaborations, from Ref. [22].

The specific procedure how the hadronic spectrum is extracted by lattice observables is discussed in details in Sec. 3.8 and subsections.

1.5.1 Chiral symmetry

A better understanding of the light hadronic mass spectrum is possible by looking at the global symmetries of the action. Let us consider the fermionic action defined in eq. 1.9 for a given number of flavours N_f in the massless quark limit. By decomposing each Dirac spinor in terms of the left and right-handed Weyl spinors

$$\psi_L = P_-\psi\,, \quad \bar{\psi}_L = \bar{\psi}P_+\,, \quad \psi_R = P_+\psi\,, \quad \bar{\psi}_R = \bar{\psi}P_-\,, \tag{1.35}$$

where the chiral projectors are defined as

$$P_\pm \equiv \frac{1 \pm \gamma_5}{2}\,, \tag{1.36}$$

at the classical level the fermionic sector of the massless QCD action can be written as

$$S_f[\psi_L, \psi_R, \bar{\psi}_L, \bar{\psi}_R, A] = \int \mathrm{d}^4x \left[\bar{\psi}_L\gamma_\mu D_\mu\psi_L + \bar{\psi}_R\gamma_\mu D_\mu\psi_R\right]. \tag{1.37}$$

The action is clearly invariant under independent global rotations of the left and right-handed spinor. This invariance is expressed in terms of two independent unitary groups $U(N_f)$, which define the so-called *chiral group*. The total symmetry group is therefore

$$U(N_f)_L \times U(N_f)_R = U(1)_L \times U(1)_A \times SU(N_f)_L \times SU(N_f)_A\,. \tag{1.38}$$

Given $V_L \in U(N_f)_L$ and $V_R \in U(N_f)_R$, the transformation relations for the spinor fields read

$$\psi_L \to \psi'_L(x) = V_L\psi_L(x)\,, \qquad \psi_R \to \psi'_R(x) = V_R\psi_R(x)\,, \tag{1.39}$$

and correspondingly for the adjoint fields. In the expression above the generic element of the $U(N_f)_{L/R}$ group can be written in terms of the generators of the algebra as

$$V_{L/R} = \exp\left[i\theta^a_{L/R}\tau^a\right] \approx 1 + i\theta^a_{L/R}\tau_a\,, \tag{1.40}$$

where $a = 0, \ldots, N_f^2 - 1$ and $\tau^a = \{\mathbb{1}, T^a\}$ with T_a being the $SU(N_f)$ generators. Notice that, since the chiral group acts on flavour indices only, the generators are diagonal in Dirac and colour spaces, i.e. $\tau_a = \tau_a \otimes \mathbb{1}_{\text{spin}} \otimes \mathbb{1}_{\text{colour}}$.

As a final remark it is worth noting that, for massive quarks, under the chiral group defined in eq. 1.38 the mass term in the action transforms as

$$\bar{\psi}_L M \psi_R + \bar{\psi}_R M^\dagger \psi_L = \bar{\psi}_L V_L^\dagger M V_R \psi_R + \bar{\psi}_R V_R^\dagger M^\dagger V_L \psi_L, \tag{1.41}$$

It is then formally invariant under the chiral group if the mass matrix is promoted to a *spurion field*, i.e. an external constant field which transforms under chiral transformations as

$$\begin{aligned} M' &= V_L M V_R^\dagger\,, \\ M'^\dagger &= V_R M' V_L^\dagger\,. \end{aligned} \tag{1.42}$$

Notice that such invariance is only formal, since the content of the mass matrix has now changed.

1.5.2 Ward-Takahashi identities

At quantum level the realization of chiral symmetry is quite different with respect to the classical theory. In general, the presence of some symmetry in the action does not guarantee, by any means, the invariance to survive in the corresponding QFT. If a classical theory is invariant under some transformation and the quantized theory is not, we talk about an *anomaly*. For instance, as we have already seen, even if QCD with massless fermions is scale invariant at the classical level, the process of quantization breaks down this invariance, by introducing the Λ-parameter. The breaking of scale invariance can be traced back to the fact that the QCD energy-

momentum tensor is traceless at classical level, but it is not in the quantized theory. This kind of anomaly is called *trace anomaly*.

The standard way to study the presence of any symmetry at quantum level is by means of Ward-Takahashi identities (WTIs), namely identities between correlation functions which provide the quantum extension to the current conservation laws arising from Noether's theorem. The core concept under WTIs is that, under infinitesimal transformations of the fields, if the symmetry is not *anomalous*, it holds

$$\langle \delta O \rangle = \langle O \delta S \rangle \,, \tag{1.43}$$

where δO is the variation of the operator under the transformation and δS is the variation of the action.

It is convenient to rewrite the chiral symmetry group in terms of vector and axial subgroups. Consider the transformations of the left and right-handed spinor under the infinitesimal chiral transformations defined in eq. 1.39 and 1.40 and recall that $\psi = \psi_L + \psi_R$, then

$$\psi \;\to\; \psi' = \left[1 + \frac{\theta_L^a + \theta_R^a}{2}\,\tau^a \;+\; i\,\frac{\theta_L^a - \theta_R^a}{2}\,\gamma_5\,\tau^a\right]\psi\,. \tag{1.44}$$

Consequently we define the infinitesimal parameters for vector and axial transformations as

$$\begin{cases} \epsilon_V^a \;=\; \frac{1}{2}\left[\theta_L^a + \theta_R^a\right] \\ \epsilon_A^a \;=\; \frac{1}{2}\left[\theta_L^a - \theta_R^a\right] \end{cases} \quad . \tag{1.45}$$

In order to extract WTIs one usually promotes the global transformations to *local* ones, otherwise, if no symmetry-breaking term appears in the action, $\delta S = 0$.

Vector WTIs

Consider for the moment only local vector transformations, i.e.

$$\begin{aligned} \delta\psi(x) &= i\epsilon_V^a(x)\tau^a\psi(x) \\ \delta\bar{\psi}(x) &= -i\bar{\psi}(x)\epsilon_V^a(x)\tau^a\,. \end{aligned} \tag{1.46}$$

The most general WTIs are obtained by including the symmetry-breaking term in the action, i.e. $M \neq 0$. Assuming the chiral transformation to be localized in such a way that $\epsilon_V^a(x) = \epsilon_V^a\delta(x-z)$, then by using eq. 1.43 we obtain

$$-i\epsilon_V^a\partial_\mu\langle V_\mu^a(x)O(y)\rangle = -i\epsilon_V^a\langle\bar{\psi}(x)\,[M,\tau^a]\,\psi(x)O(y)\rangle + \langle\delta O(y)\rangle\,, \tag{1.47}$$

where the singlet ($a = 0$) and non-singlet ($a \neq 0$) *vector currents* are defined as

$$V_\mu^a(x) = \bar{\psi}(x)\gamma_\mu\tau^a\psi(x)\,. \tag{1.48}$$

So far we have never specified neither the field content nor the support of the composite operator $O(y)$, however by doing so a couple of interesting WTIs can be derived.

On one hand, one can choose $O(y)$ such that it is localized at $y \neq x$ and that it holds $\langle\delta O(y)\rangle = 0$ under vector transformations in eq. 1.46. In such case the WTI in eq. 1.48 simplifies to

$$\partial_\mu\langle V_\mu^a(x)O(y)\rangle = \langle\bar{\psi}(x)\,[M,\tau^a]\,\psi(x)O(y)\rangle\,. \tag{1.49}$$

A couple of comments are in order:

- By restricting ourselves to the singlet vector transformations, i.e. $\tau^0 \sim \mathbb{1}$, independently of the structure of the mass matrix M in flavour space, the right-hand side of eq. 1.49 vanishes leading to the well-known *baryon number* conservation law

$$\partial_0\langle\bar{V}_0^0(x_0)O(y)\rangle = 0\,, \tag{1.50}$$

where the baryon number is defined as

$$\bar{V}_0^0 = \int \mathrm{d}^3x\, V_0^0(x)\,. \tag{1.51}$$

Thus the baryon number is a *conserved charge* in QCD independently of the number of flavour and of the mass of the quarks.

- If we restrinct to the non-singlet vector transformations, i.e. $\tau^a = T^a$, the right-hand side of eq. 1.49 vanishes only if $M \sim m\mathbb{1}$, i.e. if the N_f quarks are degenerate, which implies the conservation of $\bar{V}_0^a$, defined analogously to the baryon number. Notice that this symmetry is the N_f extension of the *isospin* symmetry for $N_f = 2$. In physical QCD, since quarks are not degenerate, it is just an approximate symmetry, in which the breaking term is proportional to the difference between the quark masses. For this reason, isospin is a good approximation especially for $N_f = 2$ and, to a smaller extent, for $N_f = 3$, while it is badly broken for $N_f = 4$ due to heavy mass of the charm quark.

On the other hand a particular case is recovered by choosing as composite operator a non-singlet vector current $O(y,z) = V_\nu^b(y)\tilde{O}(z)$ for $b \neq 0$. Assume the external operator $\tilde{O}(z)$ to be invariant under non-singlet vector transformations and recall that, by taking into account a local transformation, it holds for the vector current

$$\delta V_\nu^b(y) = \epsilon_V^a \delta(x-y) f^{abc} V_\nu^c(y)\,, \tag{1.52}$$

where f^{abc} are the structure constants of the $SU(N_f)$ group which satisfy the relations in App A.1. By assuming isospin symmetry, i.e. $M \sim m\mathbb{1}$, The corresponding WTI we obtain is

$$\partial_\mu \langle V_\mu^a(x) V_\nu(y)^b \tilde{O}(z)\rangle = i\delta(x-y) f^{abc} \langle V_\nu^c(y)\tilde{O}(z)\rangle\,, \tag{1.53}$$

which reproduces in the $N_f = 2$ case the expected euclidean current algebra of the $SU(2)$ vector group. As a final remark, notice that the introduction of the operator $\tilde{O}(z)$ is crucial, otherwise the WTI obtained in eq. 1.53 would vanish, being $\langle V_\nu^b(y)\rangle = 0$ due to Lorentz invariance of the vacuum.

Non-singlet axial WTIs

Consider now axial transformations, i.e.

$$\begin{aligned}\delta\psi(x) &= i\epsilon_A^a(x)\tau^a\gamma_5\psi(x)\\ \delta\bar{\psi}(x) &= -i\bar{\psi}(x)\gamma_5\epsilon_A^a(x)\tau^a\,.\end{aligned} \tag{1.54}$$

Since singlet axial transformations ($a = 0$) lead to chiral anomaly, it is useful to treat the singlet and non-singlet cases separately. For this reason we restrict ourselves to the non-singlet sector of the axial transformations in eq. 1.54 and at the end of this section we just give the formal definition of the anomalous WTI, while we postpone the detailed discussion on the singlet case to Chapter 3. By following the very same procedure as for the case of vector transformations and employing eq. 1.43 we obtain for non-singlet axial transformations

$$-i\epsilon_A^a\partial_\mu\left\langle A_\mu^a(x)O(y)\right\rangle = -i\epsilon_A^a\left\langle\bar{\psi}(x)\gamma_5\left\{T^a,M\right\}\psi(x)O(y)\right\rangle + \left\langle\delta O(y)\right\rangle\,, \tag{1.55}$$

where the non-singlet ($a \neq 0$) *axial current* is defined as

$$A_\mu^a(x) = \bar{\psi}(x)\gamma_\mu\gamma_5 T^a\psi(x)\,. \tag{1.56}$$

Notice that a crucial difference arises in the case of axial transformations with respect to the vector case. In eq. 1.55 an anti-commutator appears in the symmetry-breaking term on the right-hand side, which implies that this symmetry is not explicitly broken only if $M = 0$ for each flavours. By considering some specific composite operator we can recover some particularly interesting WTIs:

- As we have done for the vector sector of the chiral transformation we may expect to recover the current algebra for the axial transformations by simply taking into account the composite operator $O(y) = A_\nu^b(y)$, which implies

$$\delta A_\nu^b(y) = \epsilon_A^a\delta(x-y)f^{abc}V_\nu^c(y)\,, \tag{1.57}$$

  Notice that, in contrast with the non-singlet vector case, the variation of a non-singlet axial current leads to a vector current. As a consequence, for

massless quarks, the corresponding WTI reads

$$\partial_\mu \langle A^a_\mu(x) A^b_\nu(y) \tilde{O}(z) \rangle = i f^{abc} \delta(x-y) \langle V_\nu(y) \tilde{O}(z) \rangle \,, \tag{1.58}$$

where for the appearance of the interpolating operator $\tilde{O}(z)$ a similar discussion for what has been done in the vector case holds. Again, eq. 1.58 reproduces the correct euclidean current algebra for the axial generators. Notice that, as a direct consequence of eq. 1.58, the non-singlet axial transformations do not form a group.

- Next we consider as composite operator a pseudoscalar density, defined as

$$O(y) = P^b(y) = \bar{\psi}(y) \gamma_5 T^a \psi(y) \,, \tag{1.59}$$

which leads, by taking into account local transformations, to the variation

$$\delta P^b(y) = i \epsilon^a_A \delta(x-y) \bar{\psi}(y) \left\{ T^a, T^b \right\} \psi(y) \tag{1.60}$$

which provides, if inserted into eq. 1.55, to the so-called *partial conserved axial current (PCAC) relation*

$$\begin{aligned} \partial_\mu \langle A^a_\mu(x) P^b(y) \rangle = & \langle \bar{\psi}(x) \gamma_5 \{ T^a, M \} \psi(x) P^b(y) \rangle \\ & - \delta(x-y) \langle \bar{\psi}(y) \left\{ T^a, T^b \right\} \psi(y) \rangle \,. \end{aligned} \tag{1.61}$$

As we will see in Sec. 1.5.3, this relation has deep implication in the phenomenon of spontaneous breaking of chiral symmetry and will provide a clear explanation of the mass spectrum of flavour non-singlet pseudoscalar mesons. In particular, assuming a diagonal mass matrix, i.e. $M \sim m\mathbb{1}$ and using the anti-commutation relation between two $SU(N_f)$ algebra generators, the PCAC reads

$$\partial_\mu \langle A^a_\mu(x) P^b(y) \rangle = 2m \langle P^a(x) P^b(y) \rangle - \frac{\delta^{ab}}{N_f} \delta(x-y) \langle S^0(y) \rangle \,, \tag{1.62}$$

where we exploited the fact that the additional term $d_{abc} \langle S^c(y) \rangle$ arising from the anti-commutator of two generators is zero, since the non-singlet vector

symmetry remains unbroken. In eq. 1.62 the *singlet scalar density* is defined as

$$S^0(y) = \bar{\psi}(y)\psi(y)\,, \tag{1.63}$$

and as we will see in Sec. 1.5.3 its vacuum expectation value provides the order parameter of spontaneous chiral symmetry breaking.

Let us briefly discuss the $U(1)_A$ anomalous transformations. In this case the relation in eq. 1.43 has to be modified to take into account the anomalous contribution coming from the non-invariance of the path integral integration measure. Therefore eq. 1.43 becomes

$$\langle \delta S O \rangle + \langle \ln[\mathcal{J}]\, O \rangle = \langle \delta O \rangle\,, \tag{1.64}$$

where $\mathcal{J}$ is the determinant of the Jacobian of the transformation. In this way, the anomalous WTIs read[4]

$$-i\epsilon_A^0 \partial_\mu \langle A_\mu^0(x) O(y) \rangle = -2i\epsilon_A^0 N_f \langle q(x) O(y) \rangle + \langle \delta O(y) \rangle\,, \tag{1.65}$$

where $q(x)$ is non-zero topological charge density which is defined in the classical continuum limit as

$$q(x) = \frac{1}{32\pi^2}\epsilon_{\mu\nu\rho\sigma}\,\mathrm{Tr}\left[F_{\mu\nu}(x)F_{\rho\sigma}(x)\right]\,. \tag{1.66}$$

1.5.3 Spontaneous chiral symmetry breaking

At quantum level, a symmetry is said to be *spontaneously broken* if the action is invariant under this symmetry but the vacuum of the theory is not. Let us consider a general infinitesimal transformation $U \sim 1 + i\alpha_j \mathcal{Q}_j$, where α_j is an infinitesimal parameter, $\mathcal{Q}_j$ is a generator of the algebra of the symmetry group and j is a generic quantum number related to that specific symmetry. The vacuum of the

[4]Here we just give a formal definition of the anomalous WTIs. Those can be properly derived in the context lattice regularization by using Ginsparg-Wilson fermions and *Lüscher symmetry*, see Chapter 3 for the detailed discussion.

theory is not invariant under this transformation if

$$\mathcal{Q}_j \left|0\right\rangle \neq 0 \,. \tag{1.67}$$

First of all, recall that any WTI is valid only after the theory has been properly renormalized, i.e the PCAC relation in eq. 1.62 holds only if expressed in terms of renormalized composite operators as

$$\partial_\mu \left\langle A_\mu^{R,a}(x) P^{R,b}(y)\right\rangle = 2m^R \left\langle P^{R,a}(x) P^{R,b}(y)\right\rangle - \frac{\delta^{ab}}{N_f}\delta(x-y)\left\langle S^{R,0}(y)\right\rangle \,, \tag{1.68}$$

where the superscript "R" identifies renormalized operators. On one hand, the singlet scalar density transforms as a $(N_f, \bar{N}_f) + (\bar{N}_f, N_f)$ representation under chiral transformations, i.e. exactly as a mass term. For this reason the scalar density renomalizes multiplicatively only in the massless quark limit, while for massive fermions the renormalized scalar density mixes with the spurionic mass fields. On the other hand, all the other composite operators appearing in eq. 1.68 only get a multiplicative renormalization [5]. Therefore, in the chiral limit the renormalized WTI is totally equivalent to the one written in terms of bare composite operators[6]. By setting $y = 0$, in the chiral limit it reads

$$\left\langle \partial_\mu A_\mu^a(x) P^b(0)\right\rangle = -\frac{\delta(x)\delta^{ab}}{N_f}\left\langle S^0\right\rangle \,. \tag{1.69}$$

Notice that the singlet scalar density is invariant under the flavour (vector) subgroup of the chiral group, while it is not invariant under non-singlet axial transformation and in the chiral limit its vacuum expectation value plays the rôle of order parameter of chiral symmetry. In particular, even if the action is invariant under non-singlet axial transformations, if $\left\langle S^0\right\rangle \neq 0$ the axial current is not conserved and the symmetry is spontaneously broken. On the other hand if $\left\langle S^0\right\rangle = 0$ chiral symmetry is restored. In the language of statistical mechanics the symmetric phase

[5] The axial current does not renormalize at all ($Z_A = 1$) and the renormalization constant related to the pseudoscalar density is exactly the inverse of the renormalization constant of the mass term, i.e. $Z_P = Z_m^{-1}$. In this way in the chiral limit we obtain for the singlet scalar density $Z_S^0 = Z_P$.

[6] For this reason, in the following we omit the superscript "R".

is called *disordered phase* while, in the case of spontaneous breaking we talk about *ordered phase*.

By carefully studying the PCAC relation in eq. 1.69, if $x \neq 0$ no contact term arises on the right-hand side and by exploiting Lorentz invariance, the two-point correlation function on the left-hand side can be written as

$$\langle A^a_\mu(x) P^b(0) \rangle = \delta^{ab} k \frac{x_\mu}{x^4} , \tag{1.70}$$

where the constant k can be determined by simply integrating the WTI over a 4-sphere of radius R centered in $x = 0$, i.e

$$\int_{|x|=R} \mathrm{d}\sigma_\mu \, \langle A^a_\mu(x) P^b(0) \rangle = -\frac{\delta^{ab}}{N_f} \langle S^0 \rangle . \tag{1.71}$$

Since the integral is evaluated for $x \neq 0$, we can put eq. 1.70 into eq. 1.71, which fixes the value of k to

$$k = -\frac{1}{N_f} \frac{\langle S^0 \rangle}{2\pi^2} , \tag{1.72}$$

and finally the two-point correlation function reads

$$\langle A^a_\mu(x) P^b(0) \rangle = -\delta^{ab} \frac{x_\mu}{x^4} \frac{\langle S^0 \rangle}{2\pi^2 N_f} . \tag{1.73}$$

Notice that if chiral symmetry is spontaneously broken, i.e. $\langle S^0 \rangle \neq 0$, this two-point correlation function has a power-like suppression for large separations. If we project it to zero momentum, if the theory had a mass gap we would expect an exponential suppression dictated by the lowest energy state. By integrating the two-point function ($\mu = 0$) in space coordinates we get

$$\int \mathrm{d}^3x \, \langle A^a_0(x) P^b(0) \rangle \equiv \langle \bar{A}^a_0(x_0) P^b(0) \rangle = -\frac{\delta^{ab}}{2N_f} \langle S^0 \rangle , \tag{1.74}$$

which is constant in euclidean time, i.e. the integrated two-point correlation function does not show any exponential suppression and then no massive state is present.

As a final remark, notice that *Goldstone theorem* [53] relates the spontaneous breaking of any continuous symmetry to the underlying energy spectrum. It states that for every spontaneously broken continuous symmetry, the spectrum of the theory contains one massless scalar particle known as *Nambu-Goldstone boson* [54, 55]. The number of Nambu-Goldstone bosons is equal to the number of broken generators, namely symmetry generators which do not preserve the ground state, and the Nambu-Goldstone bosons quantum numbers are fixed by the quantum numbers of the broken generators.

In the case of chiral symmetry we have $N_f^2 - 1$ broken generators leading to $N_f^2 - 1$ massless Nambu-Goldstone bosons with $J^P = 0^-$ quantum numbers, i.e pseudoscalar mesons, which correspond to the pions in the case of $N_f = 2$ and to the octet in table 1.1 for $N_f = 3$.

1.5.4 Matrix elements and GMOR relation

In QCD with physical quark masses chiral symmetry is explicitly broken and neither pions nor kaons are massless. In this context no Nambu-Goldstone boson arises and we refer to the physical pseudoscalar mesons as *pseudo* Nambu-Goldstone bosons. Since the term responsible for the explicit breaking, namely the quark mass, is small, one could expect such breaking effects to be small too. If this is the case, we might hope to be able to relate some features of the spectrum in the massless limit to the physical spectrum with massive quarks.

By introducing a set of normalized pseudoscalar states $|\pi^a\rangle$ and by making explicit the action of the pseudoscalar density and of the axial current on the vacuum, the left-hand side of the PCAC relation in eq. 1.62 can be written in terms of

$$\langle \pi^b(p)| P^a(x) |0\rangle = -i\delta^{ab} G_\pi e^{E_\pi(p)x_0} e^{-i\mathbf{p}\cdot\mathbf{x}} \tag{1.75}$$

$$\langle 0| A^a_\mu(x) |\pi^b(p)\rangle = i\delta^{ab} p_\mu F_\pi e^{-E_\pi(p)x_0} e^{+i\mathbf{p}\cdot\mathbf{x}}\,, \tag{1.76}$$

where we used the fact that the pseudoscalar density creates a pseudoscalar state with energy $E_\pi = -ip_0$ and momentum $\mathbf{p}$ when acting on the vacuum in eq. 1.75. In the same way, the structure in eq. 1.76 is completely fixed by Lorentz invariance. By

combining these two expressions with the integrated two-point correlation function in eq. 1.74 we obtain

$$\langle \bar{A}_0^a(x_0) P^b(0) \rangle = \delta^{ab} \left(\frac{G_\pi F_\pi}{2} \right) e^{-E_\pi(0) x_0} \xrightarrow{x_0 \to \infty} \frac{\delta^{ab}}{2} F_\pi G_\pi \,, \tag{1.77}$$

since as we have seen in the previous section, the two-point correlation function projected to zero momentum has no dependence on the euclidean time. By combining this relation with eq. 1.74, we obtain for the matrix element in the massless limit

$$G_\pi = -\frac{\langle S^0 \rangle}{F_\pi N_f} \,. \tag{1.78}$$

If we now focus on the massive case, the integrated two-point function at $x_0 \neq 0$ reads

$$\partial_0 \langle \bar{A}_0^a(x_0) P^b(0) \rangle = 2m \langle \bar{P}^a(x_0) P^b(0) \rangle \,, \tag{1.79}$$

where $\bar{P}^a$ is the non-singlet pseudoscalar density integrated over space coordinates. By introducing a complete set of pseudoscalar states and making use of the relations in eq. 1.76 and 1.75 we obtain

$$\partial_0 \left\{ \delta^{ab} \frac{G_\pi^m F_\pi^m}{2} e^{-M_\pi x_0} \right\} = 2m \left\{ -\delta^{ab} \frac{(G_\pi^m)^2}{2M_\pi} e^{-M_\pi x_0} \right\} \,, \tag{1.80}$$

where $M_\pi = E_\pi(0)$ and the superscript "m" denotes we are in the massive case. This relation leads to

$$G_\pi^m = \frac{M_\pi^2}{2m} F_\pi^m \,. \tag{1.81}$$

Notice that the limit for $m \to 0$ of both F_π^m and G_π^m is perfectly defined being valid the relation in eq. 1.78. Thus we may take the massless limit of eq. 1.81 and combine it with the massless result in eq. 1.78 to obtain the so-called Gell-Mann-

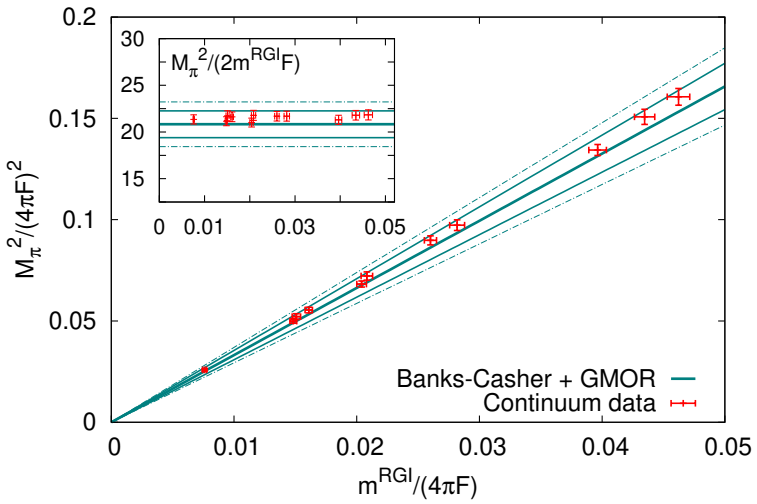

Figure 1.6: The pion mass squared as a function of the RGI quark mass normalized to $(4\pi F_\pi)^2$. The central line is the contribution coming from eq. 1.83 by directly measuring the expectation value of the singlet scalar density as in Ref. [56]. Upper and lower solid lines represent the statistical error, while the dotted lines represent the total error. From Ref. [57].

Oakes-Renner *(GMOR)* relation [58]

$$\lim_{m\to 0} \frac{\left(M_\pi F_\pi^m\right)^2}{2m} = \lim_{m\to 0} G_\pi^m F_\pi^m \overset{(1.78)}{=} -\frac{\langle S^0\rangle}{N_f}\,. \tag{1.82}$$

Finally, by expanding for small quark masses we obtain

$$M_\pi^2 = -2m\,\frac{\langle S^0\rangle}{N_f F_\pi^2} + O(m^2)\,, \tag{1.83}$$

where $F_\pi = \lim_{m\to 0} F_\pi^m$. Recalling that in the massless theory dimensional transmutation implies that the only dimensionful scale of the theory is $\Lambda_{\rm QCD}$, it is straightforward to see that, by dimensional analysis, it holds

$$M_\pi \sim \sqrt{m\Lambda_{\rm QCD}}\,. \tag{1.84}$$

The results in eq. 1.83 and 1.84 are remarkable since we were able to relate the massless theory which shows spontaneous chiral symmetry breaking to the ex-

plicitly broken massive theory and to trace back the origin of the pseudoscalar mesons masses to the order parameter of chiral symmetry breaking. Notice that pseudoscalar mesons masses have a strong dependence on the quark masses which implies we recover the spontaneous symmetry breaking pattern and the presence of $N_f^2 - 1$ massless Nambu-Goldstone bosons in the massless limit. In fig. 1.6 we show the non-perturbative determination of the pion mass, for $N_f = 2$, as a function of the renormalization group invariant quark mass together with the theoretical prediction provided by the GMOR relation, see eq. 1.83, based on the direct calculation of the scalar density by using the spectral density of the Dirac operator as in Ref. [56]. On the other hand, for all the other hadrons dimensional transmutation implies $M_H \sim \Lambda_{\rm QCD}$, which somehow explains the difference between the pseudoscalar mesonic masses and all the other masses of the light hadronic spectrum.

Chapter 2

QCD at finite temperature

In this chapter we discuss the behaviour of the theory of strong interaction at non-zero temperature. In this regime QCD plays a crucial rôle in understanding a large number of physical processes spanning from the cosmological evolution of the early universe to the interpretation of the experimental results of heavy ions collisions (RHIC).

The natural way to introduce the path integral formulation for a thermal field theory is given by a thermodynamic approach, called Mastubara formalism [59]. A thermal quantum field theory is described in terms of the grand canonical partition function, defined as

$$Z = \mathrm{Tr}\left[e^{-\beta(H-\mu_B Q)}\right] = \int DAD\bar{\psi}D\psi\, e^{-S_{QCD}}\,, \tag{2.1}$$

where we included, as most general situation, also the finite baryon number chemical potential μ_B corresponding to the conserved quark number $Q = \bar{\psi}\gamma_0\psi$. The crucial difference with respect to the zero-temperature case in eq. 1.11 lies in the integration limits over the temporal direction in the action. Being $\mathcal{L}_{QCD}$ the QCD lagrangian density, the action at finite temperature reads

$$S_{QCD}\left[A,\bar{\psi},\psi\right] = \int_0^\beta \mathrm{d}x_0 \int \mathrm{d}^3\mathbf{x}\,\mathcal{L}_{QCD}\,, \tag{2.2}$$

where β is the usual inverse of the temperature ($k_B = 1$)

$$\beta = \frac{1}{T}\,. \tag{2.3}$$

Notice that in the path integral definition of a thermal field theory the temperature amounts to a *boundary effect* only, i.e. it is an IR effect. For this reason the UV behaviour is left untouched and, as a consequence, the renormalization of the theory can be carried out at zero temperature (or vice versa) and has to be temperature independent.

Due to the compactification in the temporal extent, suitable boundary conditions have to be imposed on quark and gauge fields. Since those fields have to satisfy Fermi-Dirac and Bose-Einstein statistics respectively, it must follows

$$\begin{aligned} \psi(x_0+\beta,\mathbf{x}) &= -\psi(x_0,\mathbf{x}) \\ \bar{\psi}(x_0+\beta,\mathbf{x}) &= -\bar{\psi}(x_0,\mathbf{x}) && (2.4) \\ A_\mu(x_0+\beta,\mathbf{x}) &= A_\mu(x_0,\mathbf{x})\,. && (2.5) \end{aligned}$$

Such boundary conditions then extent to composite operators obtained by combining fermionic and gluonic fundamental fields. As a consequence, since the temporal extent is compactified and the energy levels get quantized in this direction, it is easy to see that the energy levels for fermionic and bosonic operators satisfy respectively

$$\begin{aligned} k_n &= \pi T\,(2n+1)\,, && (2.6) \\ k_n &= 2\pi T n\,, && (2.7) \end{aligned}$$

where $n \in \mathbb{Z}$. In analogy with statistical thermal field theory these energy levels are called *Matsubara frequencies*.

In the following sections we will briefly discuss the main features that QCD exhibits at high temperatures, i.e. the restoration of chiral symmetry and the so-called *deconfinement*. Then we will focus on one of the approaches used for a quantitative study of the high temperature regime of QCD, the dimensional reduced effective field theory. As we will see, at asymptotically high temperatures

QCD effectively behaves as a three-dimensional effective gauge theory, whose dynamics is completely non-perturbative, with gauge fields coupled to static heavy quarks and to a scalar Higgs-like field.

2.1 Colour deconfinement and chiral symmetry restoration

As we have seen in Sec. 1.5.3, at zero temperature the non-zero expectation value of the singlet scalar density leads to the spontaneous breaking of chiral symmetry and to the appearance of massive pseudo Nambu-Goldstone bosons. On the contrary, there is much numerical evidence that at non zero temperature, the vacuum expectation value of the scalar density rapidly drops to zero due to thermal effects, giving rise to an effective restoration of chiral symmetry [60].

Similarly, at zero temperature the $U(1)_A$ symmetry is broken by a non-trivial topological structure of the vacuum which leads to the chiral anomaly. At finite temperature, both in the pure Yang-Mills theory [61] and in full QCD [62, 63, 64, 65] numerical and analytical results show that the topological charge distribution is extremely peaked at $Q = 0$. In particular, in QCD with three degenerate flavours of mass m the semiclassical analysis provided by the dilute instanton gas approximation predicts the topological susceptibility to be proportional to $T^{-b}m^3$ with $b \sim 8$. As a consequence, only the zero topological sector is relevant if the temperature is large enough and an effective restoration of the $U(1)_A$ symmetry is expected.

Quark deconfinement is the other distinctive property of QCD at high temperature. As seen in Sec. 1.4.3 at zero temperature the non-abelian nature of QCD makes quarks and gluons strongly interacting, leading to colour confinement. At non-zero temperature there is both numerical and experimental evidence that QCD undergoes a transition from a confined phase, in which the relevant degrees of freedom are colour-singlet particles to a deconfined phase. Even if there is currently no analytical proof of such behaviour, quark confinement can be partially understood by scrutinizing the functional dependence of the static potential between two heavy quarks $q\bar{q}$. At zero temperature the static potential grows linearly with the

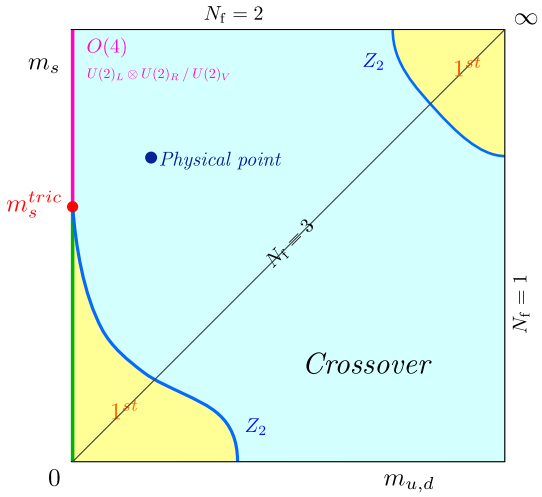

Figure 2.1: Columbia plot showing different possible scenarios for the transition from a confined phase with colour-singlet degrees of freedom to a deconfined phase. The blue point represents the smooth cross-over for physical light and strange quark masses. From Ref. [66].

quark-antiquark separation until the string breaking and the $q\bar{q}$ pair production. Thus the binding energy can be seen, in a pictorial way, to be stored in a flux tube connecting the quark-antiquark pair, whose energy increases with the separation. At high temperature the situation is quite different. Indeed the functional dependence of the static potential is modified by colour screening and in this pictorial representation, flux tubes begin to fluctuate producing complex structures, or networks, which results in a competition between binding energy and entropy. At sufficiently high temperatures entropy becomes dominant because of the high number of possible configurations of flux tubes. These complex networks lead to the loss of information about quark and antiquark bound state, which is interpreted as the deconfinement transition.

Large efforts have been devoted to the study of this transition in the last few years, in particular on the lattice (for a recent review see Ref. [67]). The behaviour of such transition has been studied for different number of flavours N_f and different values of the quark masses. Most of the studies were performed in the pure $SU(3)$ gauge theory with infinitely heavy quarks (quenched approximation), where the transition from a confined to a deconfined phase can be directly traced back to the

spontaneous breaking of the global center symmetry $Z(3)$, for which the vacuum expectation value of the Polyakov loop provides the order parameter. For physical quark masses it was argued that there is no non-analytical phase transition [68, 69], but a smooth crossover between the two phases [70, 71]. Recent studies pointed out the pseudo-critical temperature to be $T = 156$ MeV [72]. Finally, away from the physical point the situation is more involved and the nature of the transition is still debated, in particular for small quark masses. Currently our best knowledge about this phase transition is encoded in the so-called Columbia plot, see fig. 2.1. Notice that, we restricted the discussion to the zero baryon number chemical potential case. If also the $\mu_B \neq 0$ case is included possible extensions to the Columbia plot have been proposed and the appearance of new exotic states of matter in the QCD phase diagram is expected [73].

The existence of such new state of matter, called *quark-gluon plasma* (QGP), in which colour charges are screened, was first proposed in the seventies [74, 75] and widely studied in the past twenty years through relativistic heavy ions collisions experiments [76, 77, 78]. To date it is believed to be a strongly-coupled fluid both from experimental [9, 10], and theoretical evidence [11].

2.2 Effective theory description

In this section we review the main ingredients to build the effective field theory (EFT) approach to thermal QCD. As usual for an effective field theory, it is based on the appearance of a scale hierarchy, which, in this case, implies also a dimensional reduction.

On one hand, dimensional reduction is strictly related to the compactification of the temporal extent in which the thermal QFT is defined and can be related to the fact that field fluctuations are suppressed for separations smaller than the inverse temperature. On the other hand, the appearance of a scale hierarchy is due to the fact that the coupling constant at asymptotically high temperature vanishes thanks to asymptotic freedom.

Once the scale hierarchy is properly identified, in order to construct the effective field theory for thermal QCD, we follow the standard prescription which involves the following steps:

- Identify the soft and heavy degrees of freedom
- Identify the action symmetries
- Write down the most general lagrangian for the soft degrees of freedom which is invariant under the symmetries of the system and contains higher dimensional operators
- Fix the value of the effective lagrangian parameters, i.e. the *low energy constants* by matching with the original theory.

Since EFT are typically low energy description of the full theory, the last step is somehow crucial to guarantee that the IR behaviour of the theory is correctly reproduced.

2.2.1 Dimensional reduction

Due to the compact temporal extent at finite temperature the Fourier transform for gauge and quark fields reads

$$\begin{aligned} A_\mu^a(x_0,\mathbf{x}) &= T\sum_n \int \frac{\mathrm{d}^3\mathbf{p}}{(2\pi)^2} e^{i(p_n x_0+\mathbf{p}\cdot\mathbf{x})}\,\tilde{A}_\mu^a(p_n,\mathbf{p})\,, \\ \psi(x_0,\mathbf{x}) &= T\sum_n \int \frac{\mathrm{d}^3\mathbf{p}}{(2\pi)^2} e^{i(p_n x_0+\mathbf{p}\cdot\mathbf{x})}\,\tilde{\psi}_\mu(p_n,\mathbf{p})\,, \end{aligned} \tag{2.8}$$

where the sum is meant to be over bosonic and fermionic Matsubara frequencies respectively. By employing this definition for the Fourier transform and by setting the gauge fixing parameter $\lambda_0 = 1$ in eq. 1.12, the kinetic term of the gluonic action and the gauge fixing term can be written as

$$S_{\text{kin}} + S_{GF} = \frac{T}{2g_0^2}\sum_n \int \frac{\mathrm{d}^3\mathbf{p}}{(2\pi)^2}\tilde{A}_\mu^a(p_n,\mathbf{p})\left[p_n^2+\mathbf{p}^2\right]\tilde{A}_\mu^a(p_n,\mathbf{p})\,, \tag{2.9}$$

where p_n are the bosonic Matsubara frequencies. Notice that, in such a way, the action is completely factorized into each Matsubara mode contribution. Being the probability distribution for the gauge field proportional to the Boltzmann factor $e^{-S_g-S_{GF}}$, we notice that in the high temperature limit, if we consider large fluctuations, i.e. small spatial momentum $|\mathbf{p}|$, gauge field configurations related to

non-zero Matsubara frequencies are suppressed by the temperature and the only relevant contribution in eq. 2.9 comes from the zero Matsubara mode, $n = 0$.

Equivalently, eq. 2.9 can be seen as a sum of three-dimensional actions for vector fields with mass p_n. In the large temperature limit, non-zero Matsubara modes are infinitely heavy and decouple from the theory so that the dynamics of the gauge fields is completely dominated by the zero modes, which are, however, possibly affected by infrared divergences.

A similar discussion holds for fermion fields with the only, relevant, difference that fermion fields have no zero Matsbura mode, i.e. $p_0 \neq 0$. By performing a Fourier transform in the temporal extent, the action for a free massless fermion can be written in mixed coordinate-momentum space as

$$S_f = T \sum_n \int \mathrm{d}^3\mathbf{x}\, \tilde{\bar{\psi}}(p_n, \mathbf{x}) \left[i p_n \gamma_0 + \partial_k \gamma_k \right] \tilde{\psi}(p_n, \mathbf{x}) \,, \tag{2.10}$$

with $k = 1, 2, 3$ and now $p_n = \pi T(2n + 1)$ are the fermionc Matsubara frequencies. Notice that, since no zero Matsubara mode exists for fermions, at high temperatures quarks can be treated as heavy, static fields with mass $\sim \pi T$.

In the language of effective field theories we can identify the zero modes with the *soft* degrees of freedom which are, however, infrared sensitive. While, non-zero modes are the *heavy* degrees of freedom which must be integrated out, when taking into account physical processes that take place at energies much lower than the temperature, or equivalently which involve distances much larger than the compact temporal extent.

Given the analysis we performed in the free case, since for sufficiently large temperatures we do not expect any difference, in the following we will assume that the relevant degrees of freedom are given by the zero Matsubara modes for the gauge fields, while the fermionic fields will be treated as heavy fields. Based on such field content, in the following sections, the high temperature effective field theory is derived.

2.2.2 Electrostatic QCD

With the definitions given in Sec. 2.2.1 we are now able to build the effective theory which describes thermal QCD at distances much larger than $\beta = 1/T$. As mentioned, the relevant soft degrees of freedom are given by the zero modes appearing in the gauge action. The corresponding effective action has to preserve rotational and translational invariance in the spatial directions, along with gauge invariance. Notice that, since we are integrating out field fluctuations at much smaller distance than the temporal extent, the soft degrees of freedom are constant in the temporal direction. This implies that the effective action has to be invariant under a three-dimensional gauge transformation. Equivalently the $SU(3)$ element appearing in the gauge transformation in eq. 1.2 has to be x_0-independent. This leads to the gauge field transformations

$$\begin{aligned} A'_j(\mathbf{x}) &\longrightarrow \Omega(\mathbf{x}) A_j(\mathbf{x}) \Omega^\dagger(\mathbf{x}) + \frac{i}{g} \Omega(\mathbf{x}) \partial_j \Omega^\dagger(\mathbf{x}) \,, \\ A'_0(\mathbf{x}) &\longrightarrow \Omega(\mathbf{x}) A_0(\mathbf{x}) \Omega^\dagger(\mathbf{x}) \,, \end{aligned} \tag{2.11}$$

which implies that at high temperature the field content of the effective theory is given by a three-dimensional gauge field A_i and by a scalar field A_0 transforming under the adjoint representation of the $SU(3)$ gauge group. This has implications on the possible higher order operators to be included in the effective lagrangian, since three-dimensional gauge invariance does not forbid any mass term for the scalar field A_0, which is, on the contrary, not allowed at zero temperature by four-dimensional gauge invariance.

By combining all these ingredients we can write the effective action for what is usually called Electrostatic QCD (EQCD), which reads

$$\begin{aligned} S_{\mathrm{EQCD}} = \int \mathrm{d}^3\mathbf{x} \Bigg\{ & \frac{1}{2} \mathrm{Tr}\left[F_{ij} F_{ij}\right] + \mathrm{Tr}\left[\left(D_j A_0\right)\left(D_j A_0\right)\right] + m_E^2 \, \mathrm{Tr}\left[A_0^2\right] \\ & + \lambda_{\mathrm{E}}^{(1)} \left(\mathrm{Tr}\left[A_0^2\right]\right)^2 + \lambda_{\mathrm{E}}^{(2)} \, \mathrm{Tr}\left[A_0^4\right] \Bigg\} + \ldots \end{aligned} \tag{2.12}$$

where the dots stand for higher dimensional operators. Those are operators with mass dimension $d \geq 4$ which are then suppressed as $1/T^{d-3}$ [79, 80]. Notice that

in eq. 2.12 $i = 1,2,3$ and $F_{ij} = i/g_{\rm E}\,[D_i, D_j]$ with the covariant derivative defined as $D_i = \partial_i - ig_{\rm E}A_i$[1]. With this normalization the gluonic fields appearing in the EQCD action are three-dimensional fields with mass dimension $[A_i] = [A_0] = 1/2$. The parameters appearing in eq. 2.12 can be perturbatively matched by computing Green's function in the effective theory and in the corresponding full theory. For instance, $m_{\rm E}$ and $g_{\rm E}$ are obtained at several orders in Ref. [81, 82, 83, 84]. At leading order their expression reads

$$\begin{aligned} m_{\rm E}^2 &= g^2T^2\left(\frac{N_c}{3} + \frac{N_f}{6}\right) + O(g^4T^2)\,, \\ g_{\rm E}^2 &= g^2T + O(g^4T)\,. \end{aligned} \tag{2.13}$$

In this context the scalar field mass $m_{\rm E}$ is often called *Debye mass* [85] and is responsible of the screening of the chromo-electric field at high temperature. Notice that the appearance of the non-zero thermal mass for the scalar field A_0 makes it less sensitive to potential non-perturbative IR effects.

Given the scales appearing in eq. 2.13 it is natural to define, up to some numerical factor, the following scale hierarchy

$$\frac{g_{\rm E}^2}{\pi} \ll m_{\rm E} \ll \pi T\,. \tag{2.14}$$

2.2.3 Magnetostatic QCD

Once Matsubara non-zero modes have been integrated out, the degrees of freedom of the resulting effective theory (EQCD) are given by a three dimensional $SU(3)$ gauge field coupled to a massive scalar field A_0. At asymptotically high temperature, due to the scale hierarchy in eq. 2.14, the Debye mass can be interpreted as a high energy scale and the corresponding field A_0 is a heavy degree of freedom. Following the same steps as before, if we consider physical processes at energy scales which are much lower than $m_{\rm E}$, then we can integrate out the scalar field to obtain a new effective theory, whose degrees of freedom are just the three-dimensional

[1] To be consistent with previous works in the literature, in the context of the dimensional reduced effective theory we use the perturbative definition for the covariant derivatives and for the field strenght tensor.

$SU(3)$ gauge fields. Such effective theory is named Magnetostatic QCD (MQCD) and its action reads

$$S_{\mathrm{MQCD}} = \int \mathrm{d}^3\mathbf{x} \left\{ \frac{1}{2} \mathrm{Tr}\left[F_{ij}F_{ij}\right] \right\} + \dots . \tag{2.15}$$

Notice that three-dimensional gauge invariance does not allow, at this order, any mass term for the gauge field, which will be at least $O(g^2T)$. As a consequence, we expect physics related to the chromo-magnetic field to be more subject to IR effects. The most important consequence arising from eq. 2.15 is that the effective coupling $g_{\mathrm{E}}^2 \approx g^2T$, appearing in the definition of F_{ij}, is the only energy scale of the theory. This implies that any dimensionful quantity, e.g. mass gap, potentials, string tension, at asymptotically high temperature has to be proportional to g_{E}^2 [79].

2.2.4 Infrared problem

Now that the hierarchy of the energy scales has been properly identified, we can better understand how non-perturbative effects can potentially spoil perturbative expansions at high temperature. In principle, since the coupling constant is small if the renormalization scale μ is of the same order of the temperature, one could expect perturbation theory to be a viable choice for the study of QCD dynamics at high temperature if the theory is not affected by infrared divergences.

In order to examine if a perturbative expansion is possible or not, it is convenient to define a dimensionless expansion parameter. Being the coupling of the three-dimensional Yang-Mills theory $g_{\mathrm{E}}^2 \sim g^2T$, it is natural to assume as a dimensionaless expansion parameter

$$\epsilon \approx \frac{g^2T}{M}, \tag{2.16}$$

where M represents the thermal mass of each field, or more generally, the relevant scale of each effective field theory. This leads to the following considerations [79]:

- For fermions the lowest Matsubara sector brings $M = \pi T$. As a consequence, $\epsilon \sim g^2/\pi$ and a perturbative approach is possible if $g^2 \ll \pi$.

- Zero Matsubara modes related to the scalar field A_0 develop a thermal mass $M = m_{\mathrm{E}} \sim gT$, which leads to $\epsilon \sim g$. As a consequence perturbation theory is still viable for $g \ll 1$.

- From eq. 2.15 at this order gauge invariance does not allow a mass term for the zero modes of the chromo-magnetic field. For this reason any potential mass term has to be, at least, $O(g^2T)$ which leads to $\epsilon \gtrsim 1$. As a consequence chromo-magnetic dynamics can only be treated non-perturbatively.

The non-perturbative behaviour of the chromo-magnetic dynamics is known as infrared or *Linde problem* [12] and is responsible for the limited applicability of perturbation theory up to a finite order only. An example of such effects can be found in the perturbative determination of the QCD Equation of State (EoS) which is limited at $O(g^6 \ln(1/g))$ [86, 87].

As a final remark, notice that the perturbative treatment of the theory in the framework of the dimensional reduced effective theory is then limited both by the chromo-magnetic infrared problem and by the constraint dictated by the scale hierarchy in eq. 2.14.

2.2.5 Heavy quark action

Let us now focus on the fermionc sector of the QCD action. As we have seen in Sec. 2.2.1 quarks behaves as heavy fields with mass $\sim \pi T$. By employing the non-relativistic representation for the Dirac gamma matrices defined in eq. A.17 the Dirac operator can be written as

$$\gamma_0 \not{D} = \begin{pmatrix} D_0 + iD_3 & -\epsilon_{jk} D_j \sigma_k \\ \epsilon_{jk} D_j \sigma_k & D_0 - iD_3 \end{pmatrix}, \tag{2.17}$$

where ϵ_{kj}, for $k = 1, 2$, is the totally anti-symmetric Levi-Civita symbol in two dimensions, i.e $\epsilon_{12} = -\epsilon_{21}$. This representation is particularly useful because it allows to factorize the propagation in the 3-direction and, as we will see in the following, it is suitable to study screening processes along the 3-direction. In this representation, it is convenient to write the fermionic field in terms of two components

spinors as

$$\psi_a(p_n, \mathbf{x}) = \frac{1}{\sqrt{T}} \begin{pmatrix} \chi_{p_n}(\mathbf{x}) \\ \phi_{p_n}(\mathbf{x}) \end{pmatrix}. \tag{2.18}$$

Notice that with the above normalization χ and ϕ are meant to be three-dimensional, two-components spinor fields with mass dimension $[\phi] = [\chi] = 1$. By employing eq. 2.17 and the definition in eq. 2.18 the fermionic action in the mixed coordinate-momentum representation (see eq. 2.10) for the lowest Matsubara mode ($n = 0$) can be written as

$$\begin{aligned} S_f = \int \mathrm{d}^3\mathbf{x} \, \Big\{ & i\chi^\dagger \left[p_0 - gA_0 + D_3 \right] \chi \; + i\phi^\dagger \left[p_0 - gA_0 - D_3 \right] \phi \\ & + \phi^\dagger \epsilon_{kl} D_k \sigma_l \chi - \chi^\dagger \epsilon_{kl} D_k \sigma_l \phi \Big\} . \end{aligned} \tag{2.19}$$

From this starting point, the first step to build an effective description for static quarks is to identify the heavy and the soft modes. Notice that at high temperature quarks are almost on-shell. In this region one spinor is a light field, while the other is a heavy field. For instance in the static limit, i.e. for small transverse momentum $\mathbf{p}_\perp$, close to the pole $p_3 \approx ip_0$, χ is the light component while ϕ is the heavy one. In analogy with what is usually done in the framework of the heavy quark effective theory (HQET) [88] we can integrate out heavy modes by solving the equations of motion for the heavy component and substitute it into the action. For instance, by solving the equation of motion for $\phi^\dagger$ we obtain

$$\phi = \frac{i\epsilon_{kl} D_k \sigma_l}{p_0 - gA_0 - D_3} \chi , \tag{2.20}$$

And similarly for $\chi^\dagger$. By inserting such terms into the action and expanding in powers of $1/p_0$, close to the poles $p_3 \approx \pm ip_0$, the Dirac action can be factorized into the χ and ϕ contributions as

$$\begin{aligned} S_f = \int \mathrm{d}^3\mathbf{x} \, i\chi^\dagger & \left[p_0 - gA_0 + D_3 - \frac{1}{2p_0} \left(D_k^2 + \frac{g}{4i} \left[\sigma_k, \sigma_j \right] F_{kj} \right) \right] \chi \\ & + i\phi^\dagger \left[p_0 - gA_0 - D_3 - \frac{1}{2p_0} \left(D_k^2 + \frac{g}{4i} \left[\sigma_k, \sigma_j \right] F_{kj} \right) \right] \phi + O\left(\frac{1}{p_0^2} \right) . \end{aligned} \tag{2.21}$$

Notice that, due to the different sign in the kinetic term in the 3-direction, the action above describes forward propagating χ and backward propagating ϕ fields in the 3-direction for $p_0 > 0$.

If we consider the theory with N_f degenerate heavy quarks, the action in eq. 2.21 is invariant under flavour rotations $SU(N_f)$. This symmetry is explicitly broken by any non-degenerate mass term, however, for sufficiently large temperatures any breaking effect is supposed to be small as long as the quark mass is a low energy scale with respect to $p_0 = \pi T$. Furthermore, up to the term $\frac{g}{4i}[\sigma_k, \sigma_j] F_{kj}$, the action is invariant under two independent *spin-transformations* belonging to the $SU(2)_{\text{spin}}$ group

$$\begin{cases} \phi & \to \phi' = e^{-i\epsilon_\phi \Sigma}\phi \\ \chi & \to \chi' = e^{-i\epsilon_\chi \Sigma}\chi \end{cases}, \qquad \text{where} \quad \Sigma = \{\sigma_1, \sigma_2, \sigma_3\} \ . \tag{2.22}$$

Notice that the only term in eq. 2.21 which is not invariant under spin-symmetry is the chromo-magnetic interaction term which can be written in the familiar form

$$O_{\text{mag}} = \frac{g}{4i}[\sigma_k, \sigma_j] F_{kj} = -g\, \sigma_3 \cdot \mathcal{B}_3 \,, \tag{2.23}$$

where $\mathcal{B}_3 = -\frac{1}{2}\epsilon_{kl} F_{kl}$ is the chromo-magnetic field along the 3-direction. The full symmetry for each spinor is $SU(2N_f)$ which is usually called in the HQET, *heavy-quark spin-flavour symmetry.*

At this level we integrated out the heavy degrees of freedom and the corresponding effective theory for non-relativistic quarks can be constructed by simply taking into account operators with higher mass dimension and with the correct symmetries.

In this context, before explicitly constructing the effective field theory, it is useful to define some power counting rules, to properly include all the higher dimensional operators up to some order. Being the theory described in eq. 2.21 a theory of heavy quarks only, in the construction of the EFT we proceed in analogy with the so-called Non Relativistic QCD (NRQCD) [89]. NRQCD power counting is somehow less trivial than the case of the HQET where the only two scales appearing are Λ_{QCD} (the soft scale) and the heavy quark mass m_Q (the

heavy scale). As a consequence, in the HQET any operator with mass dimension $4+d$ scales as $(\Lambda_{QCD}/m_Q)^d$. On the other hand in NRQCD the situation is more involved and the power counting is not explicit in the action due the appearance of three different energy scales, i.e. the quark mass, the quark three-momentum and the quark kinetic energy, denoted as $m_Q, m_Q v$ and $m_Q v^2$ respectively [90, 91]. Notice that in the case of the dimensional reduced non-relativistic effective theory the situation is even more involved due to the fact that the three scales depend explicitly on the running coupling (see eq. 2.14).

Power counting rules can be extracted by simply imposing each term in the action to be $O(1)$. In such a way, in analogy with the NRQCD, by defining $m = \pi T$, $v = g$, we can write each scale as:

- **ultrasoft** scale: $mv^2 \sim g^2 T$
- **soft** scale: $mv \sim gT$
- **hard** scale: $m \sim T$.

by scrutinizing each term in eq. 2.12, 2.15 and 2.21 we obtain for each fundamental field and composite operator the power counting reported in table 2.1.

By taking into account the degrees of freedom and the field content in eq. 2.21 together with the power counting we discussed so far, the most general three dimensional effective action for static quarks, which interact with soft and ultrasoft gauge fields only, including operators up to $O(g^4T^2)$, reads [92, 93]

$$\begin{aligned} S_{\mathrm{NRQCD}} \;=\; \int \mathrm{d}^3\mathbf{x}\, i\chi^\dagger \left[M - g_{\mathrm{E}} A_0 + D_3 - \frac{1}{2p_0}\left(D_k^2 + \frac{g_{\mathrm{E}}}{4i}\left[\sigma_k, \sigma_j\right] F_{kj} \right) \right] \chi \\ + \; i\phi^\dagger \left[M - g_{\mathrm{E}} A_0 - D_3 - \frac{1}{2p_0}\left(D_k^2 + \frac{g_{\mathrm{E}}}{4i}\left[\sigma_k, \sigma_j\right] F_{kj} \right) \right] \phi \,, \end{aligned} \tag{2.24}$$

where we introduced the matching coefficient $M \sim \pi T + O(g^2 T)$. Currently the matching coefficient has been computed at 1-loop order by matching the quark pole mass in the three dimensional theory and in full QCD [15]. Its expression reads

$$M \;=\; \pi T + g^2 T \frac{C_F}{8\pi} \;+\; O(g^4 T)\,. \tag{2.25}$$

Operator	Power counting	
gA_0	$mv^{3/2}$	$g^{3/2}T$
gA_k	mv^2	g^2T
χ, ϕ	mv	gT
p_0	mv^2	T
∂_3	mv^2	g^2T
∂_k	mv	gT
$gA_k\partial_k$	mv^3	g^3T^2
$(gA_k)^2$	m^2v^4	g^4T^2
$\partial_k (gA_k)$	m^2v^4	g^4T^2
$g[\sigma_k, \sigma_j] F_{kj}$	m^2v^4	g^4T^2

Table 2.1: Power counting for each operator appearing in the heavy quark action up to order $1/p_0$. In the second column the estimate of the power counting is given in analogy with NRQCD, while in the third column the corresponding power counting in terms of gauge coupling and temperature is provided.

As a final remark, notice that, being eq. 2.24 an effective field theory, each higher dimensional operator should in principle come with a matching coefficient c_O. However since those can be expanded in the coupling constant as $c_O \approx 1 + O(g^2)$, higher order correction would only contribute to sub-leading terms in the action.

2.3 QCD hadronic screening spectrum

In this section we review how the phase transition from a confined, chirally broken phase to a deconfined and chirally symmetric regime impacts on the spectrum of QCD. As seen in Sec. 1.5.4 at zero temperature, masses of particles associated to some particular operators with a given set quantum numbers are obtained by probing the exponential fall-off of some suitable correlation functions at large euclidean time separations. In general at finite temperature, one can probe correlation functions in one of the spatial directions. For a generic interpolating operator O, the

correlation function in the 3-direction is defined as

$$G_{k_n}(x_3) = \int_0^\beta \mathrm{d}x_0\, e^{ik_n x_0} \int \mathrm{d}x_1\, \mathrm{d}x_2\, \langle O(x) O(0) \rangle \,, \tag{2.26}$$

where O carries the quantum number we are interested in and k_n is the Matsubara frequency we are projecting on the two-point correlation function[2]. At finite temperature such correlation functions are often referred to as *screening* correlation functions. The reason is that we can easily relate the mass which regulate the exponential fall-off of the correlator, namely the *screening mass* $m_O^{(k_n)}$, to the so called screening correlation length $\xi_O = 1/m_O^{(k_n)}$. Screening lengths describe the response of the quark and gluon plasma when an excitation with the quantum numbers carried by O is present in the system. The corresponding screening masses are defined in terms of the asymptotic behaviour of the screening correlation function in eq. 2.26 as

$$m_O^{(k_n)} = -\lim_{x_3 \to \infty} \frac{\partial_3 G_{k_n}(x_3)}{G_{kn}(x_3)} \,. \tag{2.27}$$

Before looking at the consequences of chiral symmetry restoration, we can somehow understand some properties of the screening spectrum at asymptotically high temperature by directly scrutinizing in detail each term appearing in the effective action for non-relativistic quarks, see eq. 2.24. On one hand, in the free massless theory hadronic screening masses have to be uniquely determined by the lowest Matsubara frequency of each quark. As a consequence, hadrons composed of n massless quarks in the lowest Matsubara sector will have a mass $m_n = n\pi T$. On the other hand, for asymptotically high temperature, i.e. $p_0 \to \infty$ in eq. 2.24, the theory is symmetric under both flavour and spin transformations, i.e. generic hadrons composed of n massless quarks have the same mass, regardless to the spin and the flavour composition.

Notice that at very high temperatures, any effect due to the presence of a non-zero quark mass m_q is expected to be negligible as long as $m_q \ll T$. In particular, the expected correction to the screenning mass, in the free theory, for a generic

[2]The Matsubara frequency is fermionic or bosonic (see eq. 2.6 and 2.7 respectively) depending on the operator quantum numbers.

hadron composed of n quarks is given by

$$m_n = \sum_{i=1}^{n} \sqrt{(\pi T)^2 + \left(m_q^i\right)^2} \approx n\pi T + \frac{1}{2}\sum_{i=1}^{n} \frac{{m_q^i}^2}{\pi T} + \dots . \tag{2.28}$$

It is then clear that for sufficiently large temperatures any contribution coming from the mass term is suppressed. As a representative example, the relative contribution coming from the up and down quark masses in a meson ($n = 2$) at $T = 1$ GeV is approximately $\lesssim 6 \times 10^{-5}\,\%$, while the strange quark mass contribution amounts at $0.02\,\%$ at the same temperature[3].

As a final remark notice that spatially-separated two-point correlation functions like the one in eq. 2.26 are related to spectral functions $\rho_{k_n}(\omega, p_3)$ by the spectral representation

$$G_{k_n}(x_3) = \int_0^\infty \frac{\mathrm{d}\omega}{\pi\omega} \int_{-\infty}^{+\infty} \frac{\mathrm{d}p_3}{2\pi} e^{ip_3 x_3} \rho_{k_n}(\omega, p_3) \, . \tag{2.29}$$

Analogously, we can derive the spectral representation for temporal correlation functions, which however involves a kernel which is in general temperature dependent and depends on the spin-statistics nature of the interpolating operator associated to the correlation function [94].

At zero temperature due to Lorentz invariance, spectral densities extracted from spatial and temporal correlators contain the same physical information with poles due to the presence of physical particles. At finite temperature, spectral functions encode modifications of the hadronic structures due to the thermal medium. Thermal effects modify the characteristic structure of resonance peaks appearing in the spectral functions. Since for asymptotically high temperatures the screening mass approaches the free field theory value in eq. 2.28, the study of thermal effects on screening masses can provide insight on the in-medium modifications of hadronic states due to thermal effects which are then expected to shift and broaden characteristic peaks in spectral functions. As $T \to 0$, since the theory is Lorentz invariant, the screening mass in eq. 2.27 goes to the zero-temperature value of the

[3]We quote $m_u = 2.20(8)$ MeV, $m_d = 4.69(5)$ MeV and $m_s = 93.1(6)$ MeV. Here we use the values of the quark masses reported in Ref. [22]. Those are obtained by lattice simulations and converted to the standard $\overline{\mathrm{MS}}$ scheme at the renormalization scale $\mu = 2$ GeV by using continuum perturbation theory.

pole-mass which is extracted by probing the large distance behaviour of temporal correlation functions, see Sec. 3.8. In this sense, screening correlation functions are particularly suitable to probe thermal modifications to the spectral functions [95], since those can be studied at very large separations, while temporal correlation functions are limited by the compact temporal extent.

2.3.1 Chiral symmetry

At zero temperature non-singlet chiral symmetry is spontaneously broken and the singlet axial group is broken by the anomaly. On the other hand above the deconfinement temperature not only the chiral condensate is highly suppressed leading to chiral symmetry restoration, but also the singlet axial symmetry is effectively restored due to the strong thermal suppression of non-zero topological sectors.

As a consequence we expect this restoration pattern to produce substantial effects on the hadronic spectrum. As done in Sec. 1.5.3, the clearest way to highlight such effects is to extract suitable relations between two-point correlation functions associated to different interpolating operators. In particular in the following we will make extensive use of the *PCAC* relation in eq. 1.55 and of the anomalous WTIs in eq. 1.65. For this reason it is useful to recall their expression

$$-i\epsilon^a_A \partial_\mu \langle A^a_\mu(x) O(y)\rangle = -i\epsilon^a_A \langle \bar{\psi}(x)\gamma_5 \{T^a, M\}\psi(x) O(y)\rangle + \langle \delta O(y)\rangle \,, \tag{2.30}$$

$$-i\epsilon^0_A \partial_\mu \langle A^0_\mu(x) O(y)\rangle = -2i\epsilon^0_A N_f \langle q(x) O(y)\rangle + \langle \delta O(y)\rangle \,. \tag{2.31}$$

Notice that here we follow the very same procedure as done before in Sec. 1.5.2, i.e. we will only consider local chiral transformations, e.g. $\epsilon^a_A(x) = \epsilon^a_A \delta(x-y)$. The only difference lies in the fact that at finite temperature the temporal extent is finite and when computing integrated WTIs we have to be careful about (anti-)periodic boundary conditions. This will simply translate into taking into account (anti-) periodic delta functions in the temporal extent, i.e. $\delta(x-y) = \delta^{(3)}(x-y)\delta_{\beta=1/T}(x_0 - y_0)$.

2.3.2 Mesonic Ward-Takahashi identities

Consider as interpolating operator the composite operator obtained by multiplying a non-singlet vector current by a non-singlet axial current

$$O = A^b_\sigma(z)V^c_\nu(y)\,. \tag{2.32}$$

Under local axial non-singlet transformations in eq. 1.54 the variation of such operator reads

$$\delta O = \epsilon^a_A(z)f^{abd}V^d_\sigma(z)V^c_\nu(y) + \epsilon^a_A(x)f^{acd}A^b_\sigma(z)A^d_\nu(x)\,, \tag{2.33}$$

Then the whole WTI (see eq. 2.30) reads

$$\begin{aligned} -i\epsilon^a_A\partial_\mu\langle A^a_\mu(x)A^b_\sigma(z)V^c_\nu(y)\rangle &= -i\epsilon^a_A\langle\bar\psi(x)\gamma_5\{T^a,M\}\psi(x)A^b_\sigma(z)V^c_\nu(y)\rangle \\ &+ \epsilon^a_A f^{abd}\langle V^d_\sigma(z)V^c_\nu(y)\rangle + \epsilon^a_A f^{acd}\langle A^b_\sigma(z)A^d_\nu(y)\rangle\,. \end{aligned} \tag{2.34}$$

Then if we take the massless limit $M = 0$ and $\sigma = \nu = k$, by using the anti-symmetric property of f^{abc}, it can be written as

$$-i\epsilon^a_A\partial_\mu\langle A^a_\mu(x)A^b_k(z)V^c_k(y)\rangle = f^{abc}\left[\epsilon^a_A\langle V^c_k(z)V^c_k(y)\rangle - \epsilon^a_A\langle A^b_k(z)A^b_k(y)\rangle\right]. \tag{2.35}$$

Notice that at zero temperature the l.h.s of the equation above is different from zero due to the spontaneous breaking of chiral symmetry and, as a consequence, the $\rho(770)$ mass and the $a_1(1260)$ mass are different [22] and more generally there are not degenerate parity partners in QCD. On the contrary, if chiral symmetry is restored, which is the case of the high temperature regime of QCD, the l.h.s vanishes. Then by taking into account local transformations and by integrating over space-time, by a flavour rotation, the whole integrated WTI leads to

$$\langle V^a_k(z)V^a_k(y)\rangle = \langle A^a_k(z)A^a_k(y)\rangle\,. \tag{2.36}$$

Since for large spatial separations the behaviour of these two-point correlations functions is dominated by the corresponding lowest energy state, eq. 2.36 implies the degeneracy of the vector and the axial screening masses. As we will see in the

following, similar considerations hold for other mesonic channels.

By following the very same procedure and using the interpolating operator defined as

$$\mathcal{O} = P^b(z)S^0(y)\,, \tag{2.37}$$

the corresponding variation is readily obtained

$$\begin{aligned}\delta O &= i\epsilon^a_A(z)\bar{\psi}(z)\left\{T^a,T^b\right\}\psi(z)S^0(y) + 2i\epsilon^a_A(y)P^b(z)P^a(y)\\ &= i\epsilon^a_A(z)\bar{\psi}(z)\left\{d^{abc}T^c + \frac{\delta^{ab}}{N_f}\right\}\psi(z)S^0(y) + 2i\epsilon^a_A(y)P^b(z)P^a(y)\,.\end{aligned} \tag{2.38}$$

By restricting to the case $a = b$ which implies $d_{aac} = 0$ (see App. A.1), the integrated WTI in presence of chiral symmetry leads to

$$2\left\langle P^a(z)P^a(y)\right\rangle = -\frac{1}{N_f}\left\langle S^0(z)S^0(y)\right\rangle\,, \tag{2.39}$$

and, as a consequence, to the degeneracy between the masses related to the scalar and to the pseudoscalar densities.

In a very similar way we can consider the interpolating operator

$$O = S^b(z)P^0(y) \tag{2.40}$$

which leads, similarly to eq. 2.39, to

$$2\left\langle S^a(x)S^a(y)\right\rangle = -\frac{1}{N_f}\left\langle P^0(z)P^0(y)\right\rangle\,. \tag{2.41}$$

Notice that, in principle one could try to relate the singlet to the non-singlet currents by selecting interpolating operators like $O = V^b_\mu(z)A^0_\nu(y)$ and $O' = A^b_\mu(z)V^0_\nu(y)$. However, such interpolating operators would lead to trivial two-point correlation functions like $\langle V^c_\mu(z)V^0_\nu(y)\rangle$, and similarly for O'.

In the same way, we can try to relate masses associated to different channels by using anomalous axial transformations. Let us consider, for instance, the

interpolating operator

$$O = P^0(z)S^0(y)\,, \tag{2.42}$$

and the corresponding variation under singlet transformations

$$\delta O = 2i\epsilon^0_A(z)\,\langle S^0(z)S^0(y)\rangle + 2i\epsilon^0_A(y)\,\langle P^0(z)P^0(y)\rangle\ . \tag{2.43}$$

By inserting such variation in eq. 2.31, the corresponding integrated WTI is readily derived and reads

$$\langle S^0(z)S^0(y)\rangle + \langle P^0(z)P^0(y)\rangle = N_f\,\langle QP^0(z)S^0(y)\rangle\ . \tag{2.44}$$

Notice that the above WTI explicitly depends on the value of the topological charge. At zero temperature there is no suppression of non-zero topological sectors and, as a consequence, the singlet scalar meson and the pseudoscalar one are not degenerate. On the other hand, as the temperature increases thermal effects suppress any contribution coming from non-trivial topological sectors leading to an effective restoration of the $U(1)_A$ symmetry. In such case the right-hand side of eq. 2.44 vanishes and the scalar and the pseudoscalar flavour-singlet screening masses become degenerate.

In the same way if we consider the non-singlet analogue of eq. 2.42

$$O = P^a(z)S^a(y)\,, \tag{2.45}$$

the corresponding variation reads

$$\delta O = 2i\epsilon^0_A(z)S^a(z)S^a(y) + 2i\epsilon^0_A(y)P^a(z)P^a(y)\,, \tag{2.46}$$

and, by combining with eq. 2.31, leads to the integrated WTI

$$\langle S^a(z)S^a(y)\rangle + \langle P^a(z)P^a(y)\rangle = N_f\,\langle QP^a(z)S^a(y)\rangle \tag{2.47}$$

which again implies the degeneracy of the non-singlet scalar and pseudoscalar screening masses if $Q \to 0$.

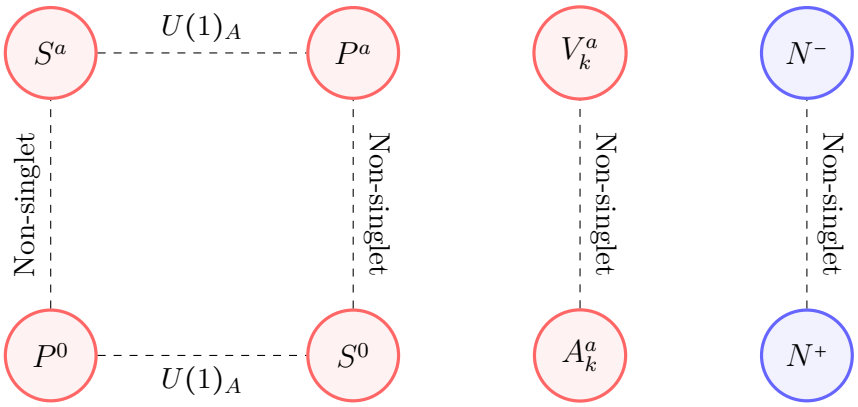

Figure 2.2: In red the degeneracy pattern of the mesonic sector of the screening masses if the axial non-singlet symmetry is not spontaneously broken and if only the $Q = 0$ topological sector is not suppressed by thermal effects. In blue the degeneracy pattern of the baryonic screening masses due to the restoration of non-singlet chiral transformations.

Similarly to what we observed for non-singlet transformations, if one tries to relate singlet currents to non-singlet ones by using singlet transformations the corresponding WTIs are trivial.

By combining the WTIs obtained in presence of non-singlet axial symmetry with the ones derived by imposing the $U(1)_A$ symmetry, a non-trivial degeneracy pattern between mesonic screening masses arises at high temperature. This leads to the standard degeneracy relations which is represented in fig 2.2.

For completeness, we mention that recently [96, 97] it has been proposed a much larger symmetry restoration pattern above the critical temperature, and in a limited range of temperatures, which would lead to the degeneracy of the screening masses related to some additional channels, including the masses associated to the singlet and non-singlet vector currents.

2.3.3 Baryonic Ward-Takahashi identities

Similar considerations hold for baryonic interpolating operators. Let us consider an interpolating operator which carries the nucleon quantum numbers. The most

general such operator is

$$N(\Gamma_A, \Gamma_B) = \epsilon^{abc} \left(u_a^T \Gamma_B d_b\right) \Gamma_A d_c \tag{2.48}$$

where Γ_A and Γ_B are specific combinations of gamma matrices, with the only constraint that Γ_B does not contain any spatial gamma matrix, which would, otherwise, produce a spin-3/2 Rarita-Schwinger operator [98]. Notice that in eq. 2.48 the transposition acts on spinor indices only, while ϵ^{abc} guarantees the operator to be an anti-symmetric, singlet operator in colour space. In general such interpolating operator has no definite parity quantum number, for this reason it is common to introduce the projector on positive and negative parity state $P_\pm$. By making the definite choice of measuring correlation functions along the 3-direction such x_3-parity projector is defined as $P_\pm = (1 \pm \gamma_3)/2$. In this thesis we restrict ourselves to the study of nucleon interpolating operators of the form

$$N^\pm = \epsilon^{abc} \left(u_a^T C\gamma_5 d_b\right) d_c P^\pm \,, \tag{2.49}$$

where we simply set $\Gamma_B = C\gamma_5$, where C is the charge-conjugation operator defined in eq. A.2 and $\Gamma_A = \mathbb{1}$. In order to make the consequences of chiral symmetry restoration clear, let us consider the interpolating operator

$$O = \mathrm{Tr}\left[\gamma_5 P_\pm N(z)\overline{N}(y)\right] , \tag{2.50}$$

where the trace has to be taken over Dirac indices. Notice that under non-singlet chiral transformations only flavour-conserving transformations lead to non-trivial WTIs. This amounts to take into account chiral transformations involving diagonal $SU(N_f)$ algebra generators only (see eq. A.7 for $N_f = 3$). Moreover, due to the flavour structure of the nucleon operator, which only contains up and down quarks, we can restrict ourselves to the $SU(2)$ sub-algebra. In such case quark fields, under diagonal chiral transformations we have

$$\begin{aligned} \delta u^a(x) &= i\epsilon\gamma_5 u^a(x) \\ \delta d^b(x) &= -i\epsilon\gamma_5 d^b(x) \,, \end{aligned} \tag{2.51}$$

and similarly for $\bar{u}^a$ and $\bar{d}^b$. Under such transformations the variation of the operator in eq. 2.50 reads

$$\delta O \;=\; \epsilon\,\mathrm{Tr}\left[P_{\pm}N(z)\overline{N}(y)\right] \;+\; \epsilon\,\mathrm{Tr}\left[P_{\mp}N(z)\overline{N}(y)\right]\,. \tag{2.52}$$

Then if combined with eq. 2.30 and assuming chiral symmetry to be not spontaneously broken, i.e $\langle\delta O\rangle = 0$, it leads to

$$\mathrm{Tr}\left[P_{\pm}N(z)\overline{N}(y)\right] \;=\; -\,\mathrm{Tr}\left[P_{\mp}N(z)\overline{N}(y)\right]\,, \tag{2.53}$$

which implies the degeneracy of the masses of the positive and the negative nucleon parity partners. Notice that at zero temperature due to the spontaneous breaking of chiral symmetry the positive (nucleon) and the negative (N^*) parity pole-masses differ by several hundreds of MeV [22]. For this reason, the comparison between these two masses provides a solid test of the restoration of chiral symmetry in the high temperature regime.

Chapter 3

Quantum Chromodynamics on the lattice

As mentioned in Sec. 1.3 the definition of the path integral given in eq. 1.11 is formal. A rigorous and mathematically well-defined definition of the path integral is obtained by defining the theory on a finite lattice and the corresponding continuum path integral is obtained by taking the limit of vanishing lattice spacing. In such a way, fields are evaluated on a finite number of lattice sites and the corresponding path integral is a well-defined mathematical object involving a finite number of degrees of freedom.

3.1 Preliminaries

Typically we define the lattice Λ as the set of points within an hypervolume $L_0 \times L_1 \times L_2 \times L_3$ in euclidean time, where L_0 is the lattice extent in the temporal direction and L_i is the extent in the ith spatial direction. More formally the lattice is defined as the subset of $\mathbb{R}^4$ [99, 100]

$$\Lambda = \left\{ x \in \mathbb{R}^4 \;\middle|\; x = \sum_{\mu=0}^{3} n_\mu a \hat{\mu}\,,\; n_\mu = -\frac{L_\mu}{2a}, -\frac{L_\mu}{a}+1, \ldots, \frac{L_\mu}{2a}-1 \right\}, \tag{3.1}$$

being $\hat{\mu} = \hat{e}_\mu$ the unit vector along the μ-direction and a the lattice spacing. In a similar way, by going to momentum space we can define the reciprocal lattice as

the set

$$\tilde{\Lambda} = \left\{ p \in \mathbb{R}^4 \;\middle|\; p_\mu = \frac{2\pi}{L_\mu} n_\mu \right\}, \qquad \text{with} \qquad -\frac{\pi}{a} \leq p_\mu \leq \frac{\pi}{a}. \tag{3.2}$$

In this way, the lattice spacing not only allows a well-defined definition for the path integral, but also naturally provides the UV cut-off in momentum space integrals, which are now restricted to the Brillouin zone (BZ).

Once the lattice has been properly defined, the next step is to define the discretized theory. Notice that this procedure is not unique and can lead to different discretized actions for the same theory. The only requirement is that, once we take the limit $a \to 0$, the correct continuum action must be obtained. The simplest way to obtain the lattice theory is to naïvely discretize each operator appearing in the continuum action.

Consider for the moment a generic field $\phi(x)$. Its lattice discretization is simply given by evaluating the field on the discrete lattice site $x \equiv na$. By taking into account finite differences, we can define the *forward* and *backward* derivatives as

$$\partial_\mu \phi(x) \to \frac{\phi(x + a\hat{\mu}) - \phi(x)}{a} \equiv \frac{\delta_{x+a\hat{\mu},y} - \delta_{x,y}}{a} \phi(y), \tag{3.3}$$

$$\partial^*_\mu \phi(x) \to \frac{\phi(x) - \phi(x - a\hat{\mu})}{a} \equiv \frac{\delta_{x,y} - \delta_{x-a\hat{\mu},y}}{a} \phi(y), \tag{3.4}$$

and the symmetrized derivative as

$$\frac{1}{2}\left(\partial^*_\mu + \partial_\mu\right)\phi(x) \to \frac{\phi(x + a\hat{\mu}) - \phi(x - a\hat{\mu})}{2a} \equiv \frac{\delta_{x+a\hat{\mu},y} - \delta_{x-a\hat{\mu},y}}{2a} \phi(y). \tag{3.5}$$

With these definitions, in the following sections we will discuss how the QCD action can be discretized on the lattice. Sec. 3.2 and 3.3 will be devoted to properly define the gauge and the fermionic sector of the action on the lattice. Along with the main definitions, we will deal with some of the main difficulties that arise when putting fermions on the lattice. The rest of the chapter is dedicated to technical details about how a proper lattice calculation is carried out, namely the renormalization of the theory on the lattice and how gauge field configurations are generated. Finally a section is dedicated to discuss how the QCD hadronic spectrum can be extracted non-pertubatively from lattice calculations.

3.2 SU(3) gauge theory on the lattice

In order to properly define the gluonic sector of the QCD action on the lattice, the main ingredient we have to take into account is gauge invariance. Notice that due to the derivative appearing in the non-abelian gauge transformation in eq. 1.2, after taking into account discretized derivatives, gauge field transformations do not hold any more at finite lattice spacing. For this reason a different approach which allows the construction of a gauge invariant discretized action is desiderable. Such different approach was provided by Wilson in Ref. [101] and is based on the continuum notion of *parallel transporter*. The parallel transporter in the continuum theory is defined as the element of the $SU(3)$ gauge group obtained by taking a path-ordered exponential of the integral of the gauge field along the path Γ

$$U(x,y) \equiv \mathcal{P}\exp\left\{-i\int_x^y \mathrm{d}z_\mu\, A_\mu(z)\right\}, \tag{3.6}$$

where Γ is the path connecting the two space-time coordinates x and y. Notice that, in eq. 3.6, the path-ordering is crucial since the $SU(3)$ group is non-abelian. Under gauge transformations, it transforms as

$$U(x,y) \to U'(x,y) = \Omega(x)U(x,y)\,\Omega^\dagger(y)\,. \tag{3.7}$$

By moving to the context of lattice regularization, the corresponding parallel transporter, which connects two nearest-neighbour lattice sites along the direction μ, can be written as[1]

$$U_\mu(x) \equiv U(x, x+a\hat{\mu}) = \mathcal{P}\exp\left\{-ia\int_0^1 \mathrm{d}z\, A_\mu(x+za\hat{\mu})\right\}. \tag{3.8}$$

The discretized version of the parallel transporter connecting two nearest-neighbour lattice points is called *link variable* and is taken as fundamental field instead of the algebra-valued fields A_μ. Notice that by taking advantage of the definition of the parallel transporter in eq. 3.6, being the link variables oriented objects, the

[1]Here A_μ is the lattice discretization of the gluonic field. In the following we will use the same notation for continuum and lattice quantities, since the ambiguity can be resolved from the context.

following relation for the inverse link variable holds

$$U_\mu^{-1}(x) = U^\dagger(x, x + a\hat{\mu}) = U(x + a\hat{\mu}, x)\,. \tag{3.9}$$

Correspondingly, under gauge transformations the link variable transforms as

$$U_\mu(x) = \Omega(x) U_\mu(x) \Omega(x + a\hat{\mu})^\dagger\,. \tag{3.10}$$

In this way, if the lattice theory is constructed by taking into account link variables as fundamental fields, rather than the gauge field A_μ, being valid eq. 3.10, we can define a theory which is gauge invariant at finite lattice spacing. Notice that, by expanding for small lattice spacing the definition of the link variable in eq. 3.8 and using eq. 3.10, one can easily recover the gauge field transformations in eq. 1.2 up to $O(a^2)$ corrections.

Starting from the definition of the link variable, we can construct gauge invariant lattice operators by simply taking the product of link variables. The simplest gauge invariant quantity one can define is the so-called *plaquette*

$$U_{\mu\nu}(x) \equiv U_\mu(x) U_\nu(x + a\hat{\mu}) U_\mu^\dagger(x + a\hat{\nu}) U_\nu^\dagger(x)\,. \tag{3.11}$$

Recalling the relations in eq. 3.9 one can see that the definition of the plaquette amounts to consider the smallest closed loop of link variables in the $(\hat{\mu}, \hat{\nu})$-plane. Its graphical representation is given in fig. 3.1. By expanding the link variable for small lattice spacing, i.e.

$$U_\mu(x) = e^{-iaA_\mu\left(x + \frac{a\mu}{2}\right)} \tag{3.12}$$

and by using the Campbell-Hausdorff formula, the plaquette field can be written in terms of the gauge field as

$$\begin{aligned} U_{\mu\nu} &= \exp\left\{-ia^2\left[\partial_\mu A_\nu(x) - \partial_\nu A_\mu(x) - i\left[A_\mu(x), A_\nu(x)\right] + O(a)\right]\right\} \\ &= \exp\left\{-ia^2\left[F_{\mu\nu} + O(a)\right]\right\} \end{aligned} \tag{3.13}$$

where ∂_μ denotes the forward derivative on the lattice and the last step is obtained

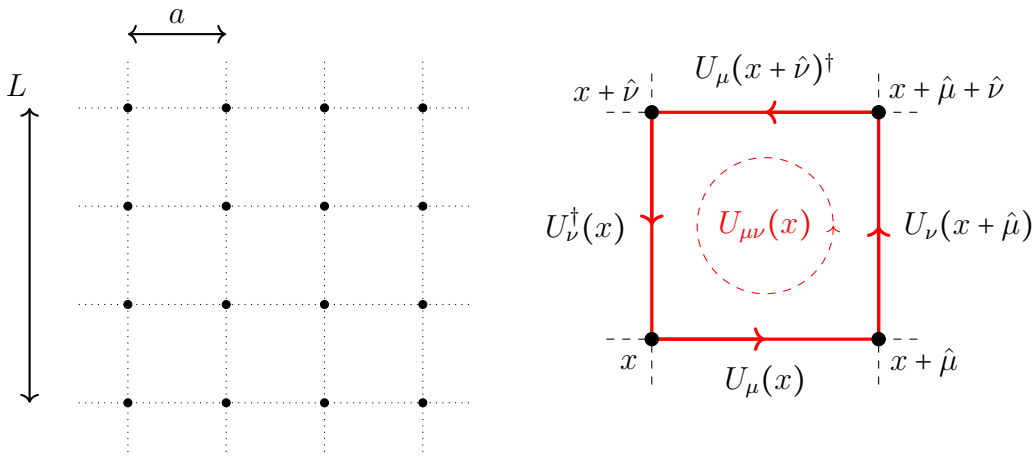

Figure 3.1: On the left, the lattice on which the theory is discretized. L is the lattice extent in the given direction, while a is the lattice spacing. On the right, the link variables and the plaquette: four different link variables define the plaquette field (red lines).

in analogy with the definition of the link variable, by writing the plaquette in terms of elements of the $SU(3)$ algebra.

By taking into account the expression above for the plaquette, a possible gauge invariant, discretized version of the Yang-Mills action is provided by the *Wilson's plaquette action* [101]

$$S_g^{(\mathrm{W})} = \frac{\beta}{2}\sum_x\sum_{\mu,\nu}\left\{\mathbb{1} - \frac{1}{2N_c}\mathrm{Re}\ \mathrm{Tr}\left[U_{\mu\nu}\right]\right\}, \tag{3.14}$$

where the bare coupling constant has been parametrized through the β-parameter as $\beta = 2N_c/g_0^2$. As done before, by expanding for small lattice spacing, it is possible to show that, by taking the continuum limit extrapolation, this reproduces the expected continuum Yang-Mills action in eq. 1.7, i.e.

$$S_g = \frac{1}{2g_0^2}a^4\sum_x\sum_{\mu,\nu}\mathrm{Tr}\left[F_{\mu\nu}(x)F_{\mu\nu}(x)\right] + O(a^2)\,. \tag{3.15}$$

The last ingredient we need for a well-defined definition of the path integral for the $SU(3)$ Yang-Mills theory is the integration measure. The functional integral is

now performed over the $SU(3)$ compact group and its integration measure reads

$$DU = \prod_{\mu} \prod_{x} \mathrm{d}U_{\mu}(x) \,. \tag{3.16}$$

Notice that the proper definition of the link integration measure relies on the so called *Haar measure* which provides the correct measure to integrate over the $SU(3)$ group manifold. Given a generic element V of the $SU(3)$ algebra, the Haar measure is invariant under left and right multiplication, i.e.

$$\mathrm{d}U_{\mu} = \mathrm{d}\left(U_{\mu}V\right) = \mathrm{d}\left(VU_{\mu}\right) \,. \tag{3.17}$$

Furthermore, being the path integral invariant under a generic change of variables, under gauge transformations in eq. 3.10, it immediately follows that the Haar measure satisfies

$$\mathrm{d}U_{\mu}(x) = \mathrm{d}\left(\Omega(x)U_{\mu}(x)\Omega^{\dagger}(x+\hat{\mu})\right) \,, \tag{3.18}$$

As a final comment, notice that, in contrast with the continuum theory in which the formal definition of the path integral requires a gauge fixing term, in lattice regularization such term is not needed anymore. Indeed the continuum gauge fixing was introduced to avoid the appearance of an infinite factor in front of the path integral when integrating over equivalent gauge field configurations, however on the lattice the integration is over compact group-valued variables which then makes the integral finite and well-defined.

3.3 Fermions on the lattice

Similarly, we can construct the fermionic action on the lattice by naïvely discretizing the corresponding continuum action. Let us consider, for the moment, the free Dirac action in the massless limit. By employing the definition of the symmetrized

derivative in eq. 3.5, the free Dirac action is readily discretized as

$$\begin{aligned} S_f &= \frac{a^4}{2} \sum_x \bar{\psi}(x) \gamma_\mu \left(\partial^*_\mu + \partial_\mu \right) \psi(x) \\ &= \frac{a^4}{2} \sum_x \left\{ \bar{\psi}(x) \gamma_\mu \psi(x + a\hat{\mu}) \; - \; \bar{\psi}(x) \gamma_\mu \psi(x - a\hat{\mu}) \right\} , \end{aligned} \tag{3.19}$$

where the second line is simply obtained by expanding the definition for the symmetrized derivative. By adding gauge interaction we need the additional requirement for the action to be gauge invariant under $SU(3)$ gauge transformations. By recalling how fermion fields transform under gauge transformations (see eq. 1.8), it is straightforward to define the lattice covariant forward and backward derivatives as

$$\nabla_\mu \psi(x) = \frac{1}{a} \left(U_\mu(x) \psi(x + a\hat{\mu}) - \psi(x) \right) , \tag{3.20}$$

$$\nabla^*_\mu \psi(x) = \frac{1}{a} \left(\psi(x) - U_\mu(x - a\hat{\mu})^\dagger \psi(x - a\hat{\mu}) \right) , \tag{3.21}$$

and correspondingly the symmetrized derivative as

$$\frac{1}{2} \left(\nabla^*_\mu + \nabla_\mu \right) = \frac{U_\mu(x) \psi(x + a\hat{\mu}) - U_\mu(x - a\hat{\mu})^\dagger \psi(x - a\hat{\mu})}{2a} . \tag{3.22}$$

Notice that, by expanding for small lattice spacing, the expressions in eq. 3.20 and 3.21 correctly reproduce the continuum limit covariant derivatives up to $O(a)$ discretization errors. By introducing a mass term, the naïve lattice Dirac action for interacting quarks can be written as

$$S_{\mathrm{w}} = a^4 \sum_x \bar{\psi}(x) \left\{ \frac{\gamma_\mu}{2} \left(\nabla^*_\mu + \nabla_\mu \right) + M_0 \right\} \psi(x) , \tag{3.23}$$

which, by naïvely taking the continuum limit extrapolation, reduces to the continuum Dirac action for massive fermions in eq. 1.9.

As done for the gluonic path integral, the last step to regularize the fermionic partition function on the lattice is the definition of the corresponding integration

measure. It reads

$$D\psi = \prod_x \prod_{\{f,\alpha,c\}} \mathrm{d}\psi_\alpha^{f,c}(x)\,, \tag{3.24}$$

and similarly for the $\bar{\psi}$ field. In the above equation the integration measure for fermions involves the product over each quantum number of the set $\{f, \alpha, c\}$ where $f = 1, \ldots, N_f$ is a flavour index, $\alpha = 1, \ldots, 4$ denotes the spin index and finally $c = 1, 2, 3$ is the colour index.

3.3.1 The doubling problem

Being D the Dirac operator for a free, massless fermion, and $\tilde{D}$ its Fourier transform, a good lattice discretization has to guarantee the following properties

(a). $\tilde{D}(p) \overset{a\to 0}{=} i\gamma_\mu p_\mu$

(b). $\tilde{D}(p)$ is a smooth function of p_μ with period $\frac{2\pi}{a}$

(c). $\tilde{D}(p)$ is invertible, besides $p_\mu = 0$

These conditions are dictated by the properties of the Dirac operator in the continuum theory. By performing a Fourier transform, the action in eq. 3.19 can be written as

$$S_f(p) = \int_{-\pi/a}^{\pi/a} \frac{\mathrm{d}^4 p}{(2\pi)^4} \tilde{\bar{\psi}}(-p)\, \frac{i}{a}\gamma_\mu \sin(a p_\mu)\, \tilde{\psi}(p)\,, \tag{3.25}$$

where the integral is restricted to the Brillouin zone due to the relation in eq. 3.2 dictated by the reciprocal lattice. By doing so, we can identify

$$\tilde{D}(p) = \frac{i}{a}\gamma_\mu \sin(a p_\mu)\,, \tag{3.26}$$

which defines the Dirac operator in momentum space, see fig. 3.2. By expanding for small lattice spacing, at *fixed* p_μ, we recover the expected behaviour of the continuum operator. On the other hand, notice that the Dirac operator in eq. 3.26 vanishes not only for $p_\mu = 0$ but also for $p_\mu = \pm\pi/a$, i.e. on the corners of the

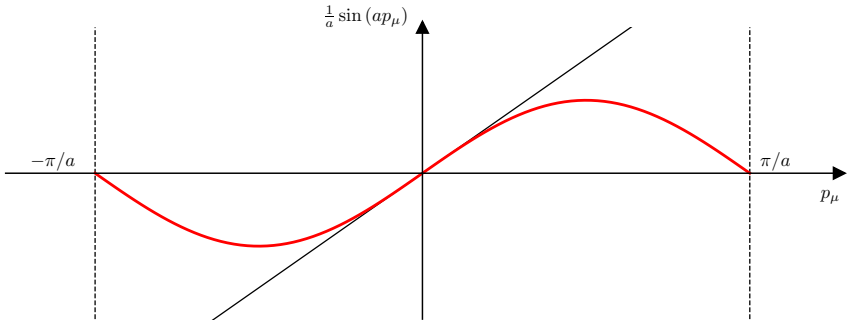

Figure 3.2: Plot of $\frac{1}{a}\sin(ap_\mu)$ as a function of p_μ. The solid line represents the continuum result, while the red curve is the naïve lattice discretization which vanishes at $p_\mu = 0$ and at each corner of the Brillouin zone.

Brillouin zone. As a consequence, the fermion propagator in momentum space, $\tilde{D}^{-1}(p)$, has a pole in

$$p_\mu = 0 \qquad |p_\mu| = \frac{\pi}{a}\,. \tag{3.27}$$

Thereby, even if the Dirac operator in eq. 3.26 satisfies relations (a), (b), it violates property (c). In d dimensions the spectrum of the resulting theory contains 2^d massless fermions, but only the one related to the pole in $p_\mu = 0$ is the physical one. Such additional states are called *doublers*. Notice that close to the edge $p_\mu = \pi/a$, even if we take the continuum limit, the quark propagator still exhibits a pole. As a consequence, the doublers do not disappear from the spectrum of the Dirac operator in the continuum limit.

In the following section, we will introduce Wilson fermions which is the discretization we will employ throughout this thesis.

3.3.2 Wilson fermions

In 1975, in order to remove fermion doublers, Wilson suggested a different lattice discretization for fermions, obtained by simply adding the so-called *Wilson term* to the discretized Dirac operator. Starting from the Dirac action for free massless

quarks in eq. 3.19 we define the Wilson-Dirac operator as [102]

$$D_{\mathrm{w}} = \frac{1}{2}\left\{\gamma_\mu\left(\partial_\mu^* + \partial_\mu\right) - a\partial_\mu^*\partial_\mu\right\}, \tag{3.28}$$

where the second term on the right-hand side represents the Wilson term. This procedure is completely legitimate since lattice discretizations are not unique and the only requirement for the discretized action is that the continuum action has to be recovered as $a \to 0$. Notice that, even if this discretization correctly reproduces the continuum action, it explicitly breaks naïve chiral symmetry in the massless limit.

We may now proceed as before, by taking the Fourier transform of the Wilson-Dirac operator, the Dirac action in momentum space reads

$$S_f = \int_{-\pi/a}^{\pi/a} \frac{\mathrm{d}^4 p}{(2\pi)^4} \tilde{\bar{\psi}}(-p)\, \frac{1}{a}\left\{i\gamma_\mu \sin\left(ap_\mu\right) - 2\sin^2\left(\frac{ap_\mu}{2}\right)\right\} \tilde{\psi}(p)\,, \tag{3.29}$$

which leads to the Wilson-Dirac operator in momentum space

$$\tilde{D}(p) = \frac{i}{a}\gamma_\mu \sin\left(ap_\mu\right) + \frac{2}{a}\sin^2\left(\frac{ap_\mu}{2}\right). \tag{3.30}$$

Notice that the Wilson term is analogous to a mass term, which then breaks chiral symmetry even in the massless limit. More generally in the massive case, the Wilson-Dirac operator can be written in momentum space as

$$\tilde{D}(p) = \frac{i}{a}\gamma_\mu \sin\left(ap_\mu\right) + \frac{2}{a}\sin^2\left(\frac{ap_\mu}{2}\right) + M_0\,, \tag{3.31}$$

where M_0 is the bare quark mass. Notice that, for fixed $|p_\mu| \neq \pi/a$, by expanding close to the continuum limit, the mass term correctly reproduces M_0. On the other hand, close to the corners of the Brillouin zone the mass term becomes

$$M\left(\pm\frac{\pi}{a}\right) = M_0 + \frac{2}{a}\,, \tag{3.32}$$

which then diverges as we take the limit $a \to 0$. In this sense, by using Wilson discretization of fermions, close to the continuum limit the doublers become excitations of the Wilson-Dirac operator with infinitely large masses which decouple

from the theory.

The corresponding Wilson-Dirac operator in coordinate space for interacting quarks in the massive theory reads

$$D_{\mathrm{w}} = \frac{1}{2}\left\{\gamma_\mu\left(\nabla^*_\mu + \nabla_\mu\right) - a\nabla^*_\mu\nabla_\mu\right\} + M_0\,. \tag{3.33}$$

As a final remark, notice that due to the presence of the Wilson term in the action, the quark mass term is not protected anymore from additive renormalization [103, 104].

In the following we will have a deeper insight about the nature of the doubling problem, which manifests itself, not simply as a computational issue, but rather as a consequence of a well known no-go theorem which relates the presence of such doublers to the possibility of defining a discretized chirally symmetric Dirac action.

3.3.3 Nielsen-Ninomiya no-go theorem

A well-known result demonstrated by Nielsen and Ninomiya in 1981 [105, 106, 107] relates the presence of fermion doublers to chiral symmetry. It states that it is not possible to define a discretized Dirac operator which satisfies the properties in Sec. 3.3.1 and, at the same time, is invariant under naïve chiral symmetry.

In general, each discretization of the Dirac operator must deal with this no-go theorem and at least one of the conditions above has to be waived in order to preserve chiral symmetry. As a result, any discretization which is free of fermion doublers must break naïve chiral symmetry. As we have seen, Wilson removed fermion doublers from the spectrum, by introducing the Wilson term which explicitly breaks naïve chiral symmetry [108]. Another possibility, explored by Ginsparg and Wilson in 1982 in Ref. [109], is to allow a mild breaking of chiral symmetry on the lattice together with a modified lattice version of chiral symmetry transformations.

In the following, some time is devoted to Ginsparg-Wilson fermions which will be used to properly derive the anomalous WTI that we formally defined in eq. 1.65.

3.3.4 Ginsparg-Wilson relation and anomalous WTI

In Ref. [109] Ginsparg and Wilson proposed to explicitly break chiral symmetry on the lattice, by modifying the continuum relation $\{\gamma_5, D\} = 0$ to

$$\{\gamma_5, D\} = aD\gamma_5 D\,. \tag{3.34}$$

The expression in eq. 3.34 provides an explicit breaking of chiral symmetry at finite lattice spacing, while the usual relation is recovered for $a \to 0$. By multiplying eq. 3.34 by the quark propagator D^{-1} on both sides, if there are no zero modes, we obtain

$$\left\{D^{-1}(x,y), \gamma_5\right\} = a\gamma_5\delta_{xy}\,. \tag{3.35}$$

With respect to the usual relation, now the chiral properties of the quark propagator are slightly modified by the contact term on the r.h.s. In this sense this is a soft and controlled breaking of chiral symmetry [18].

Notice that, when Ginsparg and Wilson introduced their relation, no Dirac operator was known to satisfy eq. 3.34 and only later it was realized that many different discretizations introduced to deal with chiral fermions on the lattice were formal solutions of the Ginsparg-Wilson relation. Some examples of such discretizations are the domain wall fermions introduced by Kaplan [110, 111], and the related Neuberger overlap operator [112, 113], and the perfect action by Hasenfratz [114, 115]. In 1998, Lüscher realized that fermionic actions constructed from a Dirac operator which satisfies the Ginsparg-Wilson relation exhibits a modified, but exact, chiral symmetry at finite lattice spacing which reproduces the original axial singlet transformations as $a \to 0$ [116]. Such modified symmetry is known as Lüscher symmetry.

Lüscher symmetry is the key ingredient we need to properly derive the formal expression we gave in eq. 1.65. Under infinitesimal Lüscher transformations, fermionic fields transform as

$$\begin{aligned}\delta\psi(x) &= i\epsilon^0_A\hat{\gamma}_5\psi(x)\,,\\ \delta\bar{\psi}(x) &= \bar{\psi}(x)i\epsilon^0_A\gamma_5\,,\end{aligned} \tag{3.36}$$

where $\hat{\gamma}_5 = \gamma_5 (1 - aD)$ which allows us to rewrite the Ginsparg-Wilson relation as $\gamma_5 D + D\hat{\gamma}_5 = 0$. By writing fermionic fields in terms of left and right handed spinors as

$$\begin{aligned} \psi_R &= \hat{P}_R \psi\,, \qquad \bar{\psi}_R = \bar{\psi} P_L \\ \psi_L &= \hat{P}_L \psi\,, \qquad \bar{\psi}_L = \bar{\psi} P_R\,, \end{aligned} \tag{3.37}$$

where the projectors are defined as

$$\hat{P}_{R/L} = \frac{1 \pm \hat{\gamma}_5}{2}\,, \qquad P_{R/L} = \frac{1 \pm \gamma_5}{2}\,, \tag{3.38}$$

the Dirac lagrangian can be written as

$$\bar{\psi} D \psi = \bar{\psi} P_R D \hat{P}_L \psi + \bar{\psi} P_L D \hat{P}_R \psi\,, \tag{3.39}$$

and correspondingly, by promoting the global transformations to a local ones, i.e. $\epsilon^0_A(x) = \epsilon^0_A \delta_{xy}$, under Lüscher transformations the action variation reads

$$\delta S = -i a^4 \epsilon^0_A \partial_\mu \mathcal{A}^0_\mu(x)\,. \tag{3.40}$$

The singlet axial current $\mathcal{A}^0_\mu(x)$ in eq. 3.40 is defined in terms of left and right projectors as [117]

$$\begin{aligned} \mathcal{A}^0_\mu(x) &= \bar{\psi} \left\{ P_L K_\mu(x) \hat{P}_R - P_R K_\mu(x) \hat{P}_\mu \right\} \psi \\ &= \frac{1}{2} \bar{\psi} \left\{ -\gamma_5 K_\mu(x) + K_\mu(x) \hat{\gamma}_5 \right\} \psi\,, \end{aligned} \tag{3.41}$$

where the kernel $K_\mu(x)$ reads

$$K_\mu(x) = -i \frac{\delta D(U^{(\alpha)})}{\delta \alpha_\mu(x)} \bigg|_{\alpha=0}\,, \tag{3.42}$$

where $\alpha_\mu = -\partial_\mu \epsilon^0_A(x)$ and $U^{(\alpha)}_\mu = e^{i\alpha_\mu(x)} U_\mu(x)$. In contrast to non-singlet chiral symmetry transformations, under Lüscher transformations in eq. 3.36 the path integral fermionic measure is no more invariant. In fact, under such transformations

the measure transforms as

$$\begin{aligned} d\bar{\psi}' d\psi' &= \left[\det\left(e^{i\epsilon_A^0 \hat{\gamma}_5}\right) \det\left(e^{i\epsilon_A^0 \gamma_5}\right)\right] d\bar{\psi} d\psi \\ &= \left[e^{-i\,\mathrm{Tr}\left(\epsilon_A^0 \hat{\gamma}_5\right)} \underbrace{e^{-i\,\mathrm{Tr}\left(\epsilon_A^0 \gamma_5\right)}}_{=1}\right] d\bar{\psi} d\psi \,, \end{aligned} \tag{3.43}$$

where the second exponential on the second line is one since $\mathrm{Tr}\,\gamma_5 = 0$. On the other hand, the first exponential on the r.h.s. can be expanded to give

$$\mathrm{Tr}\left[\epsilon_A^0(x)\hat{\gamma}_5\right] = -N_f \epsilon_A^0\, a\,\mathrm{tr}\left[\gamma_5 D(x,x)\right] \,, \tag{3.44}$$

where the N_f factor appearing on the r.h.s. is due to the trace over flavour indices, i.e. $\mathrm{tr}\left(\mathbb{1}_{N_f \times N_f}\right)$ and the remaining trace $\mathrm{tr}[\cdot]$ is over Dirac indices only. Finally we define the topological charge density as

$$a^4 q(x) = -\frac{a}{2}\mathrm{tr}\left[\gamma_5 D(x,x)\right] \,, \tag{3.45}$$

which implies that the anomalous contribution to the singlet WTI arising from the non-invariance of the path integral measure takes the form

$$i\,\mathrm{Tr}\left[\epsilon_A^0(x)\hat{\gamma}_5\right] = -iN_f \epsilon_A^0\, a\,\mathrm{tr}\left[\gamma_5 D(x,x)\right] = 2iN_f a^4 \epsilon_A^0 q(x) \,. \tag{3.46}$$

Finally by taking into account the action variation in eq. 3.40 and the anomalous contributions in eq. 3.46, one can easily recover the expression for the anomalous WTI, for a generic composite operator O, that we formally defined in eq. 1.65.

As a final comment, notice that the topological charge can be related to the spectral properties of the Ginsparg-Wilson operator in a form which recalls the *index theorem* [118, 119], i.e.

$$Q = a^4 \sum_x q(x) = -\frac{a}{2}\mathrm{tr}\left[\gamma_5 D\right] = n_+ - n_- = \mathrm{index}\,(D) \,, \tag{3.47}$$

where n_+ and n_- are the number of right and left handed zero modes of the Ginsparg-Wilson operator respectively. As a consequence of eq. 3.47, $Q \in \mathbb{Z}$ at finite lattice spacing.

3.4 Renormalization on the lattice

As we have seen in Sec. 1.4 renormalization is a key step to obtain a Quantum Field Theory. On the lattice renormalization is typically achieved by imposing a *hadronic renormalization scheme* in which the functional dependence of the bare parameters on the lattice spacing is obtained by fixing the value of some hadronic observable, which can be efficiently computed on the lattice, to a particular value. Let us restrict ourselves to observables depending on the bare coupling only and consider an observable Θ with mass dimension $d = 1$. Its physical value, provided by experiments, is Θ_{phys}, while $\hat{\Theta}(g_0, a) = a\Theta(g_0)$ is the corresponding dimensionless observable computed by lattice simulations at finite lattice spacing, for a fixed value of the bare coupling. The lattice scale is then set by imposing that the value of the physical quantity Θ_{phys} is kept constant at finite lattice spacing, i.e. $\hat{\Theta}(g_0, a) = a\Theta_{\text{phys}}$. This provides the relation

$$a = \frac{\hat{\Theta}(g_0, a)}{\Theta_{\text{phys}}}\,, \tag{3.48}$$

which implicitly defines the functional dependence of the bare coupling on the lattice spacing. Indeed, by inverting the above relation we find

$$g_0 = g_0(a\Theta_{\text{phys}})\,. \tag{3.49}$$

Similarly, when quark masses are included an additional set of hadronic observables must be chosen to fix the value of the bare masses. More generally, if the theory depends on N free bare parameters, then N different observables must be selected to fix their values. The relation in 3.48 together with the relations employed for fixing the bare quark masses defines the so called *lines of constant physics*, namely the trajectories in parameters space where the physics is kept constant for a given lattice spacing.

In full QCD, the set of bare parameters to be fixed is given by the bare coupling constant and the $N_f = 6$ bare quark masses. However, for practical simulations,

any scale E, in order to be efficiently described on the lattice, must satisfies

$$aE \ll 1\,, \tag{3.50}$$

namely, the lattice spacing has to be fine enough to resolve the scale E. This constraint limits *de facto* the possibility of simulating heavy quarks. For this reason most of the current lattice simulations are performed in presence of up, down and strange dynamical quarks and only recently the charm quark has been included [41].

3.5 Continuum limit and topological freezing

Once the functional dependence in eq. 3.48 is known we can probe the UV regime, i.e. the small lattice spacing regime, where perturbation theory is expected to work. Then by solving the corresponding beta function in the given renormalization scheme, we obtain for the bare coupling

$$g_0^2(a) \;=\; -\frac{1}{2b_0 \ln\left(a\Lambda_{\rm lat}\right)}\,, \tag{3.51}$$

wherer b_0 is the 1-loop universal coefficient in eq. 1.22 and $\Lambda_{\rm lat}$ is the Λ-parameter in the hadronic renormalization scheme. This implies that, due to renormalization group equations, for small lattice spacing the running of the bare coupling constant gives

$$\lim_{a\to 0} g_0 \;\equiv\; g^* \;=\; 0\,. \tag{3.52}$$

As a consequence, the beta function vanishes at g^* which represents a critical point of the theory. In this sense, different lattice discretizations that converge to the same continuum limit belongs to the same universality class. The universality of the continuum limit is assumed to be a general requirement at the non-perturbative level [120] and it has been proven in perturbation theory for some of those discretizations [121, 122].

In general, the continuum path integral in presence of periodic boundary con-

ditions can be defined as a sum of distinct contributions coming from disconnected topological sectors. On the other hand, at finite lattice spacing this is not true and the tunnelling between different topological sectors is allowed. In particular, at finite lattice spacings, the probability of visiting different topological sectors drops dramatically as $a \to 0$ leading to the so called *topological freezing* [123, 124, 125]. In this sense the tunnelling between different sectors is just a cut-off effect which vanishes in the continuum limit producing the expected disconnected sectors[2]. In such a way, topological freezing directly affects the correctness of standard algorithms (see Sec. 3.7) and the cost of the numerical computation for small lattice spacings, by making simulations close to the continuum limit extremely demanding.

3.6 Symanzik's effective action

A deeper insight on the continuum limit extrapolation is provided in the context of the *Symanzik's effective theory*. In his seminal papers [128, 129], Symanzik proposed to consider the lattice theory as a formal fundamental theory at the hard scale $1/a$. In this context, we can define a continuum effective field theory which describes the low energy regime by simply taking into account the most general action which includes all the possible operators with mass dimension $d > 4$ with the correct symmetry properties. The Symanzik's effective continuum action reads

$$S_{\text{eff}} = S_0 + aS_1 + a^2 S_2 + \dots , \tag{3.53}$$

where S_k contains operators with mass dimension $d = 4 + k$ and S_0 is the standard QCD continuum action which is recovered by sending $a \to 0$. In the same way, in an effective field theory approach, renormalized fields ϕ_R can be written as effective fields obtained by taking into account linear combinations of higher dimensional composite operators with the appropriate symmetries, i.e.

$$\phi_{\text{eff}}(x) = \phi_0(x) + a\phi_1(x) + a^2\phi_2(x) + \dots , \tag{3.54}$$

[2]Numerical evidence shows that the size of the barrier between two distinct topological sectors grows as a^{-6}. See Ref. [126, 127] for possible solutions to overcome this problem.

where again ϕ_0 represents the usual field in the continuum limit. Starting from these definitions we can study how the continuum limit is approached, by simply matching a generic n-point correlation function computed on the lattice with the same quantity computed in the context of the Symanzik's effective theory. By assuming that the ϕ field renormalizes multiplicatively and that the renormalized correlation function does not mix with any other operator, the lattice correlation function reads

$$G_n^{\mathrm{R}}(x_1, \ldots, x_n) = (Z_\phi)^n \langle \phi(x_1) \ldots \phi(x_n) \rangle_{\mathrm{lat}} \,, \tag{3.55}$$

where it has been evaluated at non-zero separation of space-time coordinates to avoid any possible contact term. Similarly, by using eq. 3.53 and 3.54, the n-point function in the continuum effective theory can be expanded for small a as

$$\begin{aligned} G_n^{\mathrm{R}}(x_1, \ldots, x_n) &= \langle \phi_0(x_1) \ldots \phi_0(x_n) \rangle_{\mathrm{cont}} \\ &\quad - a \langle \phi_0(x_1) \ldots \phi_0(x_n) S_1 \rangle_{\mathrm{cont}} \\ &\quad + a \sum_{k=1}^{n} \langle \phi_0(x_1) \ldots \phi_1(x_k) \ldots \phi_0(x_n) \rangle_{\mathrm{cont}} + O(a^2) \,, \end{aligned} \tag{3.56}$$

where $\langle \cdot \rangle_{\mathrm{cont}}$ denotes that the expectation value has been computed with respect to the continuum action S_0. Notice that in principle any contact term can be absorbed in a redefinition of ϕ_1. In this way, by matching eq. 3.55 and eq. 3.56 we obtain

$$\begin{aligned} (Z_\phi)^n \langle \phi(x_1) \ldots \phi(x_n) \rangle_{\mathrm{lat}} &= \langle \phi_0(x_1) \ldots \phi_0(x_n) \rangle_{\mathrm{cont}} \\ &\quad - a \langle \phi_0(x_1) \ldots \phi_0(x_n) S_1 \rangle_{\mathrm{cont}} \\ &\quad + a \sum_{k=1}^{n} \langle \phi_0(x_1) \ldots \phi_1(x_k) \ldots \phi_0(x_n) \rangle_{\mathrm{cont}} + O(a^2) \,, \end{aligned} \tag{3.57}$$

where the second and the third line on the r.h.s. provide the leading correction in the lattice spacing with respect to the continuum result. Notice that in general, depending on the discretization effects of the discretized action, the leading correction will be proportional to a^p with $p \geq 1$ [130]. For instance for the gluonic Wilson action we expect $p = 2$, while for the Wilson discretization of the Dirac

action we expect $p = 1$.

As a final remark, notice that, as usual in the context of effective field theories, any higher dimensional operator comes multiplied by a dimensionless coefficient which explicitly depends on the cut-off. As a consequence the coefficients multiplying the $O(a)$ correction can themselves depend on the lattice spacing [131] and it can be proven in perturbation theory that this dependence is at most logarithmic [132, 133].

3.6.1 $O(a)$-improvement

The Symanzik's effective action allows a deeper understanding on how lattice observables approach the continuum limit. The obvious outcome is taking advantage of this knowledge to construct lattice discretizations with a better behaviour as we approach the continuum limit. Indeed, this is in principle possible, thanks to the fact the there is quite a freedom in the definition of the discretized action.

The idea is then to modify the lattice action by adding the discretized version of the irrelevant operators appearing in the continuum Symanzik's effective action with some coefficients which are properly tuned to remove cut-off effects at a given order.

For instance, we have seen that Wilson's formulation for fermions suffers from $O(a)$ discretization effects. In order to remove them we focus on the $O(a)$ corrections appearing in S_1, by taking into account all the operators with mass dimension $d = 5$ which preserve the symmetries of the continuum action, i.e. gauge and rotational invariance, parity and charge conjugation. Only five different operators are found to satisfy these conditions [134]. Those read in the continuum

$$O_1 = \bar{\psi}\sigma_{\mu\nu}F_{\mu\nu}\psi\,, \tag{3.58}$$

$$O_2 = \bar{\psi}D_\mu D_\mu\psi + \bar{\psi}\overleftarrow{D}_\mu\overleftarrow{D}_\mu\psi\,, \tag{3.59}$$

$$O_3 = m\,\mathrm{Tr}\left\{F_{\mu\nu}F_{\mu\nu}\right\}\,, \tag{3.60}$$

$$O_4 = m\left\{\bar{\psi}\gamma_\mu D_\mu\psi - \bar{\psi}\overleftarrow{D}_\mu\gamma_\mu\psi\right\}\,, \tag{3.61}$$

$$O_5 = m^2\bar{\psi}\psi\,, \tag{3.62}$$

where $\sigma_{\mu\nu} = \frac{i}{2}[\gamma_\mu, \gamma_\nu]$ and D_μ is covariant derivative. Notice that in principle not all the dimension 5 operators above are independent. By applying the field equations for the fermionic fields, one finds the relations

$$O_1 - O_2 + 2O_5 = 0\,, \tag{3.63}$$

$$O_4 + 2O_5 = 0\,. \tag{3.64}$$

In such a way, only three of them are independent and the remaining two can be removed, say O_2 and O_4. As a consequence the corresponding lattice action can be modified with the additional term

$$S_1 = a^5 \sum_x \left\{ c_1 O_1^{\text{lat}} + c_3 O_3^{\text{lat}} + c_5 O_5^{\text{lat}} \right\}\,, \tag{3.65}$$

being O_i^{lat} the lattice version of the operators appearing in eq. 3.58, 3.60 and 3.62 and c_i the coefficients which have to be tuned in the lattice spacing to remove $O(a)$ cut-off effects. O_3 and O_5 can be further removed by properly redefining the bare coupling constant and the bare quark masses if those are discretized by using the plaquette field the local scalar density respectively. The remaining action then reads

$$S_1 = a^5 \sum_x c_{\text{sw}} \bar{\psi}(x) \frac{1}{4} \sigma_{\mu\nu} F_{\mu\nu}^{\text{lat}} \psi(x)\,, \tag{3.66}$$

where $F_{\mu\nu}^{\text{lat}}$ is a proper discretization of the field strength tensor and c_{sw} is known as *Sheikholeslami-Wohlert coefficient* [134]. Its value is, in general, a function of the bare coupling constant and has to be properly tuned to remove $O(a)$ discretization effects [135]. A common choice for $F_{\mu\nu}^{\text{lat}}$ is given by the symmetrized *clover* discretization

$$F_{\mu\nu}^{\text{lat}} \equiv \hat{F}_{\mu\nu} = -\frac{i}{8a^2}\left[Q_{\mu\nu}(x) - Q_{\nu\mu}(x)\right] \tag{3.67}$$

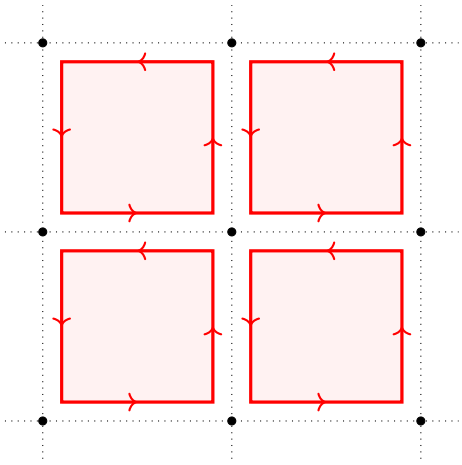

Figure 3.3: Graphical representation of the sum of plaquette fields $Q_{\mu\nu}$ as defined in eq. 3.68.

with

$$\begin{aligned} Q_{\mu\nu} \;=\; & U_\mu(x)U_\nu(x+a\hat{\mu})U_\mu^\dagger(x+a\hat{\nu})U_\nu^\dagger \\ & + U_\nu(x)U_\mu^\dagger(x-a\hat{\mu}+a\hat{\nu})U_\nu^\dagger(x-a\hat{\mu})U_\mu(x-a\hat{\mu}) \\ & + U_\mu^\dagger(x-a\hat{\mu})U_\nu^\dagger(a-a\hat{\mu}-a\hat{\nu})U_\mu(x-a\hat{\mu}-a\hat{\nu})U_\nu(x-a\hat{\nu}) \\ & + U_\nu^\dagger(x-a\hat{\nu})U_\mu(x-a\hat{\nu})U_\nu(x+a\hat{\mu}-a\hat{\nu})U_\nu^\dagger(x)\,. \end{aligned} \tag{3.68}$$

In this way the lattice $O(a)$-improved Dirac operator can be written as

$$D \;=\; D_{\rm w} + aD_{\rm sw}\,, \tag{3.69}$$

where $D_{\rm w}$ is the standard Wilson discretization of fermions provided in eq. 3.33 and $D_{\rm sw}$ is the Sheikholeslami-Wohlert operator

$$D_{\rm sw} \;=\; c_{\rm sw}(g_0)\frac{1}{4}\sigma_{\mu\nu}\hat{F}_{\mu\nu}(x)\,. \tag{3.70}$$

At leading order in perturbation theory it holds $c_{\rm sw} = 1$ [134], while at 1-loop the Sheikholeslami-Wohlert coefficient has been computed in Ref. [136] and its non-perturbative determination, for the Wilson plaquette action, is provided in Ref.

[137], leading to the expression for $N_f = 3$ quarks

$$c_{\rm sw}(g_0) = \frac{1 - 0.194785 g_0^2 - 0.110781 g_0^4 - 0.0230239 g_0^6 + 0.137401 g_0^8}{1 - 0.460685 g_0^2} . \tag{3.71}$$

Notice that in general, in order to achieve a complete $O(a)$-improvement, fields and composite operators have to be improved as well, by properly identifying higher dimensional operators with the same symmetries, see eq. 3.54. However if we are only interested in spectral quantities, e.g. hadron masses, it is sufficient to achieve an $O(a)$-improvement at the action level to guarantee that such quantities approach the continuum limit with $O(a^2)$ cut-off effects [138].

Given these definitions we can finally give the path integral formulation for $O(a)$-improved Wilson fermions. The partition function reads

$$Z_{\rm lat} = \int DU D\psi D\bar{\psi}\, e^{-S_g^{(\rm W)} - S_{\rm w}} , \tag{3.72}$$

where $S_g^{(\rm W)}$ is the Wilson's plaquette action defined in eq. 3.14, $S_{\rm w}$ is the fermionic action with the $O(a)$-improved Wilson-Dirac operator obtained in eq. 3.69 and finally the gluonic and fermionic integration measures are defined in eq. 3.18 and 3.24 respectively.

3.7 Monte Carlo methods for lattice QCD

In this section we provide a brief overview of the main computational strategies an tools which are currently used in numerical simulations of QCD and which we exploited in this thesis.

For the time being, we consider the path integral for a generic fundamental field ϕ. The analogy between the path integral formulation of a QFT in euclidean space-time and a purely statistical system implies the identification of the normalized probability density for a gauge field configuration with

$$P[\phi] = \frac{1}{Z} e^{-S[\phi]} . \tag{3.73}$$

Notice that this interpretation holds as long as the action is purely real and

bounded. With the correspondence provided in eq. 3.73, the vacuum expectation value of a generic composite operator $\mathcal{O}$ is interpreted as the statistical average of such operator over the field configurations as

$$\langle \mathcal{O} \rangle = \frac{1}{Z} \int D[\phi]\, \mathcal{O}(\phi) e^{-S[\phi]}\,. \tag{3.74}$$

In this context Monte Carlo methods provide the ideal tool to numerically compute high dimensional integrals like the one in eq. 3.74. In this way, given a representative ensable of gauge fields distributed according to the probability density in eq. 3.73, the best estimate of the expectation value is

$$\bar{\mathcal{O}} \equiv \frac{1}{N} \sum_{i=1}^{N} \mathcal{O}(\phi_i) = \langle \mathcal{O} \rangle + O\left(\frac{1}{\sqrt{N}}\right) \tag{3.75}$$

where N is the size of the ensamble. Remarkably the uncertainty provided by the Monte Carlo integration scales as $1/\sqrt{N}$ and has a purely statistical interpretation.

Representative ensambles are usually generated by Markov Chains, which are defined by a transition probabiliy $T(\phi \to \phi')$, which describes the probability of extracting the field ϕ' starting from ϕ. In general, for an ergodic Markov Chain, in order to generate field configurations according the expected probability distribution in eq. 3.73, the so called *equilibrium distribution*, it is sufficient for the corresponding transition probability to satisfy the *detailed balance* condition. The easiest way to construct transition probabilities which satisfy detailed balance is by using the Metropolis-Hastings algorithm [139, 140]. In such a way a new field configuration is extracted according to a proposal probability and then it is accepted or rejected according to an acceptance probability based on some criterion. In this sense, generating field configurations in an efficient way will translates into having a high acceptance rate. Notice that in practical lattice QCD simulations, when dynamical fermions are included, a local application of the Metropolis algorithm with a single-link update is not feasible. The reason is that, as we will see in the following section, once the integral over fermionic fields is explicitly performed, the resulting functional integral is non-local in the gauge fields. This in turn would imply a tremendous computational cost to have a reasonable acceptance rate. A different, global, approach is discussed in the following section.

3.7.1 Hybrid Monte Carlo for QCD

One of the most efficient way to generate gauge field ensambles is represented by the Hybrid Monte Carlo (HMC) algorithm [141]. Before focusing on the details of the HMC algorithm, let us consider the lattice QCD partition function in eq. 3.72. By expanding the fermionic action, it reads

$$Z_{\text{lat}} = \int DUD\psi D\bar{\psi} e^{-S_g[U]-\bar{\psi}D[U]\psi}\,, \tag{3.76}$$

where S_g and $D[U]$ are the Wilson's plaquette action and the Wilson-Dirac operator for fermions. Since the integration over fermionic fields is a gaussian integral on Grassmann variables, it can be carried out explicitly and leads to

$$Z_{\text{lat}} = \int DU\ (\det D[U])^{N_f}\, e^{-S_g[U]}\,. \tag{3.77}$$

A few comments are in order. On one hand notice that the Dirac operator is a $V \times V$ sparse matrix and a direct calculation of its determinant is not feasible in terms of computer time. On the other hand, in general, it is not guaranteed that the determinant of the Wilson-Dirac operator is positive. As a consequence, in presence of an odd number of non-degenerate quarks, the correspondence between the QFT path integral and the statistical interpretation provided by eq. 3.73 is potentially spoiled.

In the case of an even number of degenerate flavours, thanks to γ_5-hermiticity of the Dirac operator, the squared of the quark determinant is positive-defined. Furthermore, it can be written in terms of bosonic *pseudofermion* fields ϕ and $\phi^\dagger$. For instance for $N_f = 2$ [142]

$$(\det D[U])^2 = \det Q^2 \propto \int D\phi^\dagger D\phi\, e^{-S_{\text{pf}}}\,, \tag{3.78}$$

where in order to correctly reproduce the quark determinant by performing the bosonic gaussian integration, the pseudofermionic action is defined as

$$S_{\text{pf}} = \sum_x \phi^\dagger Q^{-2}\phi\,, \tag{3.79}$$

with $Q = \gamma_5 D$. The core idea behind the HMC algorithm is to write down the corresponding hamiltonian system and evolving the degrees of freedom by numerically integrating the Hamilton's equation. In this way the evolved gauge field provides the proposal in the Metropolis-Hastings algorithm. In order to write the corresponding hamiltonian system, let us introduce the algebra-valued conjugate momentum variables $\pi_\mu(x) = T^a \pi^a_\mu(x)$, which we assume to be sampled from a gaussian distribution at each step in the Markov Chain. The corresponding hamiltonian reads

$$H[U,\pi] = \frac{1}{2}(\pi,\pi) + S_g[U] + S_{\rm pf}[U,\phi,\phi^\dagger], \tag{3.80}$$

where $(\pi,\pi) = \sum_{x,\mu,a} |\pi^a_\mu(x)|^2$ denotes the $SU(3)$ algebra scalar product. In this formalism, the evolution of the gauge field is controlled, in terms of simulation time t, by the Hamilton's equation

$$\partial_t U_\mu(x) = \pi_\mu(x) U_\mu(x), \tag{3.81}$$

$$\partial_t \pi_\mu(x) = -F^g_\mu(x) - F^{\rm pf}_\mu(x), \tag{3.82}$$

where, by recalling the expression for the Wilson's plaquette action in eq. 3.14 and the pseudofermionic action in eq. 3.79, the gluonic and pseudofermionic forces are respectively defined as

$$F^g_\mu(x) = \frac{\partial}{\partial U_\mu(x)} S_g[U] \tag{3.83}$$

$$F^{\rm pf}_\mu(x) = \frac{\partial}{\partial U_\mu(x)} S_{\rm pf}[U]. \tag{3.84}$$

The hamiltonian evolution described by the equations above is often referred to as *molecular dynamics* evolution. Notice that in the molecular dynamics, the pseudofermion fields are kept fixed. By explicitly performing the derivative in eq. 3.84, the pseudofermion force involves a double inversion of the Dirac operator, which represents the most expensive part of a simulation in terms of computer time. The numerical integration of the Hamilton's equation is performed by discretizing the trajectory τ into smaller intervals with finite step-size and by using generic symplectic integrators [143, 144]. Once the dynamical integration has been performed

and the fields have evolved from the initial configuration $\left(U_\mu^{(i)}, \pi_\mu^{(i)}\right)$ to the final configuration $\left(U_\mu^{(f)}, \pi_\mu^{(f)}\right)$, an accept-reject step is performed in order to guarantee that the new configuration is distributed according to the desired equilibrium distribution. Notice that this last step is somehow crucial, since the numerical integration does not preserve the hamiltonian.

It is worth noticing, however, that in real simulations, in particular for small quark masses [145], the use of a single pseudofermion is impractical. The reason is that the pseudofermion force is often affected by large fluctuations which drastically reduce the acceptance rate of the HMC algorithm. Such fluctuations are possibly tamed by the frequency splitting introduced in Ref. [146, 147], which can produce sensible improvements if combined with multiple-step integration [148].

3.7.2 Rational HMC

So far we discussed only the case of two degenerated flavours. This case is particularly interesting given the very small difference in the up and down quark masses. However, when the strange quark is introduced, the positivity of the probability distribution in the path integral is, in general, no more guaranteed. The positivity is guarateed only for discretizations which preserve chiral symmetry [149], which is not the case of Wilson fermion. In such case, it is possible to encounter regions, in configuration space, which provides a negative-valued quark determinant and, as a consequence, the entire construction based on the statistical interpretation of the path integral is spoiled. In general, it is assumend that such regions give a negligible contribution to the path integral and then can be neglected. The reason relies on the fact that the Dirac operator for the strange quark has a large mass-gap provided by the strange quark mass, and, as a consequence, only few exceptional gauge field configurations can lead to negative-valued determinant, see Ref. [150] for a further discussion on this topic. If this is the case, then we can simply write the strange quark determinant as [151, 152]

$$\det\left(Q_s\right) \to \det\left(\sqrt{Q^2}\right) = \det\left(W\right)\det\left(R^{-1}\right), \tag{3.85}$$

where in the last step we introduced the operators $W = |Q|R$ and R. The latter provides a rational approximation for the function $1/\sqrt{Q^2}$. In general the rational approximantion is a Zolotarev rational function of degree (n, n) which depends on the spectral properties of the operator Q^2. It can be written as

$$R = r_b R_{n,\epsilon}\left(r_b^{-2} Q^{-2}\right) , \tag{3.86}$$

where $\epsilon = (r_a/r_b)^2$ and r_a and r_b are two numbers such that most of the eigenvalues λ of the operator $\sqrt{Q^2}$ belongs to the interval $[r_a, r_b]$, in order to guarantee that the operator R^{-1} is a good approximation of $\sqrt{Q^2}$ for most of the gauge field configurations. The rational approximation $R_{n,\epsilon}$ is then provided by

$$R_{n,\epsilon}(x) = A\frac{(x+a_1)\dots(x+a_{2n-1})}{(x+a_2)\dots(x+a_{2n})} \approx \frac{1}{\sqrt{x}} , \tag{3.87}$$

where $a_1 > \dots > a_{2n}$ and $A > 0$ are free parameters which have to be properly tuned in order to minimize the error of the approximation $\delta = \max_{\epsilon \le x \le 1} |1 - \sqrt{x} R_{n,\epsilon}(x)|$. In such a way, we can proceed as before by writing the quark determinant in terms of pseudofermions actions, i.e. from eq. 3.85 the pseudofermion action reads

$$S_{\mathrm{pf,s}} = \left(\phi_1, W^{-1}\phi_1\right) + \left(\phi_2, R\phi_2\right) . \tag{3.88}$$

In standard algorithms, only the second term on the r.h.s enters into the molecular dynamics, while the first one is treated as a reweighting factor, which can be computed stochastically and included, *a posteriori*, as part of the observables.

Notice that, similarly to the case of $N_f = 2$ described in the previous section, the use of a single pseudofermion is impractical in realistic simulations and methods like the frequency splitting described above can be used for the strange quark determinant as well.

The purpose of this section was to give a pedagogical introduction to the most widely used algorithm to generate gauge field configurations. Other technical, but relevant, details, such as the various type of solvers employed in the inversion of the Dirac operator [153], as well as any algorithmic technique used to allow a faster inversion for small quark masses were completely omitted [154, 155]. For those

and other relevant topics we refer to Ref. [149] for a more complete and detailed discussion.

3.8 QCD hadronic spectrum

As we have seen in Chapter 1, some peculiar features of the QCD spectrum can be direcly inferred by the study of the QCD lagrangian symmetries. However the explicit values of the hadron masses still remains inaccessible to any analytic calculation, due to the non-perturbative nature of QCD at low energies. For this reason, a determination of the hadronic spectrum from first principle is only possible in the context of the lattice regularization.

Historically, the determination on the lattice of the QCD spectrum has been both a fundamental check of the theory and a remarkable success of the lattice framework as well. While the first lattice determinations were restricted to the quenched approximation and were affected by large and not fully under control systematic errors, current lattice calculations provide a detailed and satisfactory representation of the masses of the light pseudoscalar mesons as well as of the baryonic octet, see fig. 1.5. In the following sections we will describe how the hadronic spectrum can be extracted from lattice calculations.

3.8.1 Transfer matrix

The partition function for an euclidean field theory discretized on a lattice with periodic temporal extent L_0, can be written in terms of the so-called *transfer matrix*, $\mathcal{T}$, as

$$Z = \mathrm{Tr}\left[\mathcal{T}_0^N\right], \tag{3.89}$$

where $N = L_0/a$ and the trace is over the Hilbert space of the physical states $|\epsilon_n\rangle$ of the theory. The underlying meaning of the transfer matrix formalism is to describe the probability for a quantum state to propagate in the infinitesimal time-interval $[t, t+a]$. By construction, the transfer matrix is a unitary matrix

and can be written as

$$\mathcal{T} = e^{-a\hat{H}}, \qquad \text{where} \qquad \hat{H}\,|\epsilon_n\rangle = E_n\,|\epsilon_n\rangle\,, \tag{3.90}$$

where $\hat{H}$ is a hermitian matrix which corresponds, up to discretization errors, to the hamiltonian of the system. As a consequence, the expectation value of a generic time-ordered two-point correlation function involving the operators $\hat{O}_1$ and $\hat{O}_2$ evaluated at euclidean time t_1 and t_2, with $t_1 > t_2$ can be written as

$$\langle \hat{O}_1(t_1)\hat{O}_2(t_2)\rangle_{L_0} = \frac{1}{Z}\,\mathrm{Tr}\left[\mathcal{T}^{N-(n_1-n_2)}\,\hat{O}_2\,\mathcal{T}^{n_1-n_2}\,\hat{O}_1\right], \tag{3.91}$$

where $n_i = t_i/a$ for $i = 1, 2$ are the temporal coordinates expressed in terms of lattice units. Here $\langle\cdot\rangle_{L_0}$ refers to the fact that the correlation function is computed at finite temporal extent L_0. By making explicit the trace over the Hilbert space, it reads

$$\begin{aligned}\langle \hat{O}_1(t_1)\hat{O}_2(t_2)\rangle_{L_0} &= \frac{1}{\sum_k \langle\epsilon_k|\,\mathcal{T}^N\,|\epsilon_k\rangle}\left\{\sum_k \langle\epsilon_k|\,\mathcal{T}^{N-(n_1-n_2)}\,\hat{O}_2\,\mathcal{T}^{n_1-n_2}\,\hat{O}_1\,|\epsilon_k\rangle\right\} \\ &= \frac{1}{\sum_k e^{-E_k L_0}}\left\{\sum_k e^{-E_k(L_0-t_1+t_2)}\,\langle\epsilon_k|\,\hat{O}_2\,\mathcal{T}^{n_1-n_2}\hat{O}_1\,|\epsilon_k\rangle\right\},\end{aligned} \tag{3.92}$$

where the second line is simply obtained by inserting a complete set of eigenstates of the hamiltonian and using eq. 3.90. Notice that by keeping the lattice spacing constant and taking the infinite volume limit, $L_0 \to \infty$, the exponential functions at numerator and denominator are dominated by the lowest energy state $|\epsilon_0\rangle$, i.e the vacuum of the theory. The correlation function then reads

$$\langle \hat{O}_1(t_1)\hat{O}_2(t_2)\rangle_{\infty} = e^{E_0(t_1-t_2)}\,\langle\epsilon_0|\,\hat{O}_2\,\mathcal{T}^{n_1-n_2}\,\hat{O}_2\,|\epsilon_0\rangle\,. \tag{3.93}$$

As a final step, by inserting a complete set of eigenstates of the hamiltonian $\hat{H}$ and taking the large separation limit, i.e. $\Delta t \equiv t_1 - t_2 \to \infty$, the two-point correlation

function can be written in the final form

$$\lim_{\Delta t\to\infty}\langle\hat{O}_1(t_1)\hat{O}_2(t_2)\rangle_\infty = \lim_{\Delta t\to\infty}\sum_n e^{-(E_n-E_0)\Delta t}\langle\epsilon_0|\hat{O}_2|\epsilon_n\rangle\langle\epsilon_n|\hat{O}_1|\epsilon_0\rangle$$
$$= e^{-(\bar{E}-E_0)\Delta t}\langle\epsilon_0|\hat{O}_2|\bar{\epsilon}\rangle\langle\bar{\epsilon}|\hat{O}_1|\epsilon_0\rangle\,, \tag{3.94}$$

where $\bar{E}$ is the lowest energy state which provides a non-zero matrix element for the operators $\hat{O}_1$ and $\hat{O}_2$. Notice that the mass gap $\bar{E}-E_0$ depends on the quantum number of $\hat{O}_1$ and $\hat{O}_2$ and the convergence rate, due to the exponential suppression of the excited states, depends on the relative magnitude of the first excited state.

As a final remark, notice that the correlation function in eq. 3.94 is not projected to a definite value of spatial momentum. In such case $\bar{E} = \bar{E}(\mathbf{p})$ and the corresponding mass is related to $\bar{E}$ by a dispersion relation. In order to isolate zero-momentum states and then to extract the mass of the ground state it is sufficient to project to zero momentum, by simply summing over the spatial coordinates of one of the two interpolating operators. In this way, the two-point correlation function in the infinite volume limit, at finite lattice spacing reads

$$C_{O_1,O_2}(t_1-t_2) = e^{-(\bar{E}-E_0)\Delta t}\langle\epsilon_0|\hat{O}_2|\bar{\epsilon}\rangle\langle\bar{\epsilon}|\hat{O}_1|\epsilon_0\rangle\,, \tag{3.95}$$

where now $\hat{O}_i$ are meant to be averaged over the spatial coordinates. In the equation above the dependence on the euclidean time is entirely provided by the exponential, which then determines the asymptotic behaviour of the correlation function for large temporal separations.

3.8.2 Hadronic correlation functions on the lattice

The key step to extract hadron masses from two-point correlation functions on the lattice is two construct the correct interpolating operators carrying the desired quantum numbers, see Chapters 1 and 2 for the corresponding definitions in the continuum limit. Notice that in principle there is quite a freedom in this procedure, being the only constraint given by the set of quantum numbers.

In general, on the lattice, the calculation of correlation functions involving quark fields is performed by explicitly carrying out Wick contractions between

two distinct quark fields. As a consequence, the basic element in such calculations is the quark propagator

$$S_{ab}^{\alpha\beta}(x,y) \equiv D^{-1}(x,y) = \langle \psi_a^\alpha(x) \bar{\psi}_b^\beta(y) \rangle_F \,, \tag{3.96}$$

where the expectation value $\langle \cdot \rangle_F$ is taken by integrating over the fermionic fields. In the above expression, we often refer to the quark field $\psi(x)$ as the *sink* operator and to $\bar{\psi}(y)$ as the *source* operator. With this definition, the most general fermionic correlation function can be directly written in terms of quark propagators only.

In principle, one could construct interpolating operators of arbitrary complexity, describing exotic states composed of n valence quark with the only constraint for them to be singlet operators in colour space. However, for the purpose of this thesis we are mainly interested in mesonic and baryonic lattice operators. The most general mesonic interpolating operator reads

$$O^a(x) = \bar{\psi}(x) \Gamma_O \tau^a \psi(x) \,, \tag{3.97}$$

where $\tau^a = \left\{ \mathbb{1}/\sqrt{2N_f}, T_a \right\}$ defines the flavour composition of the interpolating operator, while Γ_O is a generic combination of Dirac gamma matrices which defines the spin structure and the transformation properties of the operator under parity and charge-conjugation transformations, see App. B.1. In such a way, O^a would describe flavour singlet ($a = 0$) or flavour non-singlet ($a \neq 0$) states with the usual J^{PC} quantum numbers. The corresponding euclidean time two-point correlation function projected to zero spatial momentum reads on the lattice

$$C_O^a(x_0) = a^3 \sum_{\mathbf{x}} \langle O^a(x) O^a(0) \rangle \,, \tag{3.98}$$

where no summation over flavour index a is understood. Notice that it is always possible to define the source operator at $y = 0$ due to translational invariance. By inserting the expression of the interpolating operator in eq. 3.97 and applying Wick's theorem, the correlation function can be written in terms of all the possible

Wick contractions as

$$C_O^a(x_0) = a^3 \sum_{\mathbf{x}} \Big\{ - \langle \mathrm{Tr}\left[\tau^a \Gamma_O S(x,0) \tau^a \Gamma_O S(0,x)\right] \rangle + \langle \mathrm{Tr}\left[\tau^a \Gamma_O S(x,x)\right] \mathrm{Tr}\left[\tau^a \Gamma_O S(0,0)\right] \rangle \Big\} . \tag{3.99}$$

where the trace is over colour, spin and flavour indices. Notice that, since the quark propagator is diagonal in flavour space, the trace over flavour indices can be carried out explicitly by simply using the relations in App. A.1. Eq. 3.99 can then be written as

$$C_O^a(x_0) = a^3 \sum_{\mathbf{x}} \Big\{ - \frac{1}{2} \langle \mathrm{Tr}\left[\Gamma_O S(x,0) \Gamma_O S(0,x)\right] \rangle + \frac{N_f}{2} \delta^{a0} \langle \mathrm{Tr}\left[\Gamma_O S(x,x)\right] \mathrm{Tr}\left[\Gamma_O S(0,0)\right] \rangle \Big\} . \tag{3.100}$$

On one hand, the first term on the r.h.s., the *connected contribution*, takes into account quark propagation between two displaced space-time coordinates, while, on the other hand, the second term, the *disconnected contribution*, which appears only for singlet two-point correlation functions, includes quark loops. Finally, by using γ_5-hermiticity of the Dirac operator, which translates at the level of the quark propagator to $S^\dagger(x,y) = \gamma_5 S(y,x) \gamma_5$, the mesonic correlation function can be written in its final form as

$$C_O^a(x_0) = \frac{a^3}{2} \sum_{\mathbf{x}} \Big\{ - \langle \mathrm{Tr}\left[\Gamma_O S(x,0) \Gamma_O \gamma_5 S^\dagger(x,0) \gamma_5\right] \rangle + \delta^{a0} N_f \langle \mathrm{Tr}\left[\Gamma_O S(x,x)\right] \mathrm{Tr}\left[\Gamma_O S(0,0)\right] \rangle \Big\} . \tag{3.101}$$

Notice that by taking the conjugate transpose of the correlation function in eq. 3.101 one can easily see that it holds $C_O^a(x_0) = C_O^a(x_0)^\dagger$, i.e. the correlation function is real, as long as $\Gamma_O^\dagger = \pm \gamma_5 \Gamma_O \gamma_5$, see App. B.2 for a more detailed discussion. This is the case, for instance, of flavour non-singlet ($a \neq 0$) operator with spin structure dictated by $\Gamma_O = \{\mathbb{1}, \gamma_5, \gamma_\mu, \gamma_\mu \gamma_5\}$, on which we will focus in this thesis.

A similar analysis can be carried out for the nucleon interpolating operator in eq. 2.49 which describe a $J^P = \frac{1}{2}^\pm$ state. In such case, by making explicit the

flavour content of the operator, the corresponding two-point nucleon correlation function can be written as

$$\begin{aligned} C_{N^\pm}(x_0) &= a^6 \sum_{\mathbf{x}} \langle \mathrm{Tr}\left[P_\pm N(x)\overline{N}(0)\right]\rangle \\ &= a^6 \sum_{\mathbf{x}} \langle \left[W_\pm^1(x,0) - W_\pm^2(x,0)\right]\rangle \,, \end{aligned} \tag{3.102}$$

where in the first line the trace is over Dirac indices only and $P_\pm$ is the parity projector $P_\pm = (1 \pm \gamma_0)/2$, while $W_\pm^1$ and $W_\pm^2$ in the second line are the Wick contractions obtained by integrating over the fermion fields. Their expressions read

$$\begin{aligned} W_\pm^1(x,0) &= \mathrm{Tr}\left[S_{ag}^T(x,0) C\gamma_5 S_{bf}(x,0) C\gamma_5\right] \mathrm{Tr}\left[S_{ce}(x,0) P_\pm\right] \epsilon^{abc}\epsilon^{feg} \\ W_\pm^2(x,0) &= \mathrm{Tr}\left[S_{ag}^T(x,0) C\gamma_5 S_{be}(x,0) P_\pm S_{cf}(x,0) C\gamma_5\right] \epsilon^{abc}\epsilon^{feg} \,, \end{aligned} \tag{3.103}$$

where we made explicit colour indices in the quark propagators. As for mesonic correlation functions, it is possible to see that the nucleon correlation function in eq. 3.102 is purely real. In App. B.3 we give a proof of the reality of this correlation function, based on the derivation performed in Ref. [156].

To conclude this section, notice that in principle it is also possible to define an interpolating operator for a $J^P = \frac{3}{2}^\pm$ state by simply modifying the gamma content in the diquark operator (Γ_B in eq. 2.48). In such case the resulting interpolating operator receives contributions both by spin-1/2 and spin-3/2 states and a further spin-projection, which is in general momentum-dependent, is required in order to correctly decouple the spin-3/2 and the spin-1/2 state [157].

3.8.3 Signal-to-Noise ratio for hadronic observables

By combining the knowledge of the tranfer matrix we defined in Sec. 3.8.1 with the hadronic lattice correlation functions we constructed in Sec. 3.8.2, the QCD spectrum can be extracted by probing the large euclidean time separation of such correlation functions.

In general, since the spectrum is extracted by the asymptotics of the correlation function, having a good signal at large separation is somehow crucial to keep

systematic uncertainties under control. Unfortunately, one of the main difficulties which arise in the study of the hadronic correlation functions is the exponential deplation of the signal which occurs when correlators are evaluated at large distance.

It was argued by Parisi [158] and Lepage [159] that the probabilistic path integral formulation of the theory could give an insight on the behaviour of the correlation function at large euclidean time separations. In particular, it is possible to provide an estimate of the variance of each observables in terms of path integral expectation values. Consider for instance a generic time-separated two-point correlation function involving the interpolating operator O, whose expression on the lattice reads

$$C_O(x_0) = a^q \sum_{\mathbf{x}} \langle O(x_0) O(0) \rangle \,, \tag{3.104}$$

where the exponent q is dictated by the mass dimension of the operator O. The best estimate of its expectation value is provided, on the lattice, by the Monte Carlo average (see eq. 3.75) and its variance reads

$$\sigma^2_O(x_0) = a^{2q} \sum_{\mathbf{x}} \left\{ \langle \left[O(x_0) O(0) \right] \left[O(x_0) O^\dagger(0) \right]^\dagger \rangle - \langle O(x_0) O(0) \rangle^2 \right\} . \tag{3.105}$$

Notice that, by recalling the transfer matrix formalism, in eq. 3.94 the asymptotic suppression of the second term on the r.h.s is simply dictated by $2m_O$. On the other hand, as argued in Ref. [158], for the first term the situation might be different. In this case the suppression will be driven by the lowest energy eigenstate of the transfer matrix which provides a non-zero matrix element of the interpolating operator with respect to the vacuum. Two different scenarios can occur

$$\begin{aligned} m_{O^2} &= 2m_O \\ m_{O^2} &< 2m_O \,, \end{aligned} \tag{3.106}$$

The first case is obtained when there is no state with the correct quantum numbers and lower energy with respect to $2m_O$, which provides a non-zero matrix element. In such case, both the terms appearing on the r.h.s. of eq. 3.105 exhibits the same behaviour for $x_0 \to \infty$. On the other hand the second condition in eq. 3.106

is encountered whenever the operator $O(x_0)O(0)$ acting on the vacuum creates a state with energy lower than $2m_O$. In this case, the second contribution in eq. 3.105 is more suppressed and for sufficiently large separations the variance is dominated by the first term on the r.h.s. Such considerations lead to the definition of the so-called *signal-to-noise* ratio (StN_O), which expression for large euclidean time separations reads

$$\mathrm{StN}_O(x_0) = \frac{\langle C_O(x_0)\rangle}{\sqrt{\sigma^2_O(x_0)}} \overset{x_0\to\infty}{\longrightarrow} \exp\left\{-\left[m_O - \frac{1}{2}m_{O^2}\right]x_0\right\}. \tag{3.107}$$

As a consequence of eq. 3.107, if $m_{O^2} = 2m_O$, the noise scales exactly as the signal and then the StN is constant in euclidean time, while if $m_{O^2} < 2m_O$, at large separations the signal is more suppressed than the variance. This produces an asymptotic exponential degradation of the signal which makes it hard to control the systematic uncertainty.

In such a discussion a special rôle is covered by the pion two-point correlation function, see eq. 3.101 with $a \neq 0$ and $\Gamma_0 = \gamma_5$. Being the lightest state of the theory, in this case we expect the condition in eq. 3.106 to be saturated to $m_{\pi^2} = 2m_\pi$. The explicit expression for the variance of the pion two-point correlation function reads

$$\begin{aligned}\sigma^2_\pi(x_0) = \frac{a^6}{4}\sum_{\mathbf{x}}\Big\{ &\langle \mathrm{Tr}\left[S(x,0)S^\dagger(x,0)\right]\mathrm{Tr}\left[S(x,0)S^\dagger(x,0)\right]^\dagger\rangle \\ &+ \langle \mathrm{Tr}\left[S(x,0)S^\dagger(x,0)\right]\rangle^2\Big\},\end{aligned} \tag{3.108}$$

where the correlation function appearing as the first term on the r.h.s. describes the propagation of a state composed of two quarks and two anti-quarks. Since the pion provides the mass-gap of the theory, the lightest eigenstate of the transfer matrix involving two $q\bar{q}$ pairs is a two-pion state. As a consequence, $m_{\pi^2} = 2m_\pi$ and $\mathrm{StN}_\pi(x_0)$ is a constant for large euclidean time separations.

On the contrary, if we take into account the nucleon two-point correlation

function defined in eq. 3.102, its variance reads

$$\sigma^2_{N^\pm}(x_0) = a^{12} \sum_{\mathbf{x}} \Big\{ \langle \big[W^1_\pm(x,0) - W^2_\pm(x,0)\big] \big[W^1_\pm(x,0) - W^2_\pm(x,0)\big]^\dagger \rangle + \langle W^1_\pm(x,0) - W^2_\pm(x,0) \rangle^2 \Big\} . \tag{3.109}$$

As before, while the exponential behaviour of the second term on the r.h.s is dictated by twice the nucleon mass, the first correlation function on the r.h.s describes the propagation of three $q\bar{q}$ pairs and the corresponding lowest energy state is described by a three-pion state with mass $3m_\pi$. This leads to the StN ratio for the nucleon two-point correlation function

$$\mathrm{StN}_{N^\pm}(x_0) = \frac{\langle C_{N^\pm}(x_0) \rangle}{\sqrt{\sigma^2_{N^\pm}(x_0)}} \xrightarrow{x_0 \to \infty} \exp\left\{ -\left[m_{N^\pm} - \frac{3}{2} m_\pi \right] x_0 \right\} . \tag{3.110}$$

For instance, by restricting to the positive parity partner, i.e. the nucleon, for physical quark masses we have $m_{N^+} - \frac{3}{2} m_\pi \approx 3.7\,\mathrm{fm}^{-1}$ [22], which makes the study of such correlation function extremely difficult at large distances. As a final remark notice that such StN problem appears also for other mesonic and baryonic observables and might be possibly overcome in Monte Carlo simulations by increasing the size N of the representative ensemble used for the calculation of the Monte Carlo estimate. Nevertheless, the statistical uncertainty of the Monte Carlo average scales as $N^{-1/2}$ (see eq. 3.75) and one would need an incredibly large increase of the statistics to compensate the exponential loss of signal. Such brute force approach is not sustainable from a computational point of view and different methods, such as multilevel integration techniques [160, 161, 162, 163], are preferable for noise reduction of such pathologic observables.

Chapter 4

QCD on the lattice at very high temperature

From now on, in the following chapters we will describe the original contribution of this thesis. In particular, the present chapter is devoted to outline the strategy we implemented to simulate QCD on the lattice at very high temperatures. This strategy exploits a non-perturbative definition of the strong coupling constant in a finite volume to set the lines of constant physics. This strategy was first used in the $SU(3)$ Yang-Mills theory and allowed a precise determination of the Equation of State (EoS) up to ~ 70 GeV [14].

4.1 Shifted boundary conditions

In this thesis, the thermal field theory is discretized on a four-dimensional lattice with lattice extent L_0 in the temporal direction and L_k with $k = 1, 2, 3$ in the three spatial directions. We impose that both fermionic and gluonic fields satisfy shifted boundary conditions in the compact temporal extent [164, 165, 166], while we set periodic boundary conditions in the spatial directions. The basic idea behind shifted boundary conditions consists in shifting the fields by the spatial vector $L_0\boldsymbol{\xi}$ when crossing the boundary of the compact direction. For the gauge fields they

read

$$\begin{aligned} U_\mu(x_0 + L_0, \mathbf{x}) &= U_\mu(x_0, \mathbf{x} - L_0\boldsymbol{\xi}) \\ U_\mu(x_0, \mathbf{x} + \hat{k}L_k) &= U_\mu(x_0, \mathbf{x}) \,, \end{aligned} \tag{4.1}$$

where $\hat{k}$ denotes the unit vector in the k-direction. Due to anti-periodicity of fermionic fields, shifted boundary conditions for quarks and anti-quarks read

$$\begin{aligned} \psi(x_0 + L_0, \mathbf{x}) &= -\psi(x_0, \mathbf{x} - L_0\boldsymbol{\xi}) \,, \qquad & \psi(x_0, \mathbf{x} + \hat{k}L_k) &= \psi(x_0, \mathbf{x}) \,, \\ \bar{\psi}(x_0 + L_0, \mathbf{x}) &= -\bar{\psi}(x_0, \mathbf{x} - L_0\boldsymbol{\xi}) \,, \qquad & \bar{\psi}(x_0, \mathbf{x} + \hat{k}L_k) &= \bar{\psi}(x_0, \mathbf{x}) \,. \end{aligned} \tag{4.2}$$

At the level of path integral, a QFT defined with the usual partition function in eq. 2.1, in presence of shifted boundary conditions is equivalent to the same QFT defined in a moving reference frame with imaginary velocity given by $\mathbf{v} = i\boldsymbol{\xi}$ and euclidean partition function

$$Z\left(L_0, \boldsymbol{\xi}\right) = \mathrm{Tr}\left[e^{-L_0(H - i\boldsymbol{\xi}\cdot\mathbf{P})}\right] , \tag{4.3}$$

where H is the hamiltonian operator and $\mathbf{P}$ is the total momentum operator in the boosted reference frame, with boost characterized by the Lorentz factor $\gamma = (1 + \boldsymbol{\xi}^2)^{-1/2}$. Therefore, a relativistic thermal field theory in the presence of shifted boundary conditions is totally equivalent to the same theory with standard periodic (anti-periodic for fermionic fields) boundary conditions but with a longer temporal extent L_0/γ and temperature

$$T = \frac{\gamma}{L_0} = \frac{1}{L_0\sqrt{1 + \boldsymbol{\xi}^2}} \,. \tag{4.4}$$

By restricting ourselves to the case $\boldsymbol{\xi} = (\xi, 0, 0)$, the coordinates (x_0, x_1) of the system with shifted boundary conditions are mapped into the coordinates (x_0', x_1') of the system with periodic boundary conditions through an euclidean Lorentz transformation

$$\begin{cases} x_0' = (x_0 + \xi x_1)\,\gamma \\ x_1' = (x_1 - \xi x_0)\,\gamma \end{cases} , \tag{4.5}$$

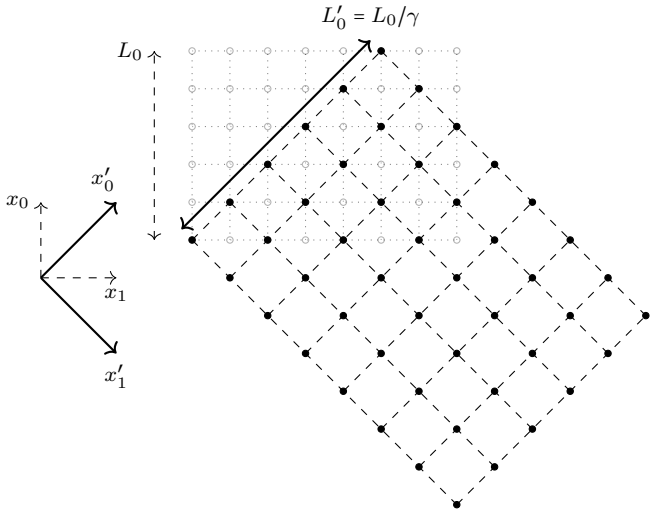

Figure 4.1: The grey horizontal lattice in the plane (x_1, x_0) represents the lattice with shifted boundary conditions and lattice extent $L_0/a = 6$ in the temporal direction. The rotated lattice represents the corresponding (x_0', x_1') frame with periodic boundary conditions and temporal extent L_0/γ, with $\boldsymbol{\xi} = (1, 0, 0)$.

while x_2 and x_3 are left unchanged, being the boost in the first spatial direction. In fig. 4.1 the transformation between the two systems is shown in the (x_1, x_0)-plane. In a shifted frame the Matsubara frequencies for fermionic and bosonic fields, that we defined in eq. 2.6 and 2.7 respectively, are accordingly modified to [167]

$$k_n = \frac{\pi}{L_0}(2n+1) - \mathbf{k}\cdot\boldsymbol{\xi}\,, \tag{4.6}$$

$$k_n = \frac{2\pi n}{L_0} - \mathbf{k}\cdot\boldsymbol{\xi}\,, \tag{4.7}$$

where n is an integer number in $[0, L_0/a - 1]$ and $\mathbf{k}$ is the spatial momentum defined in presence of periodic boundary conditions in the spatial direction. In order to make a definite choice, in this thesis we use shifted boundary conditions with $\boldsymbol{\xi} = (1, 0, 0)$ and consequently $T = 1/\left(\sqrt{2}L_0\right)$.

Shifted boundary conditions have been proven to be an efficient framework to tackle several problems that are otherwise very challenging both from the theoretical and the numerical point of view. In particular, those have already given remarkable results in the renormalization of the energy-momentum tensor [168] and in the calculation of the EoS at the permille level [169, 14] in the $SU(3)$

Yang-Mills theory and, more recently in the computation of the renormalization constant of the local vector current in QCD [170].

Even if shifted boundary conditions are not crucial for the purpose of this thesis, we have chosen to use them in order to share the cost of generating the gauge field configurations for the project which aims at the computation of the QCD Equation of State [167] in the same range of temperatures we explore in this work. Besides this cost-effective reason, there is also a technical reason for which shifted boundary conditions are a preferable framework, namely they provide milder discretization errors. Such behaviour has been observed in the pure gauge theory in Ref. [169, 14] and in QCD at leading and next-to-leading order in perturbation theory in Ref. [170]. Even in this case, the use of shifted boundary conditions makes discretization errors in the screening masses milder, at least at leading order in perturbation theory, see App. G.

4.2 Scale setting and lines of constant physics

Generally, when simulating QCD at zero-temperature the theory is renormalized by using a hadronic renormalization scheme in which the value of a given hadronic quantity $\hat{\Theta}_{\text{had}}$, computed on the lattice, is fixed to its physical value, see Sec. 3.4 for a more detailed discussion. Due to the window problem in eq. 3.50, this hadronic quantity has to be chosen so that it can be easily accommodated on the lattice and in such a way that it can be efficiently resolved by the chosen lattice spacing.

When simulating a wide range of temperature spanning several orders of magnitude, the additional scale T has to be accommodated on the lattice too [171, 172, 173]. If the temperature is sufficiently large and, in particular, much larger than the hadronic scale, the window relation to be satisfied on the lattice becomes

$$a \ll \frac{1}{T} \ll \frac{1}{\hat{\Theta}_{\text{had}}} \ll L\,, \tag{4.8}$$

which would require to accommodate on a single lattice both the temperature and the hadronic scale which may differ by several orders of magnitude. Cleary this condition makes the numerical computation prohibitively expensive for very large temperatures. A similar problem was encountered when renormalizing non-

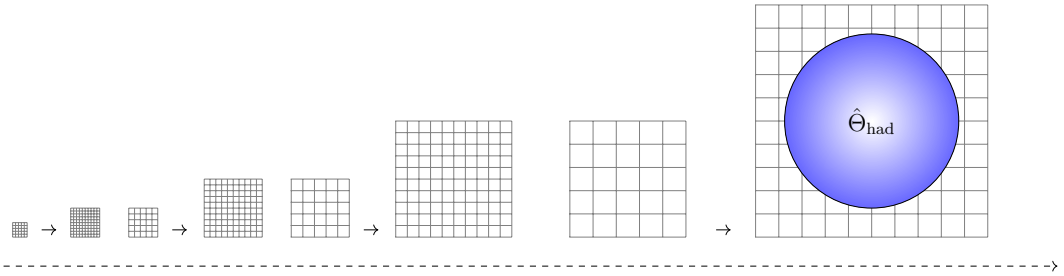

Figure 4.2: Graphical representation of step-scaling techniques which allowed us to explore a wide range of temperature. The overall scale was fixed in the low energy regime by using the results in Ref. [180].

perturbatively QCD and was solve many years ago with the introduction of step-scaling techniques [174, 175].

In this work we overcome this problem by exploiting a non-perturbative definition of the renormalized coupling constant in a finite volume $\bar{g}^2_{\rm SF}(\mu)$ which can be efficiently computed on the lattice for values of the renormalization scale μ which span several orders of magnitude. Here we refer to the definition of the coupling constant based on the Schrödinger Functional renormalization scheme (SF) [176], but other choices are possible as well. In particular, in this work we will also exploit the Gradient Flow (GF) definition [177, 178, 179].

The underlying idea is to transpose the knowledge deriving from the finite volume setup provided by the SF to the finite temperature framework. Once $\bar{g}^2_{\rm SF}(\mu)$ is known in the continuum limit for the energy scale μ which can be accommodated on the lattice, i.e. $a\mu \ll 1$ [178, 181], and the dependence of the bare coupling on the lattice spacing is known, we require $\mu \sim T$. The lines of constant physics are then fixed by requiring the value of the renormalized coupling at finite lattice spacing a to be

$$\bar{g}^2_{\rm SF}(g_0, a\mu) = \bar{g}^2_{\rm SF}(\mu)\,, \qquad \text{for} \qquad a\mu \sim aT \ll 1\,. \tag{4.9}$$

In this way we fix the dependence of the bare coupling on the lattice spacing, for values of a at which the temperature can be easily accommodated. The combination of eq. 4.9 with step-scaling techniques allows to explore a wide range of temperature without the need of simulating large volumes and then with a mod-

erate cost in terms of computer time. The detailed discussion on how the bare parameters of the lattice actions have been fixed is reported in App. D

4.3 Lattice setup

The strategy outlined in the previous section and in App. D has been implemented in the present study to simulate QCD in presence of $N_f = 3$ quarks in the chiral limit, at 12 values of the temperatures, $T_0, \ldots, T_{11}$ ranging from about 1 GeV up to 160 GeV. For the nine highest temperatures $T_0, \ldots, T_8$ we adopted, as a discretization for the gluonic sector of the QCD action, the Wilson plaquette action defined in eq. 3.14, while for the three lowest temperatures T_9, T_{10} and T_{11} the Yang-Mills sector has been discretized by using the tree-level improved gauge action defined in eq. C.1. For all the temperatures that we simulated, three massless fermions have been discretized on the lattice with the standard Wilson action in eq. 3.33 with $O(a)$-improvement, see eq. 3.71 and eq. 3.70. For all the simulations, quark masses have fixed by axial WTIs.

In order to extrapolate to the continuum limit with confidence, for each temperature, we simulated several lattice spacings corresponding to $L_0/a = 4, 6, 8$, and 10, with bare parameters fixed at each lattice spacing by using the strategy outlined in Sec. 4.2 and in App. D. In order to keep finite volume effects under control we simulated large lattices with $L/a = 288$ in all the spatial directions, see Sec. 4.5 for a further discussion on finite volume effects.

4.4 Restricting to the zero-topological sector

As already mentioned in Chapter 2 at high temperature, the topological charge distribution is expected to be extremely peaked at $Q = 0$. The semiclassical analysis provided by the dilute instanton gas approximation predicts the topological susceptibility $\chi(T)$ in the $SU(3)$ Yang-Mills theory to be proportional to T^{-b}, with $b = 8$. Such prediction has been verified explicitly on the lattice in Ref. [61]. In QCD with three light degenerate flavours with mass m, the semiclassical analysis predicts $\chi \sim T^{-8} m^3$. Even if the systematics is still difficult to control,

when fermions are included, the numerical simulations done so far confirm such behaviour [62, 63, 64, 65].

As a result, already at the lower temperature we simulated, i.e. $T \sim 1$ GeV, the probability to encounter a configuration in a non-zero topological sector in our volumes is expected to be several orders of magnitude smaller than the permille or so. Notice that, this is even less probable in presence of massless quarks. From these considerations, we can safely restrict our calculation to the zero topology sector and generate gauge field configurations as described in Sec. 3.7 and more specifically in App. C.3.

4.5 Finite volume effects

This section is dedicated to derive the relevant formula for the leading finite volume effects in spatially separated correlation functions $C_O(x_3)$ at asymptotically high temperatures. Here we follow the argumentation provided in Ref. [166, 182, 183]. The derivation is performed for a lattice with shifted boundary conditions with $\boldsymbol{\xi} = (\xi_1, 0, 0)$, see Sec. 4.1. The results can be readily generalized for any $\boldsymbol{\xi}$ by exploiting the invariance of the theory under SO(3) spatial rotations. Moreover, the result for standard periodic boundary condition is easily recovered by simply setting $\xi_1 = 0$.

Let us consider a volume $L_0 \times L^3$ and define the finite-volume residue due to the compactification in the 1-direction. It reads[1]

$$\mathcal{I}_1\left(x_3, L\right) \equiv \left[1 - \lim_{L\to\infty}\right] C_O(x_3)\,, \tag{4.10}$$

where L is the lattice extent in the first spatial direction. In order to determine the functional form of $\mathcal{I}_1$ we consider the transfer-matrix representation of the correlation function $C_O(x_3)$ along the 1-direction, see Sec. 3.8.1, i.e.

$$C_O(x_3) = \int \mathrm{d}x_0\, \mathrm{d}x_1\, \mathrm{d}x_2\, \frac{\mathrm{Tr}\left[e^{-(L\gamma_1 - x_1)\tilde{H}} O^a\left(\tilde{\boldsymbol{x}}\right) e^{-x_1\tilde{H}} O^a\left(\tilde{\mathbf{0}}\right) e^{-iL\gamma_1\xi_1\tilde{\omega}}\right]}{\mathrm{Tr}\left[e^{-L\gamma_1(\tilde{H}+i\xi_1\tilde{\omega})}\right]}\,, \tag{4.11}$$

[1] For simplicity here we refer to mesonic correlation functions, but an analogous discussion leads to the same result for the baryonic case.

where $\tilde{\boldsymbol{x}} = (x_0, x_1, x_2)$, $\gamma_1 = (1+\xi_1^2)^{-1/2}$ and the trace Tr is over the states of the corresponding Hilbert space. In eq. 4.11 $\tilde{H}$ denotes the screening Hamiltonian in the 1-direction. In analogy with the usual Hamiltonian, such operator has a discrete spectrum of states defined on a slice of dimensions $(L_0/\gamma_1) \times L \times L$ with ordinary periodic boundary conditions. The operator $\tilde{\omega}$ denotes instead the momentum operator along the 0-direction of length (L_0/γ_1). In the following we denote with $|n\rangle$ the set of simultaneous eigenstates of $\tilde{H}$ and $\tilde{\omega}$, and potentially other conserved charge operators. The energies E_n and the Matsubara frequencies ω_n are the eigenvalues of the screening Hamiltonian and of the momentum operator respectively. We now assume that the states are ordered in such a way that $E_{n+1} \geq E_n$. As a consequence, the state $|0\rangle$ is the ground state of the system, for which we conveniently set $E_0 = 0$. At large temperatures, the state $|1\rangle$ is then expected to have a positive mass, which represents the mass gap M_{gap} of the the theory.

At asymptotically high temperature QCD effectively behaves as a three dimensional theory, whose only energy scale is $\sim T$, see Sec. 2.2.2 and 2.2.3. The corresponding degrees of freedom are the zero Matsubara modes of the gauge fields A_0 and A_k with $k = 1, 2, 3$, while the non-zero gluonic Matsubara modes and the fermionic fields are heavy degrees of freedom which can be integrated out. As a consequence, we expect the lowest-lying energy states to have $E_n \ll \pi T$ and zero baryon number [184]. By inserting two complete sets of eigenstates $|n\rangle$ with zero baryon number in eq. 4.11 we get

$$C_O(x_3) = \frac{1}{Z} \int \mathrm{d}x_0 \, \mathrm{d}x_1 \, \mathrm{d}x_2 \sum_{n,n'} e^{-L\gamma_1 (E_n + i\xi_1 \omega_n)} e^{-x_1 (E_{n'} - E_n)} \times \langle n | O^a(\tilde{\boldsymbol{x}}) | n' \rangle \langle n' | O^a(\tilde{\mathbf{0}}) | n \rangle + \dots , \tag{4.12}$$

with $Z = \sum_n e^{-L\gamma_1 (E_n + i\xi_1 \omega_n)} + \dots$, where the dots stand for baryonic contributions which are suppressed exponentially with respect to the sum. Let us focus on the terms in the sum for which we have $E_n \neq E_{n'}$. For those, the integral in eq. 4.12 reads

$$e^{-L\gamma_1 E_n} \int_0^{L\gamma_1} \mathrm{d}x_1 e^{-x_1 (E_{n'} - E_n)} = \frac{e^{-L\gamma_1 E_n} - e^{-L\gamma_1 E_{n'}}}{E_{n'} - E_n} , \tag{4.13}$$

which leads, by inserting it into eq. 4.12, to

$$C_O(x_3) = \frac{1}{Z}\int \mathrm{d}x_0\,\mathrm{d}x_2 \sum_{\substack{n,n' \\ E_n \neq E_{n'}}} \frac{e^{-L\gamma_1(E_n+i\xi_1\omega_n)}}{E_{n'}-E_n} \\ \times \left\{\langle n|\,O^a(\tilde{\boldsymbol{x}})\,|n'\rangle\,\langle n'|\,O^a(\tilde{\mathbf{0}})\,|n\rangle + \langle n|\,O^a(\tilde{\mathbf{0}})\,|n'\rangle\,\langle n'|\,O^a(\tilde{\boldsymbol{x}})\,|n\rangle\right\} + \dots\,, \tag{4.14}$$

where we relabelled $n \leftrightarrow n'$ in some terms. In eq. 4.14 the terms with $E_n = E_{n'}$ are included in the dots[2]. Written in this form, it is clear that in the limit $L \to \infty$, the terms with energies $E_n \ll \pi T$ are dominant in the sum. Furthermore, within this energy range, there are no terms with $E_n = E_{n'}$ that can contribute, since O^a has non-trivial flavour quantum numbers and any flavoured mesonic state has an energy $E_n \geq 2\pi T$. Since we are interested in determining the leading finite-volume correction on the correlation function $C_O(x_3)$ we shall restrict ourselves to consider only states that satisfy the above energy constraint. These include, in particular the vacuum and 1-particle states with mass equal to the mass gap M_{gap} of the theory. Thus we introduce the two-point correlation function

$$G_n(\tau,\tilde{\boldsymbol{x}}) = \langle n|\,\mathrm{T}\left\{O^a\left(\tau,\tilde{\boldsymbol{x}}\right)O^a\left(0,\tilde{\mathbf{0}}\right)\right\}|n\rangle\,, \tag{4.15}$$

where $\mathrm{T}\{\cdot\}$ denotes the ordered product of the operators with respect to the parameter τ and $O^a\left(\tau,\tilde{\boldsymbol{x}}\right) = e^{\tau\tilde{H}}O^a(\tilde{\boldsymbol{x}})e^{-\tau\tilde{H}}$. After some trivial algebra, it is straightforward to show that

$$\int_{-\infty}^{\infty}\mathrm{d}\tau\,G_n\left(\tau,\tilde{\boldsymbol{x}}\right) = \sum_{n'}\frac{1}{E_{n'}-E_n}\left\{\langle n|\,O^a(\tilde{\boldsymbol{x}})\,|n'\rangle\,\langle n'|\,O^a(\tilde{\mathbf{0}})\,|n\rangle \right. \\ \left. + \langle n|\,O^a(\tilde{\mathbf{0}})\,|n'\rangle\,\langle n'|\,O^a(\tilde{\boldsymbol{x}})\,|n\rangle\right\}\,, \tag{4.16}$$

By combining eq. 4.16 with eq. 4.14 and by taking the limit $L \to \infty$ we find for $\mathcal{I}_1$

$$\mathcal{I}_1\left(x_3\right) = \sum_{n\left|\substack{\text{1-particle}\\ \text{states}}\right.} e^{-L\gamma_1(E_n+i\xi_1\omega_n)}\int \mathrm{d}x_0\,\mathrm{d}x_1\,\mathrm{d}\tau\left\{G_n\left(\tau,\tilde{\boldsymbol{x}}\right) - G_0\left(\tau,\tilde{\boldsymbol{x}}\right)\right\} + \dots\,, \tag{4.17}$$

[2]Notice that, in order to derive eq. 4.14 we used the fact that $C_O(x_3)$ is projected onto zero Matsubara frequency and therefore $\omega_n = \omega_{n'}$.

where the energies of the 1-particle states are confined to the range $M_{\text{gap}} \lesssim E_n \lesssim \pi T$ and the dots stand for terms which are exponentially suppressed compared to the leading ones. From this expression, it is immediate to conclude that $\mathcal{I}_1$ is exponentially suppressed as $M_{\text{gap}} L \to \infty$. Moreover, the length of the other two spatial directions can be sent to infinity on the r.h.s. of 4.17 up to sub-leading finite-volume effects. The analogous contribution from the 2-direction, $\mathcal{I}_2$ is directly obtained from $\mathcal{I}_1$ by simply replacing $L\gamma_1 \to L$, $\xi_1 \to 0$ and $x_1 \to x_2$. Its expression reads

$$\mathcal{I}_2(x_3) = \sum_{n\Big|\substack{\text{1-particle}\\ \text{states}}} e^{-LE_n} \int \mathrm{d}x_0\, \mathrm{d}x_2\, \mathrm{d}\tau \left\{G_n(\tau, \tilde{\boldsymbol{x}}) - G_0(\tau, \tilde{\boldsymbol{x}})\right\} + \dots . \tag{4.18}$$

Finite volume corrections along the 3-direction can be taken into account, as usual, by considering the backward propagation in the series of exponentials due to periodic boundary conditions in that direction. Since in this work we will extract screening masses from the asymptotic behaviour of such correlation functions, their finite-volume corrections are determined by $\mathcal{I}_1 + \mathcal{I}_2$ only.

On one hand, as we have seen in Sec. 2.2.3 at asymptotically high temperature, the only relevant scale is g_{E}^2. As a consequence finite-volume effects are expected to be exponentially small in $g_{\text{E}}^2 L \approx g^2 T L$, times a non-perturbative coefficient. On the other hand, at intermediate temperatures, as EQCD sets in, the mass gap of the theory could be different but, in any case, always proportional to the temperature. In conclusion, if the temperature is sufficiently large with respect to Λ_{QCD}, which is therefore a low energy constant, the mass gap is always expected to be proportional to the temperature times an appropriate power of the coupling constant.

Chapter 5

Mesonic screening masses

This chapter is devoted to a detailed discussion on the mesonic screening masses. In this thesis we are interested in screening masses related to flavour non-singlet fermionic bilinear operators (see eq. 3.97)

$$O^a = \bar{\psi}(x)\Gamma_O T^a \psi(x)\,, \tag{5.1}$$

where $\Gamma_O = \{\mathbb{1}, \gamma_5, \gamma_\mu, \gamma_\mu\gamma_5\}$ characterizes the structure of the operators in Dirac space. Such operators are named, as usual, as $O = \{S, P, V_\mu, A_\mu\}$ and their quantum numbers are reported in App. B.1. In order to make a definite choice, in this thesis we restrict ourselves to the case of $\mu = 2$. The non-trivial flavour structure of the operators is given by the traceless generators T^a of the $SU(3)$ flavour group, which, as usual, satisfy the properties in App. A.1.

Screening masses are extracted from spatially separated correlation function of the form in eq. 2.26. Here we restrict ourselves to the static sector of the mesonic screening masses, namely we project the screening correlation function to zero Matsubara frequency, i.e. $n = 0$. The continuum two-point correlation function, computed in the 3-direction reads

$$C_O(x_3) = \int \mathrm{d}x_0\, \mathrm{d}x_1\, \mathrm{d}x_2\, \langle O^a(x) O^a(0)\rangle\,, \tag{5.2}$$

where no summation over a is understood. Notice that, since we are simulating three degenerate quarks, see Sec. 4.2 and App. D, the l.h.s does not depend on

a. Moreover, since we are taking into account flavour non-singlet interpolating operators, the disconnected Wick contraction in eq. 3.101 does not contribute. The corresponding screening mass is extracted as in eq. 2.27 and characterizes the exponential decrease of the correlation function at large spatial distances.

At low temperatures, due to the chiral anomaly and the spontaneous breaking of chiral symmetry, the masses resulting from the above correlation functions are different. As we have seen in Chapter 2, when the temperature is large enough, the vector and the axial screening masses are expected to become degenerate thanks to the restoration of the non-singlet chiral symmetry, see eq. 2.36. Moreover, at high temperature, the topological charge distribution becomes narrower and narrower [61], and only the sector with zero topology contributes, *de facto*, to the functional integral [185, 186]. This, in practice, implies the degeneracy of the non-singlet scalar and pseudoscalar screening masses as well, see eq. 2.47 for the corresponding WTI.

5.1 Mesonic screening masses in the effective field theory

The leading term and the $O(g^2)$ correction to the non-singlet mesonic screening masses have been determined in the context of the dimensional reduced effective theory which we discussed in Sec. 2.2.2, 2.2.3 and 2.2.5. For three massless quarks, their expressions read [187, 15]

$$m_O^{\mathrm{PT}} \;=\; 2\pi T + \frac{g_{\mathrm{E}}^2}{3\pi}\left(1 + 0.93878278\right) \;=\; 2\pi T\left(1 + 0.032739961\cdot g^2\right)\,, \tag{5.3}$$

where the first two terms come from the low-energy constant M, see eq. 2.25, while the last one is generated by the interactions.

In the following subsections, the result in eq. 5.3 is derived and some time will be also dedicated to the analysis of possible higher order terms contributing to the flavour non-singlet screening masses. Such derivation is somehow pedagogical and in the following we can benefit from it, since it allows us to develop the formalism which will be used in Chapter 6 for the more complicated 1-loop perturbative

calculation of the baryonic screening masses.

Before discussing the perturbative calculation, let us write the interpolating operators in eq. 5.1 in terms of the three-dimensional spinors defined in eq. 2.18. By using the representation for the Dirac gamma matrices we provide in eq. A.17 it is straightforward to see that the general structure of such interpolating operators reads [15]

$$\begin{aligned} S &= \chi^\dagger \phi + \phi^\dagger \chi \,, \\ P &= \chi^\dagger \sigma_3 \phi - \phi^\dagger \sigma_3 \chi \,, \\ V_k &= -\epsilon_{kl} \left(\chi^\dagger \sigma_l \phi - \phi^\dagger \sigma_l \chi \right) \,, \\ A_k &= -i \left(\chi^\dagger \sigma_k \phi + \phi^\dagger \sigma_k \chi \right) \,, \end{aligned} \tag{5.4}$$

where indices $l, k = 1, 2$ label the transverse spatial directions and ϵ_{kl} is the two-dimensional anti-simmetric Levi-Civita symbol, i.e. $\epsilon_{12} = -\epsilon_{21} = 1$.

5.1.1 Free theory result

Let us consider the action for non-relativistic heavy quarks in eq. 2.24 and restrict ourselves to the free case. The free action reads

$$S_{\text{NRQCD}} = \int \mathrm{d}^3\mathbf{x} \left[i\chi^\dagger \left(p_0 + \partial_3 - \frac{\nabla_\perp^2}{2p_0} \right) \chi + i\phi^\dagger \left(p_0 - \partial_3 - \frac{\nabla_\perp^2}{2p_0} \right) \phi \right] , \tag{5.5}$$

where $p_0 = \pm\pi T$ is the lowest fermionic Matsubara frequency. From the action above, the free χ and ϕ propagators are easily worked out, see App. E.1 for the explicit derivation. Their expression is reported in eq. E.3 and E.4 for χ and ϕ respectively. Notice that the free theory propagators are diagonal in spin space. The reason is that in the free action there is no operator which directly acts on spin indices, like the one in eq. 2.23. As a consequence, all the two-point correlation functions involving the operators in eq. 5.4, at tree level, are degenerate with structure $\sim \langle \phi^\dagger(x_3)\chi(x_3)\chi^\dagger(0)\phi(0) \rangle$. Therefore, by taking into account the expression for the free propagators in App. E.1, the two-point correlation function

in eq. 5.2 at leading order in the effective field theory can be written as

$$C_O^{(0)}(x_3) \propto \int_{\mathbf{p}_\perp,\mathbf{q}_\perp} \delta^{(2)}(\mathbf{p}_\perp + \mathbf{q}_\perp)\delta(p_0+q_0)\theta(p_0)\theta(-q_0) \exp\left[-x_3\left(p_0 + |q_0| + \frac{\mathbf{p}^2}{2p_0} + \frac{\mathbf{q}^2}{2|q_0|}\right)\right], \tag{5.6}$$

where and $\int_{\mathbf{p}_\perp} \equiv \int \frac{\mathrm{d}^2\mathbf{p}_\perp}{(2\pi)^2}$ and $\mathbf{p}_\perp = (p_1, p_2)$. Furthermore, by explicitly using the conservation of energy, it is straightforward to see that for large x_3-separations, the correlation function in the static limit, i.e. for $\mathbf{p}_\perp = \mathbf{q}_\perp = 0$, is dominated by the mass $2p_0 = 2\pi T$.

Before focusing on the higher order contributions to the mesonic screening correlation function, let us stress that, by construction the correlation function in eq. 5.6 is a Green's function which satisfies the equation of motion $\left(\partial_3 - \hat{H}\right) C_O^{(0)}(x_3) = 0$, for $x_3 \neq 0$, where $\hat{H}$ is the hamiltonian of a system of two non-interacting particles.

5.1.2 1-loop order correction

In this section we compute the 1-loop order correction to the mesonic screening masses in eq. 5.3. The following discussion is mainly based on Ref. [15]. The basic idea is to compute the $O(g^2)$ corrections from the corresponding diagrams, which implies to simply use the propagators for the three-dimensional fields χ and ϕ computed at the same order. By taking into account the power counting in table 2.1, the action for non-relativistic quarks at $O(g^2)$ reads

$$S_{\mathrm{NRQCD}} = \int \mathrm{d}^3\mathbf{x}\left[i\chi^\dagger\left(M - g_{\mathrm{E}}A_0 + D_3 - \frac{\nabla_\perp^2}{2p_0}\right)\chi + i\phi^\dagger\left(M - g_{\mathrm{E}}A_0 - D_3 - \frac{\nabla_\perp^2}{2p_0}\right)\phi\right]. \tag{5.7}$$

Notice that as for the free action in eq. 5.5, also the action at $O(g^2)$ does not contain any operator which acts on spin indices. As for the free case, the 1-loop order correction to the mesonic screening masses is spin independent.

By taking into account the free correlation function in eq. 5.6, if we assume the two quarks in the sink operator to be displaced in the spatial transverse directions,

the mesonic correlation function at 1-loop order has the general form

$$\begin{aligned} C_O^{(1)}\left(\mathbf{x}_\perp, \mathbf{y}_\perp, x_3\right) &\propto \exp\left[-x_3\left(2M - \frac{\nabla_{\mathbf{x}}^2}{2M} - \frac{\nabla_{\mathbf{y}}^2}{2M}\right) + g_{\mathrm{E}}^2 \mathcal{A}\left(\mathbf{x}_\perp, \mathbf{y}_\perp, x_3\right)\right] \\ &= C_O^{(0)}(\mathbf{x}_\perp, \mathbf{y}_\perp, x_3) \,+\, g_{\mathrm{E}}^2 \mathcal{A}\left(\mathbf{x}_\perp, \mathbf{y}_\perp, x_3\right) C_O^{(0)}(\mathbf{x}_\perp, \mathbf{y}_\perp, x_3)\,, \end{aligned} \tag{5.8}$$

where $\mathbf{x}_\perp$ and $\mathbf{y}_\perp$ denote the transverse coordinates of the two quarks and in the last line we expanded for small coupling and used the tree-level result in eq. 5.6. In the equation above M is the low-energy constant in eq. 2.25 computed at 1-loop order, g_{E}^2 is the three-dimensional coupling defined in eq. 2.13 and $\mathcal{A}\left(\mathbf{x}_\perp, \mathbf{y}_\perp, x_3\right)$ is the 1-loop order correction to the correlation function. In analogy with what we have done for the free case, it is easy to see that this correlation function satisfies, for non-zero separations, the equation of motion

$$\left[\partial_3 + 2M - \frac{\nabla_{\mathbf{x}}^2}{2M} - \frac{\nabla_{\mathbf{y}}^2}{2M} - g_{\mathrm{E}}^2 \mathcal{K}\left(\mathbf{x}_\perp, \mathbf{y}_\perp, x_3\right)\right] C_O^{(1)}\left(\mathbf{x}_\perp, \mathbf{y}_\perp, x_3\right) \,=\, 0\,, \tag{5.9}$$

where we introduced the dimensionless kernel $\mathcal{K}\left(\mathbf{x}_\perp, \mathbf{y}_\perp, x_3\right) = \partial_3 \mathcal{A}\left(\mathbf{x}_\perp, \mathbf{y}_\perp, x_3\right)$. The screening mass characterizes the exponential suppression of this correlation function for large x_3-separation. Therefore, it is natural to assume for the correlation function the asymptotic functional form $C_O^{(1)}\left(\mathbf{x}_\perp, \mathbf{y}_\perp, x_3\right) = \mathcal{C}(\mathbf{x}_\perp, \mathbf{y}_\perp) e^{-E_0 x_3}$. Then by inserting this functional form in the equation above, it is straightforward to see that the lowest energy level E_0 is simply obtained by solving the eigenvalue problem, given by the 2-body Schrödinger equation

$$\left[-\frac{\nabla_{\mathbf{x}}^2}{2M} - \frac{\nabla_{\mathbf{y}}^2}{2M} + 2M + V\left(\mathbf{x}_\perp, \mathbf{y}_\perp\right)\right] \mathcal{C}(\mathbf{x}_\perp, \mathbf{y}_\perp) \,=\, E_0 \mathcal{C}(\mathbf{x}_\perp, \mathbf{y}_\perp)\,, \tag{5.10}$$

where we introduced the *static potential* $V(\mathbf{x}_\perp, \mathbf{y}_\perp) = -\lim_{x_3 \to \infty} g_{\mathrm{E}}^2 \mathcal{K}\left(\mathbf{x}_\perp, \mathbf{y}_\perp, x_3\right)$. Notice that, in general, the kernel $\mathcal{K}\left(\mathbf{x}_\perp, \mathbf{y}_\perp, x_3\right)$ might contain transverse contributions deriving from the exchange of soft and ultrasoft transverse gluons and from the transverse propagation of quarks. Furthermore, since quarks are heavy fields, i.e $\mathbf{p}_\perp \ll p_0$ and the kernel is dimensionless, we can assume to expand $\mathcal{K}\left(\mathbf{x}_\perp, \mathbf{y}_\perp, x_3\right)$ in powers of $\nabla_\perp / p_0$, with the leading contribution containing longitudinal quark propagation only. In this sense, in the static quark limit, contributions coming from

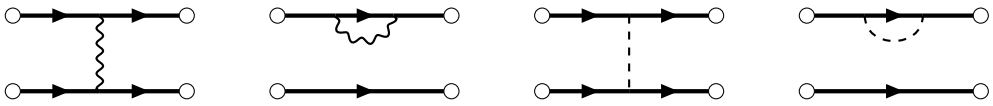

Figure 5.1: 1-loop order corrections to the screening mesonic correlation function. Straight solid lines represent the two longitudinal quark propagators. Wavy lines stand for the propagators of the gauge field A_3 and dashed lines represent the propagators of the scalar field A_0, see Sec. 2.2.2 for the details.

the fermionic transverse motion, even if those are still $O(g^2)$, are parametrically suppressed as $\left(\frac{\nabla_\perp}{p_0}\right)^n$ with $n \geq 1$. By proceeding in this way, the 1-loop order correction to the screening correlation function can be extracted by using the $O(g^2)$ longitudinal propagators for the fields χ and ϕ, which have been derived in App. E.2. By putting everything together, the 1-loop order correlation function, in the static limit, i.e. for $\mathbf{p}_\perp \to 0$, can be written as

$$C_O^{(1)}(\mathbf{x}_\perp, \mathbf{y}_\perp, x_3) = \frac{1}{N} \left\langle U_\chi^{ab}(\mathbf{x}_\perp, x_3) U_\phi^{ba}(\mathbf{y}_\perp, x_3) \right\rangle , \tag{5.11}$$

where the longitudinal propagators U_χ and U_ϕ are defined in eq. E.6 and E.7, a and b are colour indices and $N = 3$ is an irrelevant constant which can be easily computed by requiring the correct normalization for the tree-level result in eq. 5.6. The derivation of such correlation function is performed in details in App. E.3. Its final expression reads

$$C_O^{(1)}(\mathbf{r}_\perp, x_3) \propto e^{-2Mx_3} \left\{ 1 + g_{\mathrm{E}}^2 \mathcal{A}_{\mathrm{L}}(\mathbf{0}_\perp, x_3) + g_{\mathrm{E}}^2 \mathcal{A}_{\mathrm{T}}(\mathbf{r}_\perp, x_3) \right\} \tag{5.12}$$

where $\mathcal{A}_{\mathrm{L}}(\mathbf{0}_\perp, x_3)$ and $\mathcal{A}_{\mathrm{T}}(\mathbf{r}_\perp, x_3)$ are the contributions deriving from the exchange of longitudinal and transverse gluons respectively, see eq. E.13 and E.14, and $\mathbf{r}_\perp = \mathbf{x}_\perp - \mathbf{y}_\perp$. Those contributions, which are graphically shown in fig. 5.1, can be written in terms of the gluon propagators defined in eq. E.15 and E.16. By comparing eq. 5.12 together with eq. E.13 and E.14, with eq. 5.8, it is straightforward to derive the expression for the static potential, see App E.5 for the full derivation. It reads

$$V^-(\mathbf{r}_\perp) = \frac{g^2 C_F T}{2\pi} \left[\ln \frac{m_{\mathrm{E}} r}{2} + \gamma_E - K_0(m_{\mathrm{E}} r) \right] , \tag{5.13}$$

where m_{E} is the Debye mass defined in eq. 2.13, $r = |\mathbf{r}_\perp|$ and $K_0(x)$ is a modified

Bessel function. In order to find a numerical solution to the Schrödinger equation in eq. 5.10 with static potential given by eq. 5.13 it is useful to define the dimensionless parameters $\hat{r}$ and $\hat{E}_0$ as

$$\hat{r} \equiv m_{\mathrm{E}} r\,, \qquad E_0 \equiv 2M + \frac{g^2 T C_F}{2\pi}\hat{E}_0\,. \tag{5.14}$$

As a result, the Schrödinger equation, for the relative motion, can be rewritten in polar coordinates as [15]

$$\left[-\left(\frac{\mathrm{d}^2}{\mathrm{d}\hat{r}^2} + \frac{1}{\hat{r}}\frac{\mathrm{d}}{\mathrm{d}\hat{r}}\right) + \rho\left(\ln\frac{\hat{r}}{2} + \gamma_E - K_0(\hat{r}) - \hat{E}_0\right)\right]\mathcal{C}(\hat{r}) = 0\,. \tag{5.15}$$

where

$$\rho = \frac{g^2 T^2 C_F}{2m_{\mathrm{E}}^2} \overset{N_c=3}{=} \frac{4}{(6+N_f)} \overset{N_f=3}{=} \frac{4}{9} \tag{5.16}$$

A numerical solution is then easily found with standard algorithms, like the one described in App. F.2[1], and leads to the result $\hat{E}_0 = 0.469393$ and correspondingly the 1-loop order screening mass reads

$$E_0 = 2\pi T + g^2 T\frac{C_F}{2\pi}\left(\frac{1}{2} + \hat{E}_0\right) = 2\pi T\left(1 + 0.032740\cdot g^2\right)\,, \tag{5.17}$$

which perfectly agrees with the result in eq. 5.3 taken from Ref. [15], which we assume, in the following, as the reference perturbative result.

5.1.3 Higher order contributions

This section is devoted to the analysis of possible higher order terms in the perturbative expansion of the mesonic screening masses. In general, before looking at such corrections, the correct expansion parameter for the static potential as to be carried out. By combining the result that we obtained for the 1-loop order static

[1]Notice that a numerical solution to this equation suffers from bad convergence for small $\hat{r}$. A possible solution to this problem can be found in Ref. [188].

potential with dimensional analysis, the general form of the static potential is [15]

$$V(\mathbf{r}_\perp) \sim g_{\mathrm{E}}^2 \ln r + g_{\mathrm{E}}^4 r + O(g_{\mathrm{E}}^6 r^2)\,, \tag{5.18}$$

where the scale appearing in the leading logarithmic term is fixed by the 1-loop order calculation. By using the same power counting rules which have been defined in Sec. 2.2.5, one can easily see that $1/r \sim O(gT)$. Notice that this power counting somehow justifies the introduction of the dimensionless $\hat{r}$ in eq. 5.14. In such a way we can rewrite the static potential, by using $g_{\mathrm{E}}^2 \sim g^2 T$, as

$$V(\hat{r}) \sim g^2 T \left(\ln \hat{r} + g\hat{r} + O(g^2 \hat{r}^2)\right)\,, \tag{5.19}$$

from which it directly follows that the expansion parameter of the static potential is $O(g)$. Furthermore, notice that, written in this way, the potential is proportional to the temperature times a dimensionless function of the separation between quarks, a fact which is expected, since the only energy scale of the system is the temperature.

From such considerations, it follows that the perturbative expansion of the screening masses may contain also odd powers in the coupling constant. As a representative example, the first of such term is the string term $\sim \hat{r}$ which might provide $O(g^3)$ correction to the screening masses. Notice that at zero temperature the origin of the string term is purely non-perturbative, and also at non-zero temperature this term could be determined by non-perturbative effects.

Other features of the spectrum of the screening masses can be carried out by looking at the NRQCD action defined in eq. 2.24 and from its power counting. In particular, spin-dependent terms arise from the chromo-magnetic operator defined in eq. 2.23 which is $O(g^4)$. As a consequence, spin-dependent terms in the masses are expected to emerge only at this order and any contribution coming from lower orders, e.g. the string term, must be the same for each of the flavour non-singlet masses.

5.2 Mesonic screening masses on the lattice

The lattice version of the correlation function in eq. 5.2 reads

$$C_O(x_3 - y_3) = a^3 \sum_{x_0,x_1,x_2} \langle O^a(x) O^a(y) \rangle \ . \tag{5.20}$$

After integrating over the fermionic variables in the path integral, it can be written as

$$C_O\left(x_3 - y_3\right) = -\frac{a^2}{2} \sum_{x_0,x_1,x_2} \left\langle \mathrm{Tr}\left[\Gamma_O S(x,y) \Gamma_O \gamma_5 S^\dagger(x,y) \gamma_5\right] \right\rangle \ , \tag{5.21}$$

where Tr indicates the trace over colour and spin indices and $S(x,y)$ is the quark propagator, i.e. the inverse of the $O(a)$-improved Wilson-Dirac operator defined in eq. 3.33 and computed at the critical value of the quark mass, see App. D for the details. In general, at high temperature, the inverse of the lattice Dirac operator has to be done with some care. The reason is that the lowest Matsubara frequency πT provides an infrared cut-off to quark propagation and, as a result, the matrix elements of the propagator $S(x,y)$ become extremely small when $\pi T|x-y| \gg 1$. At those distances, a very accurate solution of the Dirac equation is required and the brute force approach of simply implementing higher-precision by requiring a smaller tolerance is not practicable. We have solved this problem by introducing a distance preconditioning [189] of the Dirac equation as discussed in App. C.2.

The two-point correlation functions for the scalar and pseudoscalar densities and for the vector and the axial currents have been computed on all the lattices generated, see tables D.3 and D.6. We report in tables C.1 and C.2 the number of Molecular Dynamics Units (MDUs) after the thermalization phase of each HMC chain, the number of MDUs skipped between two consecutive independent configurations and the number of local sources per configuration on which the Wilson-Dirac operator has been inverted. The best estimates of $C_O(x_3)$ on each configuration have been obtained by averaging their values from all the local sources and then by symmetrizing the correlation functions with respect to the coordinate $x_3 = L/2$. We carefully monitored the autocorrelation of the correlators, and we never observed long autocorrelation times with respect to the number of

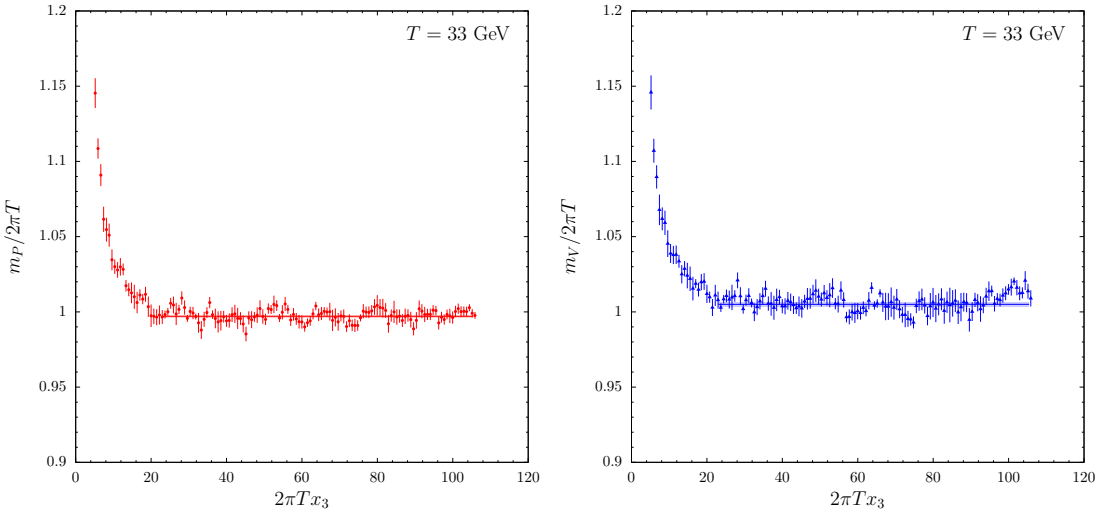

Figure 5.2: Plot of the effective masses, normalized to the free theory value $2\pi T$, for the pseudoscalar (left) and the the vector (right) correlation functions at the temperature T_3 for $L_0/a = 6$.

MDUs skipped between two consecutive measurements.

Let us anticipate that within our statistical precision, at all the temperatures simulated, we observed an excellent agreement between the scalar and the pseudoscalar correlators as well as between the vector and the axial ones at intermediate and large separations. As we have seen in Sec. 2.3.2, this is a distinctive feature of the restoration of chiral symmetry which manifests itself at high temperature. For this reason in the following sections we focus our discussion on the pseudoscalar and the vector masses and we postpone the discussion about the scalar and the axial channel to a dedicated section (see Sec. 5.2.4).

5.2.1 Mesonic effective masses

Once the two-point correlation functions in eq. 5.21 have been computed as discussed in the previous section, effective masses are defined as

$$m_O\left(x_3\right) = \frac{1}{a}\text{arcosh}\left[\frac{C_O\left(x_3+a\right)+C_O\left(x_3-a\right)}{2C_O\left(x_3\right)}\right]. \tag{5.22}$$

Two representative examples are provided in fig. 5.2. On the left panel we show the

effective mass related to the pseudoscalar density and on the right panel the one associated to the vector current, in both cases data refer to $L_0/a = 6$ at the temperature $T_3 = 32.8$ GeV. An analogous behaviour is observed for all the lattices. We obtained very long plateaux thanks to the fact that we have simulated very large spatial extensions in our volumes and that there is no signal-to-noise ratio problem if the temperature is sufficiently large. In order to determine the best estimates of the screening masses m_O, we start by fitting the symmetrized correlator to a sum of two exponentials from a minimum value of x_3/a up to the last available point. The minimum value is chosen so as to obtain, at the same time, a good quality of the two-exponential fit and a statistically non-zero contribution deriving from the sub-leading exponential. From the result of this fit, we then estimate the minimum value $x_3^{\min}/a$ from which the contamination in the effective mass due to the second exponential is negligible with respect to the statistical precision that we obtain by fitting the effective mass to a constant from $x_3^{\min}/a$ up to the last available point. We then explicitly verify that a constant value fits well the effective mass from $x_3^{\min}/a$ up to the end of the plateau, and that by increasing $x_3^{\min}/a$ by a few units the result of the fit does not change significantly. Two representative examples of such fits are provided in fig. 5.2 as straight lines for T_3 and $L_0/a = 6$. Our best estimates of the screening masses are reported in tables C.1 and C.2 for all the lattices that we have simulated. The statistcal error is at most a few permille in all the cases. Furthermore, we profit from the correlations in our data in order to reduce the statistical error, by calculating the mass diference between the vector and the pseudoscalar masses, i.e. $(m_V - m_P)\,/\,(2\pi T)$. Data regarding the mass difference are provided in tables C.1 and C.2 as well. Notice that such combination is particularly useful because it encodes any spin-dependent term, which can be computed very precisely.

Before concluding this section, let us remark that we explicitly checked that finite volume effects are totally under control and that their effects are negligible within our statistical precision: we have generated three more lattices at the highest and at the lowest temperatures for the smallest spatial volumes corresponding to $L_0/a = 6, 10$ and 8 for T_0, T_1 and T_{11} respectively. These lattices have the same extension in the temporal and in the third spatial directions as those in tables D.3 and D.6 but smaller extension in the other two spatial directions. The

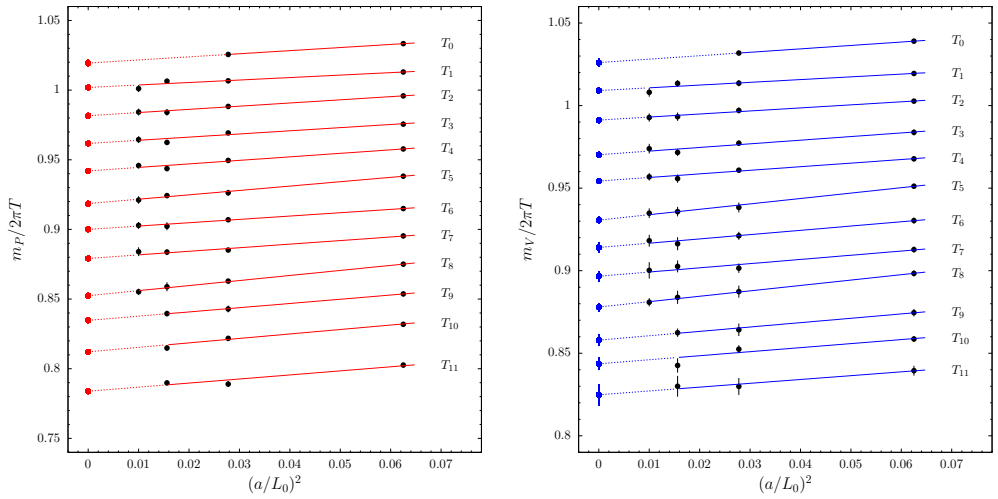

Figure 5.3: Numerical results for the tree-level improved pseudoscalar (left panel) and for the vector (right panel) screening masses at finite lattice spacing (black dots). The lines represent the linear extrapolations in $(a/L_0)^2$ to the continuum limit. Each temperature has been analyzed independently from the others. In order to improve readability data corresponding to T_i with $i = 0, \ldots, 11$ has been shifted downward by $0.02 \times i$.

screening masses computed on them are in agreement with those calculated on the larger volume as expected from the discussion in Sec. 4.5. Therefore we can safely assume that our results have negligible finite-volume corrections within the statistical precision.

5.2.2 Continuum limit of mesonic screening masses

The results that we have collected at finite lattice spacing, see tables C.1 and C.2 have to be extrapolated to the continuum in order to remove any cut-off effect. Since we are using $O(a)$-improved actions, the Symanzik effective theory predicts that the leading behaviour of the lattice artifacts has to be $O(a^2)$. In order to make continuum limit extrapolations as reliable as possible, we can further accelerate the convergence to the continuum by introducing a tree-level improved definition of the effective mass

$$m_O \longrightarrow m_O - \left[m_O^{\text{free}} - 2\pi T\right], \tag{5.23}$$

where m_O^{free} is the mass in the free theory computed on the lattice. The calculation, reported in App. G.1, shows that it is the same for all the mesonic two-point correlation function of interest. From now on, in the following discussion we will always consider the tree-level improved definition of the screening masses and, without any ambiguity, we will refer to them as m_O.

The extrapolation to the continuum limit for the pseudoscalar and the vector screening masses are represented on the left and on the right panel of fig. 5.3 respectively. For better readability data corresponding to T_i $(i = 0, \dots 11)$ are shifted downward by $0.02 \times i$. The analogous plot for the mass difference $(m_V - m_P)$ is shown in fig. 5.4. At each temperature, lattice artifacts are well described by a single $O(a^2)$ correction. Indeed, by fitting each data set linearly in $(a/L_0)^2$, the values of χ^2/dof are all around 1 except for a few outliers a fact which is, however, not surprising, given the large amount of data and fits that we have collected. The results of such fits are shown in fig. 5.3 and 5.4 as straight lines. Furthermore, for the mass difference in fig. 5.4 the linear coefficient in $(a/L_0)^2$ is always found to be compatible with zero at all the temperatures. We take the continuum limit values of these fits as our best estimated for the vector and the pseudoscalar screening masses and for their difference.

Such values are reported in table 5.1 for all the 12 temperatures that we simulated in this thesis. As a further consistency check of the extrapolations, we have fitted the data by excluding the coarsest lattice spacing, i.e. $L_0/a = 4$, for the temperatures $T_1, \dots, T_8$, for which we have 4 data points. The intercepts are in excellent agreement with those of the previous fits, albeit a slightly larger error. Furthermore, for the same data set, we also attempted to include in the fit a $(a/L_0)^2 \log(a/L_0)$ or a cubic term in the lattice spacing. The resulting coef-

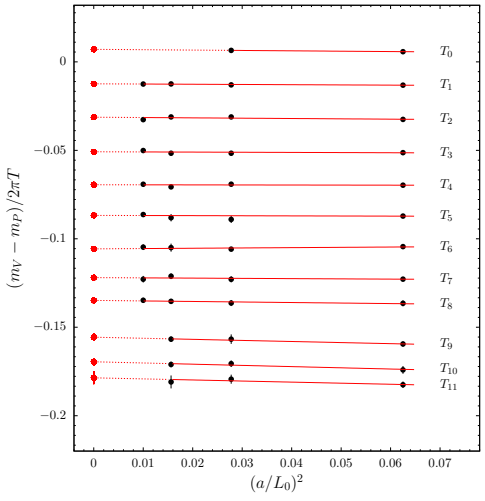

Figure 5.4: As in figure 5.3 but for the mass difference.

T	T(GeV)	$\frac{m_P}{2\pi T}$	$\frac{m_V}{2\pi T}$	$\frac{(m_V - m_P)}{2\pi T}$
T_0	164.6(5.6)	1.0194(25)	1.0261(23)	0.0071(7)
T_1	82.3(2.8)	1.0219(15)	1.0291(18)	0.0076(4)
T_2	51.4(1.7)	1.0216(16)	1.0312(18)	0.0087(4)
T_3	32.8(1.0)	1.0217(15)	1.0302(19)	0.0092(6)
T_4	20.63(63)	1.0220(15)	1.0343(17)	0.0105(6)
T_5	12.77(37)	1.0185(18)	1.0306(24)	0.0132(10)
T_6	8.03(22)	1.0200(18)	1.0341(28)	0.0143(13)
T_7	4.91(13)	1.0192(18)	1.037(3)	0.0181(14)
T_8	3.040(78)	1.0124(18)	1.0380(25)	0.0252(13)
T_9	2.833(68)	1.0147(24)	1.038(3)	0.0244(20)
T_{10}	1.821(39)	1.0122(18)	1.044(4)	0.0305(20)
T_{11}	1.167(23)	1.0039(20)	1.045(6)	0.041(4)

Table 5.1: Best estimates for the pseudoscalar, m_P, and the vector, m_V, non-singlet screening masses in the continuum limit together with their difference.

ficients were always found to be compatible with zero. As a final comment on the extrapolation, given the high quality of the data and of the fits described above, it was not necessary to model the temperature dependence of the lattice artifacts through a global fit of the data.

5.2.3 Temperature dependence and spin-splitting

In table 5.1 we collect the main results on the pseudoscalar and the vector screening masses and on their mass splitting. Those masses have been computed for the first time in a wide range of temperatures from $T \sim 1$ GeV up to 160 GeV or so with a few permille accuracy. It is clear, by looking at the continuum limit results reported in table 5.1 that the bulk of the non-singlet meson screening masses is given by the free theory value $2\pi T$, both for the pseudoscalar and the vector channel, see Sec. 5.1.1, plus a few percent positive deviation in the entire range of temperatures.

Given the high quality of our results, we can study in detail the temperature dependence induced by interactions. In order to do that, we introduce the function

$\hat{g}^2(T)$, defined as

$$\frac{1}{\hat{g}^2(T)} \equiv \frac{9}{8\pi^2}\ln\frac{2\pi T}{\Lambda_{\overline{\rm MS}}} + \frac{4}{9\pi^2}\ln\left(2\ln\frac{2\pi T}{\Lambda_{\overline{\rm MS}}}\right), \tag{5.24}$$

where $\Lambda_{\overline{\rm MS}} = 341$ MeV is taken from Ref. [40]. It corresponds to the 2-loop definition of the strong coupling constant in the $\overline{\rm MS}$ scheme at the scale $\mu = 2\pi T$. However, let us stress that, for our purpose, it is just a parametrization of the temperature dependence, suggested by the effective field theory analysis, which turns out to be useful to analyze our results[2]. In general, any function of the temperature with a leading inverse logarithmic behaviour in the temperature is valid as well.

Pseudoscalar mass

The pseudoscalar mass (third column of table 5.1) has been fitted to a quartic polynomial in $\hat{g}$. The resulting intercept turns out to be compatible with 1, as predicted by the free theory, within a large error. We have thus enforced the intercept to the free-theory value, $p_0 = 1$ and we have fitted again the data. The coefficient of the $\hat{g}^2$ term turns out to be compatible with the theoretical expectation in eq. 5.3 (see Sec. 5.1.2 for the detailed discussion) within again a large uncertainty. For this reason we have also fixed this coefficient to its analytical value, i.e. $p_2 = 0.032739961$, and we have performed again the quartic fit of the form

$$\frac{m_P}{2\pi T} = p_0 + p_2\hat{g}^2 + p_3\hat{g}^3 + p_4\hat{g}^4, \tag{5.25}$$

where now the p_0 and p_2 coefficients have been fixed to their theoretical values as explained above. As a result, for the fit parameters we obtain $p_3 = 0.0038(22)$, $p_4 = -0.0161(17)$ and $\mathrm{cov}(p_3, p_4)/\left[\sigma(p_3)\sigma(p_4)\right] = -1.0$ with an excellent $\chi^2/\mathrm{dof} = 0.75$. The quality of the fit can be appreciated in the left panel of fig. 5.5, where $m_P/(2\pi T)$ is shown as a function of $\hat{g}^4$ together with the best fit in eq. 5.25, after subtracting the analytically known contributions. If the cubic coefficient is enforced to zero, i.e. $p_3 = 0.0$, the fit returns $p_4 = -0.01323(20)$ with again an

[2]Other possible definitions of the coupling are valid as well, e.g. non perturbative definitions of the running coupling. However in such case, the comparison between our data and the analytic result in Sec. 5.1.2 would be more involved.

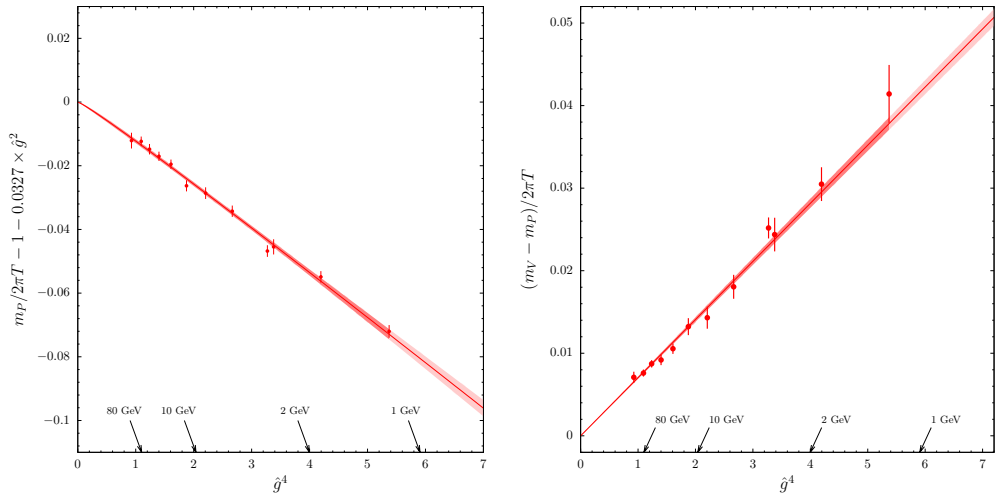

Figure 5.5: Left: the pseudoscalar mass, normalized to the free theory value $2\pi T$, subtracted of the analytically known contributions, as a function of $\hat{g}^4$. Right: the vector-pseudoscalar mass difference, normalized the the free theory value, versus $\hat{g}^4$. Red bands represent the best fits of the data obtained as explained in the text.

excellent value of $\chi^2/\text{dof} = 0.96$. The subtracted data lies on a straight line over two orders of magnitude in the temperature. The polynomial in eq. 5.25 is our best parameterization for the pseudoscalar mass over the entire range of temperatures explored.

The quartic term is necessary to explain the data over the entire temperature range. In particular at the highest temperature simulated, i.e. $T \sim 160$ GeV, its contribution is still approximately half of the total contribution due to interactions. Notice that the sign of the quartic term is negative, in contrast to the quadratic one, and its magnitude is about 2-3 times smaller than the analytic value of p_2. When the pseudoscalar mass is plotted as a function of $\hat{g}^2$, the quartic contribution competes with the quadratic one to bend down the pseudoscalar mass as shown in fig. 5.6. Toward the lower end of the range of temperatures, the competition between this term and the leading one results in an effective slope of opposite sign with respect to the analytically known one. At $T \sim 1$ GeV, the various terms cancel each other and the mass turns out to be very close the free theory value $2\pi T$.

Vector mass

The mass difference $(m_V - m_P)/(2\pi T)$ is an interesting quantity in order to investigate the magnitude of the spin-dependent contributions. We plot our results for this quantity (last column of table 5.1) as a function of $\hat{g}^4$ on the right panel of fig. 5.5. The data turn out to lie on a straight line with a vanishing intercept. By fitting them to the fit ansatz

$$\frac{(m_V - m_P)}{2\pi T} = s_4 \hat{g}^4 , \tag{5.26}$$

we obtain as best estimate of the fit parameter $s_4 = 0.00704(14)$ with $\chi^2/\text{dof} = 0.79$. It turns out that the spin-dependent contribution can be parametrized by a single $O(\hat{g}^4)$ correction in the entire range of temperatures. Moreover, such contribution is still visible even at the highest temperature, where the vector and the pseudoscalar masses are significantly different within our statistical precision. Therefore, the best polynomial that parametrizes the vector mass (fourth column of table 5.1) in our range of temperatures is

$$\frac{m_V}{2\pi T} = p_0 + p_2 \hat{g}^2 + p_3 \hat{g}^3 + (p_4 + s_4)\, \hat{g}^4 , \tag{5.27}$$

where p_i with $i = 0, \dots 4$ are the parameters obtained from eq. 5.25, while s_4 is the one obtained by fitting the mass difference in eq. 5.26. The covariance matrix elements of the p_3 and p_4 coefficient with s_4 are $\text{cov}(p_3, s_4)/[\sigma(p_3)\sigma(s_4)] = 0.08$ and $\text{cov}(p_4, s_4)/[\sigma(p_4)\sigma(s_4)] = -0.07$. As shown in fig. 5.6, the quartic contribution is necessary to explain the data over the entire range of temperatures. In particular, at the electroweak scale it is approximately 15% of the total contribution due to interactions. Also for the vector mass, the coefficient of the quartic term in eq. 5.27 has an opposite sign with respect to p_2, but it is approximately half of the analogous one for the pseudoscalar. By looking at fig. 5.6 it is clear that the quartic contribution in the vector mass competes with the quadratic one, but it is not sufficiently large to push down the mass at least up to lowest temperture considered. At the lower end of the range of temperatures, i.e. at $T \sim 1$ GeV, the entire deviation of the vector mass from the free theory value $2\pi T$ is due to the spin-dependent term, given the cancellation among the other terms.

In the literature, non-perturbative computations of these masses are available in the continuum limit only up to temperatures of 1 GeV or so [190]. Even if those results were obtained with physical quark masses, they are in agreement with ours at those temperatures within the rather large errors. From the discussion in Sec. 2.3 and in particular from eq. 2.28, this is expected, since the relevance of the quark masses is very mild if the temperature is sufficiently large with respect to them. The pattern of different contributions that we have just discussed, however, explains why it has been difficult in the past to match non-perturbative lattice results at $T \leq 1$ GeV with the expected analytic behaviour at asymptotically high temperatures. Indeed the apparently small $2-4\%$ effect on the screening masses induced by the interactions among quarks and gluons encodes a lot of interesting non-trivial information about the dynamics of the plasma. When the corresponding non-perturbative computations in the three-dimensional effective theory will become available, the matching with these results will allow to shed light on the origin of the various terms, and to verify non-perturbatively the effective theory paradigm over several orders of magnitude in the temperature.

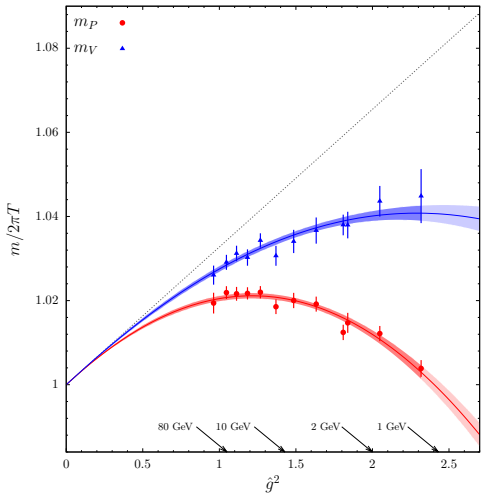

Figure 5.6: Pseudoscalar (red) and vector (blue) screening masses versus $\hat{g}^2$. The bands represent the best fits in eq. 5.25 and 5.27, while the dashed black line is the analytically known contribution.

As a final comment, the analytic calculation of the leading $O(g^4)$ spin-dependent term, in the framework of the effective field theory, is currently in progress.

5.2.4 Chiral symmetry restoration on the lattice

At low temperature the axial non-singlet symmetry of the chiral group is spontaneously broken by the non-zero value of the chiral condensate and the axial singlet symmetry is broken by the anomaly. As the temperature increases both the chiral

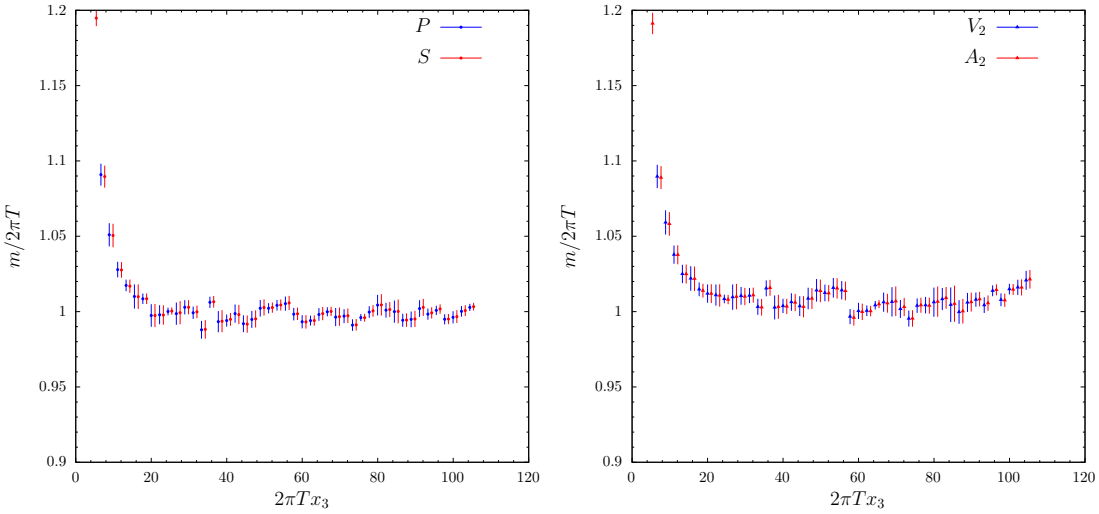

Figure 5.7: The effective mass versus the separation on the lattice for the pseudoscalar and the scalar channel (left panel) and for the vector and the axial ones (right panel) at the physical temperature $T_3 = 32.8$ GeV. To improve readability, we show one every three points and the scalar and the axial data set are shifted by a factor of 1 to the right.

condensate and the topological susceptibility are extremely suppressed, leading to an effective restoration of both non-singlet and singlet axial symmetries. This phenomenon translates into the set of non-trivial WTIs derived in Sec. 2.3.2.

As anticipated, the vector and the axial two-point correlation functions are found to be degenerate at intermediate and large separations, a fact which is consistent with eq. 2.36 if chiral symmetry is restored. Analogously, the scalar and the pseudoscalar correlators are degenerate, consistently with 2.47, if only the trivial topological sector contributes to the path integral. Such degeneracy among different correlation functions implies the degeneracy of the related screening masses which are extracted by the asymptotic behaviour of the screening correlators. In fig. 5.7 we provide the effective mass plots for the pseudoscalar and the scalar correlation function on the left panel and for the vector and the axial ones on the right panel, in both cases for the temperature $T_3 = 32.8$ GeV at $L_0/a = 6$.

The restoration pattern of chiral symmetry has been studied through the analysis of the mass difference between the pseudoscalar and the scalar masses and between the vector and the axial ones for all the temperature we have taken into

T	T(GeV)	$\frac{(m_P - m_S)}{2\pi T}$	$\frac{(m_V - m_A)}{2\pi T}$
T_0	164.6(5.6)	-0.00003(9)	-0.00018(18)
T_1	82.3(2.8)	-0.00011(16)	-0.00007(13)
T_2	51.4(1.7)	0.00004(15)	-0.00002(17)
T_3	32.8(1.0)	-0.00005(12)	-0.00012(15)
T_4	20.63(63)	0.00011(13)	0.00015(27)
T_5	12.77(37)	0.0003(4)	0.00009(30)
T_6	8.03(22)	0.00028(21)	0.00015(23)
T_7	4.91(13)	-0.00019(27)	-0.0007(5)
T_8	3.040(78)	-0.0002(5)	-0.0007(6)
T_9	2.833(68)	0.00015(12)	0.0003(3)
T_{10}	1.821(39)	0.00023(21)	0.0005(5)
T_{11}	1.167(23)	-0.00006(24)	0.0000(6)

Table 5.2: Best estimates for the mass difference between the pseudoscalar and scalar masses (third column) and for the vector and axial masses (fourth column).

account. The best estimates for these differences have been extracted by using the same strategy employed for the vector-pseudoscalar difference, in order to reduce the statistical fluctuations of the measurements by exploiting the correlation of our data. The corresponding continuum limit extrapolated mass differences are

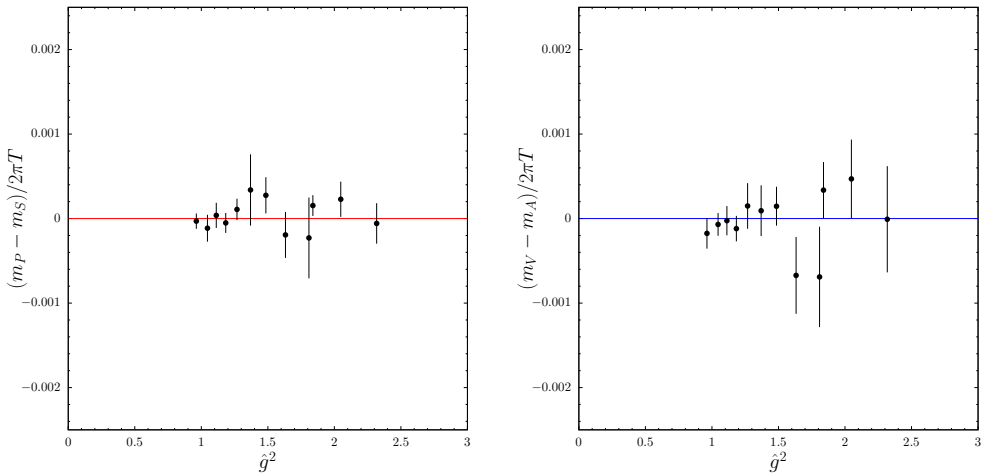

Figure 5.8: Left: mass difference between the pseudoscalar and the scalar channels. Right: mass difference between the vector and the axial channels.

reported in table 5.2.

The same data are shown as a function of $\hat{g}^2$ in fig. 5.8. On the left panel we provide the mass difference between the pseudoscalar and the scalar masses, while on the right panel the difference between the vector and the axial ones. In both cases, within our statistical precision, such differences are compatible with zero for all the temperatures simulated. On one hand, the numerical results for the pseudoscalar-scalar difference together with eq. 2.47 are compatible with the fact that we restricted our simulations to the zero topological sector. On the other hand the difference between the vector and the axial masses, if combined with eq. 2.36. provides a clear sign that chiral symmetry is effectively restored in the entire range of temperature that we explored in this thesis.

Chapter 6

Baryonic screening masses

Baryonic screening masses are important properties of the quark-gluon plasma. They characterize the large distance behaviour of two-point correlation functions composed of fields with the baryon quantum numbers. In this thesis we focus on interpolating operators of the form in eq. 3.102, i.e.

$$N = \epsilon^{abc}\left(u_a^T C\gamma_5 d_b\right) d_c\,, \qquad \overline{N} = \epsilon^{abc}\bar{d}_c\left(\bar{d}_b C\gamma_5 \bar{u}_a^T\right)\,. \tag{6.1}$$

The corresponding spatially-separated two-point correlation function, which is used to extract screening masses, read

$$C_{N^\pm}(x_3) = \int \mathrm{d}x_0\,\mathrm{d}x_1\,\mathrm{d}x_2 e^{i\frac{x_0}{L_0}\pi}\left\langle \mathrm{Tr}\left[P_\pm N(x)\overline{N}(0)\right]\right\rangle\,, \tag{6.2}$$

where $P_\pm = (1 \pm \gamma_3)/2$ are the parity projectors on positive (N^+) and negative (N^-) x_3-parity states respectively and the trace is over the free Dirac indices of the baryonic operators in eq. 6.1. Notice that, in contrast to the mesonic case, the integral select only states which are associated to the lowest Matsubara frequency π/L_0, being $L_0^{-1} = T$. The reason is that due to anti-periodic boundary conditions in the temporal extent for fermionic fields, the lowest possible Matsubara mode has non-zero energy, see eq. 2.6.

Baryonic screening masses describe the exponential fall-off of such correlation functions and, being the inverse of the correlation lengths, they are related to the response of the plasma when a baryon is injected into the system. Moreover,

similarly to the mesonic screening masses, as we have seen in Sec. 2.3.2, these masses are ideal probes to study the restoration of chiral symmetry in QCD at large temperatures.

Notice that, in presence of anti-periodic shifted boundary conditions for fermionic fields, the projection to the lowest Matsubara frequency must be modified in order to take into account that, in such framework, the periodic direction is identified by the vector $L_0\,(1, \boldsymbol{\xi})$, see Sec. 4.1 for the details, and correspondingly the temperature is modified as $T^{-1} = L_0/\gamma = L_0\sqrt{1+\boldsymbol{\xi}^2}$. Thanks to rotational invariance, we can choose one of the axis to be in the direction of the shift, and restrict our discussion to the case of interest $\boldsymbol{\xi} = (\xi, 0, 0)$. If we define (x_0, x_1) the temporal and the first spatial coordinate of a point in a system with temporal extent L_0 and shifted boundary conditions, the corresponding coordinates (x_0', x_1') in the system with periodic boundary conditions and temporal extent L_0/γ are found by using the euclidean Lorentz transformation in eq. 4.5. The projection on the lowest Matsubara frequency is then achieved by

$$C_{N^\pm}(x_3) = \int \mathrm{d}x_0\,\mathrm{d}x_1\,\mathrm{d}x_2 e^{i\frac{x_0+\xi x_1}{L_0}\gamma^2\pi}\left\langle \mathrm{Tr}\left[P_\pm N(x)\overline{N}(0)\right]\right\rangle\,, \tag{6.3}$$

where at variance of eq. 6.2 the expectation value $\langle\cdot\rangle$ is computed in presence of shifted boundary conditions.

While a rich literature is available on the mesonic sector of the screening masses, very few studies have been performed on the baryonic one. In particular, the current 1-loop order perturbative result obtained in the framework of the effective field theory is only qualitative [191]. On the other hand all the lattice calculations, both in the quenched approximation [192, 193] and in the full theory [194], are restricted to very low temperatures and no extrapolation to the continuum limit has ever been done. The chiral symmetry restoration pattern, at non-zero temperature, has been investigated by studying baryonic temporal correlation functions up to temperatures which are twice the critical one in Ref. [195, 94, 196]. For more recent efforts on the subject see Ref. [197, 198, 199].

Given the present status outlined above, a complete and systematic study, both on the lattice and on the perturbative side, is still missing in the literature. In the following sections we provide a first quantitative 1-loop perturbative estimate of

the baryonic screening masses, as well as a complete description of those masses on the lattice for temperatures ranging from 1 GeV up to the electroweak scale.

6.1 Baryonic screening masses in the effective field theory

The following discussion on the pertubative calculation of the baryonic screening masses is based on some notes by Prof. Mikko Laine which were given to us as a private communication [3]. The calculation has been independently checked and extended and allowed us to determine the 1-loop order perturbative correction to the baryonic screening masses.

As for the simpler case of the mesonic screening masses, the first step is to write the baryonic interpolating operator in terms of the fields χ and ϕ defined in the dimensional reduced effective theory. In this way, if only zero Matsubara modes contribute, it is easy to see that the Fourier transform in the temporal direction of the nucleon interpolating operator reads

$$\begin{aligned}\int dx_0\, e^{i\frac{x_0}{L_0}\pi}\, N(x) \;=\; & -i\epsilon^{abc}T^{3/2}\,\delta\left(p_0+q_0+r_0-\pi T\right) \\ & \times\left[\chi^T_{u_a,p_0}\sigma_2\phi_{d_b,q_0}\;+\;\phi^T_{u_a,p_0}\sigma_2\chi_{d_b,q_0}\right]\begin{pmatrix}\chi_{d_c,r_0}\\ \phi_{d_c,r_0}\end{pmatrix},\end{aligned} \tag{6.4}$$

where p_0, q_0 and r_0 denotes the lowest Matsubara frequencies, i.e. $\pm\pi T$, of each spinor[1]. Similar considerations lead to the expression of $\overline{N}(0)$ in the effective field theory.

6.1.1 Free theory result

The calculation in the free theory is carried out in the very same way as it has been done for the mesonic masses. If we assume to have forward propagating baryons in the third spatial direction with positive energy, then, from eq. E.3 and E.4, χ and ϕ propagate with positive and negative frequency respectively. For this reason, the

[1] Given the definite flavour structure of the interpolating operator in eq. 6.1, we also introduced an additional index, labelling the flavour content of the three-dimensional spinor.

only possible combinations which contributes to eq. 6.4 are

$$\epsilon^{abc}\left[\chi^{T}_{u_a,\pi T}\sigma_2\phi_{d_b,-\pi T}\right]\chi^{\alpha}_{d_c,\pi T} \tag{6.5}$$

$$\epsilon^{abc}\left[\phi^{T}_{u_a,-\pi T}\sigma_2\chi_{d_b,\pi T}\right]\chi^{\alpha}_{d_c,\pi T}\,. \tag{6.6}$$

Being the free theory insensitive to any spin structure, the σ_2 matrices appearing in eq. 6.4 play no rôle. In particular when doing the Wick contractions, Pauli matrices produce terms like $\mathrm{Tr}\,[\sigma_2^2]$, which amounts just to an overall constant. Then by taking into account the expressions of the free propagators in App. E.1, the baryonic spatial correlation function in the free theory is readily computed. Its expression reads

$$\begin{aligned} C^{(0)}_{N^{\pm}}(x_3) \,\propto\, \int_{\mathbf{p}_\perp,\mathbf{q}_\perp,\mathbf{r}_\perp} & \delta^{(2)}\left(\mathbf{p}_\perp+\mathbf{q}_\perp+\mathbf{r}_\perp\right)\delta(p_0+q_0+r_0-\pi T)\mathcal{M}(p_0,q_0,r_0) \\ & \exp\left[-x_3\left(|p_0|+|q_0|+|r_0|+\frac{\mathbf{p}^2}{2|p_0|}+\frac{\mathbf{q}^2}{2|q_0|}+\frac{\mathbf{r}^2}{2|r_0|}\right)\right], \end{aligned} \tag{6.7}$$

where $\mathcal{M}$ is a function of the Matsubara frequency whose form is dictated by the expressions of the free propagators in eq. E.3 and E.4. It reads

$$\mathcal{M}(p_0,q_0,r_0) \,=\, \left[3\theta(-p_0)\theta(q_0)\theta(r_0)+2\theta(p_0)\theta(-q_0)\theta(r_0)\right]. \tag{6.8}$$

It is now clear that in the static limit, for large separations, the exponential fall-off of such correlation function is dominated by $3\pi T$, which then provides the tree-level result for the baryonic screening masses. Notice that, in analogy with the mesonic case, this correlation function satisfies the equation of motion $\left(\partial_3-\hat{H}\right)C^{(0)}_{N^{\pm}}(x_3)=0$ for non-zero separations, being $\hat{H}$ the hamiltonian of a system with three non-interacting particles.

6.1.2 1-loop order correction

Similarly, the 1-loop order calculation is carried out by using the 1-loop order quark propagators derived from the NRQCD action at $O(g^2)$ in eq. 5.7. By displacing each quark in the transverse direction and by using the tree-level result in eq. 6.7

the 1-loop order baryonic correlation function has the general form

$$C^{(1)}_{N^{\pm}}(\{\mathbf{r}_i\},x_3) \propto \exp\left[-x_3\left(3M-\frac{\nabla^2_{\mathbf{r_1}}}{2M}-\frac{\nabla^2_{\mathbf{r_2}}}{2M}-\frac{\nabla^2_{\mathbf{r_3}}}{2M}\right)+g^2_{\mathrm{E}}\mathcal{A}(\{\mathbf{r}_i\},x_3)\right]$$

$$= C^{(0)}_{N^{\pm}}(\{\mathbf{r}_i\},x_3) + g^2_{\mathrm{E}}\mathcal{A}(\{\mathbf{r}_i\},x_3)\,C^{(0)}_{N^{\pm}}(\{\mathbf{r}_i\},x_3) \tag{6.9}$$

where $\mathcal{A}(\{\mathbf{r}_i\},x_3)$ encodes the 1-loop order corrections, $\{\mathbf{r}_i\}=\{\mathbf{r_1},\mathbf{r_2},\mathbf{r_3}\}$ are the transverse coordinates of each of the three quark fields and similarly $\nabla_{\mathbf{r}_i}$ denotes the derivative in the transverse directions coming from each quark propagator. For $x_3\neq 0$, this correlation function satisfies

$$\left[\partial_3+3M-\frac{\nabla^2_{\mathbf{r_1}}}{2M}-\frac{\nabla^2_{\mathbf{r_2}}}{2M}-\frac{\nabla^2_{\mathbf{r_3}}}{2M}-g^2_{\mathrm{E}}\mathcal{K}(\{\mathbf{r}_i\},x_3)\right]C^{(1)}_{N^{\pm}}(\{\mathbf{r}_i\},x_3)=0\,, \tag{6.10}$$

where the dimensionless kernel is defined as $\mathcal{K}(\{\mathbf{r}_i\},x_3)=\partial_3\mathcal{A}(\{\mathbf{r}_i\},x_3)$. Notice that the very same discussion we performed about the kernel for the simpler case of the non-singlet mesonic screening masses holds also in this case. In this way, any contribution coming from the transverse motion of quarks is parametrically suppressed in the static limit and all the transverse contribution in the kernel is only due to the exchange of gluons. For large x_3, the correlation function has the asymptotic form $C^{(1)}_{N^{\pm}}(\{\mathbf{r}_i\},x_3)=\mathcal{C}(\mathbf{r_1},\mathbf{r_2},\mathbf{r_3})e^{-E_0x_3}$. By inserting this expression in the equation above, the lowest energy state is unambiguously determined by solving the three-body Schrödinger equation

$$\left[-\frac{\nabla^2_{\mathbf{r_1}}+\nabla^2_{\mathbf{r_2}}+\nabla^2_{\mathbf{r_3}}}{2\pi T}+3M+V(\{\mathbf{r}_i\})\right]\mathcal{C}(\{\mathbf{r}_i\})=E_0\mathcal{C}(\{\mathbf{r}_i\})\,, \tag{6.11}$$

where we substituted $M\to\pi T$ at denominator of the kinetic term, since 1-loop order corrections to M give rise to subleading terms in the static limit. In the above equation, the static potential is then defined as $V(\{\mathbf{r}_i\})=-\lim_{x_3\to\infty}g^2_{\mathrm{E}}\mathcal{K}(\{\mathbf{r}_i\},x_3)$. Notice that, given the field content in eq. 6.5 and 6.6, the above Green's function is obtained by taking into account forward quark propagating χ fields with energy πT and forward propagating ϕ fields with energy $-\pi T$. The corresponding longitudinal propagators are defined in eq. E.6 and E.10. By combining them with eq. 6.5 and

6.6 and the corresponding expressions for $\overline{N}$, the correlation function at 1-loop order reads

$$C^{(1)}_{N^\pm}(\{\mathbf{r}_i\}, x_3) \equiv \frac{1}{N}\epsilon^{abc}\epsilon^{def}\Big(\left\langle U^{ad}_\phi(\mathbf{r}_1, x_3)\, U^{be}_\chi(\mathbf{r}_2, x_3)\, U^{cf}_\chi(\mathbf{r}_3, x_3)\right\rangle + \left\langle U^{ad}_\chi(\mathbf{r}_1, x_3)\, U^{be}_\phi(\mathbf{r}_2, x_3)\, U^{cf}_\chi(\mathbf{r}_3, x_3)\right\rangle\Big), \tag{6.12}$$

where N is an irrelevant constant introduced to obtain the correct normalization for the tree-level result in eq. 6.7. The full derivation of this correlation function is performed in App. E.4. Its general form is [3]

$$C^{(1)}_{N^\pm}(\{\mathbf{r}_i\}, x_3) \propto e^{-3Mx_3}\Big\{1 + 3g^2_{\mathrm{E}}\mathcal{A}_{\mathrm{L}}(\mathbf{0}_\perp, x_3) + g^2_{\mathrm{E}}\mathcal{A}^{12}_{\mathrm{T}}(\mathbf{r}_1, \mathbf{r}_2, x_3) + g^2_{\mathrm{E}}\mathcal{A}^{23}_{\mathrm{T}}(\mathbf{r}_2, \mathbf{r}_3, x_3) + g^2_{\mathrm{E}}\mathcal{A}^{13}_{\mathrm{T}}(\mathbf{r}_1, \mathbf{r}_3, x_3)\Big\}, \tag{6.13}$$

where $\mathcal{A}_{\mathrm{L}}(\mathbf{0}_\perp, x_3)$ is the term due to the exchange of longitudinal gluons which is common to the three quark propagators and $\mathcal{A}^{ij}_{\mathrm{T}}(\mathbf{r}_i, \mathbf{r}_j, x_3)$ is the trasverse term due to the exchange of gluons between two quark propagators at transverse coordinates $\mathbf{r}_i$ and $\mathbf{r}_j$ respectively. Notice that, at this order, no three-particle interactions contribute to the Green's function. By introducing the absolute value of the relative separation as $r_{ij} \equiv |\mathbf{r}_i - \mathbf{r}_j|$, the static potential, see App. E.4 and E.5 for the full derivation, reads [3]

$$V(\mathbf{r}_1, \mathbf{r}_2, \mathbf{r}_3) = \frac{1}{4}\Big[2V^-(r_{12}) + V^+(r_{23}) + V^-(r_{23}) + V^+(r_{13}) + V^-(r_{13})\Big] \tag{6.14}$$

where the potential $V^+(r)$ and $V^-(r)$ are defined in Ref. [95] and reported in App. E.5. As for the mesonic case, in order to find a numerical solution it is convenient to define the dimensionless coordinates $\hat{\mathbf{r}}_i = m_{\mathrm{E}}\mathbf{r}_i$ and consequently, by using the 1-loop expression for the low-energy constant M, we define

$$E_0 = 3M + \frac{g^2 C_F T}{2\pi}\hat{E}_0 = 3\pi T + g^2 T\frac{C_F}{2\pi}\left(\frac{3}{4} + \hat{E}_0\right). \tag{6.15}$$

Finally by reparametrizing the coupling in terms of ρ as defined in eq. 5.16, the Schrödinger equation for the three-body problem can be written as

$$\left\{-\frac{1}{2}\left(\nabla^2_{\hat{\mathbf{r}}_1}+\nabla^2_{\hat{\mathbf{r}}_2}+\nabla^2_{\hat{\mathbf{r}}_3}\right)+\rho\left[\hat{V}\left(\hat{\mathbf{r}}_1,\hat{\mathbf{r}}_2,\hat{\mathbf{r}}_3\right)-\hat{E}_0\right]\right\}\mathcal{C}\left(\{\hat{\mathbf{r}}_i\}\right)=0 \tag{6.16}$$

where $\hat{V}\left(\hat{\mathbf{r}}_1,\hat{\mathbf{r}}_2,\hat{\mathbf{r}}_3\right)$ is the static potential in eq. 6.14 obtained by reparametrizing the coupling in terms of ρ and expressed as a function of the dimensionless coordinates, see eq. 5.15 for the corresponding expression for the mesonic case.

A numerical solution has been determined as explained in App. F.1 and provides $\hat{E}_0 = 1.188$ and consequently [3]

$$E_0 = 3\pi T + g^2 T\frac{C_F}{2\pi}\left(\frac{3}{4}+\hat{E}_0\right) = 3\pi T\left(1+0.044\cdot g^2\right). \tag{6.17}$$

6.2 Baryonic screening masses on the lattice

The lattice transcription of the continuum correlation function in eq. 6.3 for $\boldsymbol{\xi} = (1,0,0)$ reads

$$\begin{aligned} C_{N^\pm}(x_3) &= a^6\sum_{x_0,x_1,x_2} e^{i\frac{x_0+x_1}{2L_0}\pi}\left\langle \mathrm{Tr}\left[P_\pm N(x)\overline{N}(0)\right]\right\rangle \\ &= a^6\sum_{x_0,x_1,x_2} e^{i\frac{x_0+x_1}{2L_0}\pi}\left\langle\left[W^1_\pm - W^2_\pm\right]\right\rangle, \end{aligned} \tag{6.18}$$

where in the second line we used the two Wick contractions, defined in eq. 3.103, which have been obtained by integrating over the fermionic fields. As for the mesonic screening masses, since the quark propagator is extremely suppressed for large separations, in order to obtain an accurate solution of the Dirac equation we employed the distance preconditioning described in App. C.2.

The two-point correlation functions in eq. 6.18 have been computed on all the lattice generated, see tables D.3 and D.6. For each ensemble, in tables C.3 and C.4 we report the total number of MDUs after the thermalization phase and the number of local sources per configuration on which the Wilson-Dirac operator has been inverted. Notice that in this case, at variance of the mesonic case, we always skipped 10 MDUs between two consecutive measurements, in order to enlarge

the statistics and benefit from a reduced statistical error. In any case, we never observed long autocorrelation times with respect to the number of MDUs skipped.

In the following we will focus on the positive parity correlators, since, at all the temperatures we simulated, we found excellent agreement, up to a sign, between the positive and the negative parity partners correlation functions. As discussed in Sec. 2.3.2 this is a clear manifestation of the chiral symmetry restoration which occurs at high temperatures. For this reason we studied the mass difference $(m_{N^+} - m_{N^-})/(3\pi T)$, which is a particularly interesting observable, since it is a measure of the chiral symmetry restoration. To this restoration pattern is devoted a dedicated section as a conclusion of this chapter.

6.2.1 Signal-to-noise ratio for baryonic correlation functions

From a technical point of view the calculation of the baryonic screening masses is feasible because, at asymptotically large temperatures, baryonic two-point correlation functions do not suffers from the exponential fall-off of the signal-to-noise ratio as they do at low and zero temperatures, see Sec. 3.8.3 and Ref. [158, 159] for more details on this topic.

As we have seen in Sec. 3.8.3, at zero temperature the exponential decay of the signal, for baryonic correlation functions, is dominated by the baryon mass, while the leading suppression of the variance is dictated by the pion mass, a fact which leads to a severe degradation of the signal at large separation, see eq. 3.110. However, at asymptotically high temperatures, up to corrections due to interaction, $m_{N^\pm} \to 3\pi T$ and $m_P \to 2\pi T$, where m_P is the pseudoscalar screening mass computed in Chapter 5. As a result, for very large temperatures, the signal-to-noise ratio becomes

$$\mathrm{StN}_{N^\pm}(x_3) = \frac{C_{N^\pm}(x_3)}{\sqrt{\sigma^2_{N^\pm}(x_3)}} \xrightarrow{x_3 \to \infty} \exp\left\{-\left[m_{N^\pm} - \frac{3}{2} m_P\right] x_3\right\} \sim \text{const.} \tag{6.19}$$

As a consequence, no exponential depletion of the signal-to-noise ratio is expected for large x_3 when $T \to \infty$. In fig. 6.1 we provide some representative examples of the signal-to-noise ratio as a function of the separation on the lattice for high, low

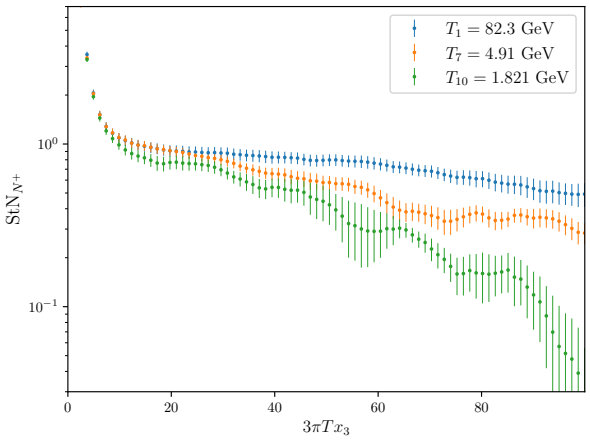

Figure 6.1: Signal-to-noise ratio as defined in eq. 6.19 for different values of the temperatures. For the highest temperature (blue points) the signal-to-noise is almost constant. As the temperature decreases the signal-to-noise starts to degrade (orange and green points). The signal-to-noise ratio for the sample mean is obtained by dividing by $1/\sqrt{N}$, where N is the number of gauge field configurations. For all the temperatures data refers to $L_0/a = 6$.

and intermediate temperatures. As expected, the degradation of the signal-to-noise ratio is less severe at high temperature. On the other hand when the temperature is lowered, the depletion becomes more severe and the Monte Carlo estimate of the correlation function becomes noisier.

6.2.2 Baryonic effective masses

Once the two-point correlation functions, in eq. 6.18, have been computed, the corresponding effective masses are defined as

$$m_{N^\pm}(x_3) = -\frac{1}{a}\ln\left[\frac{C_{N^\pm}(x_3+a)}{C_{N^\pm}(x_3)}\right]. \tag{6.20}$$

As a representative example of the data, the nucleon effective mass for $T_1 = 82.3$ GeV and $L_0/a = 4$ is shown in fig. 6.2 . In order to determine the value of the screening mass, we start by fitting the effective mass to a constant plus a correction deriving from the contamination of the first excited state from a minimum value up

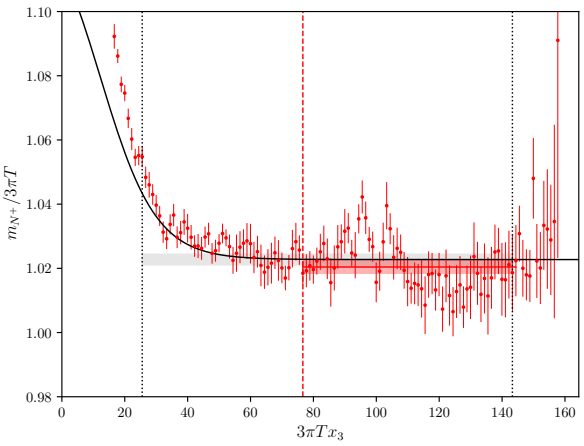

Figure 6.2: Plot of the effective mass m_{N^+}, normalized to the free theory value $3\pi T$, as a function of the separation on the lattice. The vertical black dotted lines show the interval in which the effective mass has been fitted, while the red vertical line indicates the starting point from which we averaged the plateau. The black curve and the red horizontal line represent the correlated fit and the average of the plateau respectively. Black and red bands are the corresponding errors of the best estimates of the mass. Data refers to the temperature $T_1 = 82.3$ GeV for $L_0/a = 4$.

to the last point where we have a good signal. The minimum value is chosen to have a good quality of the fit and to have, at the same time, a non-vanishing contribution from the first excited state. On one hand, for the ensembles where the signal is good enough at large distance, from this fit we estimate the minimum value $x_3^{\min}/a$ from which the excited state contamination is below the target statistical precision. The screening mass is then obtained by averaging the plateau from $x_3^{\min}/a$ up to the last point where we have a good signal. On the other hand, for the lowest temperatures and for the ensembles corresponding to $L_0/a = 10$, where the loss of signal is more relevant at large distance, the screening mass is directly estimated from the result of the effective mass fit. See fig. 6.2 for a representative example of such fits.

Our best estimates of the screening masses are reported in tables C.3 and C.4 for all the lattices simulated. The statistical error varies from a few permille to at most 6 permille for the lowest temperatures. As for the mesonic masses, in order to profit from the correlation in our data for reducing the statistical error, we also

T	T(GeV)	$\frac{m_{N^+}}{3\pi T}$	$\frac{m_{N^+} - m_{N^-}}{3\pi T}$
T_0	164.6(5.6)	1.047(3)	0.0006(4)
T_1	82.3(2.8)	1.0544(19)	-0.0001(3)
T_2	51.4(1.7)	1.0569(28)	0.0002(3)
T_3	32.8(1.0)	1.0583(27)	0.0003(4)
T_4	20.63(63)	1.0596(28)	-0.0011(4)
T_5	12.77(37)	1.0662(28)	0.0001(4)
T_6	8.03(22)	1.068(3)	0.0001(4)
T_7	4.91(13)	1.075(4)	0.0004(9)
T_8	3.040(78)	1.077(4)	0.0003(9)
T_9	2.833(68)	1.076(4)	0.0009(12)
T_{10}	1.821(39)	1.089(4)	0.0007(20)
T_{11}	1.167(23)	1.078(6)	0.0016(15)

Table 6.1: Best results for the nucleon mass, m_{N^+}, and the mass difference with its parity partner, $m_{N^+} - m_{N^-}$, in the continuum limit. In both cases results are normalized to the free theory value $3\pi T$.

compute the mass difference $(m_{N^+} - m_{N^-})\,/\,(3\pi T)$ and report its values in tables C.3 and C.4 as well.

In analogy with what we have done for the mesonic screening masses we explicitly checked that finite volume effects are negligible within our statistical precision. We computed the baryonic screening masses on the same smaller lattices as for the mesonic masses and checked that those are in agreement with the ones obtained on the corresponding larger volume. As expected from the theoretical analysis provided in Sec. 4.5, we can safely assume that our results have negligible finite-volume effects within the statistical precision that has been reached.

6.2.3 Continuum limit of baryonic screening masses

The results that we have collected at finite lattice spacings have to be extrapolated to the continuum limit, along the lines of constant physics. As for the mesonic masses, the Symanzik effective theory predicts $O(a^2)$ lattice artifacts. Furthermore, the convergence to the continuum limit has been accelerated by introducing the

tree-level improved definitions

$$m_{N^\pm} \longrightarrow m_{N^\pm} - \left[m_{N^\pm}^{\text{free}} - 3\pi T\right], \tag{6.21}$$

where $m_{N^\pm}^{\text{free}}$ is the mass in the free lattice theory, which has been computed in App. G.2. The improved data have been extrapolated to the continuum limit. Such

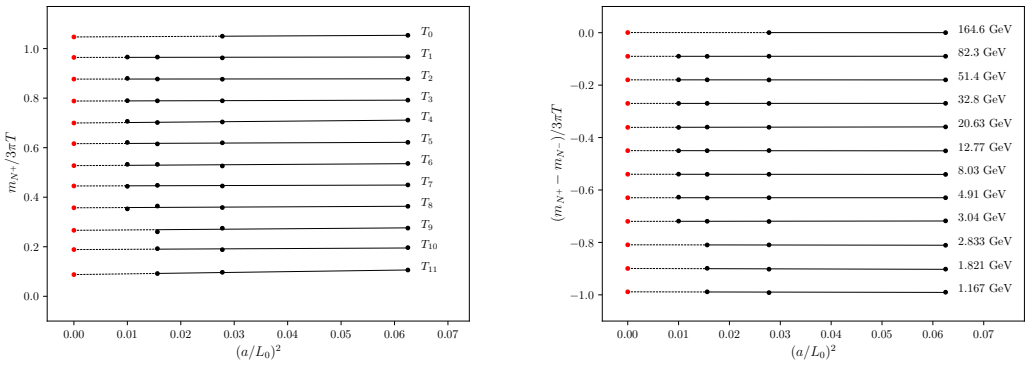

Figure 6.3: Left: Numerical result for the tree-level improved nucleon screening mass at finite lattice spacing (black dots). The lines in the panel represent the linear extrapolations in $(a/L_0)^2$ to the continuum limit. Each temperature is analyzed independently from the others. Data corresponding to T_i $(i = 0, \ldots, 11)$ have been shifted downward by $0.09 \times i$ for better readability. Right: same as the left panel but for the mass difference $(m_{N^+} - m_{N^-})$.

extrapolations are represented in fig. 6.3 where, in order to improve readability, data corresponding to T_i with $i = 0, \ldots, 11$ are shifted downward by $0.09 \times i$. As it is clear from fig. 6.3, data are well described by a single correction proportional to $(a/L_0)^2$. In general, by fitting with a linear ansatz in the squared lattice spacing, we obtained values of χ^2/dof all around 1, with just for a few outliers, a fact which is, however, not surprising given the large amount of data and fits. The results of the fits are shown in fig. 6.3 on the left panel as straight lines. For the mass difference $(m_{N^+} - m_{N^-})$ the coefficient of $(a/L_0)^2$ is found to be proportional with zero at all the temperatures, see left right panel of fig. 6.3. The continuum values obtained from these fits are taken to be our best estimates of the nucleon screening masses in this range of temperatures. The continuum limit extrapolated values for the positive parity screening mass are reported in the third column of

table 6.1 for all the temperatures that have been simulated and in the same way the corresponding values for the mass difference $(m_{N^+} - m_{N^-})$ are reported in the fourth column.

As a further check of the quality of our extrapolations, data have been fitted by excluding the coarsest lattice spacing, i.e. $L_0/a = 4$, for the temperatures $T_1, \ldots, T_8$. As it was observed for the mesonic screening masses, the intercept are in good agreement with those of the previous fit. Further checks include fitting the data with fit ansatz $(a/L_0)^2 \ln(a/L_0)$ and $(a/L_0)^3$ and the corresponding parameters turn out to be compatible with zero for each data set. Finally, given the high quality of the tree-level improved data and the robustness of the independent continuum limit extrapolations, it was not necessary to model the temperature dependence of the lattice artifacts by a global fit of the data.

6.2.4 Temperature dependence

From the results reported in the third column of table 6.1 it is clear that the bulk of the nucleon screening mass is given by the free-theory value $3\pi T$, plus a 4–8% positive contribution due to interactions over the entire range of temperature explored.

Thanks to the high precision of our results, we can scrutinize in detail the temperature dependence induced by the non-trivial dynamics. As done for the mesonic case, we decide to parametrize our data in terms of the function of the temperature defined in eq. 5.24. Again, let us stress that any function with a leading inverse logarithmic behaviour in the temperature is a good choice as well, and that the choice of eq. 5.24 is suggested by the effective field theory analysis.

We fit the values of m_{N^+} reported in the third column of table 6.1 to a quartic polynomial in $\hat{g}$ of the form

$$\frac{m_{N^+}}{3\pi T} = b_0 + b_2\hat{g}^2 + b_3\hat{g}^3 + b_4\hat{g}^4 \,. \tag{6.22}$$

The intercept turns out to be compatible with the free theory value 1, with a large error. We thus enforce it to the free theory value $b_0 = 1$ and we fit again the data. From the resulting fit, the coefficient of the $\hat{g}^2$ term results to be compatible with the 1-loop order correction that has been computed in Sec. 6.1.2 within again

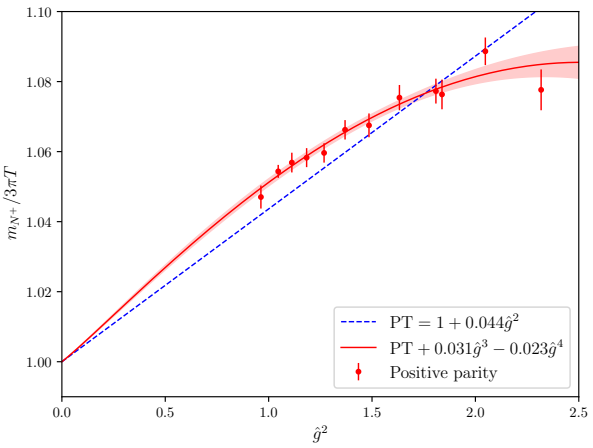

Figure 6.4: Nucleon screening mass versus $\hat{g}^2$. The band represents the best fit in eq. 6.22, while the dashed line is the analytically known contribution.

a large uncertainty. We have thus set the quadratic coefficient to its theoretical expectation, i.e. $b_2 = 0.044$, and we have performed again the quartic fit of the form in eq. 6.22.

As a result, for the fit parameters we obtain $b_3 = 0.031(4)$ and $b_4 = -0.023(3)$ with $\mathrm{cov}(b_3, b_4)/[\sigma(b_3)\sigma(b_4)] = -0.992$. The fit provides an excellent value of $\chi^2/\mathrm{dof} = 0.638$ and we thus take the polynomial in eq. 6.22 as the best parameterization of our results in the entire range of temperatures. Let us notice, however, that if a cubic ansatz in $\hat{g}$ is used instead of the one in eq. 6.22, the quadratic coefficient does not result to be compatible with the theoretical prediction at 1-loop order. This is even more evident from the plot in fig. 6.4 where the lattice data are shown together with the 1-loop order theoretical prediction and with the fit in eq. 6.22. In general the 1-loop order correction to the free theory value lies below lattice data almost in the entire range of temperatures that we considered.

In any case, it is clear that the leading perturbative correction in the coupling constant cannot explain our results even at the highest temperature, where cubic and quartic terms are still relevant. In particular, given the best parameterization of our data in eq. 6.22, at the electroweak scale, the strong competition between these terms amounts to approximately 20% of the total contribution due to interactions. On the other hand, at the lower end of the temperature range that has

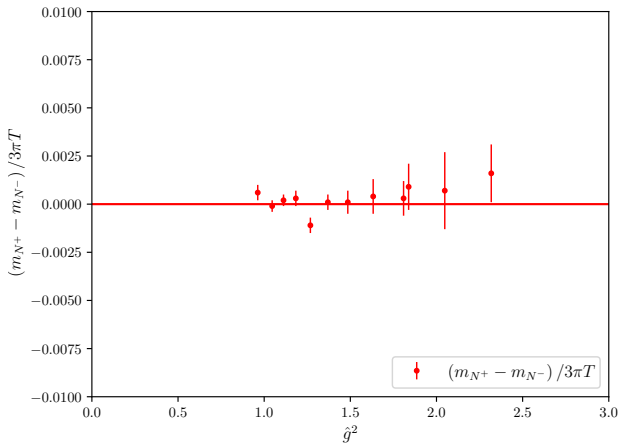

Figure 6.5: Mass difference between the positive and negative parity partners masses as a function of $\hat{g}^2$.

been considered, the presence of a quartic term is crucial to explain the flattening of the lattice data at $T \approx 1$ GeV.

To conclude, by combining lattice data with the known leading correction to the free theory, it is evident that the validity regime of the 1-loop order perturbative result is restricted to temperatures which are several order of magnitude above the electroweak scale.

6.2.5 Chiral symmetry restoration on the lattice

Baryonic screening masses are a good measure of chiral symmetry restoration. From the discussion in eq. 2.3.2 it is clear, that if the non-singlet axial symmetry is restored, then the positive and negative parity partners are expected to become degenerate. This is at variance of the zero temperature case, where the screening masses m_{N^+} and m_{N^-} correspond to the chiral limit values of the nucleon and of the N^* masses. Due to the spontaneous breaking of chiral symmetry, see Sec. 1.5.3 that occurs at zero temperature, they differ by several hundreds of MeV [22]. As anticipated, the screening correlation functions related to different parity partners are found to be degenerate, within our statistical precision, for large and intermediate separations on the lattice. In fig. 6.3 on the right the continuum limit

extrapolations of the mass differences are shown and the corresponding results in the continuum limit are provided in the fourth column of table 6.1. In fig. 6.5 we show the results in the continuum limit as a function of $\hat{g}^2$. In general, the mass difference is compatible with zero in the entire range of temperatures that has been simulated. These numerical results, together with the WTI in eq. 2.53, provides a measure of the restoration pattern of chiral symmetry at high temperature.

Chapter 7

Conclusions and outlook

In this thesis we exploited the steady theoretical and algorithmic progress in the simulations of lattice QCD, as well as in the HPC hardware which make it possible to simulate lattices with a very large number of points. Based on this progress, we implemented a new strategy to simulate very high temperatures on the lattice with a moderate computational effort. This strategy is built on the knowledge deriving from a non-perturbative definition of the strong coupling constant in a finite volume, combined with step-scaling techniques.

The strategy has been outlined in Chapter 4. It has been implemented in our lattice simulations, by discretizing three flavours of massless quarks with the $O(a)$-improved Wilson's discretization for fermions. Monte Carlo simulations have been carried out at 12 values of the temperatures in the range between ~ 1 GeV up to the electroweak scale for the first time on the lattice. For each temperature, we simulated three or four different lattice spacings in order extrapolate our results to the continuum limit. Furthermore finite volume effects have been explicitly checked to be negligible within our statistical precision.

The main physics results of this work are the hadronic screening masses, both mesonic and baryonic. In Chapter 5, we focused on the flavour non-singlet mesonic screening masses. These are maybe the simplest observables in thermal QCD. However, despite the simplicity of the calculation, they encode a lot of non-trivial interesting features. They are ideal probes of chiral symmetry restoration in the high temperature regime and can provide relevant information on the reliability of

next-to-leading order perturbation theory up to the electroweak scale.

Thanks to the permille accuracy of our results we were able to analyze in detail the temperature dependence of the non-trivial dynamics induced by interactions. In general, the bulk of the non-singlet mesonic screening masses is given by the free theory value $2\pi T$ with a few percent positive deviation in the entire range of temperatures. Quartic contributions in the coupling constant are still relevant both at low and high temperatures. On one hand, at low temperatures, such terms bend down the pseudoscalar mass, which has a value close to $2\pi T$, at $T \sim 1$ GeV. On the other hand spin-dependent terms, which have been observed to be $O(g^4)$ in the entire range of temperatures, are responsible, at low temperature, for the deviation of the vector mass from the free theory value $2\pi T$. Furthermore, those terms still remain visible even at the highest temperatures that we simulated, where the vector and the pseudoscalar screening masses are clearly different within our statistical precision. It is crucial to notice that such behaviour cannot be explained by the next-to-leading order perturbative result in Ref. [15]. The pattern of different contributions that we have found explains why it has been difficult in the past to match non-perturbative lattice results at $T \lesssim 1$ GeV with the known analytic behaviour at asymptotically high temperatures.

In Chapter 6 we carried out the first non-perturbative calculation of the baryonic screening masses in the same wide range of temperatures. While a rich literature is available on the mesonic spectrum, very few studies have been performed on the baryonic sector. In particular the only analytical result is just qualitative [191] and all the lattice calculations, both in the quenched approximation and in the full theory, are restricted to the low temperature regime and no extrapolation to the continuum limit has ever been performed. From the technical view point, the calculation is feasible, because at very large temperatures baryonic two-point correlation functions do not suffer from the dramatic depletion of the signal-to-noise ratio as they do at low and zero temperature. Baryonic screening masses were obtained with a few permille accuracy, for the first time in a wide range of temperatures. In the entire range of temperature explored, their values show at most a 8% positive deviation with respect to the free theory value $3\pi T$.

At the electroweak scale, cubic and quartic terms compete to give a final correction which is about 20% of the total contribution due to interactions. Furthermore,

at low temperatures these contributions are crucial to explain the temperature dependence of the baryonic screening masses.

In this work, we also provided the first quantitative determination of the 1-loop order correction to the free theory value. This correction has been obtained in the framework of the dimensional reduced effective theory defined in Chapter 2. However, as for the mesonic case, given the non-trivial temperature dependence induced by interactions, the 1-loop order perturbative correction is not able to explain our non-perturbative results.

Finally, both in the mesonic and in the baryonic sectors, we observed chiral symmetry restoration which manifests itself through the degeneracy of several masses. This degeneracy pattern is compatible with a set of WTI derived in Chapter 2.

In conclusion, our results are compatible with the dimensional reduced effective theory predictions. However, thanks to the high accuracy of our results we are able to resolve the different contributions due to interactions and, if compared with the corresponding next-to-leading order correction, these findings provide a clear indication that a 1-loop order perturbative description of these observables is not satisfactory even at very large temperatures. These results, together with other findings in the literature obtained in the $SU(3)$ Yang-Mills theory, suggest that a higher order description in perturbation theory is needed, if the perturbative expansion is not spoiled by non-perturbative effects, but, most of all, they motivate a non-perturbative exploration of thermal QCD up to the electroweak scale.

7.1 Future perspectives

The non-perturbative results provided in this thesis, together with the comparison with the analytical results obtained in the context of the effective field theory, call for a non-perturbative study of the high temperature regime of QCD. In this work, we propose a general strategy which allows to do that with a moderate computational effort. This strategy clears the way to compute many other interesting properties of thermal QCD in the high temperature regime, e.g. the Equation of State. Indeed this work is part of a larger effort which aims at studying thermal QCD non-perturbatively up to the electroweak scale [167].

Within this long-term project, it would be interesting to extend such calculations to screening masses related to different interpolating operators, like the ones related to spin-3/2 states. In such case, we could perform a detailed analysis of the spin-dependent terms similarly to the one we performed for the vector-pseudoscalar mass difference. The other obvious outcome is the calculation of the non-static sector, i.e. the non-zero Matsubara sector, of the mesonic screening masses. Indeed, the non-static sector is somehow related to the production of soft dileptons and photons in the quark-gluon plasma [95]. In both cases, the calculation on the lattice of these observables is expected to be more challenging than the ones we focused on in this work. For the non-static sector of the mesonic screening masses we expect a dramatic degradation of the signal-to-noise ratio, while for the spin-3/2 baryon the correct implementation of the spin projection at finite temperature is not trivial, since it is in general momentum-dependent. In any case, both these non-perturbative calculations would put additional constraints on the validity of the perturbative approach at temperatures above 1 GeV.

On the perturbative side, the high quality of our results call for a higher order calculation of the mesonic and baryonic screening masses, if possible, namely if the perturbative expansion is not spoiled by any non-perturbative infrared effect. In this case, the analytical results for cubic terms in the coupling constant and spin-dependent terms would give a further insight on the reliability of perturbation theory.

Finally, from a theoretical point of view, when the corresponding non-perturbative computations in the three-dimensional effective theory will become available, the matching with the results provided in this thesis will allow to shed light on the origin of the various terms and to verify at the non-perturbative level the effective field theory paradigm.

Appendix A

Conventions & definitions

A.1 SU(N) conventions

The Lie algebra of $SU(N)$ may be identified with a linear space of dimensions N^2-1. The $SU(N)$ group is composed of unitary matrices with unitary determinant. As a consequence, its algebra is the linear space spanned by hermitian, traceless $N \times N$ matrices T_a, i.e.

$$\mathrm{Tr}\left[T^a\right] = 0\,, \quad T^{a\dagger} = T^a \qquad T^a \in \mathfrak{su}(N)\,. \tag{A.1}$$

In order to make a definite choice, we assume the normalization given by

$$\mathrm{Tr}\left[T^a T^b\right] = \frac{\delta^{ab}}{2}\,. \tag{A.2}$$

The product of two generators of the algebra leads to following relation

$$T^a T^b = \frac{1}{2N}\delta^{ab}\mathbb{1}_{N\times N} + \frac{1}{2}\sum_{c=1}^{N^2-1}\left(if^{abc} + d^{abc}\right)T^c\,, \tag{A.3}$$

where f^{abc} are totally anti-symmetric structure constants and d^{abc} are totally symmetric coefficients, which expressions reads

$$d^{abc} = 2\,\mathrm{Tr}\left[\left\{T^a, T^b\right\}T^c\right]\,, \tag{A.4}$$

and the Casimir operator is defined by

$$T^a T^a = C_F \mathbb{1}_{N\times N}\,, \tag{A.5}$$

where $C_F = (N^2-1)/(2N)$. These definitions lead to the following (anti-)commutation relations

$$\begin{aligned}\left[T^a, T^b\right] &= i f^{abc} T^c \\ \left\{T^a, T^b\right\} &= d^{abc} T^c + \frac{\delta^{abc}}{N}\,.\end{aligned} \tag{A.6}$$

In this thesis we will extensively use the case $N = 3$, both for the number of colours and flavours. For this reason it is useful to define the Gell-Mann matrices

$$\begin{gathered}\lambda_1 = \begin{pmatrix}0&1&0\\1&0&0\\0&0&0\end{pmatrix}, \quad \lambda_2 = \begin{pmatrix}0&-i&0\\i&0&0\\0&0&0\end{pmatrix}, \quad \lambda_3 = \begin{pmatrix}1&0&0\\0&-1&0\\0&0&0\end{pmatrix}, \\ \lambda_4 = \begin{pmatrix}0&0&1\\0&0&0\\1&0&0\end{pmatrix}, \quad \lambda_5 = \begin{pmatrix}0&0&-i\\0&0&0\\i&0&0\end{pmatrix}, \\ \lambda_6 = \begin{pmatrix}0&0&0\\0&0&1\\0&1&0\end{pmatrix}, \quad \lambda_7 = \begin{pmatrix}0&0&0\\0&0&-i\\0&i&0\end{pmatrix}, \\ \lambda_8 = \frac{1}{\sqrt{3}}\begin{pmatrix}1&0&0\\0&1&0\\0&0&-2\end{pmatrix},\end{gathered} \tag{A.7}$$

which provide a basis T^a for the $\mathfrak{su}(3)$ algebra given by $T^a = \lambda^a/2$.

A.2 Clifford algebra

In a four-dimensional euclidean space-time Dirac gamma matrices are covariant matrices which define a basis for the Clifford algebra $\mathrm{Cl}_4(\mathbb{C})$ [1]. Those satisfy the anti-commutation relation

$$\{\gamma_\mu, \gamma_\nu\} = 2\delta_{\mu\nu}\mathbb{1}_{4\times4}\,. \tag{A.8}$$

In the so called *chiral representation* Dirac gamma matrices read

$$\gamma_0 = \begin{pmatrix} 0 & -\mathbb{1}_{2\times2} \\ -\mathbb{1}_{2\times2} & 0 \end{pmatrix}, \quad \gamma_i = \begin{pmatrix} 0 & -i\sigma^i \\ i\sigma^i & 0 \end{pmatrix} \qquad i = 1,2,3\,, \tag{A.9}$$

where σ^i are the 2×2 Pauli matrices, which are defined as

$$\sigma_1 = \begin{pmatrix} 0 & 1 \\ 1 & 0 \end{pmatrix}, \quad \sigma_2 = \begin{pmatrix} 0 & -i \\ i & 0 \end{pmatrix}, \quad \sigma_3 = \begin{pmatrix} 1 & 0 \\ 0 & -1 \end{pmatrix}. \tag{A.10}$$

Then we define the γ_5 matrix as the product of the four gamma matrices

$$\gamma_5 = \gamma_0\gamma_1\gamma_2\gamma_3 = \begin{pmatrix} \mathbb{1}_{2\times2} & 0 \\ 0 & -\mathbb{1}_{2\times2} \end{pmatrix}, \tag{A.11}$$

which anti-commutes with all the other γ-matrices, i.e.

$$\{\gamma_5, \gamma_\mu\} = 0\,. \tag{A.12}$$

Following from these definitions, the charge-conjugation operator is given by the product

$$C = i\gamma_0\gamma_2 = \begin{pmatrix} \sigma_2 & 0 \\ 0 & -\sigma_2 \end{pmatrix}. \tag{A.13}$$

[1] In Minkowski space the Clifford algebra is defined as $\mathrm{Cl}_{1,3}(\mathbb{R})$ which is, by rotating to euclidean time, isomorphic to $\mathrm{Cl}_4(\mathbb{C})$.

This satisfies the following identities

$$C\gamma_\mu C = -\gamma_\mu^{\mathrm{T}}\,, \quad C^{\mathrm{T}} = -C\,, \quad C\gamma_5 = \gamma_5 C\,, \tag{A.14}$$

where the superscript "T" refers to the transposed matrix. Dirac gamma matrices satisfy the following trace relations

$$\mathrm{Tr}\{[\gamma_\mu\gamma_\nu]\} = 4\delta_{\mu\nu}\,, \tag{A.15}$$

$$\mathrm{Tr}\{[\gamma_\mu\gamma_\nu\gamma_\rho\gamma_\sigma]\} = 4\left(\delta_{\mu\nu}\delta_{\rho\sigma} - \delta_{\mu\rho}\delta_{\nu\sigma} + \delta_{\mu\sigma}\delta_{\rho\nu}\right)\,, \tag{A.16}$$

while the trace of an odd number of gamma matrices vanishes.

In the effective field theory, in order to properly factorize the propagation along different space directions, it is useful to define the Dirac gamma matrices in a different representation with respect to eq. A.9. In this representation they read

$$\gamma_0 = \begin{pmatrix} 0 & \mathbb{1} \\ \mathbb{1} & 0 \end{pmatrix}, \quad \gamma_1 = \begin{pmatrix} \sigma_2 & 0 \\ 0 & -\sigma_2 \end{pmatrix}, \quad \gamma_2 = \begin{pmatrix} -\sigma_1 & 0 \\ 0 & \sigma_1 \end{pmatrix}, \quad \gamma_3 = \begin{pmatrix} 0 & -i\mathbb{1} \\ i\mathbb{1} & 0 \end{pmatrix}. \tag{A.17}$$

As a consequence, in this representation for the γ_5 matrix and the charge-conjugation operator it holds

$$\gamma_5 = \begin{pmatrix} -\sigma_3 & 0 \\ 0 & \sigma_3 \end{pmatrix}, \quad C = \begin{pmatrix} 0 & i\sigma_1 \\ -i\sigma_1 & 0 \end{pmatrix} \quad \text{and} \quad C\gamma_5 = \begin{pmatrix} 0 & \sigma_2 \\ \sigma_2 & 0 \end{pmatrix}, \tag{A.18}$$

where σ_i are the 2×2 Pauli matrices defined in eq. A.10.

Appendix B

Correlation functions on the lattice

B.1 Parity and charge-conjugation transformations

In this appendix we review how hadronic interpolating operators, used on the lattice to extract the QCD hadronic spectrum, transform under global symmetries, such as parity and charge conjugation. First of all, recall how quark and anti-quark transforms under charge conjugation transformations

$$\begin{aligned} \psi(x) &\xrightarrow{C} C^{-1}\bar{\psi}(x)^T\,, \\ \bar{\psi}(x) &\xrightarrow{C} -\psi(x)^T C\,, \end{aligned} \tag{B.1}$$

where C is the charge-conjugation matrix defined in App. A.2. Analogously under generalized parity transformations the fermionic fields transform as

$$\begin{aligned} \psi(x) &\xrightarrow{\mathcal{P}_\mu} \gamma_\mu\,\psi(X) \\ \bar{\psi}(x) &\xrightarrow{\mathcal{P}_\mu} \bar{\psi}(X)\,\gamma_\mu \end{aligned} \tag{B.2}$$

where X denotes the coordinate vector x with flipped sign except for the coordinate in the μ-direction.

Operator	Γ_O	C	$\mathcal{P}$
S	$\mathbb{1}$	+1	+1
P	γ_5	+1	−1
V_μ	γ_μ	−1	−1
A_μ	$\gamma_\mu\gamma_5$	−1	+1

Table B.1: Transformation properties for mesonic interpolating operators under parity and charge-conjucation transformations.

Starting from the transformation properties of the quark and anti-quark fields it is straightforward to see that the mesonic interpolating operators defined in eq. 3.97 transform as

$$O^a = \bar{\psi}(x)\Gamma_O\tau^a\psi(x) \xrightarrow{C} \bar{\psi}(x)\left(C\Gamma_O C^{-1}\right)^T\tau^a\psi(x)\,, \tag{B.3}$$

$$O^a = \bar{\psi}(x)\Gamma_O\tau^a\psi(x) \xrightarrow{\mathcal{P}_\mu} \bar{\psi}(X)\left(\gamma_\mu\Gamma_O\gamma_\mu\right)\tau^a\psi(X)\,. \tag{B.4}$$

By resctricting ourselves to the interpolating operators of interest in this work it immediately follows the transformation properties reported in table B.1

In a similar way one can see that the nucleon interpolating operator in eq. 2.48 transforms under parity transformations as

$$\begin{aligned} N &\xrightarrow{\mathcal{P}_\mu} \gamma_\mu N^{\pm}(X) \\ \overline{N} &\xrightarrow{\mathcal{P}_\mu} \overline{N}^{\pm}(X)\gamma_\mu\,, \end{aligned} \tag{B.5}$$

and the corresponding operators with definite parity quantum numbers are constructed by projecting the operators in eq. B.5 with the parity projector $P_\pm = \left(1 \pm \gamma_\mu\right)/2$.

B.2 Reality of mesonic two-point correlation functions

Let us consider the mesonic correlation function defined in eq. 3.101. It reads

$$C_O^a(x_0) = \frac{a^3}{2}\sum_{\mathbf{x}}\Big\{ -\langle \mathrm{Tr}\left[\Gamma_O S(x,0)\Gamma_O\gamma_5 S^\dagger(x,0)\gamma_5\right]\rangle + \delta^{a0}N_f\,\langle \mathrm{Tr}\left[\Gamma_O S(x,x)\right]\mathrm{Tr}\left[\Gamma_O S(0,0)\right]\rangle\Big\}. \tag{B.6}$$

Let us consider, for the moment, the connected contribution and its conjugate transpose, which reads

$$\begin{aligned} C_O^a(x_0)^\dagger &= -\frac{a^3}{2}\sum_{\mathbf{x}}\langle \mathrm{Tr}\left[\gamma_5 S(x,0)\gamma_5\Gamma_O^\dagger S^\dagger(x,0)\Gamma_O^\dagger\right]\rangle \\ &= -\frac{a^3}{2}\sum_{\mathbf{x}}\langle \mathrm{Tr}\left[S(x,0)\gamma_5\Gamma_O^\dagger S^\dagger(x,0)\Gamma_O^\dagger\gamma_5\right]\rangle\ , \end{aligned} \tag{B.7}$$

where in the second line we used the cyclic property of the trace. It is now clear that the connected contribution to the mesonic two-point correlation function is purely real, if it holds

$$\Gamma_O^\dagger = \pm\gamma_5\Gamma_O\gamma_5\,. \tag{B.8}$$

In this thesis we mainly focus on flavour non-singlet interpolating operators with $\Gamma_O = \{\mathbb{1}, \gamma_5, \gamma_\mu, \gamma_\mu\gamma_5\}$ which then provide real two-point correlation functions. Similar considerations holds for the disconnect contribution. Its conjugate transpose reads

$$C_O^0(x_0)^\dagger = -\frac{a^3}{2}\sum_{\mathbf{x}} N_f\,\langle \mathrm{Tr}\left[S^\dagger(x,x)\Gamma_O^\dagger\right]\mathrm{Tr}\left[S^\dagger(0,0)\Gamma_O^\dagger\right]\rangle\ . \tag{B.9}$$

By using γ_5-hermiticity of the quark propagator, it can be rewritten as

$$C_O^0(x_0)^\dagger = -\frac{a^3}{2}\sum_{\mathbf{x}} N_f\,\langle \mathrm{Tr}\left[S(x,x)\gamma_5\Gamma_O^\dagger\gamma_5\right]\mathrm{Tr}\left[S(0,0)\gamma_5\Gamma_O^\dagger\gamma_5\right]\rangle\ , \tag{B.10}$$

which again implies that the disconnected contribution is real if the relation in eq. B.8 is satisfied.

B.3 Reality of the nucleon two-point correlation function

In this section we provide brief demonstration of the reality of the lattice baryonic correlation function defined in Sec. 3.8.2. In order to keep the discussion as general as possible we do not project the baryonic correlation function to any definite value of momentum. After integrating fermionic variables, its expression, in terms of path integral expectation value, reads

$$C_{N^{\pm}}(x) = \frac{1}{Z}\int DU\,(\det D\,[U])^{N_f}\,e^{-S_g[U]}\left\{W_{\pm}^{1}[U]+W_{\pm}^{2}[U]\right\}\,, \tag{B.11}$$

where we made explicit the dependence on the link variable U and where $W_{\pm}^{1}$ and $W_{\pm}^{2}$ are two Wick contractions defined in eq. 3.103. By taking into account the gauge field transformation $U \to U^{*}$, it is easy to show that the reality of the gauge action directly implies

$$S_g[U] = S_g[U^{*}]\,. \tag{B.12}$$

In a similar way it is possible to show that under the same transformation of the link variable it holds for the Wilson-Dirac operator

$$D^{*}[U] = \tilde{C}D[U^{*}]\tilde{C}^{-1}\,, \tag{B.13}$$

where $\tilde{C}$ is defined in terms of the charge-conjugation matrix as $\tilde{C} = C\gamma_5$. This implies that

$$\det D^{*}[U] = \det D[U] = \det D[U^{*}]\,, \tag{B.14}$$

where the equality on the l.h.s comes from the reality of the fermion determinant, and the one on the r.h.s from eq. B.13. As a consequence of eq. B.12 and B.14,

it is straightforward to see that gauge field configurations U and U^* are sampled with the same statistical weight. In this case the correlation function in eq. B.11 can be written as

$$C_{N^\pm}(x) = \frac{1}{2}\left\{\frac{1}{Z}\int DU\,(\det D\,[U])^{N_f}\,e^{-S_g[U]}\Big\{W_\pm^1[U]+W_\pm^2[U] \right. \\ \left. +W_\pm^1[U^*]+W_\pm^2[U^*]\Big\}\right\}. \tag{B.15}$$

The condition on the Dirac operator in eq. B.13 translates to the following conditions for the quark propagator $S[U]$

$$S^*[U] = \tilde{C}S[U^*]\tilde{C}^{-1}\,, \tag{B.16}$$
$$S^*[U]^T = \tilde{C}^{-1}S[U^*]^T\tilde{C}\,, \tag{B.17}$$

and consequently the expressions for the complex conjugate of the Wick contractions in presence of a background field U can be derived. After a little bit of algebra, their expressions read

$$W_\pm^{1*}[U] = \mathrm{Tr}\left[S_{ag}^T[U^*]C\gamma_5 S_{bf}[U^*]C\gamma_5\right]\mathrm{Tr}\left[S_{ce}[U^*]P_\pm\right]\epsilon^{abc}\epsilon^{feg} \tag{B.18}$$
$$W_\pm^{2*}[U] = \mathrm{Tr}\left[S_{ag}^T[U^*]C\gamma_5 S_{be}[U^*]P_\pm S_{cf}[U^*]C\gamma_5\right]\epsilon^{abc}\epsilon^{feg}\,,$$

and by comparing eq. B.18 with eq. 3.103, it immediately follows that $W_\pm^i[U^*] = W_\pm^{i*}[U]$ for $i = 1,2$, and the two-point correlation function is now manifestly a purely real function, since it can be written as

$$C_{N^\pm}(x) = \frac{1}{Z}\int DU\,(\det D\,[U])^{N_f}\,e^{-S_g[U]}\,\mathrm{Re}\Big[W_\pm^1[U]+W_\pm^2[U]\Big]. \tag{B.19}$$

Notice that this result is independent on the choice of the parity projectors, i.e. it holds if $P_\pm = (1\pm\gamma_\mu)/2$ for any value of μ. As a consequence, this result holds also if the two-point correlation function is a spatially-separated correlation function and the parity projector defines a generalized x_μ-parity transformation, see App. B.1.

Appendix C

Simulation details

In this appendix we report most of the technical details of the lattice simulations we performed in this work. In the following sections the definitions of the lattice actions are provided. Some time will be also devoted to the specific algorithm we used for the inversion of the Wilson-Dirac operator, which is somehow critical at high temperature and finally a dedicated section is devoted to report the details of the HMC algorithm we used throughout all the simulations, together with the results for the mesonic and baryonic screening masses at finite lattice spacing.

C.1 Lattice actions

In this thesis we exploited the results from Ref. [181] and [179] on the Schrödinger Functional and the Gradient Flow renormalized coupling respectively. For this reason we used both the Wilson plaquette action and the tree level Symanzik improved action $S_g^{(I)}$. The former is defined in eq. 3.14 and was used as a discretization for gluonic fields at the nine highest temperatures $T_0, \dots, T_8$, while the latter was used for the three lowest temperatures T_9, T_{10} and T_{11} and is defined as [138]

$$S_g^{(I)} = \frac{1}{g_0^2} \sum_x \sum_{\mu,\nu} \mathrm{Re} \left\{ \frac{5}{3} \mathrm{Tr}\left[\mathbb{1} - U_{\mu\nu}(x)\right] - \frac{1}{12} \mathrm{Tr}\left[\mathbb{1} - \tilde{U}_{\mu\nu}(x)\right] \right\}, \tag{C.1}$$

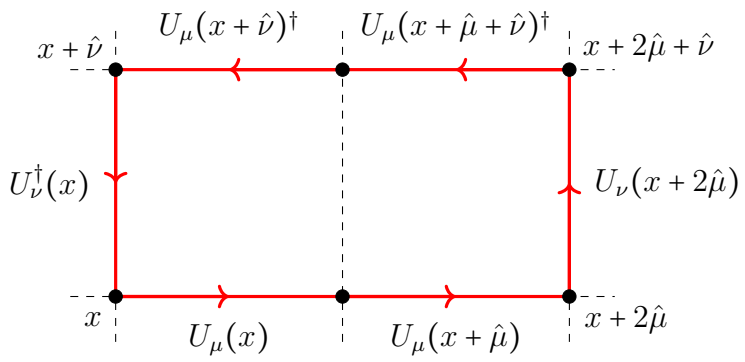

Figure C.1: Graphical representation of the rectangular two-plaquette field appearing the tree level Symanzik improved action.

where $U_{\mu\nu}(x)$ is the standard plaquette field defined in eq. 3.11 and $\tilde{U}_{\mu\nu}(x)$ is the rectangular two-plaquette field, shown in fig. C.1, and defined as

$$\tilde{U}_{\mu\nu}(x) = U_\mu(x)U_\mu(x+a\hat{\mu})U_\nu(x+2a\hat{\mu})U_\mu^\dagger(x+a\hat{\mu}+a\hat{\nu})U_\mu^\dagger(x+a\hat{\nu})U_\nu^\dagger(x)\,. \quad \text{(C.2)}$$

The fermionic sector of the action has been discretized by using the Wilson-Dirac operator defined in eq. 3.33 with $O(a)$-improvement provided by the Sheikholeslami-Wohlert operator defined in eq. 3.70. The non-perturbative tuning of the $c_{\rm sw}(g_0)$ coefficient removes all the $O(a)$ cut-off effects generated by the fermionic action in on-shell correlation functions [134, 135]. The corresponding expression for the Wilson plaquette action has been obtained in Ref. [137] and is reported in eq. 3.71, while for the tree-level Symanzik improved action it has been determined in Ref. [200] and reads

$$c_{\rm sw}^{(I)} = \frac{1-0.1921g_0^2-0.1378g_0^4+0.0717g_0^6}{1-0.3881g_0^2}\,. \quad \text{(C.3)}$$

Given this lattice setup the bare parameters of the actions have been fixed following the strategy described in App. D.

C.2 Inversion of the Dirac operator

The usual stopping criterion used in iterative methods for the numerical solution of the Dirac equation

$$D\psi = \eta \tag{C.4}$$

require that the norm of the residual $\rho = D\psi - \eta$ is sufficiently small, i.e. the global condition $r = \|\rho\|/\|\eta\| < \varepsilon$ has to be satisfied for a value of the tolerance ε small enough that the error introduced by using an approximate solution of the Dirac equation must be negligible with respect to the statistical fluctuations of the observables of interest. However, the tolerance cannot be smaller than what is allowed by the finite-precision arithmetic of a given implementation.

At high temperature, the lowest Matsubara frequency πT provides an infrared cut-off to quark propagation. As a consequence, the matrix elements of $S(x, y)$ become very small for large separations. The brute force approach of simply implementing higher-precision and requiring a smaller tolerance is not always practicable. In this case, a solution is achieved by introducing a preconditioned version of the Dirac equation,

$$\tilde{D}\tilde{\psi} = \tilde{\eta}\,, \tag{C.5}$$

where

$$\tilde{D} = M^{-1}DM \quad \tilde{\psi} = M^{-1}\psi\,, \quad \tilde{\eta} = M^{-1}\eta\,, \tag{C.6}$$

with the preconditioning matrix M chosen in such a way the the various components of the solution $\tilde{\psi}$ are comparable in magnitude [189].

The quark propagators needed for the two-point mesonic and baryonic correlation functions considered in this thesis have been computed by implementing the preconditioning matrix

$$M(x, y) = \cosh\left\{m_M\left(x_3 - y_3 - L/2\right)\right\} \cdot \mathbb{1}\,, \tag{C.7}$$

where $\mathbb{1}$ refers to the identity matrix in the indices not explicitly indicated, i.e. colour, spin and the first three components of the space-time coordinates (x_0, x_1, x_2). After some tuning, for the lattices with $L_0/a = 4, 6, 8$ and 10 we have chosen $m_M = 0.4, 0.3, 0.2$ and 0.15 respectively, with the shift parameter being always $\boldsymbol{\xi} = (1, 0, 0)$. This indeed guarantees that the components of $\tilde{\psi}$ are always comparable in magnitude. We have also monitored explicitly *a posteriori* that the global condition $r < \epsilon$ is always satisfied by the solution vector.

C.3 Simulation details and results

We have simulated three flavours QCD with a HMC algorithm by using the `openQCD-1.6` package [201, 202] modified so as to allow for shifted boundary conditions. We have employed several efficient algorithms in order to speed up simulations. More precisely, the up and down quarks have been simulated with an optimazed twisted-mass Hasenbusch preconditioning of the quark determinant [201, 146]. The determinant has been split in three factors with twisted masses value $a\mu = 0.0, 0.1$ and 1.0. The strange quark has been simulated through a RHMC algorithm [151, 152] with an optimized frequency splitting of the rational approximation in two separate contributions. Even-odd preconditioning has been used for both the light and the strange quarks. The integration of the molecular dynamics equations has been performed on a three-level integration scheme. The gauge force has been integrated on the finest level using a 4th-order Omelyan-Mryglod-Folk (OMF4) integrator [144] with step-size 1, while the fermionic forces have been integrated on the two coarsest levels. On the finest of these we have used a OMF4 integrator with step-size 1, while on the coarsest a 2nd-order OMF integrator with step-size between 7 and 9. The solution of the Dirac equation along the molecular dynamics evolution has been obtained by using standard conjugate gradient with chronological inversion. The length of each trajectory is 2 MDUs for all the lattices. More details on the exact implementation of these algorithms can be found in Ref. [201, 202].

For each ensemble we generated, we have started the thermalization phase by simulating a lattice with length $L/a = 48$ in all the three spatial directions and the same bare parameters as the target one. After approximately 1000 MDUs, we have

T	L_0/a	n_{mdu}	n_{skip}	n_{nsrc}	$\frac{m_P}{2\pi T}$	$\frac{m_V}{2\pi T}$	$\frac{(m_V - m_P)}{2\pi T}$
T_0	4	90	10	4	0.9659(5)	0.9716(7)	0.00577(20)
	6	90	10	2	0.9934(14)	0.9996(12)	0.0065(4)
T_1	4	90	10	4	0.9656(7)	0.9721(8)	0.0068(3)
	6	270	30	2	0.9945(14)	1.0014(19)	0.0070(8)
	8	450	50	2	1.0078(18)	1.0148(20)	0.0075(5)
	10	900	100	2	1.0090(25)	1.0160(27)	0.0075(4)
T_2	4	90	10	4	0.9685(7)	0.9753(8)	0.0075(3)
	6	270	30	2	0.9961(14)	1.0049(18)	0.0089(5)
	8	450	50	2	1.0055(23)	1.0147(25)	0.0089(5)
	10	900	100	2	1.0122(25)	1.0207(25)	0.0073(6)
T_3	4	90	10	4	0.9682(11)	0.9764(18)	0.0087(5)
	6	270	30	2	0.9971(11)	1.0050(16)	0.0084(10)
	8	450	50	2	1.0039(18)	1.0130(22)	0.0083(7)
	10	810	90	2	1.0124(25)	1.0219(29)	0.0099(7)
T_4	4	90	10	4	0.9704(7)	0.9804(14)	0.0103(4)
	6	270	30	2	0.9973(14)	1.0087(14)	0.0109(8)
	8	450	50	2	1.0051(20)	1.0172(25)	0.0093(9)
	10	540	60	2	1.0138(20)	1.0248(23)	0.0108(7)
T_5	4	90	10	4	0.9708(8)	0.9838(12)	0.0128(4)
	6	180	20	2	0.9941(22)	1.006(3)	0.0109(20)
	8	450	50	2	1.0057(18)	1.0172(29)	0.0119(21)
	10	540	60	2	1.0090(27)	1.0228(29)	0.0137(10)
T_6	4	90	10	4	0.9676(10)	0.9830(18)	0.0156(11)
	6	180	20	2	0.9948(15)	1.0089(24)	0.0142(11)
	8	450	50	2	1.0037(29)	1.018(4)	0.0150(23)
	10	540	60	2	1.0108(25)	1.026(4)	0.0153(16)
T_7	4	90	10	4	0.9679(8)	0.9854(18)	0.0172(11)
	6	180	20	2	0.9930(15)	1.0093(28)	0.0171(17)
	8	450	50	2	1.0051(22)	1.024(4)	0.0188(16)
	10	900	100	2	1.012(3)	1.028(5)	0.0171(19)
T_8	4	90	10	4	0.9677(8)	0.9910(18)	0.0235(17)
	6	180	20	4	0.9907(16)	1.015(4)	0.0237(17)
	8	450	50	4	1.000(3)	1.025(4)	0.0247(14)
	10	900	100	4	1.0032(23)	1.0288(25)	0.0252(14)

Table C.1: Results for the pseudoscalar, m_P, and the vector, m_V, non-singlet meson masses together with their difference $(m_V - m_P)$ all normalized to $2\pi T$ at finite lattice spacing for the temperatures $T_0, \ldots, T_8$. The number of MDUs generated, n_{mdu}, those skipped between two consecutive measurements, n_{skip}, and the number of local sources per configuration on which the two-point correlation functions have been computed, n_{nsrc}, are also reported.

T	L_0/a	n_{mdu}	n_{skip}	n_{nsrc}	$\frac{m_P}{2\pi T}$	$\frac{m_V}{2\pi T}$	$\frac{(m_V - m_P)}{2\pi T}$
T_9	4	90	10	4	0.9663(16)	0.9872(23)	0.0205(15)
	6	90	10	4	0.9907(24)	1.012(4)	0.0233(27)
	8	90	10	4	1.0010(20)	1.0238(25)	0.0233(16)
T_{10}	4	90	10	4	0.9645(13)	0.9912(17)	0.0259(22)
	6	90	10	4	0.9896(11)	1.0203(24)	0.0294(18)
	8	90	10	4	0.9963(22)	1.024(4)	0.0290(16)
T_{11}	4	90	10	4	0.9552(16)	0.992(3)	0.0375(18)
	6	90	10	8	0.9768(20)	1.018(5)	0.0406(26)
	8	90	10	8	0.9912(16)	1.031(6)	0.039(4)

Table C.2: As in Table C.1 but for T_9, T_{10} and T_{11}.

duplicated the lattice in each direction so that $L/a = 96$. We have then run the HMC for approximately 500 MDUs, after which we have triplicated the lattice in all the spatial directions so has to have $L/a = 288$. Finally we have completed the thermalization phase by running the HMC for a number of MDUs between 100 and 200, and then we have started the computation of the correlation functions. During all the phases of thermalization we have always monitored the action and the various components of the energy-momentum tensor. We have also constantly monitored the topological charge computed with the Wilson flow, and we have explicitly checked that at the end of each thermalization process we always ended up in the $Q = 0$ topological sector.

Once the thermalization has been concluded, we have accumulated a certain number of configurations for the computation of the EoS and we have selected some of those for the computation of the screening masses. In particular in tables C.1 and C.2 we report the number of MDUs considered, the number of MDUs skipped between two consecutive independent configurations, and the number of local sources per configuration, on which the mesonic two-point correlation functions have been computed. In tables C.3 and C.4 we report the same records for the baryonic two-point correlation function. In the latter case we always kept the number of skipped MDUs fixed to 10 in order to maximize data collection. For each configuration, the best estimate of the two-point correlation function has

T	L_0/a	n_{mdu}	n_{nsrc}	$\frac{m_{N^+}}{3\pi T}$	$\frac{m_{N^+}-m_{N^-}}{3\pi T}$
T_0	4	300	4	0.9863(15)	0.0002(3)
	6	390	4	1.0178(17)	0.00041(19)
T_1	4	300	4	0.9892(18)	0.0001(3)
	6	310	4	1.0204(20)	0.0002(4)
	8	500	4	1.0371(18)	-0.00013(23)
	10	500	4	1.0438(28)	0.0003(5)
T_2	4	300	4	0.9909(23)	0.0001(4)
	6	320	4	1.0242(24)	-0.00017(28)
	8	490	4	1.0385(30)	0.00026(29)
	10	500	4	1.048(5)	0.0005(6)
T_3	4	300	4	0.9945(25)	0.0006(4)
	6	340	4	1.027(3)	0.0002(4)
	8	490	4	1.0406(23)	0.00050(3)
	10	500	4	1.048(6)	0.0003(7)
T_4	4	440	4	1.0040(16)	0.0007(5)
	6	310	4	1.0317(26)	-0.0007(4)
	8	490	4	1.0430(29)	-0.0001(4)
	10	500	4	1.054(5)	-0.0013(6)
T_5	4	310	4	1.004(3)	-0.0007(6)
	6	310	4	1.038(3)	0.0005(8)
	8	500	4	1.0466(26)	-0.0001(3)
	10	500	4	1.059(4)	-0.0001(5)
T_6	4	300	4	1.0089(25)	-0.0006(9)
	6	320	4	1.034(3)	-0.0002(7)
	8	500	4	1.054(4)	-0.0002(5)
	10	500	4	1.061(6)	0.0004(10)
T_7	4	320	4	1.012(4)	0.0005(12)
	6	310	4	1.043(4)	0.0006(7)
	8	500	4	1.059(3)	-0.0001(8)
	10	500	4	1.062(6)	0.0026(17)
T_8	4	320	8	1.016(4)	0.0023(14)
	6	300	8	1.046(4)	-0.0001(11)
	8	500	4	1.066(4)	-0.0007(8)
	10	500	5	1.061(4)	0.0013(13)

Table C.3: Results for the nucleon screening mass, m_{N^+}, and the mass difference with it parity partner ($m_{N^+} - m_{N^-}$) normalized to $3\pi T$ at finite lattice spacing for the temperatures $T_0, \ldots, T_8$. The number of MDUs generated, n_{mdu}, and the number of local sources per configuration on which the two-point correlation functions have been computed, n_{nsrc}, are also reported. The latter are always calculated by skipping $n_{\mathrm{skip}} = 10$ MDUs between two consecutive measurements.

T	L_0/a	n_{mdu}	n_{nsrc}	$\frac{m_{N^+}}{3\pi T}$	$\frac{m_{N^+}-m_{N^-}}{3\pi T}$
T_9	4	400	4	1.0180(26)	-0.0008(12)
	6	390	4	1.0526(28)	0.0005(10)
	8	390	4	1.052(5)	0.0002(10)
T_{10}	4	410	4	1.029(4)	-0.0019(21)
	6	400	4	1.056(3)	-0.0021(14)
	8	390	4	1.074(3)	0.0013(17)
T_{11}	4	400	4	1.029(4)	0.0001(21)
	6	390	4	1.055(6)	-0.0015(17)
	8	390	4	1.063(5)	0.0016(11)

Table C.4: As in Table C.3 but for T_9, T_{10} and T_{11}.

been obtained by properly averaging their values from all local sources and, for the mesonic correlation function, by symmetrizing the correlators with respect to $x_3 = L/a$. The screening masses have been extracted as reported in Chapters 5 and 6 and their values are reported in tables C.1 and C.2 for the mesonic case and in tables C.3 and C.4 for the baryonic one.

To explicitly check that finite volume effects are negligible within our statistical errors, we have generated three more lattices at T_0 ($L_0/a = 6$), T_1 ($L_0/a = 10$) and T_{11} ($L_0/a = 8$) at three smaller spatial volumes, namely $6 \times 144^2 \times 288$, $10 \times 96^2 \times 288$ and $8 \times 144^2 \times 288$ (direction 3 the longest) respectively. On these lattices we have computed the screening masses following the same procedure as described before. Those are in very good agreement with the analogous reported in tables C.1 and C.2 for the mesons and C.3 and C.4 for the baryons, and therefore they confirm the theoretical expectations that finite volume effects are negligible at high temperatures.

Appendix D

Scale setting

Either for quarks and gluons we imposed shifted boundary conditions in the compact temporal direction, with shift parameter $\boldsymbol{\xi} = (1, 0, 0)$ and consequently $T = 1/\left(\sqrt{2}L_0\right)$. The twelve values of the temperature have been imposed by specifying the value of the renormalized coupling in a finite volume in a specific renormalization scheme. In particular, for the nine highest temperature $T_0, \ldots, T_8$, the temperatures have been fixed by using the Schrödinger Functional definition of the renormalized coupling, while for the three lowest temperatures T_9, T_{10} and T_{11} the corresponding value has been fixed with the Gradient Flow definition. In the following appendices we provide the details for the scale setting and the determination of the bare parameters of the lattice actions by separating the discussion for the highest and the lowest temperatures.

D.1 High temperatures

The highest temperatures we simulated in this work, namely $T_0, \ldots, T_8$ are fixed from the results reported in Refs. [178, 181, 203] by imposing the relation

$$T = \frac{1}{L_0\sqrt{2}} = \frac{\mu}{2}, \tag{D.1}$$

where μ is the renormalization scale of the Schrödinger Functional renormalized coupling $\bar{g}^2_{\mathrm{SF}}$ which has been determined in a finite volume with linear extension

T	$\bar{g}^2_{\rm SF}\left(\mu = T\sqrt{2}\right)$	T (GeV)
T_0	-	164.6(5.6)
T_1	1.11000	82.3(2.8)
T_2	1.18446	51.4(1.7)
T_3	1.26569	32.8(1.0)
T_4	1.3627	20.63(63)
T_5	1.4808	12.77(37)
T_6	1.6173	8.03(22)
T_7	1.7943	4.91(13)
T_8	2.0120	3.040(78)

Table D.1: Values of the SF couplings corresponding to the lines of constant physical temperature that we consider.

$L_0^{\rm SF} = 1/\mu$ and SF boundary conditions, i.e. $L_0 = L_0^{\rm SF}$. From [204] we obtain

$$\bar{g}^2_{\rm SF}(\mu_0) = 2.0120 \quad \longrightarrow \quad \mu_0 = 4.30(11)\,\text{GeV} = T_8\sqrt{2}\,, \tag{D.2}$$

where the contributions coming from the charm and bottom quarks can be safely neglected given the current level of precision on the combination of the pion and kaon decay constants used to set the overall scale at low energy, see Ref. [205] and [180] for further details. Once the corresponding value of the renormalized coupling is known at the reference scale μ_0 or equivalently at T_8, larger values of the temperature can be directly inferred by integrating the non-perturbative beta-function in the SF scheme

$$\ln\left(\frac{\mu}{\mu_0}\right) = \int_{\bar{g}_{\rm SF}(\mu_0)}^{\bar{g}_{\rm SF}(\mu)} \frac{\mathrm{d}g}{\beta_{\rm SF}\left(g\right)}\,, \tag{D.3}$$

which can be parametrized in the range of couplings of interest as [181, 203]

$$\beta_{\rm SF}(\bar{g}) = -\bar{g}^3 \sum_{n=0^3} b_n \bar{g}^{2n}\,, \qquad \bar{g}^2 \in [0, 2.45]\,, \tag{D.4}$$

where b_0 and b_1 are the usual perturbative universal coefficients of the beta-function defined in eq. 1.22, b_2 is the three-loop perturbative coefficient in the SF scheme.

L_0/a	$\delta am_{\rm cr}^{(0)}$	$\delta am_{\rm cr}^{(1)}$
4	0.0015131	0.0120930
6	0.0006384	0.0008250
8	0.0003209	0.0001878
10	0.0001835	0.0000751
12	0.0001145	0.0000403
16	0.0000531	0.0000168

Table D.2: Tree-level and one-loop cut-off effects for the critical mass in the SF for setup A with background gauge field, $\theta = \pi/5$ and improvement coefficients as specified in Ref. [206]. Note that the one-loop coefficient depends on the flavour number N_f as $\delta am_{\rm cr}(1) = \delta am_{\rm cr}(1,0) + \delta am_{\rm cr}(1,1)N_f$, with numerical values taken from Ref. [206].

For $N_f = 3$ they read

$$(4\pi)\, b_0 = \frac{9}{4\pi}\,, \qquad (4\pi)^2\, b_1 = \frac{4}{\pi^2}\,, \qquad (4\pi)^3\, b_2 = -0.064(27)\,, \tag{D.5}$$

and $b_3^{\rm eff}$ is an effective coefficient extracted from non-perturbative data, which encodes higher order contributions. Its expression reads

$$(4\pi)^4\, b_3^{\rm eff} = 4(3)\,. \tag{D.6}$$

With the beta-function, obtained in such a way, we integrated eq. D.3 numerically using the value of the reference scale μ_0 reported in eq. D.2, and we obtained the values for the temperatures reported in table D.1

D.1.1 Bare parameters

For the nine highest temperature we employed the Wilson plaquette action in eq. 3.14. This allowed us to fix the value of the bare parameters along the lines of constant physics by exploiting the known results for the SF coupling computed *de facto* at the critical mass. For $L_0/a = 6, 8, 10$ those are given in table 3 of [181], while those for $L_0/a = 4$ were given to us by the authors of that reference as a private communication. For each value of L_0/a, the values of β at which the SF renormalized coupling has the value reported in table D.1 were extracted by fitting

$\bar{g}^2_{\rm SF}(\mu)$ to the functional form[1]

$$\frac{1}{\bar{g}^2_{\rm SF}} = \frac{1}{g_0^2} + \sum_{k=0}^{n_p} c_k g_0^{2k} . \tag{D.7}$$

For $L_0/a = 4$ we have fitted 16 data points in the ranges $\bar{g}^2_{\rm SF} \in [2.0451, 1.1077]$ and $\beta \in [5.9949, 8.3130]$ with $n_p = 3$ obtaining $\chi^2/\text{dof} \approx 1$. The results for the interpolated β-values are reported in table D.3. For $L_0/a = 6, 8$, the values of β reported in table D.3 are taken from Ref. [203], which were obtained by interpolating the data of Ref. [181] as well. As an independent check, we performed our own fits using the functional form in eq. D.7 with $n_p = 2$ including always all the available data and we obtained $\chi^2/\text{dof} = 0.38$ and $\chi^2/\text{dof} = 0.74$ for $L_0/a = 6$ and 8 respectively. For the values of β we extracted from our interpolation we found excellent agreement within errors with the determinations of Ref. [203]. We decided to take as central values the results of this reference as this will allow us in the future to directly profit from the determination of renormalization factors obtained on the ensembles generated in Ref. [203]. The six data point for $L_0/a = 10$ have been fitted to the same functional form with $n_p = 2$ obtaining $\chi^2/\text{dof} \approx 0.7$ and provided the interpolated values reported in table D.3. Notice that, since $T_0 = 2T_1$, the values of β for $L_0/a = 4, 6$ are the ones for T_1 at $L_0/a = 8$ and 12 respectively, obtained with renormalized coupling $\bar{g}^2_{\rm SF} = 1.11$ from table 6 in [203].

Once the lines of constant physics have been defined, the values of the critical mass $m_{\rm cr}$ have been determined from Ref. [207]. They fix $m_{\rm cr}$ by requiring that the PCAC mass, computed in finite volume with SF boundary conditions, vanishes. They obtain

$$am_{\rm cr}\left(g_0^2, a/L_0\right) = am_{\rm cr}^{\rm 2lp}\left(g_0^2, a/L_0\right) + c_1^{L/a} g_0^6 + c_2^{L/a} g_0^8 + c_3^{L/a} g_0^{10} , \tag{D.8}$$

where the coefficients $c_i^{L/a}$ with $i = 1, 2, 3$ are provided by Ref. [207]. The rest of

[1] The results for $\bar{g}_{\rm SF}$ from Ref. [181] come with an error which includes both the statistical and the systematic uncertainties. The latter is an estimate for the remaining $\mathrm{O}(ag_0^8)$ effects stemming from the SF boundary counter-terms after the known perturbative improvement is implemented. We have explicitly checked that, once propagated to the mesonic and baryonic screening masses, these errors are negligible within the statistical uncertainties. We can therefore safely assume that the screening masses are free from $O(a)$ contamination deriving from the conditions which fix the lines of constant physics.

T	L_0/a	β	$\kappa_{\mathrm{cr}}^{(W)}$	$c_{\mathrm{sw}}^{(W)}$
T_0	4	8.7325	0.131887597685602	1.224666388699756
	6	8.9950	0.131885781718599	1.214293680665697
T_1	4	8.3033	0.132316223701646	1.244443949720750
	6	8.5403	0.132336064110711	1.233045285565058
	8	8.7325	0.132133744093735	1.224666388699756
	10	8.8727	0.131984877002653	1.218983546266290
T_2	4	7.9794	0.132672230374640	1.262303345977765
	6	8.2170	0.132690343212428	1.248924515099129
	8	8.4044	0.132476707113024	1.239426196162344
	10	8.5534	0.132305706323476	1.232451001338001
T_3	4	7.6713	0.133039441274476	1.282333503658225
	6	7.9091	0.133057201010874	1.266585617959733
	8	8.0929	0.132831173856378	1.255711356539447
	10	8.2485	0.132638399517155	1.247267216254281
T_4	4	7.3534	0.133449711446233	1.307002958449583
	6	7.5909	0.133469338865844	1.288146969458134
	8	7.7723	0.133228362183550	1.275393611340024
	10	7.9322	0.133013578229002	1.265160978064686
T_5	4	7.0250	0.133908723921720	1.338089264736139
	6	7.2618	0.133933679858703	1.315030958783770
	8	7.4424	0.133674531074371	1.299622821237046
	10	7.6042	0.133438165920285	1.287166774665371
T_6	4	6.7079	0.134386271436463	1.375352693193284
	6	6.9433	0.134421953633166	1.346919223092444
	8	7.1254	0.134141768774467	1.327878356622864
	10	7.2855	0.133888442235086	1.312909828079458
T_7	4	6.3719	0.134926677491050	1.425561566301377
	6	6.6050	0.134982857878749	1.389385004928746
	8	6.7915	0.134676613758678	1.364706438701718
	10	6.9453	0.134412950133538	1.346697162567041
T_8	4	6.0433	0.135481632961481	1.489790983990814
	6	6.2735	0.135571353236717	1.442967721668930
	8	6.4680	0.135236172024848	1.409845308468962
	10	6.6096	0.134976206524104	1.388734449325687

Table D.3: Parameters of the Monte Carlo simulations performed with the Wilson plaquette action. The bare gauge coupling is expressed in terms of $\beta = 6/g_0^2$.

the expression corresponds to the two-loop critical mass,

$$\begin{aligned} am_{\rm cr}^{\rm 2lp}\left(g_0^2, a/L_0\right) &= \left(am_{\rm cr}^{(0)} + \delta am_{\rm cr}^{(0)}\left(a/L_0\right)\right) \\ &+ \left(am_{\rm cr}^{(1)} + \delta am_{\rm cr}^{(1)}\left(a/L_0\right)\right) g_0^2 + am_{\rm cr}^{(2)} g_0^4 \,, \end{aligned} \tag{D.9}$$

where

$$am_{\rm cr}^{(0)} = 0\,, \qquad am_{\rm cr}^{(1)} = -0.270075349459\,, \qquad am_{\rm cr}^{(2)} = -0.039772\,, \tag{D.10}$$

are the asymptotic coefficients in the limit $L_0/a \to \infty$ while the coefficients due to cut-off effects are reported in table D.2. The interpolated values for $\kappa_{\rm cr} = 2am_{\rm cr} + 8$ as well as those for $c_{\rm sw}$ obtained from eq. D.9 and 3.71 respectively are reported in table D.3 and indicated with $\kappa_{\rm cr}^{(W)}$ and $c_{\rm sw}^{(W)}$, where the superscript refers to the Wilson plaquette action in eq. 3.14.

D.2 Low temperatures

The three lowest temperatures T_9, T_{10} and T_{11} are fixed in a similar way to the highest ones but from the renormalized coupling in the Gradient Flow definition. The temperature value is fixed by imposing the relation

$$T = \frac{1}{L_0\sqrt{2}} = 2\mu\,, \tag{D.11}$$

where μ, again, is the renormalization scale of the GF coupling $\bar{g}^2_{\rm GF}(\mu)$ defined in a finite volume with spatial and temporal extensions satisfying $L^{\rm GF} = L_0^{\rm GF} = 1/\mu$, i.e. $L_0 = L_0^{\rm GF}/2$.

In order to determine the physical values of the temperatures, we start from the results of Ref. [204],

$$\bar{g}^2_{\rm GF}\left(\mu_{\rm had,1}\right) = 11.31 \qquad \longrightarrow \qquad \mu_{\rm had,1} = 196.9(3.2)\,{\rm MeV}\,, \tag{D.12}$$

where $\mu_{\rm had,1}$ is inferred, as for μ_0 in App. D.2, from the experimental value of the combination of the pion and kaon decay constants which has been used to fix the overall scale [180]. The value of the temperatures corresponding to the coupling of

T	$\bar{g}_{\rm GF}\left(\mu = T/\sqrt{2}\right)$	T (GeV)
T_9	2.7359	2.833(68)
T_{10}	3.2029	1.821(39)
T_{11}	3.8643	1.167(23)

Table D.4: Values of the GF couplings corresponding to the lines of constant physica temperature that we consider.

interest can be extracted by integrating the beta-function

$$\ln\left(\frac{\mu}{\mu_{\rm had,1}}\right) = \int_{\bar{g}_{\rm GF}(\mu_{\rm had,1})}^{\bar{g}_{\rm GF}(\mu_{\rm had})} \frac{{\rm d}g}{\beta_{\rm GF}\left(\mu\right)} \,. \tag{D.13}$$

Using the results of Ref [179, 203] the non-perturbative beta-function of the GF coupling can be parameterized in the range of couplings of interest as

$$\beta_{\rm GF}\left(\bar{g}\right) = -\frac{\bar{g}^3}{\sum_{n=0}^{2} p_n \bar{g}^{2n}} \,, \qquad \bar{g}^2 \in [2.1, 11.3] \,, \tag{D.14}$$

with fit parameter $p_0 = 16.07, p_1 = 0.21$ and $p_2 = -0.013$ and covariance matrix

$$\mathrm{cov}(p_i, p_j) = \begin{pmatrix} 5.12310 \times 10^{-1} & 1.77401 \times 10^{-1} & 1.32026 \times 10^{-2} \\ 1.77401 \times 10^{-1} & 6.60392 \times 10^{-2} & 5.10305 \times 10^{-3} \\ 1.32026 \times 10^{-2} & 5.10305 \times 10^{-3} & 4.06114 \times 10^{-4} \end{pmatrix} . \tag{D.15}$$

Given this representation, we integrated eq. D.13 numerically by using the result for $\mu_{\rm had,1}$ in eq. D.12. The values of the temperature so obtained and the corresponding renormalized couplings are reported in table D.4.

D.2.1 Bare parameters

For the three lowest temperatures T_9, T_{10} and T_{11} we adopted the tree-level Symanzik improved gauge action in eq. C.1 so as to be able to use the results from Ref. [179]. on the Gradient Flow coupling computed in the massless theory.

For each value of L_0/a, the bare parameters are taken from table 8 of Ref. [203] and they are reported in table D.6. To verify that the temperature is constant

Coeff.	$L_0/a = 4$	$L_0/a = 6$	$L_0/a = 8$
ζ_0	+1.005834130000000	+1.002599440000000	+1.001463290000000
μ_0	−0.000022208694999	−0.000004812471537	−0.000001281872601
μ_1	−0.202388398516844	−0.201746020772477	−0.201520105247962
ζ_1	−0.560665657872021	−0.802266237327923	−0.892637061391273
ζ_2	+3.262872842957498	+4.027758778155415	+5.095631719496583
ζ_3	−5.788275397637978	−6.928207214808553	−8.939546687871335
ζ_4	+4.587959856400246	+5.510985771180077	+7.046607832794273
ζ_5	−1.653344785588201	−2.076308895962694	−2.625638312722623
ζ_6	+0.227536321065082	+0.320430672213824	+0.405387660384441
μ_2	+0.090366980657738	+0.128161834555849	+0.139461345465939
μ_3	−0.600952105402754	−0.681097059845447	−0.847457204378732
μ_4	+0.934252532135398	+0.991316994385556	+1.261676178806362
μ_5	−0.608706158693056	−0.606597739050552	−0.754644691612547
μ_6	+0.140501978953879	+0.129031928169091	+0.153135714480269

Table D.5: Coefficients for the parameterization Eq. (D.16). The three leading coefficients ζ_0, μ_0, and μ_1 in the upper part of the table are combinations of known perturbative coefficients while the others were determined by a fit.

within each set, we have fitted the result in table 1 of Ref. [179] for each value of L_0/a using the functional form in eq. D.7 but with $\bar{g}^2_{\rm SF}(\mu)$ replaced by $\bar{g}^2_{\rm GF}(\mu)$ and by taking into account that in this case, the relation between the lattice extent in the temporal direction and the renormalization scale is modified as $\mu = 1/(2L_0)$. By including all the nine data points for each value of L_0/a, and by choosing $n_p = 2$ for $L_0/a = 4, 6$ and $n_p = 3$ for $L_0/a = 8$, we obtained excellent fits with $\chi^2/\text{dof} \approx 0.93, 0.16$ and 1.07 respectively. The results confirm that the temperature is constant within errors for the lattices within each set[2].

Once the lines of constant physics have been fixed, the corresponding values of the critical mass have been computed from the results in Ref. [179]. Its expression reads

$$am_{\rm cr}\left(g_0^2, a/L_0\right) = \left(\sum_{k=0}^{6} \mu_k g_0^{2k}\right) \times \left(\sum_{i=0}^{6} \zeta_i g_0^{2i}\right)^{-1}, \tag{D.16}$$

[2]Considerations analogous to those in footnote 1 apply also here for the case of the GF coupling.

T	L_0/a	β	$\kappa_{\rm cr}^{(I)}$	$c_{\rm sw}^{(I)}$
T_9	4	4.764900	0.134885548000448	1.335350323996506
	6	4.938726	0.134507608658235	1.308983384364439
	8	5.100000	0.134168886219319	1.288203306487197
T_{10}	4	4.457600	0.135606746160064	1.39574103127591
	6	4.634654	0.135199857298424	1.358462476494125
	8	4.800000	0.134821158536685	1.329646151978636
T_{11}	4	4.151900	0.136325892438363	1.482418125298923
	6	4.331660	0.135926636004668	1.427424655158656
	8	4.500000	0.135525721037715	1.386110343557152

Table D.6: Parameters of the Monte Carlo simulations performed with the tree-level improved Symanzik action. The bare gauge coupling is expressed in terms of $\beta = 6/g_0^2$.

with parameters μ_k and ζ_i reported in table D.5 for the L_0/a of interest. As for the case of the Wilson-plaquette gauge action, the values of $m_{\rm cr}\,(g_0^2, a/L_0)$ depend on L_0/a because it has been determined by requiring the PCAC mass to vanish in a finite volume [179].

Once the values of the bare couplings β have been determined, the corresponding values for the critical hopping parameter $\kappa_{\rm cr} = 2am_{\rm cr} + 8$ as well as those for $c_{\rm sw}$ are obtained from eq. D.16 and eq. C.3 respectively. The corresponding values are reported in table D.6 as $\kappa_{\rm cr}^{(I)}$ and $c_{\rm sw}^{(I)}$, where the superscript denotes the Symanzik improved action.

Appendix E

Perturbation theory

The following appendices are devoted to collect the relevant formulae for the perturbative calculation of the mesonic and baryonic screening masses in the framework of the dimensional reduced effective theory which was outlined in Chapter 2.

E.1 Free propagators

In this appendix we explicitly derive the expression for the free theory quark propagators in the effective field theory. Starting from the free effective action in eq. 5.5 it is straightforward to see that, in momentum space, the free propagators for the fields χ and ϕ, in the lowest Matsubara sector, respectively read

$$G_\chi(p_3) = \frac{1}{i\left[p_0 + ip_3 + \frac{\mathbf{p}_\perp^2}{2p_0}\right]}, \tag{E.1}$$

$$G_\phi(p_3) = \frac{1}{i\left[p_0 - ip_3 + \frac{\mathbf{p}_\perp^2}{2p_0}\right]}. \tag{E.2}$$

These are conveniently expressed in a mixed coordinate-momentum representation. In particular, since the screening mass characterizes the exponential fall-off of the correlation function, it is natural to perform a Fourier transform in the third spatial direction. Then, by assuming forward propagation for $x_3 > 0$, which implies $p_0 > 0$

for the χ field and $p_0 < 0$ for the ϕ field, a Fourier transform leads to

$$\left\langle \chi\left(\mathbf{p}, x_3\right) \chi^\dagger(0) \right\rangle \overset{x_3>0}{=} -i\theta\left(p_0\right) e^{-x_3\left(p_0+\frac{\mathbf{p}^2}{2p_0}\right)} \tag{E.3}$$

$$\left\langle \phi\left(\mathbf{p}, x_3\right) \phi^\dagger(0) \right\rangle \overset{x_3>0}{=} +i\theta\left(-p_0\right) e^{-x_3\left(|p_0|+\frac{\mathbf{p}^2}{2|p_0|}\right)} . \tag{E.4}$$

As a final remark, notice that such free propagators are diagonal both in spin and colour space.

E.2 1-loop order propagators

Starting from the $O(g^2)$ action for non-relativistic quarks in eq. 5.7, the longitudinal propagators for the fields χ and ϕ are defined as the Wilson's lines satisfying

$$\begin{aligned} \left(\partial_3 + M - g_{\mathrm{E}} A_0 - i g_{\mathrm{E}} A_3\right) U_\chi(\mathbf{x}_\perp, x_3) &= 0 , \\ \left(-\partial_3 + M - g_{\mathrm{E}} A_0 + i g_{\mathrm{E}} A_3\right) U_\phi(\mathbf{x}_\perp, x_3) &= 0 , \end{aligned} \tag{E.5}$$

which have solutions given in the usual form of path-ordered exponentials. By suppressing, for readability, any colour and spin index, those read

$$\begin{aligned} U_\chi(\mathbf{x}_\perp, x_3) &= \mathcal{P} \exp\left\{ \int_0^{x_3} dz' \left[-M + g_{\mathrm{E}} A_0(\mathbf{x}_\perp, z') + i g_{\mathrm{E}} A_3(\mathbf{x}_\perp, z') \right] \right\} \\ &= e^{-M x_3} \mathcal{P} \exp\left\{ \int_0^{x_3} dz' \left[g_{\mathrm{E}} A_0(\mathbf{x}_\perp, z') + i g_{\mathrm{E}} A_3(\mathbf{x}_\perp, z') \right] \right\} , \end{aligned} \tag{E.6}$$

$$\begin{aligned} U_\phi(\mathbf{x}_\perp, x_3) &= \mathcal{P} \exp\left\{ \int_{x_3}^{0} dz' \left[M - g_{\mathrm{E}} A_0(\mathbf{x}_\perp, z') + i g_{\mathrm{E}} A_3(\mathbf{x}_\perp, z') \right] \right\} \\ &= e^{-M x_3} \mathcal{P} \exp\left\{ \int_0^{x_3} dz' \left[g_{\mathrm{E}} A_0(\mathbf{x}_\perp, z') - i g_{\mathrm{E}} A_3(\mathbf{x}_\perp, z') \right] \right\} . \end{aligned} \tag{E.7}$$

Notice that in the expression for U_ϕ, the bounds of integration are flipped, since the action in eq. 5.7 describes a backward propagating ϕ field for any positive-valued M. Since such longitudinal quark propagators are obtained starting from the $O(g^2)$ NRQCD action in eq. 5.7, those can be safely expanded for small g_{E} up to the same order. By exploiting the expansion of the path ordered exponential

the quark propagator for the χ field reads

$$U_{\chi}^{be}(\mathbf{x}_{\perp}, x_3) = e^{-Mx_3}\left\{\delta^{be} + \int_0^{x_3} dz' \left[g_{\mathrm{E}}A_0 + ig_{\mathrm{E}}A_3\right]^{be}(\mathbf{x}_{\perp}, z') \right. \tag{E.8}$$
$$\left. + \int_0^{x_3} dz' \int_0^{z'} dz'' \left[g_{\mathrm{E}}A_0 + ig_{\mathrm{E}}A_3\right]^{bm}(\mathbf{x}_{\perp}, z') \left[g_{\mathrm{E}}A_0 + ig_{\mathrm{E}}A_3\right]^{me}(\mathbf{x}_{\perp}, z'') + O(g_{\mathrm{E}}^3)\right\},$$

where we now made explicit colour indices. Correspondingly the propagator for the ϕ field is simply obtained by flipping the sign of the term containing the A_3 field. Then the propagator for a backward propagating ϕ field at $O(g^2)$ is

$$U_{\phi}^{be}(\mathbf{x}_{\perp}, x_3) = e^{-Mx_3}\left\{\delta^{be} + \int_0^{x_3} dz' \left[g_{\mathrm{E}}A_0 - ig_{\mathrm{E}}A_3\right]^{be}(\mathbf{x}_{\perp}, z') \right. \tag{E.9}$$
$$\left. + \int_0^{x_3} dz' \int_0^{z'} dz'' \left[g_{\mathrm{E}}A_0 - ig_{\mathrm{E}}A_3\right]^{bm}(\mathbf{x}_{\perp}, z') \left[g_{\mathrm{E}}A_0 - ig_{\mathrm{E}}A_3\right]^{me}(\mathbf{x}_{\perp}, z'') + O(g_{\mathrm{E}}^3)\right\}.$$

As a final remark, notice that baryonic correlation functions involve the forward propagation of ϕ fields with negative Matsubara frequency. At 1-loop order, the corresponding propagator is simply obtained from the propagator for the backward propagating field in eq. E.7 by flipping the bounds of integration and the sign of the matching coefficient M. The final form for a forward propagating ϕ field with negative Matsubara frequency is then given by

$$U_{\phi}^{ad}(\mathbf{x}_{\perp}, x_3) = e^{-Mx_3}\left\{\delta^{ad} + \int_0^{x_3} dz' \left[-g_{\mathrm{E}}A_0 + ig_{\mathrm{E}}A_3\right]^{ad}(\mathbf{x}_{\perp}, z') \right. \tag{E.10}$$
$$\left. + \int_0^{x_3} dz' \int_0^{z'} dz'' \left[-g_{\mathrm{E}}A_0 + ig_{\mathrm{E}}A_3\right]^{am}(\mathbf{x}_{\perp}, z') \left[-g_{\mathrm{E}}A_0 + ig_{\mathrm{E}}A_3\right]^{md}(\mathbf{x}_{\perp}, z'') + O(g_{\mathrm{E}}^3)\right\}.$$

E.3 1-loop order mesonic Green's function

This section is devoted to perform the 1-loop order calculation of the mesonic Green's function which lead to the expression reported in eq. 5.12. By taking into account the quark propagators in eq. E.6 and E.7, the correlation function in eq.

5.11 can be written, at $O(g_{\rm E}^2)$, as

$$
\begin{aligned}
C_O^{(1)}\left(\mathbf{x}_\perp,\mathbf{y}_\perp,x_3\right) \;=\; & \frac{e^{-2Mx_3}}{N}\Bigg\langle \delta^{ab}\delta^{ba} \\
+ & \int_0^{x_3}\mathrm{d}z'\left[g_{\rm E}A_0\left(\mathbf{x}_\perp,z'\right)+ig_{\rm E}A_3\left(\mathbf{x}_\perp,z'\right)\right]+\int_0^{x_3}\mathrm{d}z'\left[g_{\rm E}A_0\left(\mathbf{y}_\perp,z'\right)-ig_{\rm E}A_3\left(\mathbf{y}_\perp,z'\right)\right] \\
+ & \int_0^{x_3}\mathrm{d}z'\int_0^{z'}\mathrm{d}z''\left[g_{\rm E}A_0\left(\mathbf{x}_\perp,z'\right)+ig_{\rm E}A_3\left(\mathbf{x}_\perp,z'\right)\right]\left[g_{\rm E}A_0\left(\mathbf{x}_\perp,z''\right)+ig_{\rm E}A_3\left(\mathbf{x}_\perp,z''\right)\right] \\
+ & \int_0^{x_3}\mathrm{d}z'\int_0^{z'}\mathrm{d}z''\left[g_{\rm E}A_0\left(\mathbf{y}_\perp,z'\right)-ig_{\rm E}A_3\left(\mathbf{y}_\perp,z'\right)\right]\left[g_{\rm E}A_0\left(\mathbf{y}_\perp,z''\right)-ig_{\rm E}A_3\left(\mathbf{y}_\perp,z''\right)\right] \\
+ & \int_0^{x_3}\mathrm{d}z'\int_0^{x_3}\mathrm{d}z''\left[g_{\rm E}A_0\left(\mathbf{x}_\perp,z'\right)+ig_{\rm E}A_3\left(\mathbf{x}_\perp,z'\right)\right]\left[g_{\rm E}A_0\left(\mathbf{y}_\perp,z''\right)-ig_{\rm E}A_3\left(\mathbf{y}_\perp,z''\right)\right]\Bigg\rangle,
\end{aligned}
\tag{E.11}
$$

where the first term provides the normalization $N = 3$ and for readability we suppress the colour indices in the other terms. Notice that, the second line vanishes since it involves traces of a single $SU(3)$ group generator. The non-vanishing $O(g_{\rm E}^2)$ terms are the contributions deriving from the exchange of longitudinal gluons, i.e. the third and fourth lines, and the one in the fifth line coming from the exchange of transverse gluons. By making explicit colour indices and using the relation in eq. A.5, the above correlation function can written in terms of gluon propagators as

$$
C_O^{(1)}(\mathbf{r}_\perp,x_3) \;=\; e^{-2Mx_3}\left\{1+\,g_{\rm E}^2\mathcal{A}_{\rm L}(\mathbf{0}_\perp,x_3)+g_{\rm E}^2\mathcal{A}_{\rm T}(\mathbf{r}_\perp,x_3)\right\}\,, \tag{E.12}
$$

which is the expression in eq. 5.12, with the 1-loop order longitudinal and transverse corrections which respectively read

$$
\mathcal{A}_{\rm L}(\mathbf{0}_\perp,x_3) \;=\; 6C_F\int_0^{x_3}\mathrm{d}u\int_0^{u}\mathrm{d}v\,\left[\Delta_{00}\left(\mathbf{0}_\perp,u-v\right)-\Delta_{33}\left(\mathbf{0}_\perp,u-v\right)\right] \tag{E.13}
$$

$$
\mathcal{A}_{\rm T}(\mathbf{r}_\perp,x_3) \;=\; 3C_F\int_0^{x_3}\mathrm{d}u\int_0^{x_3}\mathrm{d}v\,\left[\Delta_{00}\left(\mathbf{r}_\perp,u-v\right)+\Delta_{33}\left(\mathbf{r}_\perp,u-v\right)\right]\,, \tag{E.14}
$$

where $\mathbf{r}_\perp = \mathbf{x}_\perp - \mathbf{y}_\perp$ since the gluonic field propagators depend only on the relative distance between the two quark lines. Notice that eq. E.12 is not gauge invariant, but, as we show in App. E.6, the final result for the static potential is gauge invariant as we take the limit of large separations. In the dimensional reduced

effective field theory the spatial and the temporal components of the gluon fields behaves differently. Indeed the latter develop a mass, i.e. the Debye mass, which provides an infrared cutoff to its propagation. The expressions for their propagators read [15, 79]

$$\Delta_{00}(\mathbf{x}) = \int_{\mathbf{p}} \frac{e^{i\mathbf{p}\cdot\mathbf{x}}}{\mathbf{p}^2 + m_{\mathrm{E}}^2}, \tag{E.15}$$

$$\Delta_{ij}(\mathbf{x}) = \int_{\mathbf{p}} e^{i\mathbf{p}\cdot\mathbf{x}} \left[\frac{\delta_{ij}}{\mathbf{p}^2} + (\xi - 1)\frac{p_i p_j}{(\mathbf{p}^2)^2}\right], \tag{E.16}$$

where m_{E} is the Debye mass in eq. 2.13 and ξ is the gauge-fixing parameter. In the expressions above $\mathbf{p} = (\mathbf{p}_\perp, p_3)$, $\mathbf{x} = (\mathbf{x}_\perp, x_3)$ and the integral $\int_{\mathbf{p}} \equiv \int \frac{\mathrm{d}^2\mathbf{p}_\perp}{(2\pi)^2} \int \frac{\mathrm{d}p_3}{2\pi}$.

E.4 1-loop order baryonic Green's function

This appendix is devoted to determine the functional form of the baryonic correlation function at 1-loop order in the effective field theory, see eq. 6.13. By taking into account the forward propagators in eq. E.6 and E.10 the correlation function in eq. 6.12 reads

$$
\begin{aligned}
C(\mathbf{r}_1,\mathbf{r}_2,\mathbf{r}_3;x_3) \;=\; & \frac{e^{-3Mx_3}}{N}\epsilon_{abc}\epsilon_{def}\Bigg\langle\Bigg\{\delta^{be}\delta^{cf}\delta^{ad} \\
& + \int_0^{x_3} dz' \left[-g_{\mathrm{E}}A_0 + ig_{\mathrm{E}}A_3\right](\mathbf{r}_1,z') \\
& + \int_0^{x_3} dz' \left[g_{\mathrm{E}}A_0 + ig_{\mathrm{E}}A_3\right](\mathbf{r}_2,z') + \int_0^{x_3} dz' \left[g_{\mathrm{E}}A_0 + ig_{\mathrm{E}}A_3\right](\mathbf{r}_3,z') \\
& + \int_0^{x_3} dz' \int_0^{z'} dz''\Big[g_{\mathrm{E}}A_0(\mathbf{r}_1,z')g_{\mathrm{E}}A_0(\mathbf{r}_1,z'') - g_{\mathrm{E}}A_3(\mathbf{r}_1,z')g_{\mathrm{E}}A_3(\mathbf{r}_1,z'') \\
& + g_{\mathrm{E}}A_0(\mathbf{r}_2,z')g_{\mathrm{E}}A_0(\mathbf{r}_2,z'') - g_{\mathrm{E}}A_3(\mathbf{r}_2,z')g_{\mathrm{E}}A_3(\mathbf{r}_2,z'') \\
& + g_{\mathrm{E}}A_0(\mathbf{r}_3,z')g_{\mathrm{E}}A_0(\mathbf{r}_3,z'') - g_{\mathrm{E}}A_3(\mathbf{r}_3,z')g_{\mathrm{E}}A_3(\mathbf{r}_3,z'')\Big] \\
& + \int_0^{x_3} dz' \int_0^{z'} dz''\Big[-g_{\mathrm{E}}A_0(\mathbf{r}_1,z')g_{\mathrm{E}}A_0(\mathbf{r}_2,z'') - g_{\mathrm{E}}A_3(\mathbf{r}_1,z')g_{\mathrm{E}}A_3(\mathbf{r}_2,z'') \\
& - g_{\mathrm{E}}A_0(\mathbf{r}_1,z')g_{\mathrm{E}}A_0(\mathbf{r}_3,z'') - g_{\mathrm{E}}A_3(\mathbf{r}_1,z')g_{\mathrm{E}}A_3(\mathbf{r}_3,z'') \\
& + g_{\mathrm{E}}A_0(\mathbf{r}_2,z')g_{\mathrm{E}}A_0(\mathbf{r}_3,z'') - g_{\mathrm{E}}A_3(\mathbf{r}_2,z')g_{\mathrm{E}}A_3(\mathbf{r}_3,z'')\Big]\Bigg\} + (\mathbf{r}_1 \leftrightarrow \mathbf{r}_2)\Bigg\rangle + O(g_{\mathrm{E}}^4),
\end{aligned}
\tag{E.17}
$$

where the first term on the r.h.s. is the contribution coming from the free theory which fixes the constant N and the second and the third lines vanish since those terms involves traces of a single generator of the $SU(3)$ group. The fourth, fifth and sixth lines contain the contributions coming from the exchange of longitudinal gluons and finally the remaining terms involve the exchange of transverse gluons between different quark lines. As done for the mesonic case, by taking into account the relation in eq. A.5, this correlation function can be written as

$$
\begin{aligned}
C^{(1)}_{N^\pm}(\{\mathbf{r}_i\},x_3) \;=\; & e^{-3Mx_3}\Big\{1 + 3g_{\mathrm{E}}^2\mathcal{A}_{\mathrm{L}}(\mathbf{0}_\perp,x_3) \\
& + g_{\mathrm{E}}^2\mathcal{A}_{\mathrm{T}}^{12}(\mathbf{r}_1,\mathbf{r}_2,x_3) + g_{\mathrm{E}}^2\mathcal{A}_{\mathrm{T}}^{23}(\mathbf{r}_2,\mathbf{r}_3,x_3) + g_{\mathrm{E}}^2\mathcal{A}_{\mathrm{T}}^{13}(\mathbf{r}_1,\mathbf{r}_3,x_3)\Big\},
\end{aligned}
\tag{E.18}
$$

where the longitudinal corrections, which are equal for each quark line, are expressed in terms of the gauge field propagators defined in eq. E.15 and E.16 as

$$\mathcal{A}_{\mathrm{L}}(\mathbf{0}_\perp, x_3) = 2C_F \int_0^{x_3} du \int_0^{u} dv \left(\Delta_{00}(\mathbf{0}_\perp, u-v) - \Delta_{33}(\mathbf{0}_\perp, u-v)\right) . \tag{E.19}$$

Similarly, we can write the transverse contributions as

$$\mathcal{A}_{\mathrm{T}}^{12}(\mathbf{r}_1, \mathbf{r}_2, x_3) = \frac{C_F}{2} \int_0^{x_3} du \int_0^{x_3} dv \left(\Delta_{00}(\mathbf{r}_{12}, u-v) + \Delta_{33}(\mathbf{r}_{12}, u-v)\right) \tag{E.20}$$

$$\begin{aligned}\mathcal{A}_{\mathrm{T}}^{23}(\mathbf{r}_2, \mathbf{r}_3, x_3) = {} & \frac{C_F}{4} \int_0^{x_3} du \int_0^{x_3} dv \left(\Delta_{00}(\mathbf{r}_{23}, u-v) + \Delta_{33}(\mathbf{r}_{23}, u-v)\right) \\ & - \frac{C_F}{4} \int_0^{x_3} du \int_0^{x_3} dv \left(\Delta_{00}(\mathbf{r}_{23}, u-v) - \Delta_{33}(\mathbf{r}_{23}, u-v)\right)\end{aligned} \tag{E.21}$$

$$\begin{aligned}\mathcal{A}_{\mathrm{T}}^{13}(\mathbf{r}_1, \mathbf{r}_3, x_3) = {} & \frac{C_F}{4} \int_0^{x_3} du \int_0^{x_3} dv \left(\Delta_{00}(\mathbf{r}_{13}, u-v) + \Delta_{33}(\mathbf{r}_{13}, u-v)\right) \\ & - \frac{C_F}{4} \int_0^{x_3} du \int_0^{x_3} dv \left(\Delta_{00}(\mathbf{r}_{13}, u-v) - \Delta_{33}(\mathbf{r}_{13}, u-v)\right) ,\end{aligned} \tag{E.22}$$

where, for the sake of notation we introduced $\mathbf{r}_{ij} \equiv \mathbf{r}_i - \mathbf{r}_j$. Notice that, here, at variance of the mesonic case, the transverse corrections do not give the same contribution for each of the quark lines due to the appearance of the additional correlation function in eq. 6.12. The above integrals are readily computed, see App. E.5 and lead to the expression for the static potential in eq. 6.14.

E.5 The static potential

In this appendix we provide the full calculation which yields the final expression for the static potential at next-to-leading order in the effective field theory description. Since the final result must be gauge invariant, see App. E.6 for a further discussion, we set $\xi = 1$ in eq. E.16 in order to simplify the structure of the spatial component of the gauge field propagator.

In general, both for the mesonic and the baryonic Green's function, the general

structures to be evaluated in the calculation of the static potential are

$$\mathcal{I}_1(\mathbf{0}_\perp) = -\lim_{x_3\to\infty}\int_{\mathbf{p}}\frac{\partial}{\partial x_3}\int_0^{x_3}dz'\left\{\int_0^{z'}dz''\frac{e^{ip_3(z'-z'')}}{p_3^2+\epsilon^2}\right\}, \tag{E.23}$$

$$\mathcal{I}_2(\mathbf{x}_\perp-\mathbf{y}_\perp) = -\lim_{x_3\to\infty}\int_{\mathbf{p}}e^{i\mathbf{p}_\perp\cdot(\mathbf{x}_\perp-\mathbf{y}_\perp)}\frac{\partial}{\partial x_3}\int_0^{x_3}dz'\left\{\int_0^{x_3}dz''\frac{e^{ip_3(z'-z'')}}{p_3^2+\epsilon^2}\right\}, \tag{E.24}$$

for the longitudinal and the transverse contribution respectively, where $\epsilon^2 = m_{\rm E}^2+\mathbf{p}_\perp^2$ for the integrals involving Δ_{00} and $\epsilon^2=\mathbf{p}_\perp^2$ for Δ_{33}. It is straightforward to see that $\mathcal{I}_2(\mathbf{x}_\perp-\mathbf{y}_\perp) = 2\mathcal{I}_1(\mathbf{x}_\perp-\mathbf{y}_\perp)$. After a little bit of algebra the integrals are carried out, leading to

$$\mathcal{I}_1(\mathbf{x}_\perp-\mathbf{y}_\perp) = -\int_{\mathbf{p}_\perp}e^{i\mathbf{p}_\perp\cdot(\mathbf{x}_\perp-\mathbf{y}_\perp)}\frac{1}{2\epsilon^2}\,. \tag{E.25}$$

Given such considerations, and by taking into account the expression for the mesonic Green's function, the static potential can be written as [15]

$$V^-(x_\perp-y_\perp) \equiv g^2C_FT\int_{\mathbf{p}_\perp}\left(\frac{1-e^{i\mathbf{p}_\perp\cdot(\mathbf{x}_\perp-\mathbf{y}_\perp)}}{p_\perp^2}-\frac{1+e^{i\mathbf{p}_\perp\cdot(\mathbf{x}_\perp-\mathbf{y}_\perp)}}{p_\perp^2+m_E^2}\right), \tag{E.26}$$

where $x_\perp-y_\perp = |\mathbf{x}_\perp-\mathbf{y}_\perp|$ and $p_\perp = |\mathbf{p}_\perp|$. Similar considerations for the baryonic Green's function lead to the additional term [95]

$$V^+(x_\perp-y_\perp) \equiv g^2C_FT\int_{\mathbf{p}_\perp}\left[1-e^{i\mathbf{p}_\perp\cdot(\mathbf{x}_\perp-\mathbf{y}_\perp)}\right]\left(\frac{1}{p_\perp^2}-\frac{1}{p_\perp^2+m_E^2}\right). \tag{E.27}$$

Notice that each of these integrals is both infrared and ultraviolet divergent. In order to explicitly evaluate them we put an IR-cutoff λ and we regularize the integral in the UV by using dimensional regularization. We consider the familiar integrals [15, 95]

$$\begin{aligned}\int\frac{d^{2-2\epsilon}p}{(2\pi)^{2-2\epsilon}}\frac{1}{p^2+\lambda^2} &= \frac{\mu^{-2\epsilon}}{4\pi}\left(\frac{1}{\epsilon}+2\ln\frac{\bar\mu}{\lambda}+O(\epsilon)\right)\\ \int\frac{d^2p}{(2\pi)^{2-2\epsilon}}\frac{e^{i\bar p\cdot\bar r}}{p^2+\lambda^2} &= \frac{1}{2\pi}K_0(\lambda r)\,,\end{aligned} \tag{E.28}$$

where $\mu = \bar{\mu}\left(\frac{e^{\gamma_E}}{4\pi}\right)^{1/2}$, with γ_E being the Euler gamma function and finally $K_0(x)$ is a modified Bessel function with asymptotic behaviour

$$K_0(x) \overset{x\to 0}{=} -\ln\frac{x}{2} - \gamma_E + O(x)\,. \tag{E.29}$$

Then by putting everything together, we find for the potential in eq. E.26

$$\begin{aligned} V^-(r) &= g^2 C_F T \int \frac{d^{2-2\epsilon}p}{(2\pi)^{2-2\epsilon}} \left\{ \frac{1}{p^2+\lambda^2}\Big[1 - e^{i\bar{p}\cdot\bar{r}}\Big] - \frac{1}{p^2+m_E^2}\Big[1 + e^{i\bar{p}\cdot\bar{r}}\Big] \right\} \\ &= g^2 C_F T \left[\frac{\mu^{-2\epsilon}}{4\pi}\Big(\frac{1}{\epsilon} + 2\ln\frac{\bar{\mu}}{\lambda} - \frac{1}{\epsilon} - 2\ln\frac{\bar{\mu}}{m_E}\Big) - \frac{1}{2\pi}\Big(K_0(\lambda r) + K_0(m_E r)\Big) \right] \\ &= \frac{g^2 C_F T}{2\pi}\left[\ln\frac{m_E r}{2} + \gamma_E - K_0(m_E r) \right], \end{aligned} \tag{E.30}$$

where, by going from the second to the third line, we have taken the limits $\epsilon \to 0$ and $\lambda \to 0$. Similarly for the potential in eq. E.27 it holds

$$V^+(r) = \frac{g^2 C_F T}{2\pi}\left[\ln\frac{m_E r}{2} + \gamma_E + K_0(m_E r) \right]. \tag{E.31}$$

As a final comment, notice that, due to the asymptotic behaviour of the Bessel function, while $V^+(r)$ assumes a finite value, $V^-(r)$, in contrast, is divergent in the origin.

E.6 Gauge invariance of the static potential

In this appendix we show that gauge dependent terms in the 1-loop order Green's function give rise to no contribution in the final result of the static potential. Following the discussion of the previous section, after performing the derivative with respect the third spatial coordinate, the general structure of such terms is

$$\mathcal{J}_3(\mathbf{x}_\perp) = -(\xi - 1)\lim_{x_3\to\infty}\int_{\mathbf{p}_\perp}\Big(1 - e^{i\mathbf{p}_\perp\cdot\mathbf{x}_\perp}\Big)\int_0^{x_3} dz'' \int \frac{dp_3}{2\pi} e^{ip_3(x_3 - z'')}\frac{p_3^2}{(p_3^2 + \mathbf{p}_\perp^2)^2}\,. \tag{E.32}$$

The Fourier transform along the third spatial direction and the integral over z'' are promply computed. Finally the remaining integral can be easily solved in polar coordinates (See pag 338 of Ref. [208]) and leads to

$$\mathcal{J}_3\left(\mathbf{x}_\perp\right) = -\frac{(\xi-1)}{8\pi}\lim_{x_3\to\infty}\left[1-\frac{x_3}{\sqrt{x_3^2+|\mathbf{x}_\perp^2|}}\right] = 0\,, \tag{E.33}$$

which shows that all the gauge dependent terms give rise to vanishing contributions in the static potential, if the large separation limit is taken.

Appendix F

Numerical methods for the perturbative solution

In this section we deal with the numerical methods that have been used to solve the mesonic and baryonic Schrödinger equation obtained from the perturbative analysis.

F.1 The Hyperspherical Harmonics method

This appendix is devoted to develop the strategy to solve the baryonic Schrödinger equation which occurs at 1-loop order in perturbation theory. The Hyperspherical Harmonics (HH) method, see Ref. [209] for a recent review on the subject, is usually used to solve quantum many-body problems in three dimensions. The three-body problem in eq. 6.16 is defined in two dimension. For this reason, in the first part of this appendix we aim to specialize this method to the two dimensional case, while in the second part we will apply this method to achieve a numerical solution for eq. 6.16.

F.1.1 Two-dimensional HH expansion

The following discussion is a two-dimensional generalization of the HH expansion method, see Ref. [209]. From that reference we borrow notation and the main definitions and we refer to it for a further and more detailed discussion on this

topic. Let us consider a quantum three-body problem in two spatial dimensions of the form of eq. 6.16 and perform a change of variables by going to the center of mass frame, i.e.

$$\begin{cases} \hat{\mathbf{R}} \equiv \frac{\hat{\mathbf{r}}_1+\hat{\mathbf{r}}_2+\hat{\mathbf{r}}_3}{3} \\ \hat{\boldsymbol{\xi}}_1 \equiv \hat{\mathbf{r}}_2 - \hat{\mathbf{r}}_3 = \hat{\mathbf{r}}_{32} \\ \hat{\boldsymbol{\xi}}_2 \equiv \frac{2}{\sqrt{3}}\left[\hat{\mathbf{r}}_1 - \frac{1}{2}\left(\hat{\mathbf{r}}_3 + \hat{\mathbf{r}}_2\right)\right] = \sqrt{3}\left(\hat{\mathbf{r}}_1 - \hat{\mathbf{R}}\right) \end{cases} , \tag{F.1}$$

where $\hat{\mathbf{R}}$ is the transverse coordinate vector of the center of mass. With this change of variables the laplacian operator in eq. 6.16 can be written, in the center of mass frame, as

$$\frac{1}{2}\left[\nabla^2_{\hat{\mathbf{r}}_1} + \nabla^2_{\hat{\mathbf{r}}_2} + \nabla^2_{\hat{\mathbf{r}}_3}\right] = \frac{\nabla^2_{\hat{\mathbf{R}}}}{6} + \nabla^2_{\hat{\boldsymbol{\xi}}_1} + \nabla^2_{\hat{\boldsymbol{\xi}}_2} , \tag{F.2}$$

and correspondingly, the Schrödinger equation for the relative motion can be written in terms of the new coordinates as

$$\left\{-\left(\nabla^2_{\hat{\boldsymbol{\xi}}_1} + \nabla^2_{\hat{\boldsymbol{\xi}}_2}\right) + \rho\left[\hat{V}\left(\hat{\boldsymbol{\xi}}_1, \hat{\boldsymbol{\xi}}_2\right) - \hat{E}_0\right]\right\} \mathcal{C}\left(\hat{\boldsymbol{\xi}}_1, \hat{\boldsymbol{\xi}}_2\right) = 0 \tag{F.3}$$

where it is understood that $\hat{V}$ is now the static potential expressed as a function of the dimensionless coordinates $\hat{\boldsymbol{\xi}}_1$ and $\hat{\boldsymbol{\xi}}_2$. By going to polar coordinates, i.e.

$$\begin{cases} \hat{\xi}_1^{(1)} = \hat{\xi}_1 \cos\theta_1 \\ \hat{\xi}_1^{(2)} = \hat{\xi}_1 \sin\theta_1 \end{cases} \qquad \begin{cases} \hat{\xi}_2^{(1)} = \hat{\xi}_2 \cos\theta_2 \\ \hat{\xi}_2^{(2)} = \hat{\xi}_2 \sin\theta_2 \end{cases} , \tag{F.4}$$

where $\hat{\xi}_i$ refers to the absolute value of the 2-vector $\hat{\boldsymbol{\xi}}_i$ and the superscript (j) refers to the $j = 1, 2$ components of the vector in the two-dimensional plane, the laplacian operator can be written as

$$\nabla^2_{\hat{\boldsymbol{\xi}}_1} + \nabla^2_{\hat{\boldsymbol{\xi}}_2} = \frac{\partial^2}{\partial\hat{\xi}_1^2} + \frac{1}{\hat{\xi}_1}\frac{\partial}{\partial\hat{\xi}_1} - \frac{1}{\hat{\xi}_1^2}\frac{\partial^2}{\partial\theta_1^2} + \frac{\partial^2}{\partial\hat{\xi}_2^2} + \frac{1}{\hat{\xi}_2}\frac{\partial}{\partial\hat{\xi}_2} - \frac{1}{\hat{\xi}_2^2}\frac{\partial^2}{\partial\theta_2^2} . \tag{F.5}$$

Both for $\hat{\xi}_1$ and $\hat{\xi}_2$ the angular differential operator corresponds to the two-dimensional quantum mechanical angular momentum operator

$$\mathbf{L}_i = \frac{\partial}{\partial \theta_i} \qquad \text{for} \quad i = 1, 2\,. \tag{F.6}$$

So far, the Schrödinger equation, and correspondingly the wave function of the system, depends on the two spatial extension $\hat{\xi}_i$ and on the two angles θ_i. The basic idea underlying the HH method is to write the system, by a suitable change of variables, in terms of three angular variables and one radial variable. This is achieved by going to the so called *hyperspherical coordinates* system

$$\begin{cases} \hat{\xi}_1 = \xi \sin\phi \\ \hat{\xi}_2 = \xi \cos\phi \end{cases}, \tag{F.7}$$

where ξ is called *hyper-radius* and the angular variable ϕ describe the relative lenghts of the two vectors $\hat{\boldsymbol{\xi}}_1$ and $\hat{\boldsymbol{\xi}}_2$, i.e. $\phi \in [0, \pi/2]$. Together with θ_1 and θ_2, ϕ forms a set of *hyper-angles* $\Omega_4 = \{\theta_1, \theta_2, \phi\}$. With this change of variables, the laplacian operator in eq. F.5 reads

$$\nabla^2_\xi = \nabla^2_{\hat{\boldsymbol{\xi}}_1} + \nabla^2_{\hat{\boldsymbol{\xi}}_2} = \frac{\partial^2}{\partial \xi^2} + \frac{3}{\xi}\frac{\partial}{\partial \xi} - \frac{\mathcal{L}^2(\Omega_4)}{\xi^2}\,, \tag{F.8}$$

where the hyperangular momentum operator reads

$$\mathcal{L}^2(\Omega_4) = -\left[\frac{\partial^2}{\partial^2 \phi} + 2\cot 2\phi \frac{\partial}{\partial \phi} - \frac{\mathbf{L}_1^2}{\sin^2\phi} - \frac{\mathbf{L}_2^2}{\cos^2\phi}\right]. \tag{F.9}$$

It is worth noticing the analogy with the expression of the laplacian operator in three-dimension for a two-body problem. Apart from the angular part, the only difference is due to the numerical factor in front of the first derivative, which explicitly depends on the number of dimensions and on the number of particles involved. In complete analogy with the standard case, we can define the eigenvalues and the eigenstates of the hyperangular momentum, by assuming that $\xi^L \mathcal{Y}(\Omega_4)$

is a harmonic function. This leads to

$$\mathcal{L}^2(\Omega_4)\,\mathcal{Y}(\Omega_4) = L(L+2)\,\mathcal{Y}(\Omega_4)\,, \tag{F.10}$$

where L, in analogy to the angular momentum quantum number, is called *grand orbital* quantum number. The corresponding eigenvectors of the operator defined in eq. F.9 can be written as

$$\mathcal{Y}_L(\Omega_4) = \mathcal{P}_L^{l_1 l_2}(\phi)\,Y_{l_1}(\theta_1)\,Y_{l_2}(\theta_2)\,, \tag{F.11}$$

where $Y_{l_i}(\theta)$ are the eigenvector of the $\mathbf{L}_i$ operators, i.e.

$$Y_{l_i}(\theta_i) = \frac{e^{i l_i \theta_i}}{\sqrt{2\pi}} \qquad \text{with} \qquad l_i \in \mathbb{Z}\,. \tag{F.12}$$

By looking for a solution of the type

$$\mathcal{P}_L^{l_1 l_2}(\phi) = (\cos\phi)^{|l_2|}\,(\sin\phi)^{|l_1|}\,g(\cos 2\phi) \tag{F.13}$$

and by performing the change of variables $x = \cos 2\phi$, the differential equation in eq. F.10 can be written as

$$\begin{aligned}\left(1-x^2\right)\frac{\partial^2 g}{\partial x^2} + \left[|l_2| - |l_1| - (|l_2| + |l_1| + 2)\right]\frac{\partial g}{\partial x} \\ + g(x)\,(n + |l_1| + |l_2| + 1)\,n = 0\,,\end{aligned} \tag{F.14}$$

with n which is related to the quantum numbers l_1, l_2 and L by the relation

$$L = 2n + |l_1| + |l_2| \qquad \text{with} \qquad n \in \mathbb{N}\,. \tag{F.15}$$

This differential equation has analytical solutions in terms of Jacobi polyonomials

$$g(x) = P_n^{l_1 l_2}(x) = \frac{(1+|l_1|)_n}{n!}\,{}_2F_1\left(-n, n + |l_1| + |l_2| + 1; |l_1| + 1; \frac{1}{2}(1-x)\right), \tag{F.16}$$

where $(\cdot)_n$ is the Pochhammer symbol and ${}_2F_1$ is the hypergeometric function. These polymomials are orthogonal in the interval $[-1, 1]$ with respect to the weight

function $(1-x)^{|l_1|}(1+x)^{|l_2|}$ and their normalization constant is given by

$$\int_{-1}^{1} P_n^{l_1 l_2}(x) P_{n'}^{l_1 l_2}(x)\,(1-x)^{|l_1|}(1+x)^{|l_2|}\,dx \qquad \text{(F.17)}$$
$$= \frac{\delta_{n,n'}\,2^{|l_1|+|l_2|+1}}{2n+|l_1|+|l_2|+1}\frac{\Gamma(n+|l_1|+1)\,\Gamma(n+|l_2|+1)}{\Gamma(n+1)\,\Gamma(n+|l_1|+|l_2|+1)},$$

where Γ is the Euler gamma function. By inserting the solution to the differential equation into eq. F.13 and taking into account the volume element for the angular variables $\mathrm{d}\Omega_4 = \sin\phi\cos\phi\;\mathrm{d}\theta_1\;\mathrm{d}\theta_2\;\mathrm{d}\phi$, the normalization of the eigenvector in eq. F.13 is obtain by integrating over the hyperangle ϕ

$$\mathcal{N}_n^{l_1 l_2}\int_0^{\frac{\pi}{2}}(\cos\phi)^{2|l_2|+1}(\sin\phi)^{2|l_1|+1}\,P_n^{l_1 l_2}(\cos 2\phi)P_{n'}^{l_1 l_2}(\cos 2\phi) = \delta_{n,n'}\,, \qquad \text{(F.18)}$$

where the normalization constant reads

$$\mathcal{N}_n^{l_1 l_2} = \left[\frac{2(L+1)\,\Gamma(n+1)\,\Gamma(L-n+1)}{\Gamma(n+|l_1|+1)\,\Gamma(n+|l_2|+1)}\right]^{1/2}. \qquad \text{(F.19)}$$

As a consequence, the hyperspherical harmonics $\mathcal{Y}_L$ satisfy the orthonormality relation

$$\int d\Omega_4\,\mathcal{Y}_L(\Omega_4)\,\mathcal{Y}_{L'}(\Omega_4) = \delta_{l_1,l_1'}\delta_{l_2,l_2'}\delta_{n,n'}\,. \qquad \text{(F.20)}$$

Notice that, the hyperspherical harmonics form a complete set for any function on the surface described by the angles $\{\phi,\theta_1,\theta_2\}$ at fixed ξ. As a consequence, the wave functions appearing in eq. F.3 can be expanded as

$$\mathcal{C}(\xi,\Omega_4) = \sum_{\{L\}}\mathcal{C}_{\{L\}}(\xi)\,\mathcal{Y}_{\{L\}}(\Omega_4)\,, \qquad \text{(F.21)}$$

where $\{L\}$ refers to the particular combination of quantum numbers which leads to $L = 2n+|l_1|+|l_2|$ and the expansion coefficients $\mathcal{C}_{\{L\}}$ encode the hyper-radial dependence of the wave function. By using the definition of the laplacian operator in eq. F.8 and employing the definition of the hyperangular momentum operator,

the Schrödinger equation can be written as

$$\left\{-\left[\frac{\partial^2}{\partial\xi^2}+\frac{3}{\xi}\frac{\partial}{\partial\xi}-\frac{\mathcal{L}^2(\Omega_4)}{\xi^2}\right]+\rho\left[\hat{V}(\xi,\Omega_4)-\hat{E}_0\right]\right\}\mathcal{C}(\xi,\Omega_4)=0\,. \tag{F.22}$$

By expanding the wave function in terms of hyperspherical harmonics as in eq. F.21 and by writing the expansion coefficient as $\mathcal{C}(\xi)=u(\xi)/\xi^{3/2}$ with the purpose of getting rid of the first derivative in the Schrödinger equation, by using eq. F.10, we can rewrite the Schrödinger equation as

$$\sum_{\{L'\}}\left\{-\left[\frac{\partial^2}{\partial\xi^2}+\frac{3}{4\xi^2}-\frac{L'(L'+2)}{\xi^2}\right]+\rho\left[\hat{V}(\xi,\Omega_4)-\hat{E}_0\right]\right\}u_{\{L'\}}(\xi)\,\mathcal{Y}_{\{L'\}}(\Omega_4)=0\,. \tag{F.23}$$

Finally by multiplying on the left by $\mathcal{Y}^*_{\{L\}}(\Omega_4)$ and integrating over the angular variables, the orthogonality relation for the hyperspherical harmonics, in eq. F.20, leads to the final form

$$\left\{-\left[\frac{\partial^2}{\partial\xi^2}+\frac{3}{4\xi^2}-\frac{L(L+2)}{\xi^2}\right]-\rho\hat{E}_0\right\}u_{\{L\}}(\xi)+\rho\sum_{\{L'\}}\mathcal{V}_{\{L,L'\}}(\xi)\,u_{\{L'\}}(\xi)=0, \tag{F.24}$$

where

$$\mathcal{V}_{\{L,L'\}}(\xi)=\int d\Omega_4\,\mathcal{Y}^*_{\{L\}}(\Omega_4)\,\hat{V}(\xi,\Omega_4)\,\mathcal{Y}_{\{L'\}} \tag{F.25}$$

are the potential matrix elements computed in the basis of the hyperspherical harmonics. Notice that in this way the Schrödinger equation has been reduced to a set of coupled one-dimensional Schrödinger equations which are easier to be solved numerically. With this procedure the bulk of the calculation reduces to the computation of the potential matrix elements by properly truncating the basis up to a certain value $L_{\max}$. Then the ground state is extracted by numerically solving the set of coupled one-dimensional differential equations in eq. F.24, with some suitable algorithm, like the one described in App. F.2.

Since we are only interested in the ground state we can restrict the calculation of the potential matrix elements to states with zero total angular momentum

$(l_1 = -l_2)$, which implies that the grand orbital quantum number is restricted to even values

$$L = 2\,(n + |l_1|)\ . \tag{F.26}$$

The choice of $L_{\max}$, i.e. the value of L which determines the truncation of the expansion in eq. F.25, is somehow critical and there is no general prescription for this choice. By increasing the number of states included in the calculation of the potential matrix, the result becomes increasingly stable. By taking $L_{\max} = 30$ which corresponds to include 256 states, we observed a stable result for the eigenvalue of the ground state ($\hat{E}_0 = 1.188$). In particular the relative difference between the lowest eigenvalue extracted by using $L_{\max} = 28$ and the one obtained with $L_{\max} = 30$ is of order 10^{-5}, which is then sufficient for a comparison with the lattice data, given our statistical precision, see Sec. 6.2.

F.2 The renormalized Numerov method

The Schrödinger equations for the 1-loop order corrections to the mesonic and baryonic screening masses have been solved by using the renormalized Numerov algorithm [210, 211] for numerical solutions of second order differential equations. Let us consider a second order differential equation, discretized on a mesh grid with lattice spacing a, of the form $y_n'' + g_n y_n = 0$. Then the following three-terms recurrence relation holds

$$y_{n+1}\left(1 + \frac{a^2}{12} g_{n+1}\right) - y_n\left(2 + \frac{10\,a^2}{12} g_n\right) + y_{n-1}\left(1 + \frac{a^2}{12} g_{n-1}\right) = 0 + O(a^6)\,. \tag{F.27}$$

One dimensional Schrödinger equations of the kind of eq. 5.15 and more generally the set of coupled differential equations in eq. F.24, can be easily reduced to this form by simply writing

$$\left(\mathbb{1}\frac{\partial^2}{\partial r^2} + \mathbf{Q}\,(r)\right)\mathbf{U}\,(r) = \mathbf{0}, \tag{F.28}$$

with

$$\mathbf{Q}(r) = \rho\left[\hat{E}_0 \cdot \mathbb{1} - \mathbf{V}(r)\right] \tag{F.29}$$

where bold letters refer to $M \times M$ matrices, where M is the total number of coupled differential equations, i.e. the case of a single Schrödinger equation is recovered by setting $M = 1$. Suppose now to discretize the system on a grid $r_0, r_1, ..., r_n$, then by directly applying the Numerov recurrence relation we have

$$(\mathbb{1} - \mathbf{T}_{j+1})\,\mathbf{U}_{j+1} - (2\mathbb{1} + 10\mathbf{T}_j)\,\mathbf{U}_j + (\mathbb{1} - \mathbf{T}_{j-1})\,\mathbf{U}_{j-1} = \mathbf{0}\,, \tag{F.30}$$

where the index j labels the point on the grid and

$$\mathbf{T}_j = -\frac{a^2}{12}\mathbf{Q}_j \tag{F.31}$$

where a is the grid lattice spacing. The recurrence relation can be written in a more compact way as

$$\mathbf{F}_{j+1} - \mathbf{W}_j\mathbf{F}_j + \mathbf{F}_{j-1} = \mathbf{0} \qquad \text{where} \qquad \begin{cases} \mathbf{F}_j = (\mathbb{1} - \mathbf{T}_j)\,\mathbf{U}_j \\ \mathbf{W}_j = (\mathbb{1} - \mathbf{T}_j)^{-1}(2\mathbb{1} - 10\mathbf{T}_j) \end{cases}. \tag{F.32}$$

Finally, by introducing $\mathbf{R}_j = \mathbf{F}_{j+1}\mathbf{F}_j^{-1}$ we obtain the *forward recurrence relation*

$$\begin{cases} \mathbf{R}_j = \mathbf{W}_j - \mathbf{R}_{j-1}^{-1} \\ \mathbf{R}_0^{-1} = \mathbf{0} \end{cases}, \tag{F.33}$$

where the starting point of the recurrence relation is simply obtained by imposing Dirichlet boundary conditions at r_0, i.e. $\mathbf{U}_0 = 0$ and $\mathbf{U}_1 \neq 0$, which implies $\mathbf{R}_0^{-1} = 0$. Since $\mathbf{W}_j$ only contains known terms appearing in the Schrödinger equation, by knowing $\mathbf{R}_j$ at r_j we can determine $\mathbf{R}_{j+1}$ at r_{j+1}. In the very same way we can also

obtain a *backward recurrence relation*, by defining $\hat{\mathbf{R}}_j = \mathbf{F}_{j-1}\mathbf{F}_j^{-1}$, as

$$\begin{cases} \hat{\mathbf{R}}_j = \mathbf{W}_j - \hat{\mathbf{R}}_{j+1}^{-1} \\ \hat{\mathbf{R}}_n^{-1} = \mathbf{0} \end{cases}, \tag{F.34}$$

where we imposed the condition that the wave function vanishes at the upper end of the grid. In this way we can solve iteratively the differential equation both forward and backward, up to a matching coordinate r_{M}, where we require the matching condition

$$\det\left[\mathbf{R}_{\mathrm{M}} - \hat{\mathbf{R}}_{\mathrm{M}+1}^{-1}\right] = 0\,, \tag{F.35}$$

which, when satisfied, provides the eigenvalue $\hat{E}_0$. Notice that, in practical applications, the matching condition is solved iteratively by means of numerical methods, e.g. the Newton method, given an initial trial energy $\hat{E}_0$.

Appendix G

Screening masses in the free lattice theory

This appendix is devoted to the calculation of the free-theory value of both the mesonic and baryonic screening masses. The aim of this calculation is to define tree-level improved definitions, see eq. 5.23 and 6.21, of the screening masses so as to be able to accelerate the convergence to the continuum limit. The corresponding masses in the continuum theory have been computed in Sec. 5.1.1 and 6.1.1 for the mesonic and baryonic cases respectively.

Since $D_{\rm sw}$ in eq. 3.70 does not contribute in the free case, the quark propagator in momentum space for each flavour is given by

$$S(p) = \frac{-i\gamma_\mu \bar{p}_\mu + m_0(p)}{D_F(p)} , \qquad \text{with} \qquad D_F(p) = \sum_{\mu=0}^{3} \bar{p}_\mu^2 + m_0^2(p) \tag{G.1}$$

and

$$m_0(p) = m_0 + \frac{a}{2}\sum_{\mu=0}^{3} \hat{p}_\mu^2 , \qquad \bar{p}_\mu = \frac{1}{a}\sin(ap_\mu) , \qquad \hat{p}_\mu = \frac{2}{a}\sin\left(\frac{ap_\mu}{2}\right) , \tag{G.2}$$

where we have assumed $M_0 = m_0 \cdot \mathbb{1}$. In the presence of shifted boundary conditions (see appendices A and E in Ref. [167] and Sec. 4.1), the fermionic lattice momenta

in the compact direction take the values

$$p_0 = \frac{2\pi n_0}{L_0} + \frac{\pi}{L_0} - \sum_{k=1}^{3} p_k \xi_k \quad \text{where} \quad n_0 = 0, \dots, L_0/a - 1 \tag{G.3}$$

while in the spatial directions we consider the infinite volume limit and therefore the momenta are given by $p_k \in [-\pi/a, \pi/a)$, see eq. 3.2.

Based on these definitions, in the following appendices we provide the free-theory calculation of the mesonic and baryonic screening masses.

G.1 Mesonic screening masses

In order to extract the mesonic screening masses, we compute the two-point correlation function defined in eq. 5.21 for $O = \{S, P, V_\mu, S_\mu\}$ corresponding to $\Gamma_O = \{\mathbb{1}, \gamma_5, \gamma_\mu, \gamma_\mu\gamma_5\}$ respectively. At tree-level those correlation functions are given by

$$C_{\mathcal{O}}(x_3) = -\frac{3}{2} \int \frac{d^4p}{(2\pi)^4} \frac{dk_3}{2\pi} \, \mathrm{Tr}\Big[\Gamma_{\mathcal{O}} \, S(k) \, \Gamma_{\mathcal{O}} \, S(p)\Big] e^{-i(p_3 - k_3)\, x_3} \,, \tag{G.4}$$

where $S(p)$ is the tree-level quark propagator defined in eq. G.1, $k = (p_0, p_1, p_2, k_3)$ and Tr stands for the trace over the Dirac index. From Eq. (3.613–1.^{6}) of Ref. [212] we obtain

$$\int \frac{dp_3}{2\pi} \frac{e^{-ip_3 x_3}}{D_F(p)} = \frac{e^{-2\hat{\omega}(p) x_3}}{a\omega(p)\bar{\omega}(p)} \tag{G.5}$$

where

$$\omega^2(p) = \overline{m}^2(p) + \sum_{\nu=0}^{2} \bar{p}_\nu^2 \,, \quad \bar{\omega}^2(p) = \left[\overline{m}(p) + \frac{2}{a}\right]^2 + \sum_{\nu=0}^{2} \bar{p}_\nu^2 \,, \tag{G.6}$$

$$\overline{m}(p) = m_0 + \frac{a}{2} \sum_{0}^{2} \hat{p}_n^2 \,, \quad a\hat{\omega}(p) = \frac{1}{2} \ln\left[\frac{\bar{\omega}(p) + \omega(p)}{\bar{\omega}(p) - \omega(p)}\right] . \tag{G.7}$$

L_0/a	$m^{\text{free}}/(2\pi T)$
4	0.932614077...
6	0.967811412...
8	0.981401809...
10	0.987944825...

Table G.1: Tree-level values of the mesonic non-singlet screening masses on lattices with temporal extension L_0/a, infinite spatial volume and shift vector $\boldsymbol{\xi} = (1,0,0)$.

By using the above formulae, the correlation function can be written as

$$C_{\mathcal{O}}(x_3) = -\frac{3}{a^2 L_0} \sum_{n_0} \int dp_1\, dp_2\, \bar{C}_{\mathcal{O}}(p)\, e^{-4\hat{\omega}(p)x_3}\,, \tag{G.8}$$

where

$$\bar{C}_S(p) = -\frac{4\sum_{\nu=0}^{2} \bar{p}_\nu^2}{\omega^2(p)\bar{\omega}^2(p)}\,, \tag{G.9}$$

$$\bar{C}_{V_\mu}(p) = (1-\delta_{\mu 3})\Big[\frac{1}{[\overline{m}(p)+1/a]^2} - \frac{4\bar{p}_\mu^2}{\omega^2(p)\bar{\omega}^2(p)}\Big], \tag{G.10}$$

$$\bar{C}_P(p) = \frac{1}{[\overline{m}(p)+1/a]^2} \tag{G.11}$$

$$\bar{C}_{A_\mu}(p) = -\frac{\delta_{\mu 3}}{[\overline{m}(p)+1/a]^2} + \frac{4\sum_{\nu\neq\mu,3} \bar{p}_\nu^2}{\omega^2(p)\bar{\omega}^2(p)}\,. \tag{G.12}$$

In such a way, the entire x_3-dependence is encoded in the exponential in eq. G.8 and $\hat{\omega}(p)$ encodes the contribution of each quark line to the screening mass. Notice that $\bar{C}_S + \bar{C}_P = \bar{C}_{V_\mu} - \bar{C}_{A_\mu}$. For the shift vector $\boldsymbol{\xi} = (1,0,0)$, the minimum of $\hat{\omega}$ is attained for $(p_0,p_1,p_2) = (\frac{\pi}{2L_0}, \frac{\pi}{2L_0}, 0)$ for all correlators we are interested in. The tree-level values of the mesonic screening masses are therefore all the same. They are given by the expression

$$m_{\mathcal{O}}^{\text{free}} = 4\,\hat{\omega}\Big(\frac{\pi}{2L_0}, \frac{\pi}{2L_0}, 0\Big)\,, \tag{G.13}$$

whose values normalized to $2\pi T$ are listed, for practical convenience, in Table G.1 for the temporal extensions L_0/a relevant to this paper.

G.2 Baryonic screening masses

Similarly to the mesonic screening masses, by using the definitions in the previous sections, in the infinite spatial volume limit the baryonic correlation function can be written in the form

$$C_{N^\pm}(x_3) = \pm \sum_{p_0,q_0} \int dp_1 dp_2 dq_1 dq_2 \mathcal{M}(p,q) e^{-2\,\Omega(p,q,k)x_3}\,, \tag{G.14}$$

where the function $\Omega(p,q,k)$ is given by

$$\Omega(p,q,k) \;=\; \hat{\omega}(p) + \hat{\omega}(q) + \hat{\omega}(k) \tag{G.15}$$

with $\hat{\omega}$ defined in eq. G.7, which encoded each quark line contribution to the screening correlator, while the matrix $\mathcal{M}(p,q)$ is a calculable function of the momenta which does not play any rôle in the computation of the baryonic screening masses. For the lowest Matsubara frequency and for shift vectors of the form $\boldsymbol{\xi} = (\xi,0,0)$, the energy-momentum conservation implies

$$\begin{cases} p_0 + q_0 + k_0 \;=\; \frac{\pi}{L_0}\gamma^2 \\ p_1 + q_1 + k_1 \;=\; \frac{\pi}{L_0}\xi\gamma^2 \\ p_2 + q_2 + k_2 \;=\; 0 \end{cases} . \tag{G.16}$$

The screening mass is then obtained by minimizing $\Omega(p,q,k)$ with respect to the momenta. For the shift vector $\boldsymbol{\xi} = (1,0,0)$, the minimum is attained at

$$p = \frac{\pi}{2L_0}(1,1,0)\,, \qquad q = k = \frac{\pi}{2L_0}(-1,-1,0)\,. \tag{G.17}$$

Notice that, since $\hat{\omega}$ is an even function of the momenta, each quark line gives the same contribution to Ω and, as a consequence, the value of the tree-level baryonic mass at finite lattice spacing is simply 3/2 the value we found in the mesonic case. As a consequence the tree-level values normalized to $3\pi T$ are the same as reported in table G.1 for the mesonic screening masses.

As a final comment, in fig. G.1 we show the tree-level baryonic masses normalized to $3\pi T$ as a function of the lattice spacing. Notice that the data set corre-

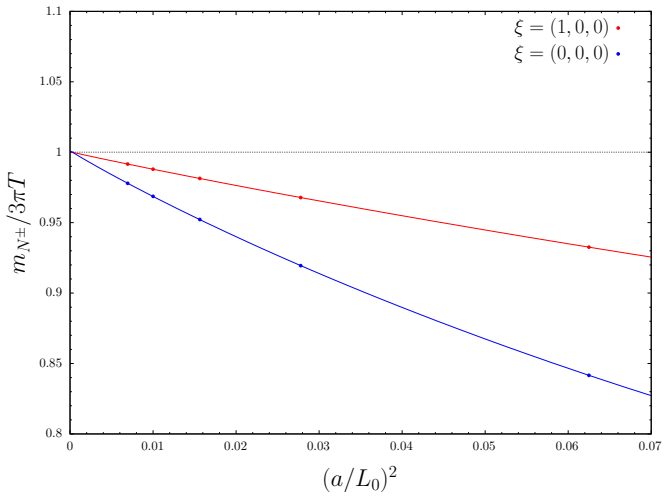

Figure G.1: Continuum limit extrapolation of the tree-level baryonic screening mass normalized to the continuum free-theory value. Red points represent the tree-level values with shifted boundary conditions and $\boldsymbol{\xi} = (1,0,0)$ which is the case of interest in this thesis. Blue point are the result with standard periodic boundary conditions, i.e. $\boldsymbol{\xi} = (0,0,0)$. Blue and red lines are polynomial fits in $(a/L_0)^2$. The dashed horizontal line is the expected continuum value.

sponding to shifted boundary conditions exhibit smaller discretization errors with respect to usual periodic boundary conditions. Such behaviour confirms previous observations in the pure gauge theory in Ref. [169, 14] and in QCD at leading and next-to-leading order in perturbation theory in Ref. [170].

Bibliography

[1] M. Dalla Brida, L. Giusti, T. Harris, D. Laudicina and M. Pepe, *Non-perturbative thermal QCD at all temperatures: the case of mesonic screening masses*, *JHEP* **04** (2022) 034 [2112.05427].

[2] L. Giusti, T. Harris, D. Laudicina, M. Pepe and P. Rescigno, "Baryonic screening masses in QCD at high temperature, *in preparation*."

[3] D.L. et al., "Analytic calculation of baryonic screening masses at 1-loop order in perturbation theory, *in preparation*."

[4] D. Laudicina, M. Dalla Brida, L. Giusti, T. Harris and M. Pepe, *Computation of QCD meson screening masses at high temperature*, *PoS* **LATTICE2021** (2022) 190 [2112.06662].

[5] M. Dalla Brida, L. Giusti, T. Harris, D. Laudicina and M. Pepe, *QCD mesonic screening masses up to high temperatures*, *PoS* **ICHEP2022** (2022) 829 [2211.11549].

[6] D. Laudicina, M. Dalla Brida, L. Giusti, T. Harris and M. Pepe, *QCD mesonic screening masses and restoration of chiral symmetry at high T*, *PoS* **LATTICE2022** (2023) 182 [2212.02167].

[7] P. Rescigno, L. Giusti, T. Harris, D. Laudicina and M. Pepe, *Baryonic Screening Masses in High Temperature QCD*, in *40th International Symposium on Lattice Field Theory*, 11, 2023 [2311.17761].

[8] H. Fritzsch, M. Gell-Mann and H. Leutwyler, *Advantages of the Color Octet Gluon Picture*, *Phys. Lett. B* **47** (1973) 365.

[9] M. Gyulassy and L. McLerran, *New forms of QCD matter discovered at RHIC*, *Nucl. Phys. A* **750** (2005) 30 [nucl-th/0405013].

[10] ALICE collaboration, *Two-particle transverse momentum correlations in pp and p-Pb collisions at LHC energies*, *Phys. Rev. C* **107** (2023) 054617 [2211.08979].

[11] E. Shuryak, *Strongly coupled quark-gluon plasma in heavy ion collisions*, *Rev. Mod. Phys.* **89** (2017) 035001 [1412.8393].

[12] A.D. Linde, *Infrared Problem in Thermodynamics of the Yang-Mills Gas*, *Phys. Lett. B* **96** (1980) 289.

[13] H.B. Meyer, *Transport Properties of the Quark-Gluon Plasma: A Lattice QCD Perspective*, *Eur. Phys. J. A* **47** (2011) 86 [1104.3708].

[14] L. Giusti and M. Pepe, *Equation of state of the SU(3) Yang–Mills theory: A precise determination from a moving frame*, *Phys. Lett. B* **769** (2017) 385 [1612.00265].

[15] M. Laine and M. Vepsalainen, *Mesonic correlation lengths in high temperature QCD*, *JHEP* **02** (2004) 004 [hep-ph/0311268].

[16] S. Weinberg, *The quantum theory of fields*, vol. 2, Cambridge university press (1995).

[17] T. Muta, *Foundation of quantum chrodinamics*, 1986.

[18] H.J. Rothe, *Lattice Gauge Theories: An Introduction Third Edition*, vol. 74, World Scientific Publishing Company (2005).

[19] C.A. Baker et al., *An Improved experimental limit on the electric dipole moment of the neutron*, *Phys. Rev. Lett.* **97** (2006) 131801 [hep-ex/0602020].

[20] J.M. Pendlebury et al., *Revised experimental upper limit on the electric dipole moment of the neutron*, *Phys. Rev. D* **92** (2015) 092003 [1509.04411].

[21] nEDM collaboration, *Measurement of the permanent electric dipole moment of the neutron*, *Phys. Rev. Lett.* **124** (2020) 081803 [2001.11966].

[22] Particle Data Group collaboration, *Review of Particle Physics*, *PTEP* **2022** (2022) 083C01.

[23] R.P. Feynman, *Space-time approach to non-relativistic quantum mechanics*, *Rev. Mod. Phys.* **20** (1948) 367.

[24] L. Faddeev and V. Popov, *Feynman Diagrams for the Yang-Mills Field*, *Phys. Lett. B* **25** (1967) 29.

[25] J. Zinn-Justin, *Quantum field theory and critical phenomena*, vol. 113, Clarendon Press, Oxford (2002).

[26] I. Montvay and G. Münster, *Quantum fields on a lattice*, Cambridge University Press (1997).

[27] R. Sommer, *Scale setting in lattice QCD*, *PoS* **LATTICE2013** (2014) 015 [1401.3270].

[28] G. 't Hooft and M.J.G. Veltman, *Regularization and Renormalization of Gauge Fields*, *Nucl. Phys. B* **44** (1972) 189.

[29] M. Peskin, *An introduction to quantum field theory*, CRC press (2018).

[30] S. Weinberg, *New approach to the renormalization group*, *Phys. Rev. D* **8** (1973) 3497.

[31] G. 't Hooft, *Dimensional regularization and the renormalization group*, *Nucl. Phys. B* **61** (1973) 455.

[32] K.G. Wilson and J. Kogut, *The renormalization group and the ϵ expansion*, *Physics reports* **12** (1974) 75.

[33] C.G. Callan Jr, *Broken scale invariance in scalar field theory*, *Physical Review D* **2** (1970) 1541.

[34] K. Symanzik, *Small distance behaviour in field theory and power counting*, *Communications in Mathematical Physics* **18** (1970) 227.

[35] H.D. Politzer, *Reliable perturbative results for strong interactions?*, *Phys. Rev. Lett.* **30** (1973) 1346.

[36] D.J. Gross and F. Wilczek, *Ultraviolet behavior of non-abelian gauge theories*, *Phys. Rev. Lett.* **30** (1973) 1343.

[37] S.A. Larin and J.A.M. Vermaseren, *The Three loop QCD Beta function and anomalous dimensions*, *Phys. Lett. B* **303** (1993) 334 [hep-ph/9302208].

[38] T. van Ritbergen, J.A.M. Vermaseren and S.A. Larin, *The Four loop beta function in quantum chromodynamics*, *Phys. Lett. B* **400** (1997) 379 [hep-ph/9701390].

[39] K.G. Wilson and J.B. Kogut, *The Renormalization group and the epsilon expansion*, *Phys. Rept.* **12** (1974) 75.

[40] ALPHA collaboration, *QCD Coupling from a Nonperturbative Determination of the Three-Flavor Λ Parameter*, *Phys. Rev. Lett.* **119** (2017) 102001 [1706.03821].

[41] Flavour Lattice Averaging Group (FLAG) collaboration, *FLAG Review 2021*, *Eur. Phys. J. C* **82** (2022) 869 [2111.09849].

[42] Flavour Lattice Averaging Group collaboration, *FLAG Review 2019: Flavour Lattice Averaging Group (FLAG)*, *Eur. Phys. J. C* **80** (2020) 113 [1902.08191].

[43] M. Beneke and M. Jamin, *alpha(s) and the tau hadronic width: fixed-order, contour-improved and higher-order perturbation theory*, *JHEP* **09** (2008) 044 [0806.3156].

[44] V. Mateu and P.G. Ortega, *Bottom and Charm Mass determinations from global fits to $Q\bar{Q}$ bound states at N^3LO*, *JHEP* **01** (2018) 122 [1711.05755].

[45] T. Cridge, L.A. Harland-Lang, A.D. Martin and R.S. Thorne, *An investigation of the α_S and heavy quark mass dependence in the MSHT20 global PDF analysis*, *Eur. Phys. J. C* **81** (2021) 744 [2106.10289].

[46] OPAL collaboration, *Determination of alpha$_s$ using OPAL hadronic event shapes at $\sqrt{s} = 91$ - 209 GeV and resummed NNLO calculations*, *Eur. Phys. J. C* **71** (2011) 1733 [1101.1470].

[47] M. Czakon, A. van Hameren, A. Mitov and R. Poncelet, *Single-jet inclusive rates with exact color at $\mathcal{O}(\alpha_s^4)$*, *JHEP* **10** (2019) 262 [1907.12911].

[48] S. Catani, S. Devoto, M. Grazzini, S. Kallweit and J. Mazzitelli, *Top-quark pair production at the LHC: Fully differential QCD predictions at NNLO*, *JHEP* **07** (2019) 100 [1906.06535].

[49] J. Haller, A. Hoecker, R. Kogler, K. Mönig, T. Peiffer and J. Stelzer, *Update of the global electroweak fit and constraints on two-Higgs-doublet models*, *Eur. Phys. J. C* **78** (2018) 675 [1803.01853].

[50] M. Gell-Mann, *The interpretation of the new particles as displaced charge multiplets*, *Nuovo Cim.* **4** (1956) 848.

[51] K. Nishijima, *Charge Independence Theory of V Particles*, *Prog. Theor. Phys.* **13** (1955) 285.

[52] M. Gell-Mann, *The Eightfold Way: A Theory of strong interaction symmetry*, 3, 1961. 10.2172/4008239.

[53] J. Goldstone, A. Salam and S. Weinberg, *Broken Symmetries*, *Phys. Rev.* **127** (1962) 965.

[54] Y. Nambu, *Quasiparticles and Gauge Invariance in the Theory of Superconductivity*, *Phys. Rev.* **117** (1960) 648.

[55] J. Goldstone, *Field Theories with Superconductor Solutions*, *Nuovo Cim.* **19** (1961) 154.

[56] L. Giusti and M. Luscher, *Chiral symmetry breaking and the Banks-Casher relation in lattice QCD with Wilson quarks*, *JHEP* **03** (2009) 013 [0812.3638].

[57] G.P. Engel, L. Giusti, S. Lottini and R. Sommer, *Chiral Symmetry Breaking in QCD with Two Light Flavors*, *Phys. Rev. Lett.* **114** (2015) 112001 [1406.4987].

[58] M. Gell-Mann, R.J. Oakes and B. Renner, *Behavior of current divergences under SU(3) x SU(3)*, *Phys. Rev.* **175** (1968) 2195.

[59] T. Matsubara, *A New approach to quantum statistical mechanics*, *Prog. Theor. Phys.* **14** (1955) 351.

[60] HotQCD collaboration, *The chiral transition and $U(1)_A$ symmetry restoration from lattice QCD using Domain Wall Fermions*, *Phys. Rev. D* **86** (2012) 094503 [1205.3535].

[61] L. Giusti and M. Lüscher, *Topological susceptibility at $T > T_c$ from master-field simulations of the SU(3) gauge theory*, *Eur. Phys. J. C* **79** (2019) 207 [1812.02062].

[62] C. Bonati, M. D'Elia, M. Mariti, G. Martinelli, M. Mesiti, F. Negro et al., *Axion phenomenology and θ-dependence from $N_f = 2 + 1$ lattice QCD*, *JHEP* **03** (2016) 155 [1512.06746].

[63] S. Borsanyi, M. Dierigl, Z. Fodor, S.D. Katz, S.W. Mages, D. Nogradi et al., *Axion cosmology, lattice QCD and the dilute instanton gas*, *Phys. Lett. B* **752** (2016) 175 [1508.06917].

[64] S. Borsanyi et al., *Calculation of the axion mass based on high-temperature lattice quantum chromodynamics*, *Nature* **539** (2016) 69 [1606.07494].

[65] A. Athenodorou, C. Bonanno, C. Bonati, G. Clemente, F. D'Angelo, M. D'Elia et al., *Topological susceptibility of $N_f = 2 + 1$ QCD from staggered fermions spectral projectors at high temperatures*, *JHEP* **10** (2022) 197 [2208.08921].

[66] F. Cuteri, O. Philipsen and A. Sciarra, *On the order of the QCD chiral phase transition for different numbers of quark flavours*, *JHEP* **11** (2021) 141 [2107.12739].

[67] G. Aarts et al., *Phase Transitions in Particle Physics - Results and Perspectives from Lattice Quantum Chromo-Dynamics*, *Prog. Part. Nucl. Phys.* **133** (2023) 104070 [2301.04382].

[68] P. Hasenfratz, F. Karsch and I.O. Stamatescu, *The SU(3) Deconfinement Phase Transition in the Presence of Quarks*, *Phys. Lett. B* **133** (1983) 221.

[69] M. Fukugita and A. Ukawa, *Deconfining and Chiral Transitions of Finite Temperature Quantum Chromodynamics in the Presence of Dynamical Quark Loops*, *Phys. Rev. Lett.* **57** (1986) 503.

[70] Y. Aoki, G. Endrodi, Z. Fodor, S.D. Katz and K.K. Szabo, *The Order of the quantum chromodynamics transition predicted by the standard model of particle physics*, *Nature* **443** (2006) 675 [hep-lat/0611014].

[71] P. de Forcrand and O. Philipsen, *The Chiral critical line of N(f) = 2+1 QCD at zero and non-zero baryon density*, *JHEP* **01** (2007) 077 [hep-lat/0607017].

[72] HotQCD collaboration, *Chiral crossover in QCD at zero and non-zero chemical potentials*, *Phys. Lett. B* **795** (2019) 15 [1812.08235].

[73] T. Schäfer and E.V. Shuryak, *Phases of QCD at high baryon density*, *Lect. Notes Phys.* **578** (2001) 203 [nucl-th/0010049].

[74] N. Cabibbo and G. Parisi, *Exponential Hadronic Spectrum and Quark Liberation*, *Phys. Lett. B* **59** (1975) 67.

[75] J.C. Collins and M.J. Perry, *Superdense Matter: Neutrons Or Asymptotically Free Quarks?*, *Phys. Rev. Lett.* **34** (1975) 1353.

[76] P. Braun-Munzinger, V. Koch, T. Schäfer and J. Stachel, *Properties of hot and dense matter from relativistic heavy ion collisions*, *Phys. Rept.* **621** (2016) 76 [1510.00442].

[77] U.W. Heinz and M. Jacob, *Evidence for a new state of matter: An Assessment of the results from the CERN lead beam program*, 1, 2000.

[78] S.A. Bass, M. Gyulassy, H. Stoecker and W. Greiner, *Signatures of quark gluon plasma formation in high-energy heavy ion collisions: A Critical review*, *J. Phys. G* **25** (1999) R1 [hep-ph/9810281].

[79] M. Laine and A. Vuorinen, *Basics of Thermal Field Theory*, vol. 925, Springer (2016), 10.1007/978-3-319-31933-9, [1701.01554].

[80] S. Chapman, *A New dimensionally reduced effective action for QCD at high temperature*, *Phys. Rev. D* **50** (1994) 5308 [hep-ph/9407313].

[81] M. Laine and Y. Schroder, *Two-loop QCD gauge coupling at high temperatures*, *JHEP* **03** (2005) 067 [hep-ph/0503061].

[82] A.K. Rebhan, *The NonAbelian Debye mass at next-to-leading order*, *Phys. Rev. D* **48** (1993) R3967 [hep-ph/9308232].

[83] P.B. Arnold and L.G. Yaffe, *The NonAbelian Debye screening length beyond leading order*, *Phys. Rev. D* **52** (1995) 7208 [hep-ph/9508280].

[84] I. Ghisoiu, J. Moller and Y. Schroder, *Debye screening mass of hot Yang-Mills theory to three-loop order*, *JHEP* **11** (2015) 121 [1509.08727].

[85] J.I. Kapusta, *Quantum Chromodynamics at High Temperature*, *Nucl. Phys. B* **148** (1979) 461.

[86] E. Braaten and A. Nieto, *Free energy of QCD at high temperature*, *Phys. Rev. D* **53** (1996) 3421 [hep-ph/9510408].

[87] K. Kajantie, M. Laine, K. Rummukainen and Y. Schroder, *The Pressure of hot QCD up to g6 ln(1/g)*, *Phys. Rev. D* **67** (2003) 105008 [hep-ph/0211321].

[88] M. Neubert, *Heavy quark symmetry*, *Phys. Rept.* **245** (1994) 259 [hep-ph/9306320].

[89] W.E. Caswell and G.P. Lepage, *Effective Lagrangians for Bound State Problems in QED, QCD, and Other Field Theories*, *Phys. Lett. B* **167** (1986) 437.

[90] M.E. Luke and A.V. Manohar, *Bound states and power counting in effective field theories*, *Phys. Rev. D* **55** (1997) 4129 [hep-ph/9610534].

[91] G.T. Bodwin, E. Braaten and G.P. Lepage, *Rigorous QCD analysis of inclusive annihilation and production of heavy quarkonium*, *Phys. Rev. D* **51** (1995) 1125 [hep-ph/9407339].

[92] A.V. Manohar, *The HQET / NRQCD Lagrangian to order alpha / m-3*, *Phys. Rev. D* **56** (1997) 230 [hep-ph/9701294].

[93] S.-z. Huang and M. Lissia, *The Dimensionally reduced effective theory for quarks in high temperature QCD*, *Nucl. Phys. B* **480** (1996) 623 [hep-ph/9511383].

[94] G. Aarts, C. Allton, D. De Boni, S. Hands, B. Jäger, C. Praki et al., *Light baryons below and above the deconfinement transition: medium effects and parity doubling*, *JHEP* **06** (2017) 034 [1703.09246].

[95] B.B. Brandt, A. Francis, M. Laine and H.B. Meyer, *A relation between screening masses and real-time rates*, *JHEP* **05** (2014) 117 [1404.2404].

[96] C. Rohrhofer, Y. Aoki, L.Y. Glozman and S. Hashimoto, *Chiral-spin symmetry of the meson spectral function above T_c*, *Phys. Lett. B* **802** (2020) 135245 [1909.00927].

[97] L.Y. Glozman, O. Philipsen and R.D. Pisarski, *Chiral spin symmetry and the QCD phase diagram*, *Eur. Phys. J. A* **58** (2022) 247 [2204.05083].

[98] W. Rarita and J. Schwinger, *On a theory of particles with half integral spin*, *Phys. Rev.* **60** (1941) 61.

[99] H. Schopper, ed., *Particle Physics Reference Library: Volume 1: Theory and Experiments*, Springer Nature, Cham (2020), 10.1007/978-3-030-38207-0.

[100] C. Gattringer and C. Lang, *Quantum chromodynamics on the lattice: an introductory presentation*, vol. 788, Springer Science & Business Media (2009).

[101] K.G. Wilson, *Confinement of Quarks*, *Phys. Rev. D* **10** (1974) 2445.

[102] K.G. Wilson, *Quarks: From Paradox to Myth*, *Subnucl. Ser.* **13** (1977) 13.

[103] M. Bochicchio, L. Maiani, G. Martinelli, G.C. Rossi and M. Testa, *Chiral Symmetry on the Lattice with Wilson Fermions*, *Nucl. Phys. B* **262** (1985) 331.

[104] M. Testa, *Some observations on broken symmetries*, *JHEP* **04** (1998) 002 [hep-th/9803147].

[105] H.B. Nielsen and M. Ninomiya, *No Go Theorem for Regularizing Chiral Fermions*, *Phys. Lett. B* **105** (1981) 219.

[106] H.B. Nielsen and M. Ninomiya, *Absence of Neutrinos on a Lattice. 1. Proof by Homotopy Theory*, *Nucl. Phys. B* **185** (1981) 20.

[107] H.B. Nielsen and M. Ninomiya, *Absence of Neutrinos on a Lattice. 2. Intuitive Topological Proof*, *Nucl. Phys. B* **193** (1981) 173.

[108] K.G. Wilson, *Quarks and Strings on a Lattice*, in *13th International School of Subnuclear Physics: New Phenomena in Subnuclear Physics*, 11, 1975.

[109] P.H. Ginsparg and K.G. Wilson, *A Remnant of Chiral Symmetry on the Lattice*, *Phys. Rev. D* **25** (1982) 2649.

[110] D.B. Kaplan, *A Method for simulating chiral fermions on the lattice*, *Phys. Lett. B* **288** (1992) 342 [hep-lat/9206013].

[111] Y. Shamir, *Chiral fermions from lattice boundaries*, *Nucl. Phys. B* **406** (1993) 90 [hep-lat/9303005].

[112] H. Neuberger, *Exactly massless quarks on the lattice*, *Phys. Lett. B* **417** (1998) 141 [hep-lat/9707022].

[113] H. Neuberger, *More about exactly massless quarks on the lattice*, *Phys. Lett. B* **427** (1998) 353 [hep-lat/9801031].

[114] P. Hasenfratz and F. Niedermayer, *Perfect lattice action for asymptotically free theories*, *Nucl. Phys. B* **414** (1994) 785 [hep-lat/9308004].

[115] P. Hasenfratz, *Prospects for perfect actions*, *Nucl. Phys. B Proc. Suppl.* **63** (1998) 53 [hep-lat/9709110].

[116] M. Luscher, *Exact chiral symmetry on the lattice and the Ginsparg-Wilson relation*, *Phys. Lett. B* **428** (1998) 342 [hep-lat/9802011].

[117] P. Hasenfratz, S. Hauswirth, T. Jorg, F. Niedermayer and K. Holland, *Testing the fixed point QCD action and the construction of chiral currents*, *Nucl. Phys. B* **643** (2002) 280 [hep-lat/0205010].

[118] M.F. Atiyah and I.M. Singer, *The index of elliptic operators on compact manifolds*, *Bull. Am. Math. Soc.* **69** (1969) 422.

[119] P. Hasenfratz, V. Laliena and F. Niedermayer, *The Index theorem in QCD with a finite cutoff*, *Phys. Lett. B* **427** (1998) 125 [hep-lat/9801021].

[120] S.R. Sharpe, *Rooted staggered fermions: Good, bad or ugly?*, *PoS* **LAT2006** (2006) 022 [hep-lat/0610094].

[121] T. Reisz, *Lattice Gauge Theory: Renormalization to All Orders in the Loop Expansion*, *Nucl. Phys. B* **318** (1989) 417.

[122] T. Reisz and H.J. Rothe, *Renormalization of lattice gauge theories with massless Ginsparg Wilson fermions*, *Nucl. Phys. B* **575** (2000) 255 [hep-lat/9908013].

[123] M. Luscher, *Topology of Lattice Gauge Fields*, *Commun. Math. Phys.* **85** (1982) 39.

[124] A. Phillips and D. Stone, *Lattice Gauge Fields, Principal Bundles and the Calculation of Topological Charge*, *Commun. Math. Phys.* **103** (1986) 599.

[125] M. Lüscher, *Properties and uses of the Wilson flow in lattice QCD*, *JHEP* **08** (2010) 071 [1006.4518].

[126] M. Luscher and S. Schaefer, *Lattice QCD without topology barriers*, *JHEP* **07** (2011) 036 [1105.4749].

[127] D. Albandea, P. Hernández, A. Ramos and F. Romero-López, *Topological sampling through windings*, *Eur. Phys. J. C* **81** (2021) 873 [2106.14234].

[128] K. Symanzik, *Continuum Limit and Improved Action in Lattice Theories. 1. Principles and φ^4 Theory*, *Nucl. Phys. B* **226** (1983) 187.

[129] K. Symanzik, *Continuum Limit and Improved Action in Lattice Theories. 2. O(N) Nonlinear Sigma Model in Perturbation Theory*, *Nucl. Phys. B* **226** (1983) 205.

[130] P. Weisz, *Renormalization and lattice artifacts*, in *Les Houches Summer School: Session 93: Modern perspectives in lattice QCD: Quantum field theory and high performance computing*, pp. 93–160, 4, 2010 [1004.3462].

[131] J. Balog, F. Niedermayer and P. Weisz, *The Puzzle of apparent linear lattice artifacts in the 2d non-linear sigma-model and Symanzik's solution*, *Nucl. Phys. B* **824** (2010) 563 [0905.1730].

[132] N. Husung, P. Marquard and R. Sommer, *Asymptotic behavior of cutoff effects in Yang–Mills theory and in Wilson's lattice QCD*, *Eur. Phys. J. C* **80** (2020) 200 [1912.08498].

[133] N. Husung, *Logarithmic corrections to O(a) and O(a^2) effects in lattice QCD with Wilson or Ginsparg–Wilson quarks*, *Eur. Phys. J. C* **83** (2023) 142 [2206.03536].

[134] B. Sheikholeslami and R. Wohlert, *Improved Continuum Limit Lattice Action for QCD with Wilson Fermions*, *Nucl. Phys. B* **259** (1985) 572.

[135] M. Luscher, S. Sint, R. Sommer and P. Weisz, *Chiral symmetry and O(a) improvement in lattice QCD*, *Nucl. Phys. B* **478** (1996) 365 [hep-lat/9605038].

[136] R. Wohlert, *Improved continuum limit lattice action for quarks*, 7, 1987.

[137] JLQCD, CP-PACS collaboration, *Non-perturbative O(a)-improvement of Wilson quark action in three-flavor QCD with plaquette gauge action*, *Phys. Rev. D* **71** (2005) 054505 [hep-lat/0406028].

[138] M. Luscher and P. Weisz, *On-Shell Improved Lattice Gauge Theories*, *Commun. Math. Phys.* **97** (1985) 59.

[139] N. Metropolis, A.W. Rosenbluth, M.N. Rosenbluth, A.H. Teller and E. Teller, *Equation of state calculations by fast computing machines*, *J. Chem. Phys.* **21** (1953) 1087.

[140] W.K. Hastings, *Monte Carlo Sampling Methods Using Markov Chains and Their Applications*, *Biometrika* **57** (1970) 97.

[141] S. Duane, A.D. Kennedy, B.J. Pendleton and D. Roweth, *Hybrid Monte Carlo*, *Phys. Lett. B* **195** (1987) 216.

[142] D.H. Weingarten and D.N. Petcher, *Monte Carlo Integration for Lattice Gauge Theories with Fermions*, *Phys. Lett. B* **99** (1981) 333.

[143] J.C. Sexton and D.H. Weingarten, *Hamiltonian evolution for the hybrid Monte Carlo algorithm*, *Nucl. Phys. B* **380** (1992) 665.

[144] I. Omelyan, I. Mryglod and R. Folk, *Symplectic analytically integrable decomposition algorithms: classification, derivation, and application to molecular dynamics, quantum and celestial mechanics simulations*, *Computer Physics Communications* **151** (2003) 272.

[145] M. Luscher and F. Palombi, *Fluctuations and reweighting of the quark determinant on large lattices*, *PoS* **LATTICE2008** (2008) 049 [0810.0946].

[146] M. Hasenbusch, *Speeding up the hybrid Monte Carlo algorithm for dynamical fermions*, *Phys. Lett. B* **519** (2001) 177 [hep-lat/0107019].

[147] M. Hasenbusch and K. Jansen, *Speeding up lattice QCD simulations with clover improved Wilson fermions*, *Nucl. Phys. B* **659** (2003) 299 [hep-lat/0211042].

[148] C. Urbach, K. Jansen, A. Shindler and U. Wenger, *HMC algorithm with multiple time scale integration and mass preconditioning*, *Comput. Phys. Commun.* **174** (2006) 87 [hep-lat/0506011].

[149] M. Luscher, *Computational Strategies in Lattice QCD*, in *Les Houches Summer School: Session 93: Modern perspectives in lattice QCD: Quantum field theory and high performance computing*, pp. 331–399, 2, 2010 [1002.4232].

[150] D. Mohler and S. Schaefer, *Remarks on strange-quark simulations with Wilson fermions*, *Phys. Rev. D* **102** (2020) 074506 [2003.13359].

[151] A.D. Kennedy, I. Horvath and S. Sint, *A New exact method for dynamical fermion computations with nonlocal actions*, *Nucl. Phys. B Proc. Suppl.* **73** (1999) 834 [hep-lat/9809092].

[152] M.A. Clark and A.D. Kennedy, *The RHMC algorithm for two flavors of dynamical staggered fermions*, *Nucl. Phys. B Proc. Suppl.* **129** (2004) 850 [hep-lat/0309084].

[153] Y. Saad, *Iterative methods for sparse linear systems*, SIAM (2003).

[154] M. Luscher, *Schwarz-preconditioned HMC algorithm for two-flavour lattice QCD*, *Comput. Phys. Commun.* **165** (2005) 199 [hep-lat/0409106].

[155] M. Luscher, *Local coherence and deflation of the low quark modes in lattice QCD*, *JHEP* **07** (2007) 081 [0706.2298].

[156] D.B. Leinweber, W. Melnitchouk, D.G. Richards, A.G. Williams and J.M. Zanotti, *Baryon spectroscopy in lattice QCD*, *Lect. Notes Phys.* **663** (2005) 71 [nucl-th/0406032].

[157] M. Benmerrouche, R.M. Davidson and N.C. Mukhopadhyay, *Problems of describing spin-(3/2 baryon resonances in the effective lagrangian theory*, *Phys. Rev. C* **39** (1989) 2339.

[158] G. Parisi, *The Strategy for Computing the Hadronic Mass Spectrum*, *Phys. Rept.* **103** (1984) 203.

[159] G.P. Lepage, *The Analysis of Algorithms for Lattice Field Theory*, in *Theoretical Advanced Study Institute in Elementary Particle Physics*, 6, 1989.

[160] M. Cè, L. Giusti and S. Schaefer, *Domain decomposition, multi-level integration and exponential noise reduction in lattice QCD*, *Phys. Rev. D* **93** (2016) 094507 [1601.04587].

[161] M. Cè, L. Giusti and S. Schaefer, *A local factorization of the fermion determinant in lattice QCD*, *Phys. Rev. D* **95** (2017) 034503 [1609.02419].

[162] L. Giusti, M.D. Brida, T. Harris and M. Pepe, *Multi-level computation of the hadronic vacuum polarization contribution to* $(g_\mu - 2)$, *PoS* **LATTICE2021** (2022) 356 [2112.02647].

[163] L. Giusti and M. Saccardi, *Four-dimensional factorization of the fermion determinant in lattice QCD*, *Phys. Lett. B* **829** (2022) 137103 [2203.02247].

[164] L. Giusti and H.B. Meyer, *Thermodynamic potentials from shifted boundary conditions: the scalar-field theory case*, *JHEP* **11** (2011) 087 [1110.3136].

[165] L. Giusti and H.B. Meyer, *Thermal momentum distribution from path integrals with shifted boundary conditions*, *Phys. Rev. Lett.* **106** (2011) 131601 [1011.2727].

[166] L. Giusti and H.B. Meyer, *Implications of Poincare symmetry for thermal field theories in finite-volume*, *JHEP* **01** (2013) 140 [1211.6669].

[167] M. Dalla Brida, L. Giusti and M. Pepe, *Non-perturbative definition of the QCD energy-momentum tensor on the lattice*, *JHEP* **04** (2020) 043 [2002.06897].

[168] L. Giusti and M. Pepe, *Energy-momentum tensor on the lattice: Nonperturbative renormalization in Yang-Mills theory*, *Phys. Rev. D* **91** (2015) 114504 [1503.07042].

[169] L. Giusti and M. Pepe, *Equation of state of a relativistic theory from a moving frame*, *Phys. Rev. Lett.* **113** (2014) 031601 [1403.0360].

[170] M. Bresciani, M. Dalla Brida, L. Giusti, M. Pepe and F. Rapuano, *Non-perturbative renormalization of the QCD flavour-singlet local vector current*, *Phys. Lett. B* **835** (2022) 137579 [2203.14754].

[171] G. Boyd, J. Engels, F. Karsch, E. Laermann, C. Legeland, M. Lutgemeier et al., *Thermodynamics of SU(3) lattice gauge theory*, *Nucl. Phys. B* **469** (1996) 419 [hep-lat/9602007].

[172] H.-T. Ding, F. Karsch and S. Mukherjee, *Thermodynamics of strong-interaction matter from Lattice QCD*, *Int. J. Mod. Phys. E* **24** (2015) 1530007 [1504.05274].

[173] S. Borsanyi, Z. Fodor, C. Hoelbling, S.D. Katz, S. Krieg and K.K. Szabo, *Full result for the QCD equation of state with 2+1 flavors*, *Phys. Lett. B* **730** (2014) 99 [1309.5258].

[174] M. Luscher, P. Weisz and U. Wolff, *A Numerical method to compute the running coupling in asymptotically free theories*, *Nucl. Phys. B* **359** (1991) 221.

[175] K. Jansen, C. Liu, M. Luscher, H. Simma, S. Sint, R. Sommer et al., *Nonperturbative renormalization of lattice QCD at all scales*, *Phys. Lett. B* **372** (1996) 275 [hep-lat/9512009].

[176] M. Luscher, R. Sommer, P. Weisz and U. Wolff, *A Precise determination of the running coupling in the SU(3) Yang-Mills theory*, *Nucl. Phys. B* **413** (1994) 481 [hep-lat/9309005].

[177] P. Fritzsch and A. Ramos, *Studying the gradient flow coupling in the Schrödinger functional*, *PoS* **Lattice2013** (2014) 319 [1308.4559].

[178] ALPHA collaboration, *Determination of the QCD Λ-parameter and the accuracy of perturbation theory at high energies*, *Phys. Rev. Lett.* **117** (2016) 182001 [1604.06193].

[179] ALPHA collaboration, *Slow running of the Gradient Flow coupling from 200 MeV to 4 GeV in $N_f = 3$ QCD*, *Phys. Rev. D* **95** (2017) 014507 [1607.06423].

[180] M. Bruno, T. Korzec and S. Schaefer, *Setting the scale for the CLS $2 + 1$ flavor ensembles*, *Phys. Rev. D* **95** (2017) 074504 [1608.08900].

[181] ALPHA collaboration, *A non-perturbative exploration of the high energy regime in $N_f = 3$ QCD*, *Eur. Phys. J. C* **78** (2018) 372 [1803.10230].

[182] H.B. Meyer, *Finite Volume Effects in Thermal Field Theory*, *JHEP* **07** (2009) 059 [0905.1663].

[183] M.T. Hansen and A. Patella, *Finite-volume effects in $(g-2)_\mu^{HVP,LO}$*, *Phys. Rev. Lett.* **123** (2019) 172001 [1904.10010].

[184] M. Laine and M. Vepsalainen, *On the smallest screening masses in hot QCD*, *JHEP* **09** (2009) 023 [0906.4450].

[185] D.J. Gross, R.D. Pisarski and L.G. Yaffe, *QCD and Instantons at Finite Temperature*, *Rev. Mod. Phys.* **53** (1981) 43.

[186] A. Boccaletti and D. Nogradi, *The semi-classical approximation at high temperature revisited*, *JHEP* **03** (2020) 045 [2001.03383].

[187] T.H. Hansson and I. Zahed, *Hadronic correlators in hot QCD*, *Nucl. Phys. B* **374** (1992) 277.

[188] V. Laliena and J. Campo, *An improved discretization of schrödinger-like radial equations*, *Journal of Physics A: Mathematical and Theoretical* **51** (2018) 325203.

[189] G.M. de Divitiis, R. Petronzio and N. Tantalo, *Distance preconditioning for lattice Dirac operators*, *Phys. Lett. B* **692** (2010) 157 [1006.4028].

[190] A. Bazavov et al., *Meson screening masses in (2+1)-flavor QCD*, *Phys. Rev. D* **100** (2019) 094510 [1908.09552].

[191] T.H. Hansson, M. Sporre and I. Zahed, *Baryonic and gluonic correlators in hot QCD*, *Nucl. Phys. B* **427** (1994) 545 [hep-ph/9401281].

[192] C.E. Detar and J.B. Kogut, *Measuring the Hadronic Spectrum of the Quark Plasma*, *Phys. Rev. D* **36** (1987) 2828.

[193] A. Gocksch, P. Rossi and U.M. Heller, *Quenched hadronic screening lengths at high temperature*, *Phys. Lett. B* **205** (1988) 334.

[194] S.A. Gottlieb, W. Liu, D. Toussaint, R.L. Renken and R.L. Sugar, *Hadronic Screening Lengths in the High Temperature Plasma*, *Phys. Rev. Lett.* **59** (1987) 1881.

[195] G. Aarts, C. Allton, S. Hands, B. Jäger, C. Praki and J.-I. Skullerud, *Nucleons and parity doubling across the deconfinement transition*, *Phys. Rev. D* **92** (2015) 014503 [1502.03603].

[196] G. Aarts, C. Allton, D. De Boni and B. Jäger, *Hyperons in thermal QCD: A lattice view*, *Phys. Rev. D* **99** (2019) 074503 [1812.07393].

[197] S. Datta, S. Gupta, M. Padmanath, J. Maiti and N. Mathur, *Nucleons near the QCD deconfinement transition*, *JHEP* **02** (2013) 145 [1212.2927].

[198] C. Rohrhofer, Y. Aoki, G. Cossu, H. Fukaya, C. Gattringer, L.Y. Glozman et al., *Symmetries of the Light Hadron Spectrum in High Temperature QCD*, *PoS* **LATTICE2019** (2020) 227 [1912.00678].

[199] JLQCD collaboration, *Study of the axial $U(1)$ anomaly at high temperature with lattice chiral fermions*, *Phys. Rev. D* **103** (2021) 074506 [2011.01499].

[200] J. Bulava and S. Schaefer, *Improvement of $N_f = 3$ lattice QCD with Wilson fermions and tree-level improved gauge action*, *Nucl. Phys. B* **874** (2013) 188 [1304.7093].

[201] M. Luscher and S. Schaefer, *Lattice QCD with open boundary conditions and twisted-mass reweighting*, *Comput. Phys. Commun.* **184** (2013) 519 [1206.2809].

[202] M. Luscher, *openQCD*.

[203] ALPHA collaboration, *Non-perturbative quark mass renormalisation and running in $N_f = 3$ QCD*, *Eur. Phys. J. C* **78** (2018) 387 [1802.05243].

[204] ALPHA collaboration, *QCD Coupling from a Nonperturbative Determination of the Three-Flavor Λ Parameter*, *Phys. Rev. Lett.* **119** (2017) 102001 [1706.03821].

[205] ALPHA collaboration, *How perturbative are heavy sea quarks?*, *Nucl. Phys. B* **943** (2019) 114612 [1809.03383].

[206] S. Kurth, *The renormalised quark mass in the Schrodinger functional of lattice QCD - a one-loop calculation with a non-vanishing background field*, Ph.D. thesis, -, Nov., 2002.

[207] ALPHA collaboration, P. Fritzsch and T. Korzec, *Simulating the QCD Schrödinger Functional with three massless quark flavors, internal notes ALPHA Collaboration, in preparation for publication.*

[208] R. Bracewell, *The Fourier Transform and Its Application*, vol. 34, McGraw-Hill (01, 2000), 10.1119/1.1973431.

[209] T.K. Das, *Hyperspherical Harmonics Expansion Techniques*, vol. 170, Springer (2016).

[210] J.M. Blatt, *Practical points concerning the solution of the schrödinger equation*, *Journal of Computational Physics* **1** (1967) 382.

[211] B.R. Johnson, *New numerical methods applied to solving the onedimensional eigenvalue problem*, *The Journal of Chemical Physics* **67** (1977) 4086.

[212] I.S. Gradshteyn and I.M. Ryzhik, *Table of integrals, series, and products*, Elsevier/Academic Press, Amsterdam, seventh ed. (2007).